DATA TRANSMISSION BY PULSE COMPRESSION

by

MUHAMMED SALEH YUSUF EL-ALEM, BSc, MS, MIEEE

Submitted for the Degree of Doctor of Philosophy

at

The University of Aston in Birmingham

June, 1978

DATA TRANSMISSION BY PULSE COMPRESSION

by

Muhammed Saleh Yusuf El-Alem, BSc, MS, MIEEE.

Submitted for the
Degree of Doctor of Philosophy

at

The University of Aston in Birmingham

1978

SUMMARY

Pulse compression techniques originated in radar. The present work is concerned with the utilization of these techniques in general, and the linear FM (LFM) technique in particular, for communications. It introduces these techniques from an optimum communications viewpoint and outlines their capabilities. It also considers the candidacy of the class of LFM signals for digital data transmission and the LFM spectrum.

Work related to the utilization of LFM signals for digital data transmission has been mostly experimental and mainly concerned with employing two rectangular LFM pulses (or chirps) with reversed slopes to convey the bits 1 and 0 in an incoherent mode. No systematic theory for LFM signal design and system performance has been available. Accordingly, the present work establishes such a theory taking into account coherent and noncoherent single-link and multiplex signalling modes. Some new results concerning the slope-reversal chirp pair are obtained.

The LFM technique combines the typical capabilities of pulse compression with a relative ease of implementation. However, these merits are often hampered by the difficulty of handling the LFM spectrum which cannot generally be expressed in closed-form. The common practice is to obtain a plot of this spectrum with a digital computer for every single set of LFM pulse parameters. Moreover, reported work has been mostly confined to the spectrum of an ideally rectangular chirp pulse with no rise or fall times. Accordingly, the present work comprises a systematic study of the LFM spectrum which takes the rise and fall times of the chirp pulse into account and can accommodate any LFM pulse with any parameters. It formulates rather simple and accurate prediction criteria concerning the behaviour of this spectrum in the different frequency regions. These criteria would facilitate the handling of the LFM technique in theory and practice.

KEY WORDS: CHIRP, DIGITAL COMMUNICATIONS, LINEAR FM (LFM), PULSE COMPRESSION, SPREAD SPECTRUM COMMUNICATIONS

ACKNOWLEDGEMENTS

The author wishes to thank Professor J. E. Flood, Head of the Department of Electrical Engineering, and Dr. R. L. Brewster, his supervisor, for their advice and encouragement throughout the course of this work.

Thanks are also due to many on the staff of the Department of Electrical Engineering who, in one way or another, helped in bringing this work to a final conclusion. A special note of thanks is due to Mrs. H. Turner for her patient typing of the manuscript.

The major part of this work was carried out while the author held a University Postgraduate Research Studentship. This support is gratefully acknowledged.

CONTENTS

GENERAL INTRODUCTION

Pulse compression techniques evolved since World War I mainly through the search for radar systems capable of target tracking at varying ranges in both isolated and dense environments. These techniques employ large duration bandwidth product signals that undergo duration and/or bandwidth compression through optimal processing. This compressibility makes such signals superior in many ways to the incompressible conventional unitary duration-bandwidth product signals (e.g. ASK, PSK and FSK signals). This superiority made it inevitable that great interest should be generated in extending pulse compression techniqu to a constantly increasing number of other fields including communications.

Investigations into the utilization of pulse compressi techniques for communications have been underway since the early sixties, often under the title "spread spectrum communications" and mainly for military purposes. It is only recently that these investigations have enjoyed some publicity. This publicity is mainly due to an increasing awareness of the commercial capabilities of pulse compression communication systems as well as to the current advances in developing new devices which are compatible with these systems.

Much effort is still needed to tackle the many hereto

GENERAL INTRODUCTION

Pulse compression techniques evolved since World War II mainly through the search for radar systems capable of target tracking at varying ranges in both isolated and dense environments. These techniques employ large duration-bandwidth product signals that undergo duration and/or bandwidth compression through optimal processing. This compressibility makes such signals superior in many ways to the incompressible conventional unitary duration-bandwidth product signals (e.g. ASK, PSK and FSK signals). This superiority made it inevitable that great interest should be generated in extending pulse compression techniques to a constantly increasing number of other fields including communications.

Investigations into the utilization of pulse compression techniques for communications have been underway since the early sixties, often under the title "spread spectrum communications" and mainly for military purposes. It is only recently that these investigations have enjoyed some publicity. This publicity is mainly due to an increasing awareness of the commercial capabilities of pulse compression communication systems as well as to the current advances in developing new devices which are compatible with these systems.

Much effort is still needed to tackle the many heretofore

unsolved problems concerning pulse compression signal design, generation, transmission, processing and performance as well as concerning the peaceful coexistence of pulse compression communication systems with the conventional, well established systems. The present work is a modest contribution in this direction.

Chapter 1 introduces the concept of pulse compression as well as the theory of signal design from an optimum communications viewpoint, providing a suitable background for the remaining chapters. Chapter 2 examines the utility of pulse compression techniques in general, and Chapter 3 examines that of the Linear FM (LFM) technique in particular for digital data transmission. Chapter 4 studies the LFM spectrum. The bulk of both Chapters 3 and 4 is new material whose outline is given in the Summary. Chapter 5 includes a brief Final Discussion. For convenience, mathematical analyses have been carried out in terms of complex signals. In order to facilitate the transformation from these signals to real signals, Appendix A outlines the theory of complex representation of deterministic real signals and considers the application of this theory to the class of LFM signals. Appendix B introduces the stationary phase principle which underlies much of the reasoning in the present work concerning Fourier and similar integrals.

unsolved problems concerning pulse compression signal design, generation, transmission, processing and performance as well as concerning the peaceful coexistence of pulse compression communication systems with the conventional, well established systems. The present work is a modest contribution in this direction.

Chapter 1 introduces the concept of pulse compression as well as the theory of signal design from an optimum communications viewpoint, providing a suitable background for the remaining chapters. Chapter 2 examines the utility of pulse compression techniques in general, and Chapter 3 examines that of the Linear FM (LFM) technique in particular, for digital data transmission. Chapter 4 studies the LFM spectrum. The bulk of both Chapters 3 and 4 is new material whose outline is given in the Summary. Chapter 5 includes a brief Final Discussion. For convenience, mathematical analyses have been carried out in terms of complex signals. In order to facilitate the transformation from these signals to real signals, Appendix A outlines the theory of complex representation of deterministic real signals and considers the application of this theory to the class of LFM signals. Appendix B introduces the stationary phase principle which underlies much of the reasoning in the present work concerning Fourier and similar integrals.

1

OPTIMUM COMMUNICATION AND PULSE COMPRESSION

This chapter introduces the concept of pulse compression from an optimum communications viewpoint and provides a suitable background for the remaining chapters.

1.1 Digital Communication System Model [1-11]

Communication theory is concerned with the transmission of information from an "information source" to an "informati sink" through a physical transmission "channel" making use of transducers to facilitate the communication process.

The information source selects (according to certain probabilistic rules) symbols from a characteristic symbol-alphabet and emits them sequentially in time in the form of a message(i.e. an information-bearing signal). Information sources are either analogue or discrete according to the type of messages they generate. An analogu message corresponds to a continuous alphabet and takes the shape of a waveform whose amplitude is a continuous functior of time and has a finite continuous dynamic range. An analogue source is thus capable of generating a noncountable set of analogue messages. The human vocal tract is, for example, an analogue source which is capable of generating a noncountable set of analogue messages that may be arbitrarily close, or different from, one another. A discr message, on the other hand, takes the form of a sequence of a finite number of abstract symbols belonging to a countable symbol-alphabet. A discrete source is thus capable of generating a countable number of discrete messag A teletype is, for example, a discrete source which can generate discrete messages in the form of pieces of English text, each message consisting of some or all of the 26

alphabetical letters, the numbers from 0 to 9 and a number of blank and punctuation marks.

An analogue message can be converted into an equivalent discrete message with minimal loss of its information content [9,12-22]. To this end, the analogue signal is first bandlimited (if not originally so) whereby it can be accommodated in an existing bandlimited channel without seriously degrading its quality. The bandlimited signal is then sampled according to the sampling principle, in order to make it discrete in time, and its dynamic range is scanned (uniformly or nonuniformly) by a finite number of quantization levels. Each sample is approximated by the closest quantization level. The analogue message is converted in this manner into an equivalent discrete message in the form of a sequence of quantized samples. The deviation between the analogue message and its discrete version is mainly determined by the sampling rate adopted and the quantization level density distribution.

In an M'ary digital communication system, the discrete message (whether original or converted from analogue form) is digitized in such a way that each of its discrete elements is transformed into a characteristic block, or word, consisting of a k-digit sequence of M'ary digits. In this manner, any discrete message can be transformed into a corresponding digit-sequence that has the same information content. It is thus possible to think of digital communications as being capable of unifying all types of messages such as data, voice, TV and facsimile messages in the common form of streams of

digits which can be transmitted over the same communication highway.

The block diagram of a digital communication system is shown in Fig. 1.1. Following the digital source in this diagram is a source encoder which may be included in order to facilitate the transmission process by modifying the structure of the source digital output.

Being abstract entities, the digits at the source encoder output cannot generally be directly transmitted through the physical channel. This can be made possible by introducing a channel encoder, or modulator. The modulator maps every digit, or block of digits, at the source encoder output into a unique physical waveform transmittable through the physical channel. This mapping is generally governed by certain selection criteria based on both theoretical and practical considerations. In this sense, the modulator design problem is essentially a signal design problem. This problem will be defined in the next section and outlined in Section 1.4.

The physical channel[1,5-7,11,23-25] takes the form of a transmission medium. Typical examples of transmission media in common use today include cable, waveguides, optical fibre, microwave and satellite relays, the troposphere and the ionosphere. The channel may be simple, consisting of a single transmission path, or multiple, consisting of many such paths. It generally distorts the signal being transmit through it. Channel disturbances are closely associated

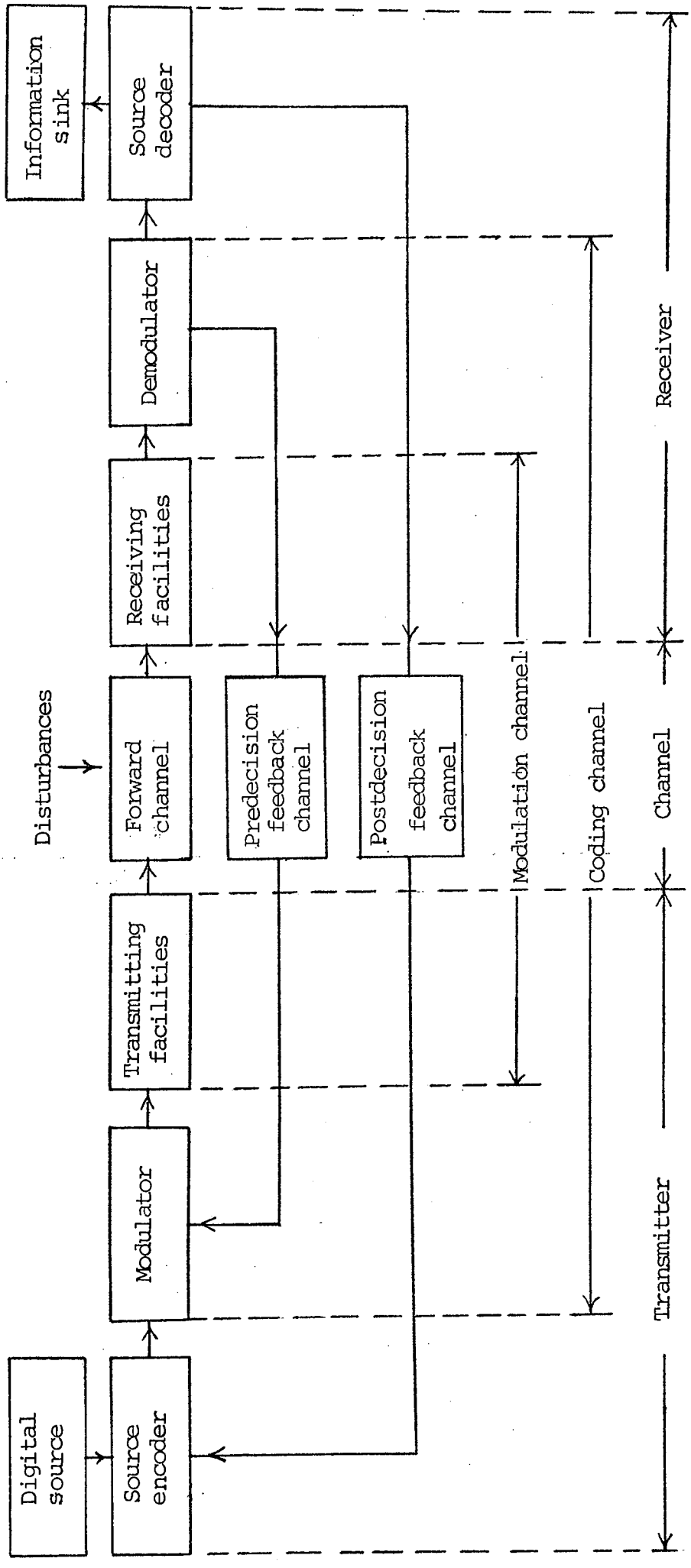

Fig. 1.1 Block Diagram of a Digital Communication System

with the complicated problem of channel characterization and design and play a key role in communication theory. Thes disturbances may be natural or man-made, static or dynamic, additive or multiplicative, and may be classified into systematic and random. A systematic disturbance is deterministic in the sense that it can be predicted as soon as the channel becomes completely known, which is rarely the case. Typical systematic disturbances include phase jitter, frequency offset, nonlinearities, dispersive characteristics of transmission media, quantization noise, ... etc. A random disturbance can only be described in probabilistic/statistical terms. Typical examples of random disturbances include impulse noise, Additive White Gaussian Noise (AWGN), Raleigh noise, ... etc. While systematic disturbances can, at least in principle, be eliminated by shrewd system design, random disturbances are much more difficult to eliminate, though measures can be taken to minimize their effects. Most existing channels have been designed originally for transmitting analogue information. Problems related to transmission quality and admissible rates arise in trying to adapt such channels for digital transmission [1,7,25].

The transmitted signal generally arrives distorted at the receiver and some of its parameters may have to be treated as random quantities by the channel decoder, or demodulator. These parameters may include its amplitude, time of arrival at the receiver, carrier frequency and

phase. Amplitude distortions are usually difficult to handle. The time of arrival at the receiver and the carrier frequency are usually assumed to be known to the receiver through the presently well developed synchronization and frequency-acquisition techniques [21,26-30]. The carrier phase may or may not be precisely known to the receiver. In the former case, the reception mode is said to be coherent. In the latter case, the reception mode is said to be incoherent differentially coherent, or partially coherent depending, respectively, on whether the carrier phase is completely unknown to the receiver, known in the form of a phase estimate based on the preceding signal as a reference, or known in the form of an estimate at the output of a phase-locked loop tracking an unmodulated carrier [7,11,21].

It is generally impossible for the demodulator to be certain of what the transmitted waveform sequence was. It usually adopts some statistical decision criterion in reaching its decisions concerning the individual received signals (asking for a retransmission over a predecision feedback link if necessary) to reconstruct the transmitted signal sequence as best as it can. It converts this signal sequence into a digital sequence which matches, either exactly or approximately, the modulator input digital sequence. The demodulator performance is usually measured by the so-called demodulator error probability, P_e, which is the average probability that the demodulator makes a wrong decision per transmitted signal.

If a source encoder is included in the transmitter, a

source decoder is required in the receiver to convert the demodulator output digital sequence into one which matches, as closely as possible, the encoder input digital sequence. The decoder should thus be capable of locating and correcting the errors in the demodulator output digital sequence (making use of a postdecision feedback link if available) before it passes its output to the information sink. This ideal situation cannot generally be achieved in practice and a difference between the decoder output and the encoder input digital sequences does usually exist in the form of an "error sequence". The number of elements in this sequence increases with the so-called decoder probability of error, P_e', which may be defined as the probability that one or more elements of the decoder output sequence are in error.

The part of the communication system that includes the physical channel together with the transmitting and receiving facilities is usually known as the modulation channel. The acronym "modem" is used to describe the modulator-demodulator pair. The part of this system which comprises the modem including the modulation channel is usually known as the coding channel. The acronym "codec" is used for the encoder-decoder pair. The modulation channel is analogue in the sense that it permits a continuum of response waveforms. The coding channel is discrete in the sense that both its input and output are sequences of digits. The problem of communication system design is usually split into two separate ones, namely, the modem and codec design problems. This separation does not

imply that these two problems are independent. It is based largely on the theoretical fact that while Fourier analysis is the main mathematical tool in the case of the former problem, linear algebra is the main tool in the case of the latter[7,10].

1.2 Communication System Optimization[3-5,10,11,21,31-42]

This section is mainly concerned with the modem, or modulator/demodulator, optimization problem.

Different criteria can be adopted for communication systems comparison and optimization. The criterion being adopted in this section is related to the reconstruction (in the receiver) of the transmitted message with the least possible number of expected errors. Thus, a suitable measure of performance must be established in this respect. The overall performance of a digital communication system in which the transmitted information is of discrete origin can be measured in terms of P_e (uncoded system) and in terms of P_e' (coded system). In a digital communication system in which the transmitted information is of analogue origin, the receiver must perform a conversion back to analogue form whereby digital errors are converted into analogue noise. Thus, the measure of performance in this case should intuitively be similar to that usually used for purely analogue communication systems. One possible performance measure in this respect is the mean-square difference between the received and transmitted messages. The adoption of such a measure obviously makes it possible to compare the performance of the purely analogue and the digitized analogue communication systems[21].

The problem of communication system optimization is

generally complicated. The central problem in this respect is that of modem optimization. This may be tackled by the detection theoretical methods of statistical decision theory. To this end, a physical modulator signal set of rather arbitrary parameters is first assumed and the prevailing transmission impairments are sufficiently characterized in appropriate statistical terms. The demodulator optimization problem is then considered by assuming that the optimum demodulator is one which applies the suitable statistical decision criterion to each distorted received signal in order to reconstruct the transmitted data sequence as closely as possible. This demodulator may be restricted to belong to a particular class, such as the class of linear devices. After deriving the exact form of the optimum demodulator, an expression for its probability of error P_e is formulated as a function of the modulator signal set parameters. Finally, the modulator optimization (or signal design) problem is considered. To this end, the optimum modulator signal set is defined as one whose parameters correspond to the minimum P_e. Obviously, such an optimum set defines the optimum modulator under the prevailing conditions. This would complete the solution of the modem optimization problem as one which consists of two basic problems, namely, the demodulator and the modulator optimization problems.

The modem optimization problem has only been considered in some relatively simple cases. The only case which has been studied in detail in this respect is the purely AWGN case[10,11, 21,32-42]. This is due to practical and theoretical reasons.

Firstly, AWGN is common to most physical situations and is predominant in the case of space communications. It displays itself in such forms as thermal noise, shot noise, cosmic noise, ... etc.[1,6,11] Secondly, the purely AWGN case seems to be the most mathematically tractable one. Thirdly, methods developed for this case can readily be applied to the case of coloured additive Gaussian noise (by making use of noise-whitening filters[11,39,40]) and can be extended to some other types of noise which may be nonstationary and/or non-Gaussian (by making use of time-variant filters and other relatively more complicated structures)[5,36,39-45].

The modulator optimization problem for the purely AWGN case is outlined in Section 1.4. The demodulator optimization problem for this case is outlined below with reference to the canonical predetection/detection (or predecision/decision) demodulator structure shown in Fig. 1.2. The detailed optimum form of this structure in general, and that of the predetection processor in particular can be derived either by making use of the so-called Signal-to-Noise Ratio (SNR) criterion or by making use of other more rigorous statistical optimization criteria[32-52]. The SNR criterion defines the optimum predetection processor as one which maximizes the output SNR (SNR_o) at one instant in time[36,39,46,49]. The statistical optimization criteria require that the demodulator optimization problem be phrased in statistical terms, either as a detection theoretical hypothesis testing problem or as a signal extraction paramete

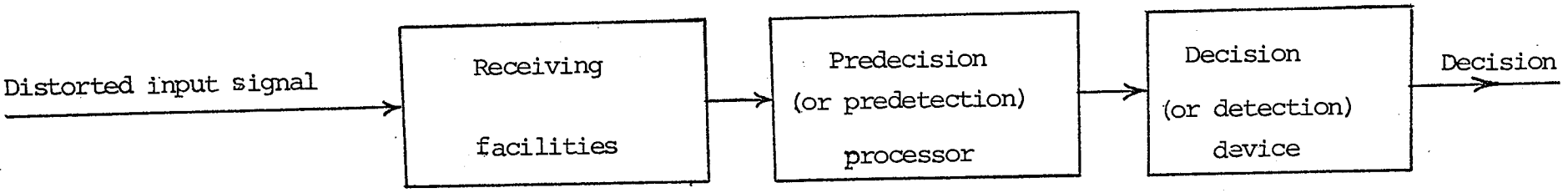

Fig. 1.2 Canonical Demodulator Structure

estimation problem. Both formulations assume that for a given physical situation, the optimum demodulator applies the appropriate optimum decision rule to every received distorted signal in such a way as to reach the decision which corresponds to the minimum expected value of the so-called loss function. The loss function is a rather arbitrary function which assumes a suitable preassigned value for every decision-observation combination. It may, or may not, be made a measure of the information loss[31,36,46,52]. Both approaches lead to essentially equivalent results. However, the former approach is generally more difficult to apply.

In any case, it can be shown[10,11,21,40] that the basic optimum predetection processor in the purely AWGN case may assume either the linear form of a multiplier-integrator compound (the so-called correlator) or the mathematically equivalent form of a matched filter-sampler compound. Both forms are treated in Section 1.5 in some detail. Here it suffices to state that each of these two forms requires a local reference to be correlated with the received signal. This local reference is generated actively in the case of the correlator and is stored in the matched filter structure in the case of the matched filter-sampler compound.

It can also be shown[10,11,21,40] that the detailed structure of the optimum predetection processor for the purely AWGN on/off communication case depends on the particular phase coherence mode under consideration. For the coherent mode, this structure assumes that of the basic optimum predetection processor which is mentioned in the preceding

paragraph. For the incoherent mode, it becomes more involved and remains essentially valid for the differentially and partially coherent modes. Here it assumes the form of a square-envelope correlator which can be implemented as a matched filter followed by an envelope detector and a sampler[1,21,40,42]. The envelope detector is a device whose output is the square root of the sum of the squares of its input and this input shifted by $\frac{\pi}{2}$ radians.

It can also be shown that the above mentioned predetection/detection demodulator structure in general, and the optimum predetection processor structures for the purely AWGN on/off communication in particular, may be extended to a variety of more involved situations. Such situations include those related to baseband and passband on/off binary or M'ary data transmission through simple or multiple channels which may be disturbed by various types of perturbations including AWGN. However, the optimum demodulator structures in these involved situations become generally more complicated than those for the simple purely AWGN on/off communication case[10,11,39,40].

The modem performance can never be made perfect in any physical situation in such a way that P_e vanishes. This fact will become clear in Section 1.4 in the purely AWGN case. Only the overall communication system performance can be made perfect with arbitrary error-free transmission at rates within the channel capacity. This can be achieved, in theory, by resorting to coding and/or feedback adaptive

techniques which usually imply considerable complication and sophistication which may turn out to be impossible to implement in practice[3-7,10,11,21,53-63].

1.3 Correlation of Deterministic Signals [11,46,64-72]

The fact stated in the previous section that correlation is the linear optimum predetection processing technique indicates the key role it plays in formulating and solving the modem optimization problem. Accordingly, this section introduces the subject of analogue correlation of deterministic signals in such a way as to provide a suitable background for the present work in this respect. The results obtained can be extended to the case of discrete correlation of deterministic signals.

1.3.1 The Correlation Function

Let σ indicate time and f indicate frequency and consider, for example, the two deterministic finite-energy complex signals $s_i(\sigma)$ and $s_k(\sigma)$ which have a common central instant and whose respective spectra $S_i(f)$ and $S_k(f)$ have a common central frequency. The two-dimensional time/frequency correlation function of these two signals may be denoted by $\chi_{ik}(t, \nu)$ and defined as

$$\chi_{ik}(t, \nu) \triangleq \int_{-\infty}^{+\infty} s_i(\sigma)\ e^{j2\pi\nu\sigma}.s_k^*(\sigma-t)d\sigma \qquad (1.1a)$$

where t is the time-shift and ν is the frequency-shift between

the signal $s_i(\sigma)e^{j2\pi\nu\sigma}$ (which is a phase-shifted version of $s_i(\sigma)$) and the signal $s_k(\sigma-t)$ (which is a time-shifted version of $s_k(\sigma)$).

As expressed in (1.1a), $\chi_{ik}(t,\nu)$ can be seen as the temporal correlation function of $s_i(\sigma)e^{j2\pi\nu\sigma}$ and $s_k(\sigma)$. However, making use of either Parseval's relation (see Subsection A.5, Appendix A) or the convolution theorem of Fourier transforms shows that

$$\chi_{ik}(t,\nu) = \int_{-\infty}^{+\infty} S_i(f-\nu)S_k^*(f)e^{j2\pi ft}\,df \qquad (1.1b)$$

which indicates that $\chi_{ik}(t,\nu)$ can be seen as the frequency correlation function of $S_k^*(f)e^{j2\pi ft}$ and $S_i^*(f)$.

It can be seen that $\chi_{ik}(t,\nu)$ measures the similarity (and, hence, the mutual interference) between the two signals $s_i(\sigma)e^{j2\pi\nu\sigma}$ and $s_k(\sigma-t)$ for different t- and ν- values. In fact, it can be shown that the separation between the two points representing these two signals in the signal space to which they both belong decreases with $\mathrm{Re}[\chi_{ik}(t,\nu)]$. This separation is given by the square root of the energy of the difference between these two signals[72], i.e. by $\left[\int_{-\infty}^{+\infty} |s_i(\sigma)e^{j2\pi\nu\sigma} - s_k(\sigma-t)|^2 d\sigma\right]^{\frac{1}{2}}$. These facts obviously imply that the separability of two given signals through correlation predetection processing decreases as their mutual correlation increases, and vice versa.

If $s_i(\sigma)$ and $s_k(\sigma)$ are strictly confined to the respectiv σ- ranges $[\sigma_{i1}, \sigma_{i2}]$ and $[\sigma_{k1}, \sigma_{k2}]$, the integration limits in

(1.1a) will be given by

$$\text{Lower limit} = \text{the larger of } \sigma_{i1} \text{ and } t+\sigma_{k1} \qquad (1.2a)$$

$$\text{Upper limit} = \text{the smaller of } \sigma_{i2} \text{ and } t+\sigma_{k2} \qquad (1.2b)$$

which can be used in (1.1a) to show that $\chi_{ik}(t,\nu)$ vanishes in this case outside the t-range $[\sigma_{i1}-\sigma_{k2},\ \sigma_{i2}-\sigma_{k1}]$.

According to Fourier transform theory, a signal cannot be strictly limited in both the time-domain and the frequency-domain [72]. However, a physical signal has finite energy and will thus be effectively, if not strictly, limited in each domain. The effective signal spread in a given domain has no unique definition. Many essentially equivalent definitions have been proposed in this respect [70,72-77]. The choice of a particular definition depends on the specific case under consideration. In any case, the dual concentration of signal energy in both domains is constrained by the "waveform uncertainty principle", so called after the formally analogous relations of quantum mechanics [46,66,70,72-77]. This principle implies that the product of signal duration (i.e. uncertainty in time) and signal bandwidth (i.e. uncertainty in frequency) is at least of the order of unity and assumes its minimum value in the case of a constant frequency carrier with a Gaussian envelope.

The fact that a physical signal strictly limited in one domain is effectively limited in the dual domain implies that if the two signals $s_i(\sigma)$ and $s_k(\sigma)$ are strictly limited to the respective σ-ranges $[\sigma_{i1},\ \sigma_{i2}]$ and $[\sigma_{k1},\ \sigma_{k2}]$, the two spectra $S_i(f)$ and $S_k(f)$ may be assumed to be effectively limited to the respective f-ranges $(f_{i1},\ f_{i2})$ and $(f_{k1},\ f_{k2})$. In this case,

the effective integration limits in (1.1b) will be given by

$$\text{Lower limit} = \text{the larger of } f_{k1} \text{ and } f_{i1}+\nu \tag{1.3a}$$

$$\text{Upper limit} = \text{the smaller of } f_{k2} \text{ and } f_{i2}+\nu \tag{1.3b}$$

whereby $\chi_{ik}(t,\nu)$ will be effectively limited to the ν-range $(f_{k1}-f_{i2},\ f_{k2}-f_{i1})$.

Clearly, both (1.2) and (1.3) are also valid in the dual case where $s_i(\sigma)$ and $s_k(\sigma)$ are effectively limited to the respective σ-ranges $(\sigma_{i1}, \sigma_{i2})$ and $(\sigma_{k1}, \sigma_{k2})$ and the two spectra $S_i(f)$ and $S_k(f)$ are strictly limited to the respective f-ranges $[f_{i1}, f_{i2}]$ and $[f_{k1}, f_{k2}]$. In this case, however, $\chi_{ik}(t,\nu)$ will be effectively confined to the t-range $(\sigma_{i1}-\sigma_{k2}, \sigma_{i2}-\sigma_{k1})$ and strictly confined to the ν-range $[f_{k1}-f_{i2}, f_{k2}-f_{i1}]$.

It is sometimes more convenient to make use of some normalized form $\chi^n_{ik}(t,\nu)$ of $\chi_{ik}(t,\nu)$. Different normalization criteria are obviously possible in this respect. It is possible, for example, to define $\chi^n_{ik}(t,\nu)$ as

$$\chi^n_{ik}(t,\nu) \triangleq \frac{\chi_{ik}(t,\nu)}{2\sqrt{E_i E_k}} \tag{1.4a}$$

$$\text{or} \quad \chi^n_{ik}(t,\nu) \triangleq \frac{\chi_{ik}(t,\nu)}{2E_k} \tag{1.4b}$$

where $2E_i$ and $2E_k$ are the respective energies of $s_i(\sigma)$ and $s_k(\sigma)$.

It will be shown in Section 1.5 that $\chi_{ik}(t,\nu)$ of (1.1)

represents the response of the basic linear optimum signal predetection processor whose local reference is $s_k(\sigma)$ to an input signal $s_i(\sigma)e^{j2\pi\nu\sigma}$. This clearly implies that $\chi_{ik}(t,\nu)$ can accommodate a variety of important studies related to signal design, weighting techniques, distortion and intereference in such areas as communications, radar and sonar, where optimum signal predetection processing is used.

Both $\chi_{ik}(t,\nu)$ and $|\chi_{ik}(t,\nu)|$ are important in communication since the various coherent and noncoherent reception modes are possible in this case. In contrast, it is $|\chi_{ik}(t,\nu)|$ which is usually more important in radar and sonar where reception is usually incoherent. In fact, radar[46,52,66,70] and sonar[78] literature often describes $|\chi_{ik}(t,\nu)|$ (or $|\chi_{ik}(t,\nu)|^2$) as the ambiguity function in the case where $i=k$ and as the cross-ambiguity function in the case where $i\neq k$. This is with reference to the fact that $|\chi_{ii}(t,\nu)|$ can be used to study the ambiguity associated with the tracking of a single moving object and $|\chi_{ik}(t,\nu)|$ can be used to study the ambiguity associated with the resolution and simultaneous tracking of several moving objects.

1.3.2 Some Properties of the Correlation Function[11,46,64-72]

It follows from (1.1) by a simple change of variable that

$$\chi_{ik}(-t,-\nu) = e^{j2\pi\nu t} \chi^{*}_{ki}(t,\nu) \tag{1.5}$$

which summarizes the symmetry properties of the correlation function.

Schwarz inequality for two complex functions $f_1(x)$ and $f_2(x)$ may be expressed as [64,72]

$$\left|\int f_1(x) f_2^*(x)\,dx\right|^2 \leq \int |f_1(x)|^2 dx \cdot \int |f_2(x)|^2 dx \qquad (1.6)$$

where the equality holds when $f_1(x)$ and $f_2(x)$ are scalar multiples of each other.

Applying (1.6) to (1.1) shows that

$$|\chi_{ik}(t,\nu)|^2 \leq |\chi_{kk}(0,0)|^2 = [2E_k]^2 \qquad (1.7)$$

which indicates that $|\chi_{ik}(t,\nu)|$ assumes its peak at the origin in the t-ν plane, in the case where the two correlated signals are identical.

It follows from the so-called self-reciprocal property of $|\chi_{ik}(t,\nu)|^2$ in the two-dimensional Fourier transform that[46,66]

$$\int\int_{-\infty}^{+\infty} |\chi_{ik}(t,\nu)|^2 dt d\nu = 2E_i \cdot 2E_k \qquad (1.8)$$

This relation expresses the invariance property (or the conservation principle) of the correlation volume between the surface $|\chi_{ik}(t,\nu)|^2$ and the t-ν plane in the sense that this volume is independent of signal form as long as signal energy remains unchanged. It implies that if signal energy is fixed, the suppression of this volume in a certain region in the t-ν plane (e.g. by proper choice of signal parameters) will lead to a corresponding spiking elsewhere in the plane.

In the special case where i=k, (1.8) is usually called the "generalized uncertainty principle of radar" , since it states that the total correlation volume (i.e. the total t-ν resolution capability) is the same for all signals having equal energies despite the fact that each signal may have its own correlation volume-distribution (i.e. its own t-ν resolution capability). In this same special case, (1.8) also indicates that the total correlation volume is fixed for the same signal. This result is often known as the "uncertainty principle of radar", since it implies that the overall t-ν resolution capability of a given signal is fixed. It can be seen that the radar uncertainty principle is closely related to the waveform uncertainty principle already mentioned in a previous paragraph.

It also follows from the self-reciprocal property of $|\chi_{ik}(t,\nu)|^2$ in the two-dimensional Fourier transform that

$$\int_{-\infty}^{+\infty} |\chi_{ik}(t,\nu)|^2 d\nu = \int_{-\infty}^{+\infty} \chi_{ii}^*(0,\nu)\chi_{kk}(0,\nu)e^{j2\pi\nu t}d\nu \qquad (1.9a)$$

$$\int_{-\infty}^{+\infty} |\chi_{ik}(t,\nu)|^2 dt = \int_{-\infty}^{+\infty} \chi_{ii}^*(t,0)\chi_{kk}(t,0)e^{-j2\pi\nu t}dt \qquad (1.9b)$$

The left-hand side of (1.9a) gives the area of a vertical cut through the correlation body parallel to the ν-axis for a particular t-setting. The right-hand side of (1.9a) is a Fourier transform of the product $\chi_{ii}^*(0,\nu)\chi_{kk}(0,\nu)$, where $\chi_{ii}(0,\nu)$ and $\chi_{kk}(0,\nu)$ are the frequency autocorrelation functions of $S_i(f)$ and $S_k(f)$ respectively. According to a relation which will be derived in Section 1.7, the width of the autocorrelation

function of a given signal in one domain is of the order of the reciprocal of the signal width in the dual domain. Thus, the widths of $\chi_{ii}(o,\nu)$ and $\chi_{kk}(O,\nu)$ are of the orders of the reciprocals of the durations of $s_i(\sigma)$ and $s_k(\sigma)$ respectively. Consequently, (1.9a) indicates that the area of a vertical cut through the correlation body parallel to the ν-axis for a particular t (and, hence, the volume of the elemental correlation body whose base is this area and whose height is dt) is determined by, and decreases with, $|t|$ and the longer of the two signal durations.

Similarly, the dual relation (1.9b) implies that the area of a vertical cut through the correlation body parallel to the t-axis for a particular ν (and, hence, the volume of the elemental correlation body whose base is this area and whose height is $d\nu$) is determined by, and decreases with, $|\nu|$ and the wider of the two signal bandwidths.

1.3.3 Correlation of Real Signals

The discussion above has been concerned with complex signals. It can be modified to accommodate the signals used in practice, namely, the real signals. To this end, use can be made of the theory of complex representation of real signals (see Appendix A).

Consider, for example, the ith and kth members of the real signal set

$$r_\ell(\sigma) \triangleq a_\ell(\sigma)\cos\left[\alpha_\ell+2\pi f_\ell\sigma+\xi_\ell(\sigma)\right] \qquad (1.10a)$$

where

$$\ell = 1, 2, 3, \ldots, i, \ldots, k, \ldots, N \tag{1.10b}$$

$$\nu \triangleq f_i - f_k \tag{1.10c}$$

$$\alpha \triangleq |\alpha_i - \alpha_k| \tag{1.10d}$$

The two-dimensional time/frequency correlation function of the two real signals $r_i(\sigma)$ and $r_k(\sigma)$ of (1.10) can be denoted by $\lambda_{ik}(t,\nu)$ and expressed as

$$\lambda_{ik}(t,\nu) = \int_{-\infty}^{+\infty} r_i(\sigma) r_k(\sigma - t)\, d\sigma \tag{1.11a}$$

or

$$\lambda_{ik}(t,\nu) = \int_{-\infty}^{+\infty} R_i(f) R_k^*(f) e^{j2\pi ft} df \tag{1.11b}$$

where $R_i(f)$ and $R_k(f)$ are the spectra of $r_i(\sigma)$ and $r_k(\sigma)$ respectively.

If the two complex signals $s_i(\sigma)e^{j2\pi\nu\sigma}$ and $s_k(\sigma)$ of (1.1) are the respective analytic complex representations of the two real signals $r_i(\sigma)$ and $r_k(\sigma)$, it is possible in this case to prove that (see relation (A.14), Appendix A)

$$\lambda_{ik}(t,\nu) = \frac{1}{2}\mathrm{Re}[\chi_{ik}(t,\nu)] \tag{1.12a}$$

$$\text{Envelope}\ [\lambda_{ik}(t,\nu)] = \frac{1}{2}|\chi_{ik}(t,\nu)| \tag{1.12b}$$

This relation becomes only approximate if $s_i(\sigma)e^{j2\pi\nu\sigma}$ and $s_k(\sigma)$ are the exponential complex representations of $r_i(\sigma)$ and $r_k(\sigma)$ unless $r_i(\sigma)$ and $r_k(\sigma)$ are bandpass signals whose bandwidths do not exceed $2f_i$ and $2f_k$ respectively (see Subsection A.4, Appendix A).

The normalised form of $\lambda_{ik}(t,\nu)$ may be defined as

$$\lambda^n_{ik}(t,\nu) \triangleq \frac{\lambda_{ik}(t,\nu)}{\sqrt{E_i E_k}} \tag{1.13a}$$

or

$$\lambda^n_{ik}(t,\nu) \triangleq \frac{\lambda_{ik}(t,\nu)}{E_k} \tag{1.13b}$$

where E_i and E_k are the energies of the two real signals $r_i(\sigma)$ and $r_k(\sigma)$ respectively.

Substituting for $\lambda_{ik}(t,\nu)$ from (1.12) in (1.13) and making use of (1.4) shows that

$$\lambda^n_{ik}(t,\nu) = \mathrm{Re}\left[\chi^n_{ik}(t,\nu)\right] \tag{1.14a}$$

$$\text{Envelope}\left[\lambda^n_{ik}(t,\nu)\right] = \left|\chi^n_{ik}(t,\nu)\right| \tag{1.14b}$$

which indicates that $\chi^n_{ik}(t,\nu)$ may be seen as the exponential complex representation of $\lambda^n_{ik}(t,\nu)$.

The importance of (1.12) and (1.14) stems from the fact that it is mathematically easier to handle complex rather than real functions. These two relations can be used to compute $\lambda_{ik}(t,\nu)$ or $\lambda^n_{ik}(t,\nu)$ and to establish their properties through $\chi_{ik}(t,\nu)$ and $\chi^n_{ik}(t,\nu)$ respectively.

1.3.4 Classification of Signal Sets According to Their Correlation Properties

The temporal correlation coefficient of the two real signals $r_i(\sigma)$ and $r_k(\sigma)$ may be taken as $\lambda_{ik}^n(0,\nu)$. Making use of (1.13), (1.11) and (1.6) shows that

$$-1 \leq \lambda_{ik}^n(0,\nu) \leq 1 \tag{1.15}$$

It can be seen from (1.11) and (1.13) that the equalities to 1 and -1 in (1.15) may correspond, respectively, to the two cases where $r_i(\sigma)$ and $r_k(\sigma)$ are identical and antipodal (i.e. equal but of opposite signs and thus lie at the antipodes of the same sphere in the signal space).

$r_i(\sigma)$ and $r_k(\sigma)$ are said to be strictly orthogonal if

$$\lambda_{ik}^n(0,\nu) = 0, \quad i \neq k \tag{1.16a}$$

However, strict orthogonality cannot be achieved in practice due to the fact that a signal cannot be both duration-limited and band-limited [72-77]. Accordingly, (1.16a) is usually replaced by the following more relaxed and realistic definition of orthogonality

$$|\lambda_{ik}^n(0,\nu)| \leq \varepsilon_{max}, \quad i \neq k \tag{1.16b}$$

where ε_{max} is an arbitrarily small positive quantity.

The correlation matrix of the signal set of (1.10) may be defined as the matrix $[\lambda_{ik}^n(0,\nu)]$, $i,k = 1,2,3,\ldots,N$. This

matrix has a total of N^2 elements, namely, N diagonal and N(N-1) off-diagonal elements. Making use of (1.15) and the fact that practical signals are physical signals shows that the total sum $\sum_{i,k=1}^{N} \lambda_{ik}^{n}(0,\nu)$ of the matrix elements satisfies the relation [42]

$$0 \leq \sum_{i,k=1}^{N} \lambda_{ik}^{n}(0,\nu) \leq N^2 \qquad (1.17a)$$

This relation and the fact that the sum $\sum_{i=k=1}^{N} \lambda_{ik}^{n}(0,\nu)$ of the diagonal matrix elements is always equal to N show that the sum $\sum_{\substack{i,k=1 \\ i\neq k}}^{N} \lambda_{ik}^{n}(0,\nu)$ of the off-diagonal matrix elements satisfies the relation

$$-N \leq \sum_{\substack{i,k=1 \\ i\neq k}}^{N} \lambda_{ik}^{n}(0,\nu) \leq N(N-1) \qquad (1.17b)$$

The case where the sum of the off-diagonal elements vanishes corresponds to an orthogonal signal set for which $\lambda_{ik}^{n}(0,\nu) = 1$, $i=k$, and $\lambda_{ik}^{n}(0,\nu) = 0$, $i\neq k$.

The upper bound in (1.17) corresponds to a signal set which consists of N identical signals for which $\lambda_{ik}^{n}(0,\nu) = 1$.

The lower bound in (1.17) may correspond to the case where the off-diagonal elements are equal in such a way that $\lambda_{ik}^{n}(0,\nu) = -\frac{1}{N-1}$, $i\neq k$ [21]. Here the signal set is usually known as the regular-simplex or transorthogonal set if it consists of signals having equal energies [10,21,40]. Such a set reduces to an antipodal pair if N=2 and to an orthogonal set if $N\to\infty$. The

regular-simplex set is like the orthogonal set in that each is a special case of the so-called equicorrelated set[10,21,40] for which $\lambda_{ik}^{n}(0,\nu) = \lambda$, $i \neq k$, where λ is a constant satisfying the relation

$$-\frac{1}{N-1} \leq \lambda \leq 1 \tag{1.18}$$

The lower bound in (1.17) may also correspond to the case where the off-diagonal elements of the correlation matrix are unequal but have the average value $-\frac{1}{N-1}$[21]. Here the signal set is usually known as the biorthogonal set if it consists of an even number of signals which have equal energies and can be ordered into $\frac{N}{2}$ antipodal pairs in addition to $\frac{N}{2}(N-2)$ orthogonal pairs[21,40,42].

1.4 Signal Design [10,11,21,31-42]

This section outlines the signal design problem for the purely AWGN case on the assumption that the demodulator is of the optimum predetection/detection type. The results obtained in this respect will be used in Chapter 3 in studying the design of chirp signal sets for data transmission.

1.4.1 Introduction

The signal design problem was introduced in Section 1.2 as the problem of selecting the modulator signal set parameters in such a way as to minimize the demodulator error probability P_e. Assuming that the demodulator is of the optimum predetection/detection type and that the signal set of (1.10) is the modulator

signal set, the formulation of this problem may be based either on $\lambda_{ik}(0,\nu)$ or on $\lambda_{ik}(t,\nu)$ as defined in (1.11) and (1.12).

The approach in which signal design is based on $\lambda_{ik}(0,\nu)$ is the conventional detection theoretical approach which assumes that the optimum demodulator decides on the received signals by first computing (in predetection), and then applying a specific decision rule (in detection) to, quantities based on the elements of the matrix $[\lambda_{ik}(0,\nu)]_{i,k=1}^{N}$ (coherent case) or on their in-phase and quadrature components (noncoherent case). This idealized demodulator model requires practically unachievable ideal elements such as precise synchronization networks, infinitely narrow sampling gates,etc. It generally results in P_e-values that are lower than those usually obtained in practice.

The approach in which signal design is based on $\lambda_{ik}(t,\nu)$ is more realistic since it can accommodate the unavoidable system imperfections. However, this approach may lead to considerable mathematical complications that are difficult to handle, even if use is made of modern computing techniques.

The direct solution of the signal design problem as a problem of optimising P_e as a function of the modulator signal set parameters is generally difficult. This explains why signal design is often done by intuition and adaptation making use of the results which have been accumulating over the years in this respect. These results may be classified into two main categories, namely, those which are based on $\lambda_{ik}(0,\nu)$ and those which are based on $\lambda_{ik}(t,\nu)$. The former category includes the

known detection theoretical results. The latter category may be viewed as complementing these detection theoretical results.

Detection theoretical results are related to uncoded and coded transmission of digital data, with or without feedback, through simple and multiple channels which are perturbed by AWGN and/or other types of disturbances. They consider the transmission of digital data by using signal sets that may consist of signals which have equal or different energies, a priori probabilities and mutual correlation coefficients[10,11,21,31-45,54-63].

Some detection theoretical results are given below. They are concerned with the relatively simple purely AWGN case where the carrier frequency is precisely known to the receiver and the modulator signal set consists of equipropable signals of equal energies. These results cover the coherent, the incoherent, the differentially coherent and the partially coherent reception modes already defined in Section (1.1). They indicate that the differences between these different reception modes tend to disappear as N increases. They also show the key role played by the correlation properties of the modulator signal set in determining P_e, and, hence, in determining the performance of this set. It will be seen that P_e increases with the mutual correlations of the signals belonging to the set, a fact which is intuitively true since the demodulator capability of separating signals decreases with their similarities (i.e. with their mutual correlations). Finally, these results also imply that the modem performance can never be made perfect in any physical situation (in such a way that $P_e=0$) and that there is no universally optimum modulator signal set which surpasses all

other sets under all circumstances.

1.4.2 Signal Design for Coherent Reception

Coherent reception corresponds to the case where the receiver knows precisely the carrier signal phase.

Consider the coherent reception, purely AWGN, case where members of the modulator signal set are given by (1.10) and are equiprobable, have the same energy E and are equicorrelated (i.e. $\lambda_{ik}^{n}(0,\nu) = \lambda$, $i \neq k, i,k = 1,2,3,\ldots,N$; λ is constant satisfying (1.18)). It can be shown in this case that[10,21,40,42]

$$P_e = 1 - \frac{1}{\sqrt{\pi}} \int_{-\infty}^{+\infty} e^{-x^2} \left[1 - \frac{1}{2}\operatorname{erfc}\left(x + \sqrt{E(1-\lambda)/N_o}\right)\right]^{N-1} dx \qquad (1.19)$$

In this relation, N_o is the one-sided noise spectral power density in Watt/Hz at the demodulator input and erfc(.) is the complementary error function defined by

$$\operatorname{erfc}(\cdot) \triangleq 1 - \operatorname{erf}(\cdot) \qquad (1.20)$$

where erf(.) is the tabulated error function which may be defined as[79]

$$\operatorname{erf}(x) \triangleq \frac{2}{\sqrt{\pi}} \int_{o}^{x} e^{-y^2} dy \qquad (1.21)$$

which implies that

$$\text{erf}(-x) = -\text{erf}(x) \tag{1.22a}$$

$$\text{erf}(x) \simeq 1 - \frac{e^{-x^2}}{\sqrt{\pi}x} \quad \text{for large } x \tag{1.22b}$$

$$\text{erf}(\infty) = 1 \tag{1.22c}$$

The right-hand side of (1.19) is usually evaluated by numerical methods. Plots of this result are available for the orthogonal set (λ=0) and can easily be applied to any other equicorrelated set such as the regular-simplex set ($\lambda = -\frac{1}{N-1}$)[21].

Relation (1.19) shows that P_e depends on the modulator signal set through the parameters N, λ and $\frac{E}{N_o}$ (the signal-to-noise ratio). N and λ are signal design parameters and $\frac{E}{N_o}$ is restricted by the usually limited transmitter power. It indicates that P_e is a decreasing function of N. Since erfc(x) is a monotonically decreasing function of x, relation (1.19) also indicates that P_e is an increasing function of λ and a decreasing function of $\frac{E}{N_o}$. These facts, together with (1.19) itself, can be used in the present case to compare two individually equicorrelated signal sets having the same size N and different correlation properties. Two possible approaches are possible in this respect:

(i) The two given sets are compared by comparing their respective P_e-values corresponding to the same $\frac{E}{N_o}$ value. This approach establishes the optimality of the regular-simplex set because this set has the minimum λ-value (i.e. $\frac{-1}{N-1}$) and, hence, has the lowest possible P_e-value.

(ii) The two given sets are compared by comparing their respective

$\frac{E}{N_o}$ -values corresponding to the same P_e-value. Again, this approach confirms the optimality of the regular-simplex set since this set requires the lowest $\frac{E}{N_o}$ -value to achieve a given P_e-value. This approach also shows that an N-signal arbitrary equicorrelated set of mutual correlation coefficient λ and signal-to-noise ratio $\frac{E}{N_o}$ has the same P_e-value as the N-signal orthogonal set which has $\frac{E(1-\lambda)}{N_o}$ as its signal-to-noise ratio[10,21,40].

Relation (1.19) can also be used to find bounds on P_e for any signal set . Consider, for example, the case of coherent communication in a purely AWGN background by making use of a signal set consisting of N equiprobable signals having the same energy E and different mutual correlation coefficients $\lambda_{ik}^{n}(0,\nu)$, $i\neq k$, which satisfy the relation $\lambda_{min} \leq \lambda_{ik}^{n}(0,\nu) \leq \lambda_{max}$. In this case, a lower bound on P_e can be obtained simply by substituting λ_{min} for λ in (1.19). Similarly, an upper bound on P_e can be obtained by substituting λ_{max} for λ in (1.19). In this manner, it can be shown that P_e for the orthogonal set is a lower bound on P_e for a quasi-orthogonal set for which $0 \leq \lambda_{ik}^{n}(0,\nu) \leq \varepsilon_{max}$, $i\neq k$ and ε_{max} is an arbitrarily small positive quantity. It can also be shown that P_e for the orthogonal set is a tight upper bound on P_e for the biorthogonal set for which $-1 \leq \lambda_{ik}^{n}(0,\nu) \leq 0$ where $i\neq k$ [21].

Relation (1.19) applies only to the simple case of an equicorrelated signal set. If the set becomes arbitrarily correlated, the problem becomes more involved. Only few

results are known in this respect. It has been shown, for example, that the orthogonal set becomes optimal between all admissible, arbitrarily correlated, sets as $N\to\infty$ with its P_e asymptotically approaching zero as $N\to\infty$ for rates up to channel capacity [21,40]. Balakrishnan[80] has shown that P_e is an increasing function of every single off-diagonal element of the correlation matrix. By making use of this fact and by expanding P_e into a Taylor's series in the vicinity of $\lambda_{ik}^{n}(0,\nu) = -\frac{1}{N-1}$, $i\neq k$, he proved that the regular-simplex set is locally optimal for all N and $\frac{E}{N_o}$ (i.e. arbitrary small variations in its correlation matrix lead to an increase in P_e) [10,21,40,80]. He also proved that if the globally optimal set is independent of $\frac{E}{N_o}$ over some $\frac{E}{N_o}$ -interval; it must be in regular-simplex form [10,80]. Ziv[81] proved that the regular-simplex set is asymptotically globally optimal as $\frac{E}{N_o}\to\infty$. The global optimality of the regular-simplex set for arbitrary $\frac{E}{N_o}$ has been proved only for N=2 (i.e. antipodal pair)[10,21,40], N=3[42] and N=4[82]. If the signals in the signal set are of arbitrary different energies and a priori probabilities in addition to being of arbitrary mutual correlations, the P_e- problem becomes formidably difficult.

The preceding discussion is based on the assumption that the signal set is not bandwidth-constrained. The case where this set is bandwidth-constrained may also be considered. It can be shown, for example, that the biorthogonal set is optimum in this case requiring a bandwidth which is only half that required by the orthogonal set [21,42] and corresponding to a P_e given by [40,83]

$$P_e = 1-\int_o^{\infty} \frac{1}{\sqrt{\pi N_o}} e^{-\frac{(x-\sqrt{E})^2}{N_o}} \left[\frac{1}{\sqrt{\pi N_o}} \int_{-x}^{x} e^{-\frac{y^2}{N_o}} dy\right]^{\frac{N}{2}-1} dx \quad (1.23)$$

which approaches P_e for the orthogonal set as both N and $\frac{E}{N_o}$ increase.

As can be seen from (1.19) and (1.23), the expressions for P_e are generally involved. Relatively simpler P_e-expressions may, however, be derived in some special cases. It can be shown, for example, that for an arbitrarily correlated set with large $\frac{E}{N_o}$, P_e can be expressed as[42]

$$P_e \approx \frac{1}{N} \sum_{i,k,i\neq k}^{N} \frac{e^{-E/N_o \cdot \delta_{ik}^2}}{2\delta_{ik}\sqrt{\pi E/N_o}} \quad (1.24a)$$

where

$$\delta_{ik} \triangleq \sqrt{\frac{1-\lambda_{ik}^n(0,\nu)}{1+\lambda_{ik}^n(0,\nu)}} \quad (1.24b)$$

which, in the case of the equicorrelated set, reduce to

$$P_e \approx \frac{1}{N} \sum_{i,k,i\neq k}^{N} \frac{e^{-E\delta^2/N_o}}{2\delta\sqrt{\pi E/N_o}} = \frac{e^{-\delta^2 E/N_o}}{2N\delta\sqrt{\pi E/N_o}} \quad (1.25a)$$

where

$$\delta \triangleq \sqrt{\frac{1-\lambda}{1+\lambda}} \quad (1.25b)$$

The preceding results can obviously be applied to the binary case where N=2. However, this approach may not be easy. Rather, the binary case is usually treated as an independent case. A variety of results can be obtained in this manner[10,21,40,42]. Consider, for example, the purely AWGN coherent case of binary transmission by making use of two equiprobable signals of the same energy E. It can be shown in this case that P_e is

given by[10,21,40,42]

$$P_e = \frac{1}{2}\,\mathrm{erfc}\left(\sqrt{\frac{E(1-\lambda)}{2N_o}}\right) \tag{1.26}$$

where λ is the mutual correlation coefficient of the two signals.

Since erfc(x) is a montonically decreasing function of x, (1.26) shows that the antipodal pair (λ=-1) is globally optimal in the present case, as stated above. Plots of (1.26) for the antipodal pair and the orthogonal pair (λ=0) are available in the literature[10,21,40].

1.4.3 Signal Design for Incoherent Reception

The precise knowledge of the carrier signal phase by the receiver is usually difficult to achieve in practice, due to the unavoidable system imperfections and channel instabilities. Moreover, the coherent receiver cannot be used in a case where it has no precise knowledge of the carrier signal phase since this may result in high error probabilities . Accordingly, noncoherent reception techniques must replace coherent techniques in any case where the carrier phase cannot be made precisely known to the receiver.

In order to make it possible to study the problem of signal design in the noncoherent modes of reception,where the carrier phase is not precisely known to the receiver, the dependence of the correlation properties of the modulator signal set on this phase must be determined. To this end, one can write

$$\lambda_{ik}^{n}(t,\nu) = \rho_{ik}(t,\nu)\cos\alpha - \hat{\rho}_{ik}(t,\nu)\sin\alpha \tag{1.27a}$$

where $\rho_{ik}(t,\nu)$ and $\hat{\rho}_{ik}(t,\nu)$ are two real quantities that may be described as the in-phase and quadrature components of $\lambda^n_{ik}(t,\nu)$ respectively and are given by

$$\rho_{ik}(t,\nu) = \left[\lambda^n_{ik}(t,\nu)\right]_{\alpha=0} = \mathrm{Re}\left[\chi^n_{ik}(t,\nu)\right]_{\alpha=0} \tag{1.27b}$$

$$\hat{\rho}_{ik}(t,\nu) = \left[\lambda^n_{ik}(t,\nu)\right]_{\alpha=3\pi/2} = \mathrm{Im}\left[\chi^n_{ik}(t,\nu)\right]_{\alpha=0} \tag{1.27c}$$

These relations can be obtained in either of the following two ways:

(i) One can substitute for $r_i(\sigma)$ and $r_k(\sigma)$ from (1.10) into (1.11a) making use of (1.13) and the fact that both $r_i(\sigma)$ and $r_k(\sigma)$ are assumed to be narrowband signals.

(ii) More conveniently, one can substitute for $\chi^n_{ik}(t,\nu)$ from (1.1a) and (1.4) into (1.14a) making use of the fact that $s_i(\sigma)e^{j2\pi\nu\sigma}$ and $s_k(\sigma)$ are the complex representations of $r_i(\sigma)$ and $r_k(\sigma)$ respectively.

Relations (1.27b) and (1.27c) imply that

$$\left[\chi^n_{ik}(t,\nu)\right]_{\alpha=0} = \rho_{ik}(t,\nu) + j\hat{\rho}_{ik}(t,\nu) \tag{1.27d}$$

which, on making use of (1.7) and (1.14), implies that

$$\left[\text{Envelope } \lambda^n_{ik}(t,\nu)\right]_{\alpha=0} = \left|\chi^n_{ik}(t,\nu)\right|_{\alpha=0} = \left[\rho^2_{ik}(t,\nu) + \hat{\rho}^2_{ik}(t,\nu)\right]^{\frac{1}{2}} \leq 1 \tag{1.27e}$$

The decomposition of $\lambda_{ik}^{n}(t,\nu)$ into in-phase and quadrature components leads to a corresponding decomposition of the correlation coefficient $\lambda_{ik}^{n}(0,\nu)$ and, hence, of the correlation matrix of the signal set under consideration . It is intuitively clear that such a decomposition will be reflected in the expressions of P_e in the noncoherent reception modes.

As developed in Section 1.3, signal classification was based on $\lambda_{ik}^{n}(0,\nu)$ which has been shown above to be a function of α. This approach may be convenient in the case of coherent reception where α is precisely known to the receiver, but cannot be so in the cases of noncoherent reception where the receiver has no precise knowledge of α. Signal classification in these noncoherent cases must be independent of α. To this end, signals may be classified according to their in-phase and quadrature correlations of (1.27). Thus [10,21]:

(i) Two signals are said to be identical if

$$\rho_{ik}(0,\nu) = 1 \tag{1.28a}$$

$$\hat{\rho}_{ik}(0,\nu) = 0 \tag{1.28b}$$

(ii) Two signals are said to be orthogonal if

$$\rho_{ik}(0,\nu) = 0 \quad , \quad i \neq k \tag{1.29a}$$

$$\hat{\rho}_{ik}(0,\nu) = 0 \quad , \quad i \neq k \tag{1.29b}$$

(iii) Two signals are said to be antipodal if

$$\rho_{ik}(0,\nu) = -1 \quad , \quad i \neq k \tag{1.30a}$$

$$\hat{\rho}_{ik}(0,\nu) = 0 \quad , \quad i \neq k \tag{1.30b}$$

This subsection considers the particular mode of incoherent reception. The other modes of noncoherent reception are considered in the following two subsections.

In the case of incoherent reception, where the receiver has neither precise nor estimated knowledge of the carrier phase, the received and reference signals may be taken respectively as the ith and kth members of the signal set (1.10). In this case, the receiver assumes that α remains essentially constant over the signal transmission interval and varies randomly under this constraint in such a way that it has a uniform probability density $p(\alpha)$ given by [10,11,21]

$$p(\alpha) = \frac{1}{2\pi} \quad , \qquad 0 \leq \alpha \leq 2\pi \tag{1.31}$$

The signal design problem for the incoherent case is considerably more difficult than that for the coherent case. Only limited results have been reported in this respect. Balakrishnan and Abrams[84] have considered the purely AWGN case where the modulator signal set of (1.10) consists of equiprobable, equi-energy but arbitrarily correlated signals. Nuttall[85] has considered the same problem under the constraint of equicorrelation. The present discussion considers this

problem only for the orthogonal set in the case where there is no bandwidth constraint [10,21,40,42].

It can be shown that between all admissible signal sets for incoherent reception, the orthogonal set satisfies the necessary conditions to be a local optimum in both $\rho_{ik}(0,0)$ and $\hat{\rho}_{ik}(0,0)$ for all $\frac{E}{N_o}$ [42]. It can also be shown that P_e for this set is given by [42,86,87]

$$P_e = 1 - \frac{1}{2\pi} \iint_{-\infty}^{+\infty} \left[1 - e^{-\frac{1}{2}(x^2+y^2)}\right]^{N-1} e^{-\frac{1}{2}\left[(x-\sqrt{\frac{2E}{N_o}})^2+y^2\right]} dxdy \tag{1.32}$$

This relation reduces to the two following forms for small $\frac{E}{N_o}$ and large $\frac{E}{N_o}$ respectively [21,40,42]

$$P_e \approx \frac{1}{N} e^{-\frac{E}{N_o}} \sum_{n=2}^{N} (-1)^n \binom{N}{n} e^{\frac{E}{nN_o}}, \quad \frac{E}{N_o} \text{ small} \tag{1.33a}$$

$$P_e \approx \frac{N-1}{2} e^{-\frac{E}{2N_o}}, \quad \frac{E}{N_o} \text{ large} \tag{1.33b}$$

These two relations coincide for the binary case where N=2. Plots of P_e as given in (1.33) are available [21,40].

The successive terms of the right-hand side of (1.33a) decrease with n and are of alternate signs. The first of these terms equals the right-hand side of (1.33b). This implies that P_e of (1.33b) is an upper bound on P_e for the orthogonal set for all $\frac{E}{N_o}$ in the incoherent case and, consequently, in the coherent case [21].

Use can be made of (1.19) and (1.33) to show that:

(i) The orthogonal set in the incoherent case requires more

transmitter power than the regular-simplex set in the coherent case in order to achieve the same P_e-value. However, this difference decreases with N [21,42].

(ii) For the orthogonal set, the difference between the two P_e-values in the coherent and incoherent cases decreases with N [21].

The preceding results obviously apply to the binary case where N=2. However, this case is usually treated as an independent case. Some of the known results in this respect include [10,11,21,34,40,42]:

(i) P_e for a pair consisting of two arbitrarily correlated signals increases with the sum $[\rho^2(0,\nu) + \hat{\rho}^2(0,\nu)]$ for all $\frac{E}{N_o}$ and is given by [21,88]

$$P_e = Q\left(\sqrt{\frac{E(1-\gamma)}{2N_o}}, \sqrt{\frac{E(1+\gamma)}{2N_o}}\right) - \frac{1}{2} I_o\left(\frac{E}{2N_o}\sqrt{\rho^2(0,\nu)+\hat{\rho}^2(0,\nu)}\right) e^{-\frac{E}{2N_o}} \tag{1.34}$$

where $\rho(0,\nu)$ and $\hat{\rho}(0,\nu)$ are, respectively, the in-phase and quadrature components of the correlation coefficient of the two signals under consideration and

$$\gamma \triangleq \sqrt{1 - [\rho^2(0,\nu) + \hat{\rho}^2(0,\nu)]} \tag{1.35}$$

, $Q(.,.)$ is the tabulated Marcum Q-function given by [89,90]

$$Q(x_1,x_2) \triangleq \int_{x_2}^{\infty} y I_o(x_1 y) e^{-\frac{(y^2+x_1^2)}{2}} dy \tag{1.36}$$

, $I_o(.)$ is the modified Bessel function of the first kind and zeroth order given by

$$I_o(x) = \frac{1}{2\pi} \int_o^{2\pi} e^{x\cos y} dy \qquad (1.37a)$$

$$\approx 1 + \frac{x^2}{4}, \quad x \to 0 \qquad (1.37b)$$

$$\approx \frac{e^x}{(2\pi x)^{\frac{1}{2}}}, \quad x \to \infty \qquad (1.37c)$$

from which it is clear that $I_o(x)$ is a monotonically increasing function for positive x.

(ii) The orthogonal pair is globally optimal for all $\frac{E}{N_o}$[42] with P_e given by[10,21]

$$P_e \approx \frac{1}{2} e^{-\frac{E}{2N_o}} \qquad (1.38)$$

which can also be obtained from (1.33).

Plots of (1.38) are available[10,21,42]. The orthogonal pair for the incoherent case can be compared with the antipodal and orthogonal pairs for the coherent case. This can be done by comparing (1.26) and (1.38) making use of (1.20) and (1.22) . It can be seen from such a comparison that the degree of phase coherence is of no great practical significance in the case of the orthogonal pair[21].

(iii) P_e for an antipodal pair consisting of two equiprobable signals of equal energies is given by[21]

$$P_e = \frac{1}{2} \quad \text{for all} \quad \frac{E}{N_o} \qquad (1.39)$$

which shows that there is no use in the antipodal pair for incoherent reception.

1.4.4 Signal Design for Differentially Coherent Reception[7,21]

In Phase-Shift Keying (PSK), digital information is transmitted in the form of a number of discretely phase-shifted versions of a suitable signal. Both Coherent PSK (CPSK) and Differentially coherent PSK (DPSK) are possible in this respect. The digits are encoded in the consecutive absolute phases of the transmitted pulses in CPSK and in the consecutive phase-differences of these pulses in DPSK. CPSK requires system and channel stability and an absolute phase reference in the receiver. CPSK system performance can be found according to subsection 1.4.4. DPSK tolerates some instability and assumes that the receiver can estimate the consecutive phase-differences.

Consider, for example, the case of binary DPSK[21] where the modulator makes use of the two real signals $r(\sigma)$ and $-r(\sigma)$. A reference $r(\sigma)$, say, is first transmitted. This reference is followed by $r(\sigma)$ itself if a 'space' is to be transmitted and by $-r(\sigma)$ if a 'mark' is to be transmitted. Thus, a space dictates no phase-change and a mark dictates a phase-change of 180^{o}. The receiver bases its decisions on the last two received signals which can be mathematically treated as a single composite signal. There are two such composite signals. These two signals are orthogonal. The receiver assumes that the absolute phase of the composite signal varies randomly with a probability density given by (1.31). Thus, the binary DPSK case reduces to a binary phase-incoherent case with a signal pair consisting of two equiprobable orthogonal signals having the same energy 2E.

This and (1.38) show that P_e for binary DPSK is given by

$$P_e \simeq \frac{1}{2} e^{-E/N_o} \tag{1.40}$$

Comparing this relation with (1.38) shows that the binary DPSK system can achieve the same P_e-value as the corresponding incoherent orthogonal binary system at exactly half the energy required by the latter. Relation (1.40) can also be compared with (1.26), making use of (1.22b), to show that binary DPSK is slightly inferior to the corresponding coherent binary CPSK.

1.4.5 Signal Design for Partially Coherent Reception

In the partially coherent mode[21], a phase estimate is made available to the receiver in the form of the output of a phase-locked loop used for tracking some unmodulated auxiliary carrier transmitted along with the data signal. The receiver assumes that α remains essentially constant over the signal duration and varies randomly under this constraint with a stationary probability density $p(\alpha)$ that may be expressed as

$$p(\alpha) = \frac{e^{\beta \cos \alpha}}{2\pi I_o(\beta)}, \quad 0 \leq \alpha \leq 2\pi \tag{1.41}$$

where β is a measure of the signal-to-noise ratio in the loop bandwidth defined by

$$\beta \triangleq \frac{\text{average signal power}}{N_o \times \text{loop bandwidth}} \tag{1.42}$$

and where $I_o(.)$ is the Bessel function given by (1.37).

Making use of (1.37c) in (1.41) and expanding cos α in a Taylor's series in the vicinity of $\alpha=0$ shows that

$$\lim_{\beta\to\infty} p(\alpha) = \delta(\alpha) \tag{1.43a}$$

which implies that the probability that $\alpha=0$ is one in this limiting case. Thus, partially coherent reception reduces to coherent reception as $\beta\to\infty$.

Again, making use of (1.37b) in (1.41) shows that

$$\lim_{\beta\to 0} p(\alpha) = \frac{1}{2\pi}, \qquad 0 \leq \alpha \leq 2\pi \tag{1.43b}$$

which coincides with (1.31) showing that partially coherent reception reduces to incoherent reception as $\beta\to 0$.

Relations (1.43a) and (1.43b) imply that the partially coherent case is the general case which includes both cases of coherent and incoherent reception as two special cases. Signal design for partial coherence is extremely difficult to handle. The only known results in this respect are mainly confined to the purely AWGN binary case where there is no bandwidth constraint and the signal pair consists of two equiprobable signals of equal energies which may be arbitrarily correlated [21,91,92]. Some of these results are given below:

(i) P_e can generally be expressed as

$$P_e = \int_0^{2\pi} p(\alpha) P_e(\alpha) d\alpha \tag{1.44}$$

where $p(\alpha)$ is given by (1.41) and $P_e(\alpha)$ is the conditional

error probability given α.

Relation (1.44) shows that P_e is obtained in the present case by averaging $P_e(\alpha)$ with respect to α. This is usually done by finding $P_e(\alpha)$, substituting it in (1.44) and integrating numerically.

(ii) For the antipodal pair, it can be shown that $P_e(\alpha)$ takes the form

$$P_e(\alpha) = \frac{1}{2} \operatorname{erfc}(\sqrt{E/N_o} \cos\alpha) \tag{1.45}$$

which, along with (1.41), can be used in (1.44) to show that P_e for the antipodal pair in the partially coherent case is given by

$$P_e = \frac{1}{2} \int_o^{2\pi} \frac{e^{\beta\cos\alpha}}{2\pi I_o(\beta)} \operatorname{erfc}(\sqrt{E/N_o}\cos\alpha)\, d\alpha \tag{1.46}$$

This relation gives P_e for the antipodal pair in the coherent case (where $\beta\to\infty$) as it is given by (1.26), i.e.

$$P_e = \frac{1}{2} \operatorname{erfc}(\sqrt{E/N_o}) \tag{1.47}$$

Relation (1.46) also gives P_e for the antipodal pair in the incoherent case (where $\beta\to 0$) as it is given by (1.39).

(iii) For the orthogonal pair, it can be shown that $P_e(\alpha)$ is given by

$$P_e(\alpha) = Q\left(\frac{\delta_2}{\sqrt{2}}, \frac{\delta_1}{\sqrt{2}}\right) - \frac{1}{2} I_o\left(\frac{\delta_1\delta_2}{2}\right) e^{-\frac{\delta_1^2+\delta_2^2}{4}} \tag{1.48}$$

where the Q-function $Q(.,.)$ is given by (1.36), the

Bessel function $I_o(.)$ is given by (1.37) and

$$\delta_1 \triangleq \sqrt{\frac{\beta^2+(2E/N_o)^2 + 4\beta(E/N_o)\cos\alpha}{2E/N_o}} \tag{1.49a}$$

$$\delta_2 \triangleq \frac{\beta}{\sqrt{2E/N_o}} \tag{1.49b}$$

Relations (1.48) and (1.41) can be used in (1.44) to show that P_e for the orthogonal pair in the partially coherent case is given by

$$P_e = \int_o^{2\pi} \frac{e^{\beta\cos\alpha}}{2\pi I_o(\beta)} \left[Q\left(\frac{\delta_2}{\sqrt{2}},\frac{\delta_1}{\sqrt{2}}\right) - \frac{1}{2} I_o\left(\frac{\delta_1\delta_2}{2}\right) e^{-\frac{\delta_1^2+\delta_2^2}{4}}\right] d\alpha \tag{1.50}$$

This relation gives P_e for the orthogonal pair in the coherent case (where $\beta\to\infty$) as it is given by (1.26), i.e.

$$P_e = \frac{1}{2}\,\mathrm{erfc}\left(\sqrt{E/2N_o}\right) \tag{1.51}$$

Relation (1.50) also gives P_e for the orthogonal pair in the incoherent case (where $\beta\to 0$) as it is given by (1.38).

(iv) For the arbitrarily correlated pair, it can be shown that $P_e(\alpha)$ and P_e take the same forms expressed in (1.48) and (1.50) respectively but with δ_1 and δ_2 now given by

$$\delta_\ell \triangleq +\sqrt{a_\ell^2+b_\ell^2+2a_\ell b_\ell\cos(\alpha-\eta_\ell)}\,, \qquad \ell=1,2 \tag{1.52a}$$

$$a_\ell \triangleq \frac{\beta}{\gamma}\sqrt{\frac{1-\rho(o,\nu)}{2E/N_o}}\,, \quad \ell=1,2 \tag{1.52b}$$

$$b_1 \triangleq +\sqrt{(1+\gamma)E/N_o} \tag{1.52c}$$

$$b_2 \triangleq -\sqrt{(1-\gamma)E/N_o} \tag{1.52d}$$

$$\eta_1 \triangleq \tan^{-1} \frac{\hat{\rho}(0,\nu)}{1+\gamma-\rho(0,\nu)} \tag{1.52e}$$

$$\eta_2 \triangleq \tan^{-1} \frac{\hat{\rho}(0,\nu)}{1-\gamma-\rho(0,\nu)} \tag{1.52f}$$

where γ is as defined by (1.35) and $\rho(0,\nu)$ and $\hat{\rho}(0,\nu)$ are, respectively, the in-phase and quadrature components of the correlation coefficient of the two signals under consideration.

It can be shown that the expression for P_e in the present case reduces exactly to (1.26) in the case of coherent reception and to (1.34) in the case of incoherent reception. This expression can also be shown to be an even function of $\hat{\rho}(0,\nu)$ and to have an absolute minimum at $\hat{\rho}(0,\nu) = 0$ for all $\rho(0,\nu), \beta, \alpha$ and E/N_o. Moreover, corresponding to this minimum, the following conclusions may be obtained.

a) From a practical viewpoint, the case where $\beta \leq \beta_1 \tilde{} 2$ may roughly be considered as an incoherent case. On the other hand, the case where $\beta \geq \beta_2 \tilde{} 8$ can roughly be considered as a coherent case. That is, the partially coherent case may be considered to correspond to the β-range (β_1, β_2).

b) For $\beta < \beta_1$, the orthogonal pair is optimum for all E/N_o and excels over any other pair (including the antipodal pair) for which $\rho(0,\nu) < 0$. For $\beta > \beta_2$, the antipodal pair is optimum for all E/N_o and excels over any other pair (including the orthogonal pair) for which $\rho(0,0) > -1$. This confirms two previous results.

No results are available for the general N'ary partially coherent case. However, it can be seen from the previous discussion that the difference between P_e for the N'ary coherent case and P_e for the N'ary incoherent case becomes practically negligible as N increases. This obviously implies that for relatively large N, the partially coherent mode is practically the same as both the coherent and incoherent modes which coincide in this case.

1.5 The Basic Optimum Predetection Processor[5,39,46,70,72]

This section introduces the two possible forms of the basic optimum predetection processor, namely, the multiplier-integrator compound (i.e. the correlator)and the matched filter-sampler compound. It also introduces spectrum processing as the dual of signal processing. The discussion is given from the viewpoint of analogue processing. It can be extended to the case of discrete processing[93].

1.5.1 The Correlator

The correlator is shown in Fig.1.3 where it can be seen to compute the value of the correlation function $\chi_{ik}(t,\nu)$ of the complex input signal $s_i(\sigma)e^{j2\pi\nu\sigma}$ and local reference $s_k(\sigma)$ for different t-settings. It acts as the optimum predetection processor of the input signal, in a purely AWGN background, in the case where i=k and $t=\nu=0$. Its response in this case is $\chi_{ii}(0,0)$, which is the value of the temporal autocorrelation

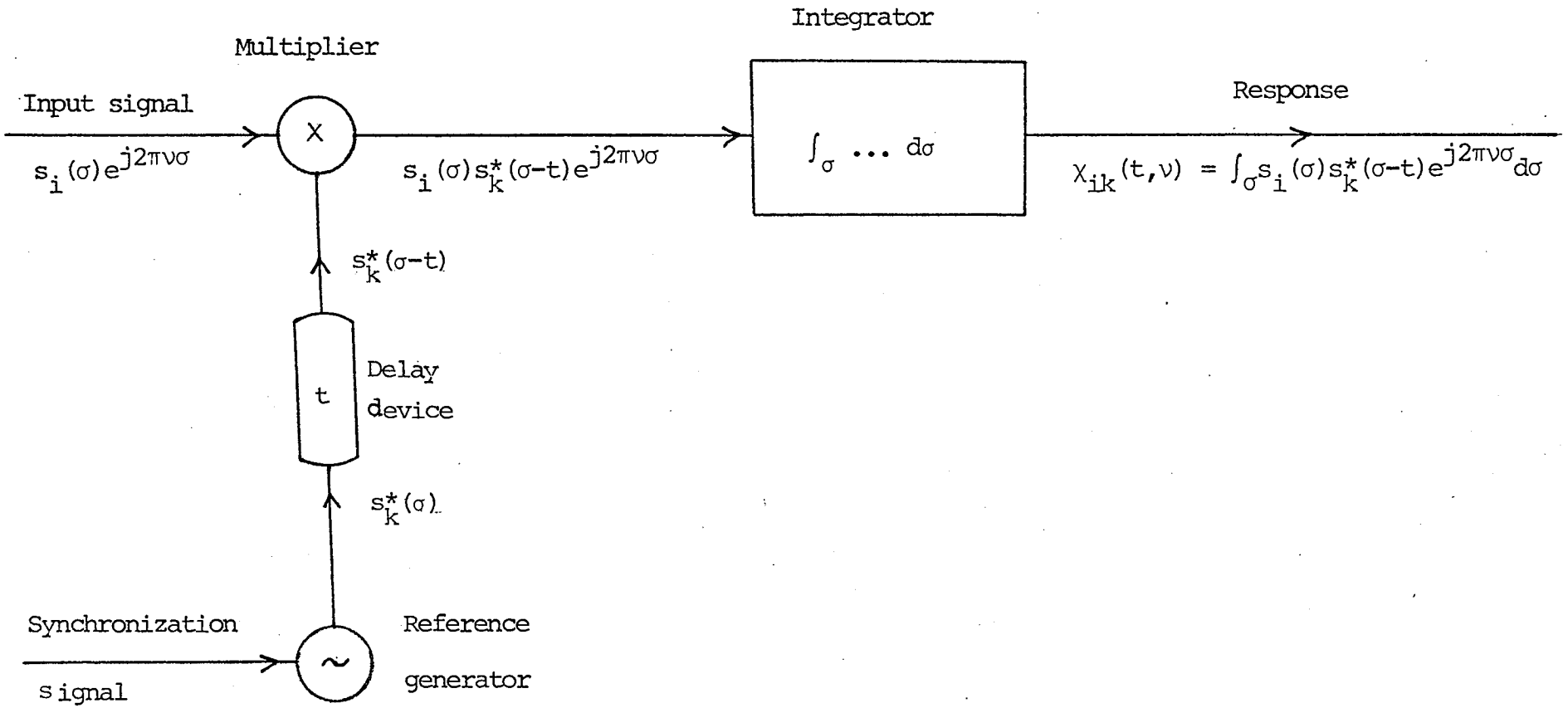

Fig. 1.3 The Basic Correlator

function $\chi_{ii}(t,0)$ of the input signal at t=0.

The correlator is relatively simple and flexible.Transition from one input signal to another is done by generating the right local reference which may be available in recorded form. However, the correlator has a major drawback. The absence of perfect synchronization between the input and reference signals may lead to a serious degradation in its response.

The correlator is frequently replaced by a matched filter-sampler compound. This is despite the fact that the matched filter is generally difficult to realize and is not flexible. It can only be matched to a single waveform and may have to be substantially changed in order to become matched to a different waveform.

1.5.2 The Matched Filter

The matched filter is a linear time-invariant passive device. The impulse response $h(\sigma)$ of a filter matched to a complex signal $s_k(\sigma)$ is an amplified, time-reversed and delayed conjugate of $s_k(\sigma)$, i.e.

$$h(\sigma) \triangleq As_k^*(\tau-\sigma) \tag{1.53a}$$

where the real constants A and τ represent the filter gain factor and the filter delay respectively.

Taking the Fourier transforms of both sides of (1.53a) shows that the transfer function H(f) of the matched filter is given by

$$H(f) = A\, e^{-j2\pi f\tau} S_k^*(f) \tag{1.53b}$$

where $S_k(f)$ is the spectrum of $s_k(\sigma)$.

A and τ are determined by the physical and practical realizability constraints and can be ignored in an essentially theoretical analysis. Thus, one can put A=1 and τ=0 whereby (1.53) reduces to

$$h(\sigma) = s_k^*(-\sigma) \tag{1.54a}$$

$$H(f) = S_k^*(f) \tag{1.54b}$$

Since the matched filter is a linear time-invariant device, the response of the matched filter of (1.54) to a complex input signal $s_i(\sigma)e^{j2\pi\nu\sigma}$ can be obtained either by convolving this signal and $h(\sigma)$ or by multiplying the spectrum of this signal and $H(f)$. This implies that the matched filter response in this case is given by $\chi_{ik}(t,\nu)$ of (1.1). That is, the matched filter processes the input signal in real time in such a way as to give the entire correlation function of this signal and the signal to which it is matched (which can be seen as a local reference stored in the filter structure). This implies that the matched filter is equivalent to a bank of correlators all of which have the same reference signal $s_k(\sigma)$ and each of which has its own t-setting. The output of one of these correlators with the delay-setting t_ℓ, say, corresponds to the output of the matched filter at the instant $t=t_\ell$, i.e. it will be given by $\chi_{ik}(t_\ell,\nu)$ (see Fig. 1.4).

The matched filter-sampler compound is shown in Fig. 1.5. In a purely AWGN background, this compound acts as the optimum

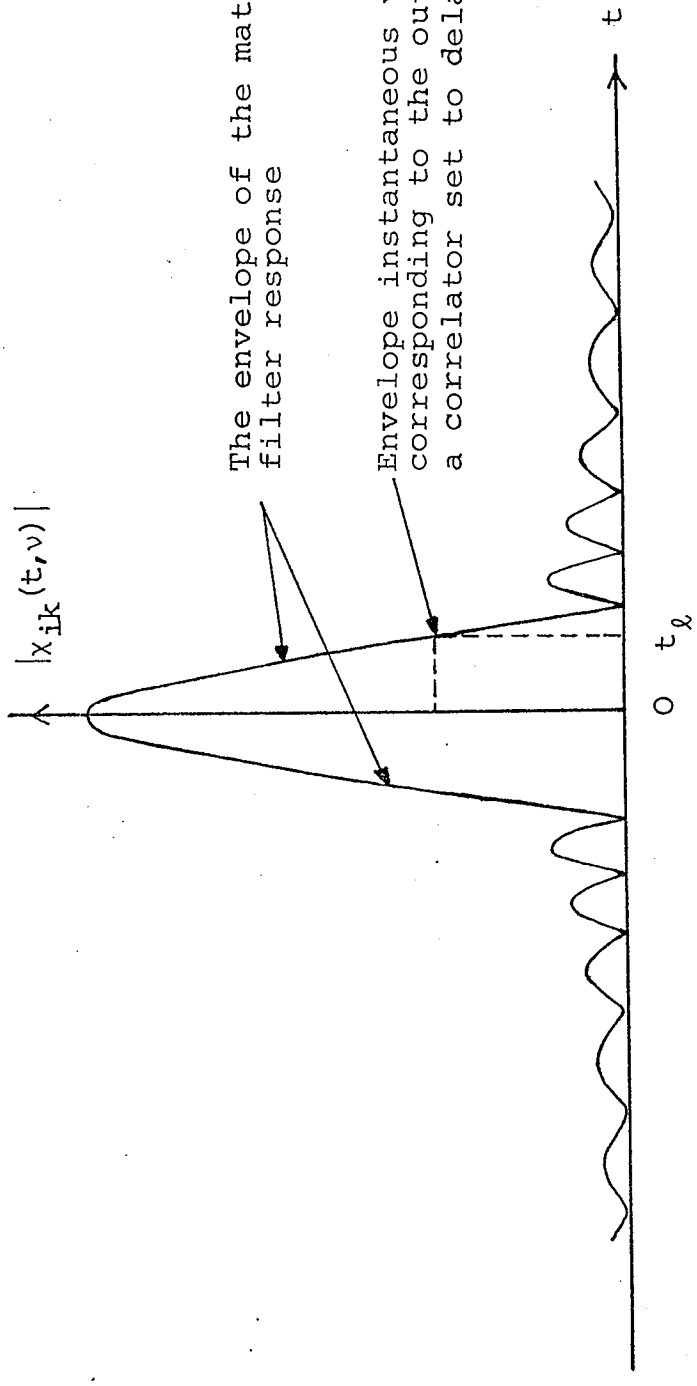

Fig. 1.4 Comparison of the Matched Filter and Correlator Responses

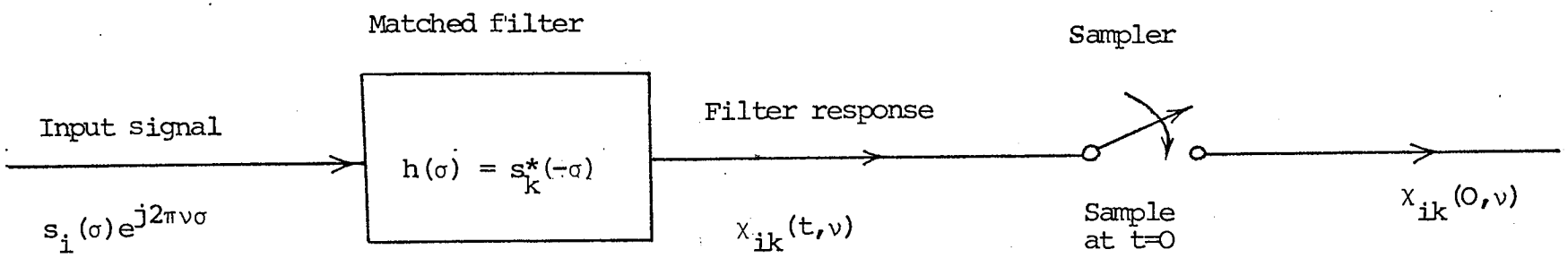

Fig. 1.5 The Matched Filter-Sampler Compound

predetection processor of the input signal in the case of matched reception where i=k and ν=0. All other cases correspond to unmatched reception.

1.5.3 The Matched Filter-Sampler Compound As A Basic Optimum Processor[39,46,49,70]

It is enough to establish the optimality of the matched filter-sampler compound as a basic optimum predetection processor since this will imply the optimality of the correlator in this respect. To this end, use can be made of the SNR-criterion (see Section 1.2) which defines the optimum predetection processor as one which maximizes SNR_o at one instant in time. Accordingly, SNR_o for an arbitrary system used as a predetection processor may be defined as

$$SNR_o \triangleq \frac{\text{peak instantaneous output signal power}}{\text{mean output noise power}} \tag{1.55}$$

This definition restricts the use of SNR_o as a definitive performance measure only to the case where the systems to be compared process the input in the same manner. Such systems may belong, for example, to the class of linear systems (filters). Thus, SNR_o as defined in (1.55) cannot be expected to be definitive, and may be misleading, if used to compare the performance of unlike systems.

Consider an arbitrary linear system (filter) whose transfer function is H(f). Let the input to this system be a complex signal $s(\sigma)$ of spectrum S(f). The filter response in this case is $\int_{-\infty}^{+\infty} S(f)H(f)e^{j2\pi ft}df$. If the peak of this response occurs at

$t=\tau$, one has

$$\text{Peak instantaneous output signal power} = \left| \int_{-\infty}^{+\infty} S(f)H(f)e^{j2\pi f\tau} df \right|^2 \tag{1.56}$$

Assuming a purely AWGN backgound, the mean noise power at the filter output will be given by[11]

$$\text{Mean output noise power} = \frac{N_o}{2} \int_{-\infty}^{+\infty} |H(f)|^2 df \tag{1.57}$$

where N_o is the single-sided noise spectral power density at the filter input in Watt/Hz.

Substituting from (1.56) and (1.57) in (1.55) gives SNR_o for the assumed arbitrary filter in a purely AWGN background as

$$SNR_o = \frac{\left| \int_{-\infty}^{+\infty} S(f)H(f)e^{j2\pi f\tau} df \right|^2}{\frac{N_o}{2} \int_{-\infty}^{+\infty} |H(f)|^2 df} \tag{1.58}$$

Applying Schwarz inequality of (1.6) to the numerator in (1.58) shows that the maximum SNR_o-value for any linear system (filter) in a purely AWGN background is given by

$$[SNR_o]_{max} = \frac{\int_{-\infty}^{+\infty} |S(f)|^2 df \cdot \int_{-\infty}^{+\infty} |H(f)|^2 df}{\frac{N_o}{2} \int_{-\infty}^{+\infty} |H(f)|^2 df} = \frac{2 \times \text{input signal energy}}{N_o} \tag{1.59}$$

which can also be obtained from (1.58) by substituting

$$H(f) = A\, S^*(f)\, e^{-j2\pi f\tau} \tag{1.60}$$

This last relation checks with (1.53b) and, thus, indicates

that the only filter which can achieve $[SNR_o]_{max}$ in a purely AWGN background is the matched filter (in the case where this filter and its input signal are in perfect match). That is, the matched filter is optimum in this respect.

Consider the purely AWGN case where the matched filter is in perfect match with its input signal and let it be followed by a sampler which samples its output at the instant of peak instantaneous output-signal power. In this case, the signal-to-noise ratio at the output of the matched filter-sampler compound is given by $[SNR_o]_{max}$. This indicates that in the purely AWGN case, where no other types of disturbances are present, a predetection processor in the form of a matched filter-sampler compound is optimum from the viewpoint of maximizing SNR_o and, hence, from the viewpoint of minimizing P_e, which is determined only by SNR_o in this case.

The conclusion that the matched filter-sampler compound is optimum in combating AWGN according to the signal-to-noise ratio criterion shows that this criterion confirms the detection theoretical result (obtained according to the statistical optimization criteria) that this compound is the optimum predetection processor for a purely AWGN coherent on/off communication system. No such definite confirmation is possible in the case of a purely AWGN noncoherent on/off communication system.[93] In this case, the statistical optimization criteria indicate that the square-envelope correlator and the matched filter envelope-detector-sampler compound are equivalent forms of the optimum predetection processor at a time when the signal-to-noise ratio criterion implies that the latter is

superior to the former in this respect. In fact, the signal-to-noise ratio criterion indicates that the SNR_o of the matched filter-envelope detector-sampler compound is roughly the same as $[SNR_o]_{max}$ (especially for large SNR_o-values) and that SNR_o of the square-envelope correlator is $\frac{1}{4}[SNR_o]_{max}$[93]. These results show how misleading the signal-to-noise ratio criterion may be if used to compare structurally unlike systems.

1.5.4 Spectrum Processing[70]

The discussion above has been concerned with the processing of signals as functions of time. Obviously, this discussion can be extended to the processing of signal spectra by making use of the Fourier time-frequency duality relations in this respect. It is possible, for example, to define the dual of the matched filter of (1.54) as a processor whose frequency impulse response $H_d(f)$ and temporal transfer function $h_d(\sigma)$ are given by

$$H_d(f) = S_k^*(-f) \tag{1.61a}$$

$$h_d(\sigma) = s_k^*(\sigma) \tag{1.61b}$$

Obviously, this processor is simply a multiplier whose local refernce is $s_k(\sigma)$. The spectrum of the response of this multiplier can be found either by convolving the input spectrum and $H_d(f)$ or by taking the Fourier transform of the product of the input signal and $h_d(\sigma)$.

1.6 Practicability of Optimum Processing

The matched filter-sampler compound is the form of the basic optimum predetection processor generally adopted in the present work. However, matched filtering cannot be judged only on theoretical grounds. Practical problems also have to be taken into consideration in this respect. This section considers, for example, the two problems of matched filter realization and distortion. Some other problems will be considered in Chapter 2. Knowing such problems is essential for a better understanding of the implications of some investigations in the following Chapters.

1.6.1 Matched Filter Realization [39,46,93-103]

It is a well known fact that a signal of duration T and bandwidth F has 2FT degrees of freedom and can uniquely be represented by any 2FT linearly independent parameters related to its form[72]. Since such a signal defines its matched filter, as can be seen from (1.54), the realization of this filter generally requires the knowledge of 2FT linearly independent parameters. Thus, the duration-bandwidth product of a given signal is a measure of the complexity of its matched filter as well as its generator. This fact implies that it is generally not easy to handle large duration-bandwidth product signals which are becoming increasingly important in practice.

It can be seen from (1.53) that the realization of the matched filter requires the specification of its gain factor A and delay τ. 'A' is usually chosen in such a way as to achieve

a unity gain filter response[46]. The choice of τ is governed by the constraint of physical realizability which requires the matched filter to be causal and not anticipatory[39,72]. However, this constraint cannot be precisely satisfied by a filter matched to a strictly bandlimited signal (since this signal is theoretically of infinite duration) and does not need to hold in the case of a non-real-time optical or parametric matched filter[39].

The practical realization of matched filters is generally difficult and cannot be precise. Practical realization methods are well covered in the literature and investigations are still underway in this respect. They can be grouped into the two main categories of the mathematically equivalent time-domain and frequency-domain methods. The time-domain methods are based on correlating the received signal with a stored replica of the transmitted waveform and may make use of either analogue or discrete processing techniques. The frequency-domain methods make use of analogue or discrete processing techniques and are based on Fourier transforming the received signal, multiplying the resulting spectrum by a stored replica of the transmitted signal spectrum and Fourier transforming the resulting product in order to obtain the corresponding matched filter response. In these frequency-domain methods, it is obvious that Fourier transforms play only a book-keeping role.

The analogue time-domain processing techniques are based on the theory of analogue correlation and may be implemented in a variety of ways. The Surface Acoustic Wave (SAW) and the Charge-Coupled Devices (CCD) technologies and the Optical methods are

of particular interest in this respect. SAW devices operate at bandpass frequencies and can be used for both the time-domain and the frequency-domain analogue processing of signals whose duration-bandwidth products may be of the order of several hundred. Methods for interfacing the SAW technology with the silicon technology are currently being developed. CCD devices operate at baseband frequencies and belong to the silicon technology. Optical arrangements are relatively cheap, simple, light, flexible, reliable, have multichannel capability and can process signals whose duration-bandwidth products may be of the order of several thousand. However, optical structures are sensitive to vibration and are unsuited for real time because of the involved photographic film processing.

The discrete time-domain processing techniques are based on the theory of discrete correlation. They are either sampled-data techniques in the case where the received and reference signals are both in sampled form or digital techniques in the case where the signal samples are coded into corresponding digital words. These techniques produce matched filters which are generally of inferior performance compared to those realized by analogue time-domain techniques. However, improved performance in this respect can be achieved by making use of interpolation at the processor output or by resorting to nonlinear time-domain processing techniques[93].

The discrete frequency-domain processing techniques are based on the theory of the Discrete Fourier Transform (DFT). They became feasible only after the advent of the Fast Fourier Transform (FFT) algorithm by Cooley and Tukey[104] which made it

possible to reduce substantially the number of operations and, hence, the time required for DFT computations. The FFT algorithm can be implemented in the form of a pipeline structure in which the DFT operation is partitioned in such a way that it is performed by separate cascaded modules. Each module performs its part of the DFT operation and passes the result to the next module for further computation. In this method, input and output buffer stages are often required to control the flow of data in and out of the processor proper. However, this problem of data flow control can be obviated by making use of the self-adaptive floating-point FFT algorithms which usually imply more complexity and higher cost.

The adoption of one matched filter realization technique or another is usually based on such factors as cost, simplicity, flexibility and reliability. At present, it seems that SAW's are preferable for high bandwidth real-time operation, CCD's for low bandwidth real-time operation and digital methods for non-real-time operation. Digital methods can make use of a reliable and ever advancing digital microelectronic technology. They are highly flexible since the reference shift registers of a digital processor can easily be reloaded with the exact or weighted form of any new reference signal. They are also more stable and can handle relatively high duration-bandwidth products.

Signals in common use are often bandpass signals. Except in the case of SAW technology, the direct matched filter realization for such signals may not be easy. It is generally more convenient to transform the bandpass signal into its in-phase and quadrature components in such a way as to transform

the single-channel bandpass matched filter into two baseband ones which are usually easier to realize[72,93].

1.6.2 Distortion[46,70]

Distortion is the main problem associated with, though not peculiar to, matched filtering. It usually refers to the condition where the relationship between the input and reference signals departs from an arbitrary desired one in general, and from the state of perfect match in particular, due to such deterministic and random distorting phenomena as channel and systematic disturbances, instabilities and imperfections. It causes the matched filter response to deviate from its desired form in one way or another and thus may lead to a degradation in system performance. It may involve the amplitude and/or phase of the received signal and/or the local reference. Distortion in the received signal is usually known as the modulation-distortion and that in the reference signal as the filter-distortion. Modulation-distortion is usually analyzed in the time-domain and filter-distortion is usually analyzed in the frequency domain.

In order to make it possible to analyze distortion and determine its effects, specific amplitude and/or phase distortion functions have to be assumed. Two types of such functions are possible in this respect, namely, the deterministic and the random types. The former type is suitable in particular in the case where the distortion sources are known. The latter type is suitable in the case where the distortion sources are unpredictable and can be described only in statistical terms.

Deterministic distortion analysis can be accommodated by the correlation function $\chi_{ik}(t,\nu)$ of (1.1). This can be done by substituting the distorted forms of the received signal and the local reference for the two correlated signals in (1.1). The explicit form of the deterministic distortion function depends on the nature of the particular distortion under consideration. Consider, for example, the case where distortion refers to the deterioration of the state of perfect match between the input and reference signals. Let a simple deterministic distortion source be modelled by a sinusoid having its own amplitude and phase functions. It can be shown in this case, for pulse compression signals, that[46,70,105]

(i) Each simple amplitude modulation-distortion source introduces two similar secondary distortion responses in the form of two paired side-bands flanking the undistorted matched filter response on the frequency-axis.

(ii) Each simple phase modulation-distortion source generally introduces an infinity of secondary distortion responses in the form of paired side-bands flanking the undistorted matched filter response on the frequency-axis. This implies the intuitively obvious fact that phase modulation-distortion is generally more serious than amplitude modulation-distortion.

(iii) Each simple amplitude filter-distortion source introduces two similar secondary distortion responses in the form of two paired echoes flanking the undistorted matched filter response on the time-axis.

(iv) Each simple phase filter-distortion source generally introduces an infinity of secondary distortion responses in the form of paired echoes of decreasing level flanking the undistorted matched filter response on the time-axis. This implies the intuitively obvious fact that phase filter-distortion is generally more serious than amplitude filter-distortion.

(v) The positions of the side-bands in (i) and (ii) on the frequency-axis as well as the positions of the echoes in (iii) and (iv) on the time-axis are determined by the frequency of the distortion source and are independent of the form of the signal involved.

(vi) In the general case of large duration-bandwidth product FM signals, the modulation-distortion paired side-bands in the frequency-domain appear as filter-distortion paired echoes in the time-domain, and vice versa.

In the particular case of the linear FM signal (see Section 3.1), the distortion side-bands and the distortion echoes are roughly related by a 1-1 correspondence (due to the fact that this signal is approximately symmetric in both the time-domain and the frequency-domain). This together with (v) implies that the filter-distortions associated with any signal can be studied through the modulation-distortions of the linear FM signal which are relatively easy to implement and analyze experimentally.

(vii) An involved deterministic distortion of a given type can be considered as being caused by a composite source which can be modelled by a linear superposition of a finite number of sinusoids each of which represents a simple distortion source. The more involved cases where many types of deterministic distortions are present at a time can also be dealt with at the cost of more complexity.

Statistical distortion analysis is usually based on the statistical trial and error Monte Carlo method. Only limited work has been reported in this respect[46,70].

Both the deterministic and statistical approaches show that if distortions exceed certain tolerable thresholds, they may lead to serious deformation of the matched filter response concerning its level, width and shape. This inevitably results in a higher demodulator error probability and affects the capability of matched filtering as an optimum predetection processing technique. Thus, distortion should be fully analyzed and controlled in such a way that it is reduced or eliminated by careful signal and filter design and/or by making use of active compensation techniques[46].

1.7 Pulse Compression[39,46,66,70]

This section introduces the two basic dual aspects of pulse compression, namely, duration compression and bandwidth compression. It presents the former as an energy and bandwidth conserving phenomenon associated with the perfect

matched filtering of signals and presents the latter as an energy and duration conserving phenomenon associated with the optimum processing of spectra. It shows that the pulse compression behaviour of a given signal is determined by its duration-bandwidth product, the figure of merit in this respect. Accordingly, it defines a pulse compression signal as a large duration-bandwidth product signal which exhibits pronounced pulse compression properties. It also shows how successive pulse compression of the same type or of different types can be used for the predetection processing of signals with arbitrarily large duration-bandwidth products in such a way as to bypass the problems associated with the direct implementation of the optimum processors for such signals.

1.7.1 Duration Compression

Consider the case where the input signal and the matched filter of (1.54) are in perfect match, i.e. where $i = k$ and $\nu = o$ in (1.1). Let $s_i(\sigma) = s_k(\sigma) \triangleq s(\sigma)$ and let $S(f)$ be the spectrum of $s(\sigma)$, where σ is strictly (or effectively) limited to the range $(-\frac{T}{2},\frac{T}{2})$ and f is effectively (or strictly) limited to the bandwidth F. It can be seen from (1.1) and (1.5) that the matched filter response in this case is given by

$$\chi(t,o) = \int_{t-T/2}^{T/2} s(\sigma)s^*(\sigma-t)d\sigma \qquad ,o\leqslant t\leqslant T \qquad (1.62a)$$

$$= \chi^*(-t,o) \qquad ,o\leqslant t\leqslant T \qquad (1.62b)$$

$$= \int |S(f)|^2 e^{j2\pi ft} df \qquad |f|\varepsilon F \qquad (1.62c)$$

where the limits of integration in (1.62a) have been found by making use of (1.2).

Relation (1.62a) expresses the fact that the matched filter response in the present case is simply the autocorrelation function of the input signal $s(\sigma)$. Relation (1.62b) expresses the time-symmetry property of this autocorrelation function. Relation (1.62c) expresses the well-known fact that the autocorrelation function of a given signal $s(\sigma)$ of spectrum $S(f)$ is the Fourier transform of $|S(f)|^2$.

In order to understand the implications of perfect matched filtering, (1.62) will now be studied in some detail. It can be seen that $S(f)$ occurs in (1.62c) as $|S(f)|^2$ whose phase is zero for all f. This behaviour stems from the fact that the perfect matching of the input signal and its matched filter implies both an amplitude-match and a phase-match between the signal spectrum $S(f)$ and the matched filter transfer function $H(f)$ in the sense that $H(f) = S^*(f)$ as indicated by (1.54b).

The amplitude-match between $S(f)$ and $H(f)$ is reflected in the fact that $|H(f)| = |S(f)|$ and results in that the signal and the filter both have the same bandwidth (i.e. matched filtering conserves signal bandwidth) and that the filter attenuation law $|H(f)|$ is defined by $|S(f)|$.

The phase-match between $S(f)$ and $H(f)$ is reflected in the fact that $H(f)$ and $S(f)$ have equal but opposite phases and results in that the filter eliminates the phase dispersion from $S(f)$ in such a way that the signal spectral components fed into the matched filter in the form $S(f)$ having different

phases emerge from this filter in the form $|S(f)|^2$ having the same zero phase. This phase cancellation and equalization can also be explained (e.g. for FM signals) in terms of the dispersive "group delay/frequency characteristics" of $s(\sigma)$ and its matched filter. To this end, $S(f)$ and $H(f)$ may be expressed as

$$S(f) = |S(f)|\, e^{j\phi(f)} \tag{1.63a}$$

$$H(f) = |S(f)|\, e^{-j\phi(f)} \tag{1.63b}$$

Making use of (B.10b), Appendix B, shows that (1.63a) gives the signal "group delay/frequency characteristic" $\sigma_g^{sig}(f)$ and that (1.63b) gives the filter "group delay/frequency characteristic" $\sigma_g^{fil}(f)$ as

$$\sigma_g^{sig}(f) = -\frac{1}{2\pi}\frac{d\phi(f)}{df} \tag{1.64a}$$

$$\sigma_g^{fil}(f) = \frac{1}{2\pi}\frac{d\phi(f)}{df} \tag{1.64b}$$

These two relations show that the dispersive "group delay/frequency characteristic" $\sigma_g^{fil}(f)$ of the filter is determined by $\phi(f)$, the spectrum phase/frequency function of the signal to which this filter is matched. They also show that the filter acts as a dispersive delay equalizer in relation to the spectral components of this signal. It advances in time the originally delayed components and delays in time the originally advanced components in such a way that all these components emerge at its output, forming the spectral components of its response, at the same instant $t = o$ (the sampling instant of this output) where they add arithmetically.

The above-mentioned fact that all the spectral components of the matched filter response emerge at the same instant $t = o$ at the filter output implies that this response has its peak at $t = o$. It can be seen that this result requires only the existence of a perfect phase-match between $S(f)$ and $H(f)$. The existence of a perfect amplitude-match between $S(f)$ and $H(f)$ is not essential in this respect. In fact, such a perfect amplitude-match is required only to limit the amount of noise power which passes through the filter and, hence, to maximize the output signal-to-noise ratio as described in Section 1.5.

It can be seen from (1.62c) that $\chi(t,o)$ may be considered as a superposition of an infinitely large number of the spectral cisoidal components $|S(f)|^2 e^{j2\pi ft}$, $|f| \varepsilon F$, which may be depicted in the form of simple sinusoidal waveforms extending over the entire t-axis and having different amplitudes and wavelengths. These spectral cisoids clearly add arithmetically only at $t = o$ and interfere at all other instants in such a way that $|\chi(t,o)|$ has its peak at $t = o$ and decreases with $|t|$ (not necessarily monotonically) for all other values of $|t| \leq T$ assuming, for example, a shape of the type shown in Fig. 1.4. This clearly agrees with (1.7) and explains (1.62b). In fact, (1.62c) indicates that the exact form of $\chi(t,o)$ is determined by the particular signal under consideration. That is, a given signal $s(\sigma)$ has its unique $\chi(t,o)$. However, (1.62c) also shows that $\chi(t,o)$ is the same for all signals with the same $|S(f)|$ but with different phase/frequency functions. That is, a given $\chi(t,o)$ does not correspond to a unique signal $s(\sigma)$.

The preceding discussion implies that the matched filter response in the case of perfect match has an effective duration T_r which is smaller than its actual duration 2T. In fact, it can be seen from (1.62c) that T_r is of the order of the reciprocal of the integration range (assuming a smooth S(f)). That is, one can in this case write

$$T_r \approx \frac{1}{F} \tag{1.65}$$

This relation is based on the assumption that S(f) and $|S(f)|^2$ (the respective spectra of the matched filter input and response) both have the same bandwidth F. However, it is obvious that $|S(f)|^2$ is generally of somewhat narrower bandwidth than S(f). This clearly indicates that T_r may slightly exceed its estimate given by (1.65).

It can be seen from (1.65) that

$$T_r < T \quad \text{if } FT > 1 \tag{1.66a}$$

$$T_r \approx T \quad \text{if } FT \approx 1 \tag{1.66b}$$

Relation (1.66a), on the one hand, shows that the perfect matched filtering of a large duration-bandwidth product signal is accompanied by an effective compression of its duration from T at the matched filter input to $\frac{1}{F}$ at the matched filter output. This is the duration compression aspect of the so-called pulse compression phenomenon usually associated with optimum processing. Relation (1.66b), on the other hand, indicates that duration compression does not accompany the perfect matched filtering of a signal whose duration-bandwidth product is of the order of unity.

The preceding paragraph shows that signals may be classified into two main classes according to their duration compression behaviour, namely, the class of unitary duration-bandwidth product signals which do not exhibit any significant duration compression properties and the class of large duration-bandwidth product signals which exhibit pronounced duration compression properties (the so-called pulse compression signals). A unitary duration-bandwidth product signal may be described as an "elementary" signal. In contrast, a pulse compression signal of duration-bandwidth product TF >> 1 may be described as a "composite" signal equivalent to FT elementary signals. Examples of elementary signals in common use include the familiar Amplitude-Shift Keyed (ASK), Frequency-Shift Keyed (FSK) and Phase-Shift Keyed (PSK) signals[8,106]. Examples of pulse compression signals will be given in Chapter 2.

Making use of (1.65) and the fact that the perfect matched filtering of a given signal of bandwidth F preserves this bandwidth shows that the matched filter response in this case has a duration-bandwidth product $\approx F.T_r \approx F.\frac{1}{F} \approx 1$. That is, the perfect matched filtering of a given signal reduces this signal to an elementary signal (which is its temporal autocorrelation function) if it is not originally so. It is this elementary signal which is sampled when the given signal is processed by its own matched filter-sampler compound.

In order to facilitate the study of the duration compression behaviour of a given signal, a duration compression ratio ρ_{dur} may be defined as

$$\rho_{dur} \triangleq T/T_r \qquad (1.67a)$$

where T is the signal duration and T_r is the effective duration of its matched filter response.

Making use of (1.65) in (1.67a) shows that

$$\rho_{dur} \approx FT \tag{1.67b}$$

This relation confirms that the duration compression behaviour of a given signal is determined by its duration-bandwidth product. It is only the order of magnitude of this product which is important in this respect. This is because this product cannot be defined in a unique manner as described in Section 1.3.

The input/output energy conservation relationship for a filter matched to a given signal $s(\sigma)$ of duration T when this signal is its input may be expressed as

$$\int_T |s(\sigma)|^2 d\sigma \approx \int_{T_r} |\chi(t,o)|^2 dt \tag{1.68}$$

where $\chi(t,o)$ is the matched filter response in this case and T_r is the effective duration of this response and where the filter gain factor has been dropped for convenience.

The average input signal power $\bar{p}$ and the peak instantaneous output signal power $\hat{p}$ are given by

$$\bar{p} = \frac{1}{T} \int_T |s(t)|^2 dt \tag{1.69a}$$

$$\hat{p} = |\chi(t,o)|^2_{max} = |\chi(o,o)|^2 \tag{1.69b}$$

Making use of (1.69) in (1.68) and assuming that T_r is small enough to make it possible to substitute $|\chi(t,o)|_{max}$ for $|\chi(t,o)|$ over T_r shows that

$$\frac{\hat{p}}{\bar{p}} \approx \frac{T}{T_r} \tag{1.70a}$$

which, by making use of (1.65), reduces to

$$\frac{\hat{p}}{\bar{p}} \approx FT \tag{1.70b}$$

This relation implies that the perfect matched filtering of a given signal is accompanied by an input-to-output signal power gain ($\triangleq \hat{p}/\bar{p}$) which increases with the signal duration-bandwidth product. This is because the compression of the duration of the input signal by its matched filter must be accompanied by a corresponding gain in its instantaneous power in such a way that a balance is maintained between the input and output signal energies.

1.7.2 Bandwidth Compression

Bandwidth compression is the dual of duration compression. Consider the case where the input signal to the multiplier of (1.61) is the complex conjugate of its local reference. Let this signal be denoted by $s(\sigma)$ and have a duration T and spectrum $S(f)$. It can be seen that the spectrum of the multiplier response in this case is given by

$$\chi^*(o,\nu) = \int S(f)S^*(f-\nu)df \tag{1.71a}$$

$$\chi^*(o,\nu) = \int_T |s(\sigma)|^2 e^{-j2\pi\nu\sigma} d\sigma \tag{1.71b}$$

where $\chi(t,\nu)$ is defined by (1.1).

Relation (1.71) can be used to study the bandwidth compression behaviour of the signal $s(\sigma)$ in a manner which is

similar to that in which (1.62) was used to study the duration compression behaviour of this signal. These facts indicate that the correlation function $\chi(t,\nu)$ associated with the signal $s(\sigma)$ can accommodate not only its duration compression behaviour but also its bandwidth compression behaviour. The duration compression behaviour can be studied through $\chi(t,o)$ and the bandwidth compression behaviour can be studied through $\chi^*(o,\nu)$.

Relation (1.71a) expresses the fact that $\chi^*(o,\nu)$ is the autocorrelation function of the input spectrum $S(f)$. This function's envelope can be seen to be symmetrically centred about an Intermediate Frequency (IF) given by $\nu = o$, where $|\chi(o,\nu)|$ has its peak value.

Relation (1.71b) shows that in the present case, the multiplier multiplies its local reference $s^*(\sigma)$ and the input signal $s(\sigma)$ in such a way as to remove the phase modulation from $s(\sigma)$ while preserving its duration T. Relation (1.71b) also shows that the effective bandwidth F_r of the multiplier response may be expressed as

$$F_r \approx \frac{1}{T} \tag{1.72}$$

This relation is the dual of (1.65) and describes the bandwidth compression aspect of the pulse compression phenomenon.

Making use of (1.72) and the fact that bandwidth compression preserves the input signal duration shows that bandwidth compression reduces this signal to a signal whose duration-bandwidth product $\approx T.F_r \approx T.\frac{1}{T} \approx 1$. That is,

bandwidth compression reduces the given input signal to an elementary signal (which is its frequency autocorrelation function) if it is not originally so. It is this elementary signal which is integrated when the given input signal is processed by its own multiplier-integrator compound.

One can define the bandwidth compression ratio ρ_{band} as

$$\rho_{band} \triangleq F/F_r \tag{1.73a}$$

where F is the uncompressed input signal bandwidth.

Making use of (1.72) in (1.73a) shows that

$$\rho_{band} \approx FT \tag{1.73b}$$

which corresponds to (1.67b) and shows that the bandwidth compression behaviour of a given signal is determined by its duration-bandwidth product.

The input/output energy conservation relationship in the case of bandwidth compression may be expressed as

$$\int_F |S(f)|^2 df \approx \int_{F_r} |\chi(o,\nu)|^2 d\nu \tag{1.74}$$

where the multiplier amplification factor has been dropped for convenience.

The average input spectral power $\bar{q}$ and the peak output spectral power $\hat{q}$ are given by

$$\bar{q} = \frac{1}{F} \int_F |S(f)|^2 df \tag{1.75a}$$

$$\hat{q} = |\chi(o,\nu)|^2_{max} = |\chi(o,o)|^2 \tag{1.75b}$$

Making use of these two relations in (1.74) and assuming that F_r is small enough to make it possible to substitute $|\chi(o,\nu)|_{max}$ for $|\chi(o,\nu)|$ over F_r shows that

$$\frac{\hat{q}}{\bar{q}} \approx \frac{F}{F_r} \tag{1.76a}$$

which, on making use of (1.72), reduces to

$$\frac{\hat{q}}{\bar{q}} \approx FT \tag{1.76b}$$

This relation corresponds to (1.70b) and implies that bandwidth compression is accompanied by an input-to-output spectral power gain ($\triangleq \hat{q}/\bar{q}$) which increases with the duration-bandwidth product of the signal whose bandwidth is being compressed.

1.7.3 Signal Processing By Progressive Pulse Compression

The duration-bandwidth product of a given signal may be so large that the implementation of a single multiplier or matched filter for its processing (using, respectively, a multiplier-integrator compound or a matched filter-sampler compound) becomes quite difficult (see Section 1.6). However, such a difficulty can be reduced through digital processing, parallel-channel processing[46] and progressive pulse compression.

In the progressive pulse compression technique, the ordinary method in which the optimum processing of a given signal in AWGN is achieved by passing it through its multiplier-integrator compound (or its matched filter-sampler compound) is replaced by another method. In this alternative method, the signal is first passed through a cascade comprising an

arbitrary number of correlators and/or matched filters, whereby it undergoes a series of partial bandwidth and/or duration compression operations to reduce its original duration-bandwidth product before it is fed into a final stage in the form of a multiplier-integrator compound (or a matched filter-sampler compound) for optimum processing.

Each multiplier or matched filter used in the progressive pulse compression processing technique has a local reference whose duration-bandwidth product is less than that of the given input signal and,thus, can readily be implemented. Each multiplication or matched filtering operation preserves the input signal energy.

The progressive pulse compression processing technique is theoretically optimal in AWGN. This can be seen from the so-called "reversibility theorem"[11] which may be stated as: 'The minimum attainable demodulator error probability P_e is not affected by the introduction of any realizable reversible operation between the channel and the receiver that transforms the channel output into a new arbitrary waveform". In practice, however, some degradation in demodulator performance is generally unavoidable in this respect.

Progressive pulse compression methods are most convenient for the processing of FM signals in general, and the Linear FM (LFM) signal in particular. A signal $s(\sigma) = |s(\sigma)|e^{j\theta(\sigma)}$ of duration T is said to be an FM signal if $\theta(\sigma)$ is smooth enough to make it possible to define a monotonic signal instantaneous frequency $f_{inst}(\sigma) \triangleq \frac{1}{2\pi}\frac{d\theta(\sigma)}{d(\sigma)}$ and, hence, an FM

law over T. The case where this law is linear corresponds to the Linear FM (LFM) signal.

Optimal signal processing by progressive pulse compression can, for example, be achieved by one of the following four basic methods:

1.7.3.1 First Method

In this method, a given input signal $s(\sigma) = |s(\sigma)|e^{j\theta(\sigma)}$ of duration T and bandwidth F is first passed through a multiplier whose local reference is $|s(\sigma)|e^{-j\theta'(\sigma)}$ which has a duration T and a bandwidth < F. It will become clear in Section 2.1 that the relationship between F and the bandwidth of the multiplier local reference is essentially determined by the phase-mismatch $\theta(\sigma) - \theta'(\sigma)$ which is usually small in the present application. Assuming that $s(\sigma)$ is an FM signal, such a phase-mismatch can obviously be obtained by varying the frequency of the local oscillator at a slower rate than that of the frequency of the input signal.

According to Subsection 1.7.2, passing $s(\sigma)$ through the multiplier as described in the preceding paragraph preserves its energy and duration and partially compresses its bandwidth around some Intermediate Frequency (IF). That bandwidth compression will only be partial is due to the existence of the phase-mismatch $\theta(\sigma) - \theta'(\sigma)$ which implies that the multiplier does not completely remove the phase modulation from the input signal. Thus, the multiplier response will have the same duration T as the input signal and an effective

bandwidth F', say, which satisfies the relation $\frac{1}{T} < F' < F$.

The partially bandwidth-compressed multiplier response is then processed optimally by passing it through a matched filter-sampler compound whose matched filter is in perfect match with this response. According to Subsection 1.7.1, the matched filter preserves the energy and bandwidth of the multiplier response and fully compresses its duration. Thus, the matched filter response will have an effective bandwidth F' and an effective duration $T' \approx \frac{1}{F'}$. That is, this response will be an elementary signal whose duration-bandwidth product $\approx F'.T' \approx F'.\frac{1}{F'} \approx 1$.

In this method, it can be seen that the receiver does not need to accommodate the full bandwidth of the input signal. In fact, the phase-mismatch $\theta(\sigma) - \theta'(\sigma)$ can be chosen in such a way as to achieve a best compromise between the maximum bandwidth F' and the maximum duration T' for which the matched filter must be designed.

The overall bandwidth/duration compression ratio in this method $\approx \frac{F}{F'}.\frac{T}{T'} \approx FT$. This is obviously the same as ρ_{dur} of (1.67b) and ρ_{band} of (1.73b). However, the overall duration compression ratio in this method is only $\frac{T}{T'} \approx TF' < TF$. This implies that the main lobe of the overall response obtained by this method is wider than that obtained by the method in which the optimum processing of the input signal is achieved by passing it through its own matched filter. Thus, this method is superior to the matched filter method from the viewpoint of combating the problems associated with the

synchronization and sampling prior to detection. However, this superiority is achieved at minimal expense of the demodulator performance.

1.7.3.2 Second Method

This method differs from the first method only in that the optimal processing of the multiplier response is achieved by passing it through a multiplier-integrator compound rather than a matched filter-sampler compound as in the first method.

In this second method, both multipliers preserve the energy as well as the duration T of the input signal. In fact, this method is essentially a bandwidth compression method in which the first multiplier compresses the input signal bandwidth from F to F' and the second multiplier compresses F' to F" (where $F'' \approx \frac{1}{T} < F' < F$) in such a way that the overall response is a unitary duration-bandwidth product elementary signal.

Obviously, this method does not require the receiver to accommodate the full bandwidth of the input signal.

1.7.3.3 Third Method

This method is the dual of the first method and can be explained accordingly.

Here a given input signal $s(\sigma)$ of duration T, bandwidth F and spectrum $S(f) = |S(f)|e^{j\phi(f)}$ is first passed through a matched filter whose transfer function is $|S(f)|e^{-j\phi'(f)}$ (which is phase-mismatched to S(f) in such a way that the

filter impulse response has a duration < T) whereby its energy and bandwidth are both conserved and its duration is partially compressed to T', say, where $\frac{1}{F} < T' < T$.

The partially duration-compressed matched filter response is then processed optimally by passing it through its own multiplier-integrator compound. Obviously, the multiplier in this compound preserves both the energy and duration T' of the matched filter response and compresses its bandwidth from F to F', say, where $F' \approx \frac{1}{T'}$. Thus, the correlator response will be an elementary signal whose duration-bandwidth product $\approx T'.F' \approx T'.\frac{1}{T'} \approx 1$.

This method does not require the receiver to accommodate the full duration of the input signal. It can also be seen that the phase-mismatch $\phi(f) - \phi'(f)$ can be chosen in such a way as to achieve a best compromise between the maximum duration T' and the maximum bandwidth F' to which the correlator (i.e. the multiplier-integrator compound) must be designed.

1.7.3.4 Fourth Method

This method differs from the previous method only in that the optimal processing of the matched filter response is achieved by passing it through its own matched filter-sampler compound rather than its own multiplier-integrator compound as in the previous method.

In this method, both matched filters preserve the energy as well as the bandwidth of the input signal. In fact, this method is essentially a duration compression method in which the first matched filter compresses the input signal duration

from T to T' and the second matched filter compresses T' to T" (where $T'' \approx \frac{1}{F} < T' < T$) in such a way that the overall response is a unitary duration-bandwidth product elementary signal.

Obviously, this method does not require the receiver to accommodate the full duration of the input signal.

The first and second methods have two limiting cases, namely, the case where $\theta(\sigma) - \theta'(\sigma) = C_1$ (constant) and the case where $\theta'(\sigma) = C_2$ (constant). Similarly, the third and fourth methods have two limiting cases corresponding to the two conditions $\phi(f) - \phi'(f) = C_3$ (constant) and $\phi'(f) = C_4$ (constant). The implications of each of these four limiting cases can readily be apprehended.

2

DATA TRANSMISSION BY PULSE COMPRESSION[98-101,107-110]

This chapter examines the utility of pulse compression techniques in general, and the FM pulse compression techniques in particular, for digital data transmission. It provides a suitable background for the special case of the linear FM pulse compression technique which will be studied in the remaining chapters.

2.1 Pulse Compression Signals[46,66,70,98,107-110]

This section establishes the dependence of the bandwidth of a given single-pulse signal on its phase/time function and the dependence of its duration on the phase/frequency function of its spectrum. It also defines some important pulse compression signal classes.

2.1.1 Signal Bandwidth and Duration

A pulse compression signal was defined in the previous section as a large duration-bandwidth product signal whose duration and/or bandwidth can be compressed through matched filtering and/or multiplication operations.

Since the duration-bandwidth product of a given signal determines its pulse compression properties, it is important to determine the dependence of signal duration and bandwidth on the other signal parameters. Consider, for example, an FM single-pulse signal $s(\sigma)$ of spectrum $S(f)$ where

$$s(\sigma) \triangleq |s(\sigma)|\, e^{j\theta(\sigma)}\,, \quad \sigma \varepsilon T \tag{2.1a}$$

$$S(f) \triangleq |S(f)|\, e^{j\phi(f)}\,, \quad f \varepsilon (f_1, f_2) \tag{2.1b}$$

The signal $s(\sigma)$ and its spectrum $S(f)$ are related by the following Fourier transform pair

$$S(f) = \int_T |s(\sigma)| e^{j[\theta(\sigma)-2\pi f\sigma]} d\sigma \tag{2.2a}$$

$$s(\sigma) = \int_{f_1}^{f_2} |S(f)| e^{j[\phi(f)+2\pi f\sigma]} df \tag{2.2b}$$

Relation (2.2a) can be shown by the stationary phase method (see Appendix B) to imply that the value of S(f), for a given f, is essentially determined by the contributions to the integral from the immediate vicinity of that value of σ which belongs to T and satisfies the following condition of stationary phase

$$\theta(\sigma) - 2\pi f\sigma = \text{constant}, \quad \sigma \varepsilon T \tag{2.3a}$$

$$\text{i.e.} \qquad f = \frac{1}{2\pi} \frac{d\theta(\sigma)}{d\sigma}, \quad \sigma \varepsilon T \tag{2.3b}$$

Relation (2.3b) implies that if T is strictly limited, S(f) effectively vanishes for all f-values which correspond, through (2.3b), to the σ-values which do not belong to T. As σ spans the strictly limited duration T, $|f|$ simultaneously spans the effective signal bandwidth.

Relation (2.3b) can also be interpreted in such a way that f stands for $f_{inst}(\sigma)$, the signal instantaneous frequency. Thus, (2.3b) can also be expressed as

$$f_{inst}(\sigma) = \frac{1}{2\pi} \frac{d\theta(\sigma)}{d\sigma}, \quad \sigma \varepsilon T \tag{2.3c}$$

These facts imply that the effective signal bandwidth is confined to the range of values which $f_{inst}(\sigma)$ assumes over T.

In the case where $\theta(\sigma)$ is linear in σ, (2.3) shows that both f and $f_{inst}(\sigma)$ remain unchanged as σ spans T. That is, S(f) is effectively concentrated at a single frequency which is the centre frequency. However, the fact that T is finite implies that the bandwidth is nonzero as can be seen from (2.2a). Thus, the case where $\theta(\sigma)$ is linear in σ implies that

$s(\sigma)$ has a narrow bandwidth regardless of the exact form of $|s(\sigma)|$. Examples of such signals in common use as modulator signals include the familiar ASK, FSK and PSK signals (see Subsection 1.7.1).

In the case where $\theta(\sigma)$ is nonlinear in σ, (2.3) shows that both f and $f_{inst}(\sigma)$ assume the same wide range of values as σ spans T. That is, the signal bandwidth is effectively broad and not confined to the immediate vicinity of a single f-value. Thus, the case where $\theta(\sigma)$ is nonlinear in σ implies that $s(\sigma)$ has a broad bandwidth regardless of the exact form of $|s(\sigma)|$. The broadness of the signal bandwidth in this case depends on the exact form of $\theta(\sigma)$ and its deviation from linearity.

The stationary phase method can also be applied to (2.2b) to show that the duration of $s(\sigma)$ is essentially determined by $\phi(f)$. A short-duration $s(\sigma)$ may be defined as one whose spectrum has an arbitrary $|S(f)|$ and a linear $\phi(f)$. A long-duration $s(\sigma)$ may be defined as one whose spectrum has an arbitrary $|S(f)|$ and a nonlinear $\phi(f)$.

2.1.2 Classification of Pulse Compression Signals

Assuming signal classification in the time-domain, pulse compression signals have two main classes : (i) the class of analogue coded signals with continuous amplitude or frequency (or phase) modulation, and (ii) the class of discrete coded signals with discrete amplitude, phase or frequency modulation. Hybrid analogue and/or discrete coded signals are also possible.

A typical example of class (i) is the FM pulse. Basic examples of class (ii) are the amplitude-shift, phase-shift and frequency-shift coded signals. In amplitude-shift coding, signal phase and frequency are unchanged and signal amplitude usually assumes a coded sequence of the two values 1 and 0 over the consecutive elemental chips of signal duration. Such a signal takes the form of a train of Time-Hopped (TH) elementary pulses. In phase-shift coding, signal amplitude and frequency are unchanged and signal phase assumes a binary or an M'ary coded sequence of discrete values over the consecutive elemental chips of signal duration. Such a signal is usually described as a Direct Sequence (DS) signal. In frequency-shift coding, or Frequency-Hopping (FH), signal amplitude and phase are unchanged and signal frequency assumes a coded sequence of discrete values over the consecutive elemental chips of signal duration. Randomly or pseudorandomly amplitude-shift, phase-shift and frequency shift coded signals belong to the class of noiselike signals which are characterised by their random or pseudorandom amplitude, phase or frequency irregularities[66,111,112].

2.2 Generation of Pulse Compression Signals[46,66,113]

This section introduces and compares the 'active' and 'passive' pulse compression signal generation techniques.

2.2.1 The Active and Passive Generation Techniques

There are two main methods for signal generation in practice, namely the 'active' and 'passive' methods. Referring to the signal $s(\sigma)$ of (2.1), the active method corresponds to generating $s(\sigma)$ actively in the time-domain by generating its desired $|s(\sigma)|$ and $\theta(\sigma)$ functions. The

passive method corresponds to generating $s(\sigma)$ passively in the frequency-domain by generating the desired $|S(f)|$ and $\phi(f)$ functions of its spectrum. The passively generated form of a given signal can be treated as the dual of its actively generated form. A signal is usually truncated in the domain in which it is generated. Thus, an actively generated signal is strictly duration-limited and a passively generated signal is strictly bandwidth-limited. A certain degree of spectrum truncation is usually unavoidable in practice. This implies that most practical signals are actually of the strictly bandwidth-limited type.

According to the previous section, $s(\sigma)$ of (2.1) has a broad bandwidth if $\theta(\sigma)$ is nonlinear in σ regardless of the exact form of $|s(\sigma)|$. Similarly, $s(\sigma)$ has a long duration if $\phi(f)$ is nonlinear in f regardless of the exact form of $|S(f)|$. These facts imply that if $s(\sigma)$ is a broadband pulse compression signal, the most efficient technique for its active generation is to generate a nonlinear $\theta(\sigma)$ along with any desired $|s(\sigma)|$. They also imply that if $s(\sigma)$ is a long duration pulse compression signal, the most efficient technique for its passive generation is to generate a nonlinear $\phi(f)$ along with any desired $|S(f)|$.

The active generation technique of $s(\sigma)$ can be explained on the assumption that it is an FM pulse compression signal. In this case, the active generation may be either "direct" or "indirect". The direct active generation can, for example, be achieved by modulating the instantaneous frequency of a voltage-controlled oscillator according to (2.3c) as illustrated

in Fig. 2.1a. The indirect active generation can, for example, be achieved by applying $\theta(\sigma)$ itself to a phase-controlled oscillator as illustrated in Fig. 2.1b.

The passive generation technique of $s(\sigma)$ is illustrated in Fig. 2.2. Here $s(\sigma)$ is generated as the response of a filter to an input time-impulse whose spectrum has zero phase and unity amplitude at least over the bandwidth F of $s(\sigma)$. This filter is the conjugate of the matched filter of $s(\sigma)$, i.e. the filter whose impulse response $h(\sigma)$ and transfer function $H(f)$ are given by

$$h(\sigma) = s(\sigma) \tag{2.4a}$$

$$H(f) = S(f) \tag{2.4b}$$

Usually, the pulse compression signal is first generated at low power level to achieve the required phase-structure. It can then be power-amplified and/or raised to a higher frequency band before transmission. Assuming good power amplifier and frequency multiplier design, the phase-structure remains accurate at the transmitter output. Amplitude Modulation (AM) can be accomplished only at the final amplification stage at the higher power level. However, a comparatively flexible AM may be difficult to achieve in this manner. Also AM requires system stability and that the receiver be linear over the entire dynamic range of the received signal. Complicated AM cannot thus be easily implemented and implies more system complexity and higher cost. Moreover, it does not permit full utilization of the peak power capability of the transmitter. This explains why it is frequently preferable to operate the transmitter at constant power level.

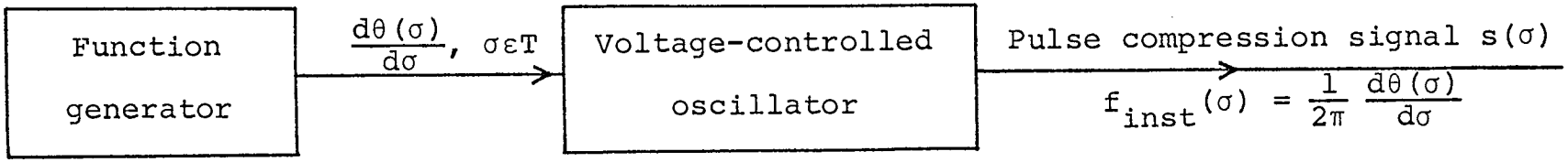

(a) Direct Method

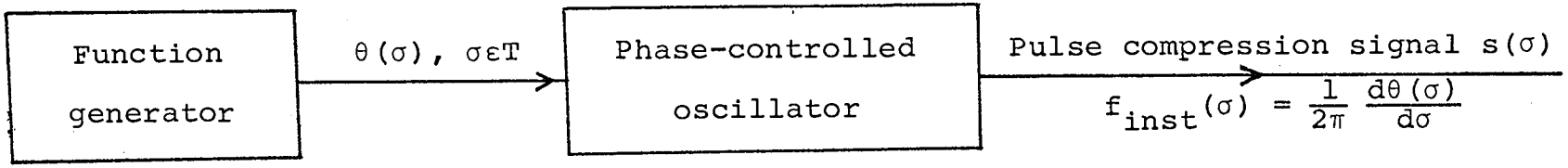

(b) Indirect Method

Fig. 2.1 Basic FM Pulse Compression Signal Active Generation Techniques

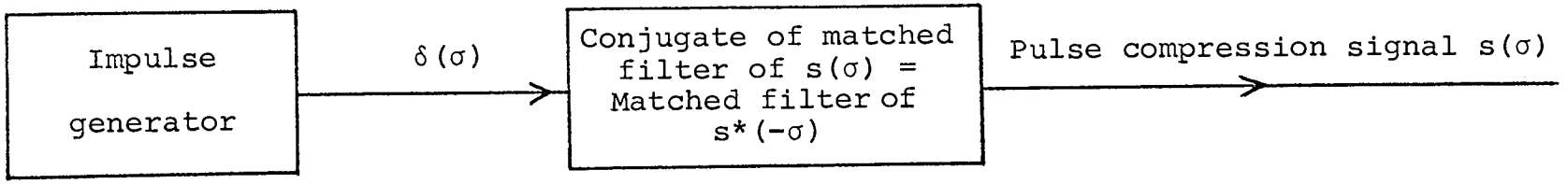

Fig. 2.2 Basic Pulse Compression Signal Passive Generation Technique

2.2.2. Comparison of Active and Passive Generation Techniques

Each pulse compression signal generation technique imposes its own problems. In the active technique, it is often difficult to achieve the desired precise amplitude/time function $|s(\sigma)|$ and phase/time function $\theta(\sigma)$ over the entire signal duration and distortions usually take place. However, the active technique is more controllable, more flexible, easier to implement and more capable of handling higher duration-bandwidth products than the passive technique which usually suffers from the inflexibility and realization difficulty of matched filters. This does not imply that the passive technique is always disadvantageous. In fact, it is often easier to achieve stability with passive filters rather than with active oscillators. The passive technique also makes it possible to reduce cost and complexity and to compensate automatically for signal distortions that may result from errors or instabilities in the generator. This is because this technique makes it possible to use the same matched filter for both signal generation and signal optimum processing in a variety of cases such as:

(i) The case where the signal is both real and even in time. In this case, the signal matched and conjugate filters are identical.

(ii) The case where the signal is, for example, a real FM signal whose amplitude/time function is even, and whose FM law is odd, in time. Here the matched filter and its conjugate are not identical but a single matched filter can still be used for both signal generation and

optimum processing by making use of sideband inversion prior to optimum processing in a way which may, for example, be illustrated as in Fig. 2.3.

It can be seen in this case that sideband inversion can be achieved only if the mixing frequency exceeds the signal carrier frequency. It can also be seen that this inversion reverses the FM sweep direction in time, has theoretically no effect on the demodulator error probability (according to the reversibility theorem[11]), and can conveniently be accomplished either at transmission or at reception in conjunction with heterodyning.

The choice of a specific pulse compression signal generation technique depends on the particular case under consideration. However, it should be noted here that

(i) It is of paramount importance to generate the desired pulse compression signal having the required precise amplitude and phase characteristics. Intolerable amplitude and phase distortions result in reduced performance as was explained in Section 1.6.

(ii) There is an increasing trend towards large duration-bandwidth product pulse compression signals. The precise generation of such signals may be difficult in practice. This is because the complexity of the generator of a given signal increases with its duration-bandwidth product, as was mentioned in Section 1.6.

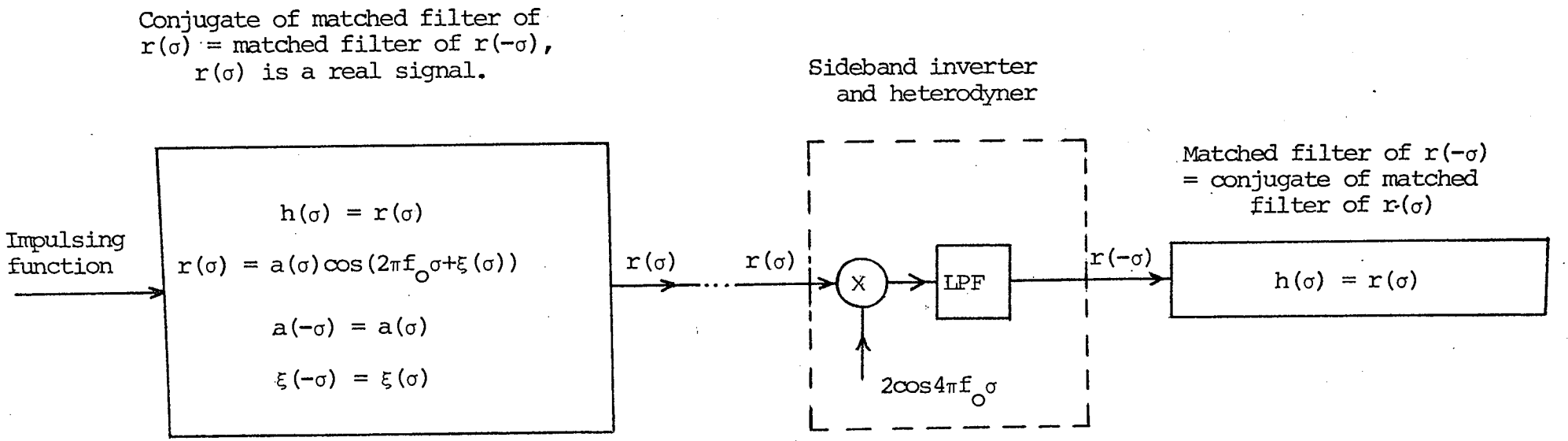

Fig. 2.3 Signal Generation and Processing Using One Matched Filter and Sideband Inversion

(iii) It is frequently important in practice to use a flexible signal generation technique which, for example, makes it possible to modify or weight the generated pulse compression signal parameters.

(iv) It is sometimes important in practice to maintain good coherency between the sequentially generated pulse compression signals.

These requirements are generally difficult to achieve by making use of the analogue active and passive pulse compression signal generation techniques. They may, however, be achieved by making use of the largely active digital generation techniques. These techniques also have the additional advantage of being compatible with the digital processing techniques.

2.3 Basic Pulse Compression Signal Generation-Processing Structures

Pulse compression signal generation may be active or passive as described in the previous section. The optimum predetection processing of a pulse compression signal may be achieved with an active correlator and/or a passive matched filter as described in Sections 1.1, 1.5 and 1.7. Accordingly, a digital pulse compression communication system may, for example, make use of the following four basic signal generating/processing structures:

(i) The active generator-active processor (i.e. correlator) structure. This structure conserves the pulse compression signal duration and makes it generally possible to achieve a perfect match between this signal and its correlator.

(ii) The passive generator-passive processor (i.e. matched filter) structure. This structure conserves the pulse compression signal bandwidth and makes it generally possible to achieve a perfect match between this signal and its matched filter.

(iii) The active generator-passive processor structure. Here the perfect match between the actively generated signal and its matched filter cannot generally be achieved.

(iv) The passive generator-active processor structure. Here the perfect match between the passively generated signal and its correlator cannot generally be achieved.

Each of these four basic structures has its important applications. However, the active generator-active/passive processor structure is becoming increasingly important in practice because it can handle larger signal duration-bandwidth products (see Subsection 1.7.3.) and because of the present trend towards the largely active signal generation and processing techniques.

2.4 Capabilities of Pulse Compression Signals[98,107-110, 114]

This section gives a rather preliminary and general description of the capabilities of pulse compression signals, assuming that these signals are optimally processed prior to detection. The discussion, which is supplemented in the following sections, is confined to the case of analogue matched filtering. It can also be extended to the case of digital matched filtering[93], correlator processing or processing by progressive pulse compression.

2.4.1. Introduction

Digital communication system performance is not constrained only by AWGN. Other natural and man-made active and passive disturbances are also becoming increasingly important as demand increases for higher communication capacity, quality, security and privacy. It is thus desirable to employ modulator signal sets which are less vulnerable to such disturbances as well as to AWGN. Accordingly, the present discussion examines the utility of pulse compression signals (and demonstrates their superiority to the ordinary ASK, PSK and FSK signals) in this respect. It is mostly confined to the case involving only one pulse compression signal form and one disturbance and can be extended to the case involving a pulse compression signal set and one or more disturbances. Expressions for P_e in the AWGN case are given in Section 1.4. However, these expressions have to be modified if other disturbances and system imperfections are also present.

A pulse compression signal is generally capable of combating any structurally similar or different interference which cannot produce enough interfering power at the sampling instant of its matched filter output. Usually, such an interference is not in perfect match with this filter (i.e. has low correlation with the signal) and, thus, undergoes minimal or no processing gain or suffers from a processing loss when passed through it. The performance of a given pulse compression signal against a defined interference depends on both and can be found by substituting them for the two correlated signals in (1.1) if the interference is deterministic, and by making use of statistical methods if it is random. If the interference environment lacks a known characterization, the performance of the pulse compression signal may be found by making use of the max-min criterion which maximizes the worst case (i.e. minimum) performance.

2.4.2. Gaussian Noise

Assuming a purely AWGN background and making use of (1.59), it can be shown that the signal-to-noise ratio corresponding to the peak instantaneous signal power at the output of a matched filter whose input is the signal to which it is matched may be expressed as

$$[SNR_o]_{m.f.} = \frac{2 \times \text{input signal energy}}{N_o} \tag{2.5}$$

where N_o is the single-sided noise spectral power density at the matched filter input in Watt/Hz.

Making use of this relation along with Subsection 1.5.3 indicates that if matched filtering is adopted as the basic predetection processing technique, the performance of a given

signal in a purely AWGN background is determined only by its energy and not by its particular form. This implies that in the same AWGN background, the performance of a large duration-bandwidth product pulse compression signal will be identical to that of a unitary duration-bandwidth product elementary signal as long as both signals have equal energies. The elementary signal may even excel over the pulse compression signal in this case because it is only the latter which undergoes duration-compression through matched filtering and, hence, becomes more vulnerable to the errors associated with the sampling of the matched filter output. However, these are misleading conclusions that could be true only if there were no transmitter power constraints and transmission rate requirements. In fact, such constraints and requirements do exist in practice and lead to the conclusion that the pulse compression signal excels over the elementary signal as is explained below.

A high output signal-to-noise ratio is always desirable in order to minimize P_e and to achieve long-range transmission communication (or, long-range capability in radar). Relation (2.5) shows that this ratio can be increased by increasing the input signal energy, i.e. by increasing its duration and/or the transmitter power. The first option is undesirable since it restricts the possible transmission rate (or, the possible range-resolution capability in radar). The second option is restricted by the transmitter peak instantaneous power constraints. Many transmitter power components cannot operate at high power conditions. The atmosphere surrounding

the transmitter may ionize if the transmitter peak power exceeds a certain maximum level. It is frequently desirable to operate the transmitter at a constant power level. These transmission rate requirements and transmitter power constraints put serious restrictions on the output signal-to-noise ratio that can be achieved with an elementary signal. However, these restrictions are less severe in the case of a pulse compression signal. Here the transmitter power constraints still exist but a high transmission rate together with a high output signal-to-noise ratio can be achieved simultaneously. The high output signal-to-noise ratio can be achieved by increasing the input pulse compression signal duration and, hence, its energy. The high transmission rate can be made possible, for example, by making use of the time-resolution properties of spread spectrum pulse compression signals which are considered in Subsection 2.4.6 below.

The preceding paragraph shows that pulse compression signals are suitable candidates for such applications as the predominantly AWGN long-range satellite and space digital communications where transmitter power considerations are of paramount importance. It also explains why pulse compression signals were used to solve the World War II problem of achieving simultaneous long-range and high range-resolution capabilities with limited peak-power radar systems [46,66,70,115]. It was the search for a solution to this problem (which could not be solved by making use of elementary signals) that led

to the advent and evolution of pulse compression techniques. In fact, the bandwidth-compression (or spectrum resolution) properties of the pulse compression signal can also be used to improve the target velocity (or range-rate) resolution capability of the radar system. This is because different target velocities lead to different Doppler shifts.

The main conclusion from the discussion above is that in a purely AWGN background, the pulse compression signal surpasses the elementary signal in making it possible to achieve simultaneous high output signal-to-noise ratio and high transmission rates under the restrictive transmitter power constraints. Obviously, these facts cannot be reconciled with the output signal-to-noise ratio of (2.5) as a measure of signal performance in a purely AWGN background. It is thus more convenient to replace this ratio by a new performance measure which can show the superiority of the pulse compression signal in this respect by taking signal compressibility (irrespective of signal form) into consideration. Such a new measure may intuitively be the signal duration-bandwidth product. It may also be the input-to-output signal-to-noise ratio gain G. These two measures are actually equivalent. To show this, G may be defined as

$$G \triangleq \frac{\text{output signal-to-noise ratio}}{\text{input signal-to-noise ratio}} \tag{2.6}$$

In this relation, the numerator is given by (2.5) and the denominator may be denoted by SNR_i and defined as

$$SNR_i \triangleq \frac{\text{average input signal power}}{\text{input noise power in the filter noise-bandwidth}} \tag{2.7a}$$

$$\approx \frac{\text{input signal energy} \div \text{input signal duration}}{N_o \times \text{input signal bandwidth}} \tag{2.7b}$$

In this relation, only the input noise power contained in the matched filter noise-bandwidth has been considered at a time when the total input noise power is virtually infinite. Moreover, the matched filter noise-bandwidth has been roughly identified with its actual bandwidth and, hence, with the bandwidth of the signal to which it is matched. In fact, the matched filter noise-bandwidth is usually defined as the bandwidth of the filter whose transfer function is $\max|H(f)|$ and whose output noise power in response to a given AWGN input is the same as that of the matched filter itself[39,116], i.e.

$$\text{Matched filter noise-bandwidth} \triangleq \frac{\int_0^\infty |H(f)|^2 df}{\max|H(f)|^2} \tag{2.8}$$

where $H(f)$ is the matched filter transfer function.

Substituting from (2.5) and (2.7) in (2.6) gives

$$G = 2 \times \text{input signal duration-bandwidth product} \tag{2.9}$$

This relation confirms the assertion made above that both the signal duration-bandwidth product and G are actually equivalent measures of signal performance in a purely AWGN background. It is to be noted in this respect that the minimum value of G or the duration-bandwidth product below which system performance becomes unacceptable can only be determined on an experimental basis.

Substituting from (1.59) for the numerator and from (2.7a) for the denominator in (2.6) shows that G can also be expressed as

$$G = \frac{\text{signal power gain}}{\text{noise power gain}} \tag{2.10a}$$

where

$$\text{Signal power gain} \triangleq \frac{\text{peak instantaneous output signal power}}{\text{average input signal power}} \tag{2.10b}$$

$$\text{Noise power gain} \triangleq \frac{\text{mean output noise power}}{\text{input noise power in filter noise-bandwidth}} \tag{2.10c}$$

Making use of (1.70) and substituting from (2.9) for G in (2.10a) show that while the perfect matched filtering of a given signal results in a signal power gain of the order of the signal duration-bandwidth product, the associated noise power gain is always of the order of unity. This is due to the obvious fact that while the matched filter compresses its signal, it neither compresses nor expands the input noise.

The preceding results concerning the performance of pulse compression techniques in combating AWGN can readily be extended to the case of coloured Gaussian noise by making use of noise whitening filters [39,40].

2.4.3 White Jamming[93,117]

Both AWGN power and bandwidth are virtually infinite. AWGN spectral power density is independent of signal parameters including signal bandwidth. White jamming has a finite power and a bandwidth ≥ the bandwidth of the signal to be jammed. Thus,

$$\text{White jamming spectral power density} \leq \frac{\text{White jamming fixed power}}{\text{jammed signal bandwidth}} \qquad (2.11)$$

These facts indicate that (2.5) may be applied to the white jamming case by replacing N_o by the white jamming spectral power density of (2.11). They also indicate that the results of the previous subsection concerning the pulse compression signal performance in the AWGN case can also be used to describe this performance in the white jamming case. However, (2.11) shows that spreading the signal spectrum in the white jamming case does not only enhance the signal duration-compressibility through matched filtering as in the AWGN case, but also forces a reduction in the white jammer's spectral power density. This implies that it is possible, under the restrictive transmitter power constraints, to combat white jamming not only by increasing the signal energy through increasing its duration, but also by forcing a reduction in the jamming spectral power density through the spectrum spreading of this signal.

2.4.4 Hostile Detection and Measures

Pulse compression techniques can combat hostile detection and, hence, passive and active hostile measures (e.g. interception, eavesdropping and jamming). This may be achieved by employing spread spectrum (duration) pulse compression signals whose spectral (temporal) power-density is less than that of the prevailing noise. This may also be achieved by employing signals which are structurally similar to the prevailing noise. Only a receiver which knows, and is matched to, the transmitted signal can readily observe it and extract its information content under such conditions.

Pulse compression techniques have higher immunity to

hostile detection and measures in the case of dense environments where, for example, many spread spectrum links share the same common wide transmission bandwidth. In this case, pulse compression techniques offer yet another dimension - the elimination of obvious frequency channelization which has usually provided the underlying basis for the traditionally frequency-selective hostile strategies.

The immunity of pulse compression techniques to hostile detection and measures can also be enhanced by making use of an automatic adaptive data rate which makes it possible to cope with what may be perceived to be the most serious current hostile threat. Moreover, this immunity can be enhanced by making use of cryptographically secure information codes and/or discrete pulse compression signal codes.

2.4.5 Bandwidth and Power Constraints

The utility of low power-density pulse compression signalling described in the previous subsection is not confined to combating hostile detection. In fact, the problem of frequency allocation for pulse compression communications may be solved by overlaying low spectral power-density pulse compression signalling on the existing narrowband conventional systems. This type of signalling affords only minimum interferences to such systems and is relatively immune to their interferences. Similarly, low temporal power-density spread duration signalling may be used, at the cost of a lower data rate, when the transmitter or receiver components have only very limited peak power capabilities.

2.4.6 Signal Overlapping

According to Section 1.7, the perfect matched filtering of a spread spectrum pulse compression signal of duration T and bandwidth F gives a response whose actual duration is 2T and effective duration $\approx \frac{1}{F} < T$. The envelope of this response is peaked at, and falls symmetrically around, its central instant. The exact forms of this response and its envelope are determined by the particular pulse compression signal under consideration. FM pulse compression signals, for example, are generally characterized by a matched filter response whose envelope has a high and relatively broad main lobe surrounded by a number of rapidly falling side-lobes as illustrated in Fig. 1.4[46,66,70].

The above-mentioned facts, along with the fact that the matched filter is a linear time-invariant device, indicate that the duration-compressibility of a spread spectrum signal may, for example, be used to enhance the resolution in time of the matched filter responses to a given set of identical input spread spectrum signals which are of overlapping durations. However, this time-domain resolution cannot be expected to be automatically achievable with any arbitrary spread spectrum signal or under any overlapping conditions. This is due to the fact that the matched filter responses in this case may interfere in such a way that their respective peaks are too close to be resolved by sampling the filter output, some original peaks may disappear or some new false peaks may be created. In fact, the desired temporal resolution may be achieved if, for

example, incoherent reception is assumed and the following two conditions are satisfied:

(i) The spread spectrum signal has a temporal autocorrelation function (i.e. a matched filter response) which is optimal from the viewpoint of enhancing the desired temporal resolution in the situation under consideration. There is no unique all-purpose optimality criterion in this respect. The logical approach is to consider several criteria and to see if they are equivalent from a practical point of view. One possible criterion defines the optimum autocorrelation function as one whose envelope has the highest and narrowest possible main lobe and the lowest possible side-lobe level[70]. This criterion cannot be definitive since the main-lobe width and the side-lobe level may be defined in a variety of ways[46,70]. Another possible criterion is based on the waveform uncertainty principle (see Section 1.3) and defines the optimum autocorrelation function as one which has the maximum of its energy simultaneously concentrated in a duration and a bandwidth whose product is a minimum[70].

(ii) If condition (i) is satisfied, the matched filter responses of two identical input pulse compression signals of overlapping durations can be resolved if, for example,

$$\text{Time-shift between the two input signals} > \text{effective duration of the matched filter response} \tag{2.12a}$$

which is a quasi-orthogonality condition for the two matched filter responses.

Making use of (1.65) shows that (2.12a) reduces to

Rate at which information < pulse compression signal
is received bandwidth (2.12b)

This relation indicates that the bandwidth required to combat temporal signal overlapping increases with the rate at which information is received.

It is thus essential to obtain the pulse compression signal whose autocorrelation function is optimal for combating temporal signal overlapping in the case under consideration. To this end, use can be made of the known pulse compression signals and their characteristic autocorrelation functions[46,66,70]. If this approach cannot solve the problem, the required pulse compression signal has to be synthesized directly from the given optimum autocorrelation function. In both approaches, use can be made of the weighting techniques to modify (usually slightly) the matched filter response of a pulse compression signal in such a way as to make this response approximate, or coincide with, the required autocorrelation function. Both the pulse compression synthesis from an optimum autocorrelation function and the weighting techniques are described below.

Pulse compression signal synthesis from an optimum autocorrelation function is a special case of the more general, and more complicated, problem of signal design as based on the correlation function of (1.1)[70]. The solution of this problem may result in a pulse compression signal which cannot be utilized in practice because of its complicated amplitude and/or phase characteristics (see Section 2.2). In any case, this solution may be accomplished in the following three main steps on the

assumption that the signal to be synthesized has the form described by (2.1)

(i) The first step is to specify both the amplitude and phase functions of the desirable optimum autocorrelation function $\chi(t,o)$. The specification of the amplitude function in this respect can be achieved through the suitable optimality criterion. The specification of the phase function is more difficult because of the arbitrariness involved. The assumed optimum autocorrelation function should be realizable and should possess the well known properties of autocorrelation functions.

It can be shown that the above-mentioned two optimality criteria lead to unrealizable optimal forms of $\chi(t,o)$[70]. However, these forms can be approximated by various realizable, practically equivalent, quasi-optimal forms. Such quasi-optimal forms include, for example, the form whose envelope is Gaussian and the form whose envelope is a $\frac{\sin \pi x}{\pi x}$ (or sinc x) function. These two envelopes are quasi-optimal under the constraints of low side-lobe level and high side-lobe level respectively[46,70]. This fact agrees with relations (1.8) and (1.9) which imply that the side-lobe level can be decreased only at the cost of a corresponding increase in the main-lobe width.

(ii) The second step is based on (1.62c), i.e. on

$$\chi(t,o) = \int |S(f)|^2 e^{j2\pi ft} df, \quad |f| \varepsilon F \qquad (1.62c)$$

where S(f) and F are, respectively, the spectrum and

bandwidth of the signal to be synthesized from its autocorrelation function $\chi(t,o)$.

In this step, $|S(f)|^2$ is computed as the Fourier transform of the specific optimum form of $\chi(t,o)$ chosen in the first step. $|S(f)|$ is effectively, if not strictly, band-limited for a realizable $\chi(t,o)$.

(iii) The third step is to obtain the pulse compression signal $s(\sigma)$ from $|S(f)|$. Relation (2.2) indicates that this problem has no unique solution since only $|S(f)|$ rather than $\phi(f)$ is specified. Should a particular $\phi(f)$ be chosen in this respect, it must lead through (2.2) to a realizable $s(\sigma)$. However, this problem becomes relatively easy to handle in the case where $s(\sigma)$ is a large duration-bandwidth product FM signal (see discussion following relation (B.9), Appendix B).

Weighting[46,66,70,118,119] is usually done at the transmitter and/or receiver by introducing a slight mismatch (or predistortion) between the input pulse compression signal and its matched filter. This mismatch may be introduced in the time-domain or in the frequency-domain. It is frequently confined to the envelopes of the input and reference signals and/or their spectra, leaving the other signal parameters in perfect match. Weighting theory can be accommodated by the correlation function $\chi_{ik}(t,\nu)$ of (1.1).

Different weighting techniques are possible. Each technique imposes its own problems. It may be suitable in a

particular situation and disadvantageous in a different situation.

The effectiveness of weighting is generally limited in practice. Firstly, weighting may imply a complicated AM-modulated signal envelope which is not easy to achieve. Secondly, weighting results in a degradation in the signal-to-noise ratio of (2.5), i.e. in the pulse compression system performance. This is because weighting disturbs the condition of perfect match between the input signal and its matched filter on which (2.5) is based. Thirdly, weighting cannot be done in isolation from the spurious systematic and channel distortive mismatching effects which may spoil any expected weighting advantages. Fourthly, the overall capability of weighting is constrained by the volume-invariance and volume distribution properties of the matched filter response whose implications were described in relation to (1.8) and (1.9) respectively.

It has been shown above that a pulse compression signal with a realizable optimal autocorrelation function does not exist. A pulse compression signal with a usually side-lobed quasi-optimal realizable autocorrelation function is the best that can be achieved in this respect. Thus, the exact P_e-value for a pulse compression system designed according to (2.12) to resolve duration-overlapping signals cannot be found by assuming that the matched filter responses of these signals are strictly orthogonal. Only a lower bound on P_e can be obtained in this manner. To find the actual P_e-value, P_e dependence on the unavoidable side-lobes and on any possible

weighting effects must also be taken into consideration.

It seems that the P_e-dependence on the side-lobes has not yet been investigated. Such an investigation may be accomplished, for example, by formulating a suitable model for the interfering side-lobes at the matched filter output (e.g. in the statistical form of a Gaussian process). P_e can be expressed, and minimized, as a function of the parameters of this model. This investigation can also be extended to the case where many pulse compression signals are involved and the demodulator comprises their respective matched filters. In this case, each signal appears as an interference at the inputs of all matched filters except its own. The effects of side-lobing on system performance can be reduced in this case if the signals are so chosen that their autocorrelation functions are optimum and their crosscorrelation functions are as low as possible so that the total interference at any matched filter output does not exceed a maximum admissible level.

The discussion above has been concerned with the possibility of using spread spectrum pulse compression techniques to resolve duration-overlapping signals. It can be extended to the dual case concerning the use of spread duration pulse compression techniques to resolve spectrum-overlapping signals. These facts together with the results of Section 1.7 can be used to define the pulse compression signal which is optimal from the viewpoint of having both temporal and spectral resolution capabilities. This signal would have a two-dimensional time/frequency correlation function $\chi(t,\nu)$ whose envelope takes a thumbtack form[46,66,70] in the shape of an impulse at the origin of the t-ν plane surrounded by a flat plateau or pedestal of the lowest possible altitude.

Signals which can approach such an optimal pulse compression signal are the noise-like signals already introduced in Section 2.1.

The time and frequency resolution properties of pulse compression signals and the associated side-lobing phenomena were first studied in relation to the range and range-rate resolution capabilities of a radar system[46,66,70]. The results obtained in this respect would also be applicable to communication systems (e.g. multipath and multiple-access systems) in which the demodulator is operated without synchronization and threshold devices are used to detect the received data signals. However, communication systems have the advantage that they can make use of the nominal transmission rate in establishing demodulator synchronization according to the well known synchronization techniques[26-30,98].

2.4.7 Frequency-Concentrated Interferences

According to Section 1.7, a large duration-bandwidth product pulse compression signal of duration T and bandwidth F may be viewed as a sequential/parallel superposition of FT unitary duration-bandwidth product elementary signals. This fact indicates that the pulse compression signal is capable of enhancing communication reliability and security against those interferences which can only destroy some, and not all, of its elementary components. This is because such interferences can only partially distort, but cannot completely destroy, the pulse compression signal.

Consider, for example, a spread spectrum pulse compression signal. Under particular conditions, this signal may be used to combat such elementary frequency-concentrated interferences as narrowband jamming and frequency-selective fading (thereby eliminating the need for frequency diversity reception). To show this, let the spread spectrum pulse compression signal in question, its spectrum, its duration and its bandwidth be denoted by $s_k(\sigma)$, $S_k(f)$, T_k and F_k respectively. Let the frequency-concentrated interference, its spectrum, its duration and its bandwidth be denoted by $s_i(\sigma)$, $S_i(f)$, T_i and F_i respectively (where $F_i << F_k$ and $F_i T_i \approx 1$). It is possible to model this interference in the time-domain by the following constant-frequency carrier

$$s_i(\sigma) = A_i \, R_{T_i}(\sigma) e^{j[2\pi f_i \sigma + \alpha_i]} \tag{2.13}$$

In this relation, σ indicates time and f_i is the carrier frequency. The amplitude A_i and the phase α_i are both assumed to be constant over T_i. $R_{T_i}(\sigma)$ is the so-called Rect function defined as

$$R_{T_i}(\sigma) \triangleq \begin{cases} 1 , & |\sigma| \leq \frac{T_i}{2} \\ 0 , & |\sigma| > \frac{T_i}{2} \end{cases} \tag{2.14}$$

Taking the integral Fourier transforms of both sides of (2.13) gives

$$S_i(f) = A_i \frac{\sin\pi(f_i - f)T_i}{\pi(f_i - f)} e^{j\alpha_i} \tag{2.15a}$$

which, for large T_i, reduces to

$$S_i(f) \approx A_i \delta(f-f_i) e^{j\alpha_i} \tag{2.15b}$$

This relation expresses the obvious fact that a frequency-concentrated interference can be modelled in the frequency-domain by a frequency-impulse.

Assuming that f_i lies within the bandwidth F_k of the pulse compression signal, use can be made of Subsections 1.3.1 and 1.5.2 to show that the output of the filter matched to this signal in response to the given frequency-concentrated interference is given by

$$\chi_{ik}(t,\nu) = A_i S_k^*(f_i) e^{j[2\pi f_i t+\alpha_i]}, \quad |t| \leq \frac{T_i+T_k}{2} \tag{2.16a}$$

which, on writing $S_k(f) = |S_k(f)| e^{j\phi_k(f)}$, reduces to

$$\chi_{ik}(t,\nu) = A_i |S_k(f_i)| e^{j[2\pi f_i t-\phi_k(fi)+\alpha_i]}, |t| \leq \frac{T_i+T_k}{2} \tag{2.16b}$$

where ν is the frequency-shift between the central frequencies of $s(\sigma)$ and $s_k(\sigma)$.

Comparing this relation with (2.13) shows that while the input interference undergoes a phase-shift $-\phi_k(f_i)$ and a processing gain $|S_k(f_i)|$, its duration is neither compressed nor expanded through processing.

Relation (2.16b) shows that the interference level at t=o (the sampling instant of the matched filter output) is given by $\chi_{ik}(o,\nu)$ where

$$\chi_{ik}(o,\nu) = A_i |S_k(f_i)| e^{j[\alpha_i-\phi_k(f_i)]} \tag{2.17}$$

This relation indicates that the interference level at t=o depends on the phase $[\alpha_i - \phi_k(f_i)]$ and cannot exceed $A_i|S_k(f_i)|$, the worst interference level. Making use of (2.17) and the fact that the value at t=o of the response resulting from passing the pulse compression signal through its matched filter is $\chi_{kk}(o,o)$ shows that

$$\text{Signal-to-interference amplitude ratio at t=o} = \frac{\chi_{kk}(o,o)}{\chi_{ik}(o,\nu)} \tag{2.18}$$

The value of this ratio determines the pulse compression signal performance against the assumed frequency-concentrated interference. The minimum value of this ratio needed to secure acceptable system performance can only be determined on an experimental basis.

It is convenient in the present case to write

$$\text{Interference power gain} \triangleq \frac{\text{maximum output interference power at t=o}}{\text{average input interference power}} \tag{2.19a}$$

The numerator in this relation is given by $A_i^2|S_k(fi)|^2$ according to (2.17) and the denominator is given by A_i^2 as can be seen from (2.13). Thus, (2.19a) reduces to

$$\text{Interference power gain} = |S_k(f_i)|^2 \tag{2.19b}$$

It is possible in the present case to make use of the terminology of Subsection 2.4.2 concerning the Gaussian noise case to write

$$\text{Input-output signal-to-interference ratio gain} \triangleq \frac{\text{signal power gain}}{\text{interference power gain}} \tag{2.20a}$$

Making use of (2.19b) and the fact that the signal power gain

is of the order of $F_k T_k$ according to (1.70), (2.20a) reduces to

$$\text{Input-output signal-to-interference ratio gain} \approx \frac{T_k F_k}{|S_k(f_i)|^2} \quad (2.20b)$$

Comparing (2.20b) with (2.9) shows that the pulse compression signal immunity to both AWGN and frequency-concentrated interference increases with its duration-bandwidth product. The minimum value of this product needed for acceptable performance can be determined on an experimental basis. However, the pulse compression signal performance does not depend on its spectrum $S_k(f)$ in the AWGN case but does depend on this spectrum in the frequency-concentrated interference case. In fact, (2.20b) implies that this performance improves as the maximum value of $|S_k(f)|$ decreases. Relation (2.20b) also indicates that if f_i is known, it is generally possible to reduce the effects of the frequency-concentrated interference by proper spectrum weighting at the receiver.

Relation (2.20b) also implies that unitary duration-bandwidth product narrowband signals (e.g. the familiar ASK, PSK and FSK signals) cannot be used to jam a spread spectrum pulse compression signal of large duration-bandwidth product. However, it can be seen that the reciprocal of (2.20b) is a measure of the efficiency with which a spread spectrum pulse compression signal can jam a narrowband signal. This efficiency increases with the duration-bandwidth product of the pulse compression signal.

The preceding results have been obtained for the case of an isolated frequency-concentrated interference which can be

modelled by $s_i(\sigma)$ of (2.13) whose amplitude A_i and phase α_i are both assumed to be constant at least over T_k. These results can also be extended to the case where many such interferences occur simultaneously. They can also be extended to the case of any frequency-concentrated interference with an arbitrary known form. This can be done by substituting this known form for $s_i(\sigma)$ in the derivations above. The extension of these results to the case where A_i and α_i are unstable or random over T_k is a more difficult problem which can be solved only by making use of statistical methods.

2.4.8 Time-Concentrated Interferences

A time-concentrated interference may be treated as the dual of a frequency-concentrated interference of the type considered in the previous subsection. While frequency-concentrated interferences can be dealt with by making use of spread spectrum pulse compression techniques, time-concentrated interferences can be dealt with by making use of spread duration pulse compression techniques.

It is obvious that a time-concentrated interference can only distort a pulse compression signal of spread duration. That is, such a signal can be used to combat impulse-like interferences including short term fading and isolated noise impulses. To show this, let the spread duration pulse compression signal, its duration and its bandwidth be denoted by $s_k(\sigma)$, T_k and F_k respectively. Let the time-concentrated interference, its duration and its bandwidth be denoted by $s_i(\sigma)$, T_i and F_i respectively (where $T_i << T_k$ and $T_iF_i \approx 1$). Such an interference

can be represented by a time-impulse. Let this impulse be centred at an instant which lies within T_k. According to Section 1.5, the output of the filter matched to $S_k(\sigma)$ in response to the interfering impulse $s_i(\sigma)$ is essentially $S_k^*(-\sigma)$. This implies that a time-concentrated interference undergoes duration expansion on passing through a filter matched to a spread duration pulse compression signal. This phenomenon is the opposite of that of duration compression considered in Section 1.7 and exhibited by the pulse compression signal itself when passed through its matched filter.

According to Section 1.7, the duration-compressibility associated with the perfect matched filtering of the pulse compression signal $s_k(\sigma)$ results in a processing power gain $\approx F_k T_k$. The same method used to prove this fact can also be used to show that the duration-expandability accompanying the processing of the time-concentrated interference $s_i(\sigma)$ by the filter matched to $s_k(\sigma)$ results in a processing power loss. This loss can be shown to be of the order of $F_k T_k$ on the assumption that the effective duration of $s_i(\sigma)$ is of the order of $\frac{1}{F_k}$ and that its processing power loss is given by the ratio: $\frac{\text{peak instantaneous input } s_i(\sigma) \text{ power}}{\text{mean output } s_i(\sigma) \text{ power}}$.

Thus, the processing signal-to-interference power ratio gain in the present case $\approx (F_k T_k)^2$. This indicates that pulse compression techniques are more capable of combating time-concentrated interferences than they are capable of combating AWGN and frequency-concentrated interferences where the processing power ratio gain is only of the order of $F_k T_k$.

2.4.9 Impulse Noise

The utility of pulse compression techniques for combating isolated frequency-concentrated and time-concentrated interferences has already been examined in the previous two subsections. The question now arises concerning the utility of these techniques for combating groups of such interferences. Most important in this respect is the impulse noise.

Impulse noise is usually unavoidable in practice. It is most serious in digital data transmission. It may introduce or destroy digits[7,25,120]. There are two known procedures for combating impulse noise. The first procedure makes use of error detection and correction coding techniques[7]. The second procedure makes use of modulation and signal design techniques. In this latter approach, the main problem is to develop a sufficiently realistic mathematical model of impulse noise. Such a model would clearly be statistical in nature and should account for the amplitudes, durations and time-distribution of impulses. Various models have been suggested in this respect[7,11,114,121,122].

In its simplest form, impulse noise can be modelled by a Gaussian process[11]. Here, impulse noise takes the form of a stream of approximately isolated statistically independent identical impulses of high mean temporal density. In this case, the central-limit theorem applies and impulse noise approaches Gaussian form. Pulse compression techniques are as efficient in combating this type of impulse noise as they are in combating Gaussian noise as was explained in Subsection 2.4.2.

The Gaussian model of impulse noise is not applicable in most practical situations. The fact that there is no universally acceptable impulse noise model makes it difficult to examine the performance of pulse compression techniques against this type of noise in any detail. In fact, some related work has been reported in this respect concerning the so-called smear-desmear techniques[7,114,123,124] which have often not performed in practice as expected in theory[7]. However, it is intuitively clear that pulse compression signals can generally be expected to excel over ordinary elementary signals in combating impulse noise although they cannot be expected to be as capable in this respect as they are capable of combating isolated impulses.

2.5 Free Space Data Transmission by Pulse Compression

Free space channels have been playing an increasingly important role in the fields of surface-surface, surface-space and space-space civil and military radio and satellite digital communications in the different frequency bands. These channels may be perturbed by a variety of man-made and natural system and channel disturbances such as imprecise synchronization, oscillator drifts and Doppler shifts, background noise, impulse noise, jamming, fading, interferences, and multipath echoes. These disturbances may result in envelope distortion, phase shifts and reduced phase coherence, and temporal and spectral overlapping of data signals which may lead to digit distortion or cancellation giving rise either to isolated errors or to bursts of errors of varying lengths.

Free space channel disturbances have been studied for a relatively long period of time and much effort is still being

devoted to analyzing, comparing and minimizing their effects, assuming different channel models and various data signal sets[6,10,23,40,100,124-128]. The principal design object in this respect is to reduce the effects of the different perturbations in such a way that the background noise becomes the main determinant of P_e. It can be seen from the previous section that it is generally easier to achieve this with large duration-bandwidth product pulse compression signals rather than with the unitary duration-bandwidth product ordinary narrowband signals. The so-called RAKE spread spectrum pulse compression techniques are the earliest known attempts in this field[5,108,129,130]. Since then, other pulse compression techniques (e.g. the LFM technique) have also been considered in this respect[98,100,107-110,131-137].

As was shown in the previous section, pulse compression techniques can solve the problem of temporal and spectral signal overlapping in general. This result may, for example, be applied to the case of temporal signal overlapping which results from multipath echoes that may be scattered off the ionosphere, land and sea. The occurrence of such echoes is usually enhanced by the fact that most free space applications make use of fixed omnidirectional or semi-directional aerials rather than steerable directional ones. Consider, for example, the case where two consecutive identical primary signals are received through the shortest direct path and an echo of the leading primary signal is received through a longer delayed path. Obviously, this situation may lead to fading through overlapping between the leading primary signal and its echo

or to intersymbol interference through overlapping between this echo and the lagging primary signal. In order to minimize the effects of this kind of fading and intersymbol interference and, hence, to enhance correct detection, the echo (whose amplitude is generally lower than that of the corresponding primary signal) must be resolvable from both primary signals. Assuming a signal of duration T and bandwidth F and making use of (2.12) show that the echo will be resolvable from the leading primary signal if

$$\text{Minimum multipath differential delay} > T_r \tag{2.21}$$

where T_r is the effective duration of the temporal autocorrelation function (i.e. the matched filter response) of the signal under consideration.

Making use of the fact that $T_r \approx \frac{1}{F}$, relation (2.21) shows that a spread spectrum pulse compression signal is generally superior to an ordinary narrowband signal from the viewpoint of resolving a primary signal from its echo received with minimum multipath differential delay.

Again, making use of (2.12) shows that the echo will be resolvable from the lagging primary signal and will not be detected as if it were an actually transmitted signal if

$$\text{Transmitted pulse repetition period} > \text{Maximum multipath differential delay} + T_r \tag{2.22}$$

This relation imposes an upper bound on the maximum possible transmission rate. It indicates that this rate

decreases with the maximum multipath differential delay and increases with signal bandwidth (since $F \approx \frac{1}{T_r}$). It also indicates that a spread spectrum pulse compression signal is generally superior to an ordinary narrowband signal from the viewpoint of resolving the lagging primary signal from the echo of the leading signal and rejecting this echo as an actually transmitted signal.

It can be seen that if both (2.21) and (2.22) are satisfied and if well-synchronized and gated sampling of the matched filter output takes place every transmission period, the demodulator will only detect the two primary signals and will ignore the echo. It can also be seen from these two relations that a spread spectrum pulse compression signal generally has a more effective echo rejection capability than an ordinary narrowband signal.

2.6 Basic Pulse Compression Communication Systems[98,107-110]

A digital pulse compression communication system makes use of a pulse compression modulator signal set (or transmitter signature). Most basic in this respect are the FM, Time-Hopping (TH), Direct Sequence (DS) and Frequency-Hopping (FH) systems which, respectively, employ FM, TH, DS and FH pulse compression modulator signal sets (see Subsection 2.1.2). A usually Pseudo Noise (PN) digital code with a rate >> data rate is used to control the discrete shifting of the TH signal amplitude (between the levels 1 and 0) in the TH system, the DS signal phase in the DS system and the FH signal frequency in the FH system. This PN code should also have the proper qualities concerning its linearity or nonlinearity, correlation

properties, length, rate and implementability, depending on the particular application under consideration.

The basic FM, TH, DS and FH digital pulse compression communication systems are all Spread Spectrum (SS) systems in the sense that each employs an RF signal transmission bandwidth which is: (i) significantly exceeding (e.g. at least 10 times) the data signal bandwidth, and (ii) relatively independent of the data signal. Usually, the choice of this RF transmission bandwidth is based on such factors as the desired SS-system capabilities, the available bandwidth and the transmission characteristics of the propagation medium.

A digital SS-communication system may be implemented in a variety of ways making use of the signal generation-processing techniques described in Section 2.3. However, the actual mechanization of the transmitter and receiver in such a system obviously depends on the type of its SS-modulator signal set and the related practical considerations. In any case, it should be noted here that AM is not usually used in most practical digital SS-communication systems. This is mainly due to the facts given in Subsection 2.2.1 and the fact that AM generally implies the transmission of a large peak power, easily observable signal instead of a constant power one with low detectability. Thus, SS-transmitters are normally operated at constant power levels. The only exception to this is the TH transmitter which is turned on and off by the keying PN code under the constant power constraint.

The general pulse compression properties and advantages outlined eariler in this chapter are shared by the various SS-techniques. This does not imply, however, that all these techniques are absolutely equivalent. In fact, each technique is characterized by its own capabilities and, thus, may only excel in certain practical situations. It is frequently necessary to employ a hybrid SS-technique combining two or more of the four basic SS-techniques. Hybrid SS-techniques generally extend the usefulness of the basic SS-techniques. They also may enhance system implementation[108].

An FM signal may, for example, be viewed as a limiting case of an FH signal in which the frequency is hopped according to the prescribed FM law. Thus, the FM law of an analogue coded FM signal lacks the arbitrariness and large number of degrees of coding freedom associated with the keying SS-code of the discrete coded TH, DS and FH signals. This implies that while the figure of merit of an FM signal is determined by its duration-bandwidth product, the figure of merit of a TH, DS or FH signal is determined by its duration-bandwidth product along with the quality of its SS-code. This also implies that FM signal generation/modulation and processing differ from the generation/modulation and processing of TH, DS and FH signals from the viewpoint of simplicity, flexibility and methods of realization. This also implies that the transmitter-receiver synchronization in an FM system may be mainly confined to carrier frequency and phase acquisition and tracking and does not involve the additional more complicated problem of SS-code and code-clock acquisition

and tracking characteristic of TH, DS and FH SS-systems. Moreover, this implies that the FM SS-technique is generally less capable than the TH, DS and FH SS-techniques from the point of view of enhancing communication privacy and, hence, immunity to hostile measures. In fact, only the discrete coded signal SS-techniques can employ cryptographically secure SS-codes (see Subsection 2.4.4) or coincident data and SS-code clocks (in such a way that the data cannot be read by a receiver having no prior knowledge of the SS-code). Nevertheless, this deficiency of the FM SS-technique can be minimized, at least in principle, by making use of the FH/FM hybrid SS-technique in which the starting frequency of an FM SS-signal is keyed by a PN code. The DS/FM hybrid SS-technique (in which the initial phase of an FM SS-signal is keyed by a PN-code) is not similarly useful in this respect, although it can improve the interference rejection capability of the FM SS-technique[108].

The TH SS-technique is characterized by the simplicity of generating the transmitted signal and is good for ranging and Time-Division Multiplexing (TDM). TH SS-signalling is vulnerable to tone jamming which is transmitted at the TH signal centre frequency, either continuously or according to the TH SS-code. This explains why the TH SS-technique is frequently replaced by the FH/TH hybrid SS-technique in which the SS-code controls both the transmitted frequency and the time of transmission. The TH SS-technique may also be combined with the DS SS-technique to form a TH/DS hybrid SS-technique employing a time-hopped DS signal. The FH/TH and TH/DS techniques can both be used to aid in traffic control and

in reducing the near-far problem in DS multiplex systems (see next section).

The coherent DS SS-technique is the most studied and widely used SS-technique. It is usually the standard against which all other SS-techniques are measured. DS SS-systems are vulnerable to frequency-concentrated interferences. According to (2.20b), this vulnerability depends on the intereference level and frequency and decreases with the employed signal duration-bandwidth product (i.e. with the SS-code length). DS SS-systems are more complex than FM SS-systems and simpler than FH SS-systems. The DS SS-technique may be combined with the FH SS-technique by hopping the centre frequency of a DS signal. The resulting FH/DS hybrid SS-technique is relatively easier to implement than either the DS or the FH SS-techniques and can be used to achieve higher spectrum-spreading and discrete address capabilities and to reduce the near-far problem in DS multiplex systems.

The usually noncoherent FH SS-technique employs a frequency synthesizer driven by an SS-code generator. FH SS-systems are becoming increasingly practicable as improved, small, light, stable, inexpensive and rapid- response and switching frequency synthesizers, which are capable of generating thousands of reasonably discrete frequency choices, become available. The FH SS-technique is generally immune to frequency-concentrated measures and interferences. It is however, vulnerable to relatively strong multitone interferences which have partially or completely identical spectral structures. Also, this technique usually suffers from the unavoidable Doppler and drift frequency-shifts and from phase-shifts accompanying the frequency-hopping action.

2.7 Multiple-Access Pulse Compression Systems

The problems of improving multiple-access techniques and of reducing redundant information by data compression are becoming increasingly important as the demand increases for both higher communication capacity and quality with minimum electromagnetic compatibility complications of both intersystem and intrasystem interferences[138,139]. Accordingly, this section gives a brief and basic account of the problem of multiple-access in general, and of the problem of multiple-access by pulse compression in particular.

The choice of a specific signal set for a particular multiple-access application is usually based on both practical and theoretical considerations. Theoretically, the necessary and sufficient condition for signals transmitted simultaneously over a common linear channel to be completely separable through linear operations in the receiver is that every one of these signals belongs to one unique signal set which is itself a member of a family of linearly separable signal sets. Two signal sets are said to be linearly separable if: (i) each one of them is linear in the sense that it contains every finite linear combination of its elements, and (ii) the two sets are mutually disjoint in the sense that they do not share a common element except the null signal[140].

The linear separability of signal sets may be based on their respective disjoint locations along the time-axis,

on their respective disjoint locations along the frequency-axis or on their respective structures. The first case corresponds to Time-Division Multiplexing (TDM), the second case to Frequency-Division Multiplexing (FDM) and the third case to the so-called Structural Multiplexing (SM). TDM generally requires time regulation and buffers. FDM generally requires frequency regulation and buffers. SM obviously permits temporal and spectral signal overlapping and, thus, may not need time and frequency regulation or may only need minimal such regulation. The former case corresponds to the so-called "random-access SM", where signals are transmitted asynchronously through the common channel in a statistically random manner. The latter case corresponds to the so-called "organized SM". Compared to TDM and FDM, SM is generally more flexible and efficient from the viewpoint of channel loading and utilization.

Consider an arbitrary family of linearly separable signal sets and let only one signal be selected from each of these sets. The number of such selected signals that can be transmitted simultaneously over a particular linear channel and completely separated through linear operations in the receiver cannot exceed an upper maximum limit which is determined by the prevailing conditions. However, it is possible to exceed this limit in two ways[139]: (i) by allowing the linearly separable signal sets (from which the transmitted signals are selected) to exhibit some degree of mutual linear inseparability (whereby the transmitted signals

will exhibit some practically tolerable degree of mutual interference), and (ii) by adopting nonlinear processing techniques in place of linear processing techniques. In any case, there is always an upper bound on the amount of information that can be transmitted over a given channel during a given time and recovered with arbitrarily small error in the receiver. For example, the maximum amount of information that can be transmitted in a time T in the form of a completely unpredictable sequence of independent bits over an AWGN channel of bandwidth F (and recovered with an arbitrarily high reliability in the receiver) cannot exceed Shannon's bound of CT bits, C is the channel capacity given by[61]

$$C = F \log_2(1 + p/N_o F) \text{ bit/sec} \tag{2.23}$$

where p is the total transmitted signal power and N_o is the one-sided noise spectral power density.

Relation (2.23) states the general conditions for reliable multiplex transmission in an AWGN background. It implies that this transmission is possible only when the bandwidth F of the channel exceeds that of the signals to be transmitted or when the signal-to-noise ratio $p/N_o F$ exceeds that required for reliable signal reconstruction in the receiver.

Consider the class of linearly independent signals and let each one of these signals be associated with the signal

set that comprises all the signals which are linearly dependent on it. It can be seen that the resulting signal sets are linearly separable. Again, consider the signal space which accommodates all signals sharing a common bandwidth F and a common duration T. It can be seen that this space is a 2FT - dimensional space which can accommodate a maximum of 2FT linearly independent signals which span it[72]. These facts imply that the maximum number of linearly independent signals that can be transmitted simultaneously during a time T over a common linear channel of bandwidth F (and are completely separable by linear operations in the receiver) is 2FT. This maximum number of 2FT signals can convey a maximum total of $2FT\log_2 L$ bits (i.e. each signal can convey a maximum of $\log_2 L$ bits) if the receiver is capable of distinguishing L signal-levels under the prevailing conditions. This result checks with the Nyquist expression which gives the maximum amount of information that can be conveyed by sequentially transmitting 2FT different voltages (or other symbols) over a noiseless channel of bandwidth F at a rate of 2F voltages per second (in the form of a signal of duration T and bandwidth F) and making use of a receiver capable of distinguishing L voltage-levels[25,139].

Orthogonality (see (1.16)) is the most common form of linear independence usually adopted in practical multiple-access systems such as the TDM, FDM and orthogonal SM systems. In TDM[23], signal orthogonality is based on

disjoint signal location along the time-axis. In FDM[23], signal orthogonality is based on disjoint signal location along the frequency-axis. In orthogonal SM, signal orthogonality is based on signal structure rather than signal location along the time- and frequency- axes. Many structurally orthogonal signal sets have been reported in this respect[72, 141].

Strict signal orthogonality cannot be achieved in practice for both theoretical and practical reasons. Thus, multiplexing with a set of supposedly orthogonal signals usually reduces to multiplexing with a signal set whose members are quasi-orthogonal, exhibiting some mutual interference. This interference increases with, and does therefore limit, the ratio between the number of the simultaneous active users of the multiplex system and the total number of subscribers.

An SM multiplex system can, for example, make use of a set of pulse compression signals each of which belongs to a unique member of a family of signal sets which are structurally linearly separable in a strict or an approximate sense. Such a pulse compression signal set may consist of signals that are strictly or approximately structurally linearly independent (e.g. orthogonal or quasi-orthogonal). A pulse compression SM system which makes use of a set of spread spectrum pulse compression signals that share the same common bandwidth is usually described as a Spread Spectrum Multiplex (SSM) system.

It has been shown that in an AWGN background, the linear correlation predetection processing techniques are optimum for signal separation in the receiver. It has also been shown that these techniques are most efficient in the case of pulse compression signals. These facts imply that in addition to its superior structural multiplexing and simultaneous random-access capabilities, a pulse compression SM multiplex system using correlation predetection processing techniques also has the following advantages:

(i) Like any other pulse compression communication system, this multiplex system has the properties outlined earlier in this chapter . For example, this multiplex system is capable of minimum temporal and spectral power-density signalling as well as of combating such phenomena as additive Gaussian noise, impulse noise, temporal and spectral signal overlapping, echoes, interferences and hostile detection (for the purposes of eavesdropping, jamming or interception).

(ii) Every subscriber in this multiplex system has his own unique subset of correlation processors. Each of these processors can optimally process only one particular pulse compression signal and suppresses, or rejects, all other signals and interferences. This implies that in this multiplex system, every subscriber is characterized by his own unique pulse

compression signal subset which must be used by the other subscribers in addressing and communicating with him. These facts imply that the organization of this multiplex system can be based on appropriate signal allocation and that this system has secure and antispoof communication capabilities.

The fact that the pulse compression signal subset assigned to each subscriber in an SM multiplex system forms his characteristic address implies that this system belongs to the general class of Code-Division Mulitplex (CDM) systems where each subscriber is characterized by his own unique address[142]. CDM systems also include the class of the so-called Multiple-Access Discrete Address (MADA) systems which may be Random-Access Discrete Address (RADA) or Self-Organizing Multiple-Access Discrete Address (SOMADA) systems[143].

(iii) A pulse compression signal is characterized by a large duration-bandwidth product and, hence, by a large number of degrees of freedom. This implies that it is possible to construct a set of a relatively large number of pulse compression signals of acceptable auto- and cross-correlation properties by applying a proper parameter selection scheme to a given generic pulse compression signal. Such

a pulse compression signal set can obviously be used for structural multiplexing between a correspondingly large number of active subscribers. Pulse compression signals are superior in this respect to the unitary duration-bandwidth product signals in common use such as the ASK, PSK and FSK signals.

The pulse compression multiple-access techniques in general, and the spread spectrum multiple-access techniques in particular, seem to be promising candidates for a variety of military and commercial applications by making use of the existing guided and radio channels in the different regions of the electromagnetic spectrum. These applications include, for example, rural telephony, air traffic control, multi-user computer communication networks and mobile and satellite multiple-access communication systems. Some progress has recently been, and continues to be, made in this direction[98, 107-110, 144]. However, many theoretical and practical problems are still either undefined or unsolved in this respect[27,98,107-110,144]. These problems include those problems which are common to all pulse compression communications applications and which are outlined in the following section. They also include those particular problems which are associated with pulse compression multiplex system implementation, channel allocation and bandwidth requirements, peaceful coexistence with the conventional multiplex systems, cost, operation, control,

active loading efficiency, possible billing difficulties and reliability and performance analysis with or without information and/or pulse compression signal coding in the presence of disturbances which can be defined or which lack a known characterization (including the multiplex system so-called near-far self-jamming).

2.8 Conclusions and Comments[98,107-110]

It can be seen from the preceding brief discussion that the large duration-bandwidth product pulse compression signals are theoretically superior in many ways to the unitary duration-bandwidth product signals such as the ASK, PSK and FSK signals. The full utilization of this superiority in practice requires, however, tackling the many heretofore unformulated or unsolved theoretical and practical problems related to the design, generation, transmission, channel requirements, processing and applications of pulse compression signals. Much effort is still needed to tackle such problems and to develop new devices which are compatible with pulse compression techniques. Moreover, the associated problem of terminology and system standardization has to be considered along with that of operator and maintenance personnel training. This would make it possible to realize and popularize the potential use and capabilities of pulse compression communication systems.

Though the basic pulse compression concepts have been known to workers in radar since World War II, the subject

of communication by pulse compression is only about 15 years old and only recently has enjoyed some publicity. This is mainly due to: (i) the fact that pulse compression techniques and applications have mostly been classified and confined to the defence community, and (ii) the fact that the implementation of pulse compression communication systems required an advanced technology which was generally either unattainable or not feasible for commercial purposes.

The recent increasing publicity of the subject of communication by pulse compression is probably due to: (i) the attractive potential capabilities of pulse compression techniques for commercial as well as military multiple-access applications, and (ii) the recent technological achievements brought about by microminiaturization, LSI, SAW and CCD techniques. Such achievements are making and continue to make pulse compression system implementation simpler and more compact and feasible.

Although much information has been published in both the West and East on the subject of communication by pulse compression, much remains classified and unknown in this respect. The published work is mainly concerned with the still challenging theoretical and practical problems related to:

(i) The design, generation, transmission and processing of large duration-bandwidth pulse compression signals in general, and the phase-shift coded and frequency-shift coded spread spectrum signals in particular.

(ii) The immunity of pulse compression communication systems, in both isolated and dense environments, to hostile detection, eavesdropping, interception and jamming as well as to known and unknown time-variant and invariant interferences which are structurally related or unrelated to the employed pulse compression signals.

(iii) The possible improvement of the pulse compression communication system performance by making use of information and/or signal coding techniques.

(iv) The guided and radio channels that can be used for different purposes for data transmission by pulse compression, either exclusively or otherwise, in such a way that pulse compression systems can coexist with the conventional systems without seriously interfering with them or degrading their performance.

(v) The potential commercial and military applications of pulse compression for data transmission (e.g. privacy antijam, antimultipath, anti-intercept, minimum power-density, satellite, navigation, interference-immune, discrete address and multiple-access signalling).

(vi) The synchronization techniques involving rapid pulse compression code, frequency and phase acquisition and tracking.

(vii) The implementation of pulse compression communication

systems and the devices required for this purpose.

Pulse compression techniques in general, and spread spectrum techniques in particular, cannot be expected to solve every problem and are not always best for every application. They represent, however, a new approach and often provide capabilities which are not shared by the older, conventional, techniques. They must be considered whenever they are advantageous.

Much effort is being spent in the field of communication by pulse compression. As a modest contribution to this effort, the following chapters investigate some of the problems associated with the utilization of the linear FM pulse compression technique for digital data transmission.

3

DATA TRANSMISSION BY LINEAR FM PULSE COMPRESSION

This chapter includes a systematic study of the candidacy of the class of Linear LFM signals for digital data transmission. It formulates the correlation properties of this class of signals and exploits these properties mainly to establish its signal design and performance criteria. The results are obtained for the case of analogue signal generation and processing and may be extended to the digital case.

3.1 Introduction

This section introduces the Linear FM (LFM) signal in general, and the LFM signal with rectangular envelope (the chirp signal) in particular.

3.1.1 The Linear FM Signal[46,66,113]

The linear FM signal may be "active" or "passive" depending on whether it is generated actively or passively (see Section 2.2). Since the active and passive forms of a given signal may be treated as duals, it is enough to confine the present discussion to the case of the active linear FM signal.

A set of N real LFM signals may be expressed in the general form (see (1.10))

$$x_\ell(\sigma) = a_\ell(\sigma)\cos\theta_\ell(\sigma), \qquad |\sigma| \leq \frac{T_\ell}{2},\ \ell=1,\ldots,N$$
$$= 0, |\sigma| > \frac{T_\ell}{2},\ \ell=1,\ldots,N \tag{3.1}$$

In this relation, σ indicates time and $x_\ell(\sigma)$ is the ℓth real LFM signal whose duration, envelope and phase-function are T_ℓ, $a_\ell(\sigma)$ and $\theta_\ell(\sigma)$ respectively. Also, $a_\ell(\sigma)$ is assumed to be real and even in σ and $\theta_\ell(\sigma)$ is assumed to have the real parabolic form

$$\theta_\ell(\sigma) \triangleq \alpha_\ell + 2\pi f_\ell \sigma + \pi\mu_\ell\sigma^2 \tag{3.2}$$

In this relation, α_ℓ is the phase of $x_\ell(\sigma)$, f_ℓ is its mean frequency and μ_ℓ is the slope of the straight line representing the relationship between its instantaneous frequency $f^{\ell}_{inst}(\sigma)$ and time, where

$$f^{\ell}_{inst}(\sigma) \triangleq \frac{1}{2\pi}\frac{d\theta_\ell(\sigma)}{d\sigma} = f_\ell + \mu_\ell\sigma \qquad (3.3a)$$

This linear FM law is depicted in Fig. 3.1 where it is assumed that μ_ℓ is expressed as

$$\mu_\ell \triangleq \frac{W_\ell}{T_\ell} \qquad (3.3b)$$

in which W_ℓ is the frequency sweep over the signal duration, i.e.

$$W_\ell = f^{\ell}_{inst}(\frac{T_\ell}{2}) - f^{\ell}_{inst}(-\frac{T_\ell}{2}) \qquad (3.3c)$$

This relation implies that a positive W_ℓ (or μ_ℓ) corresponds to a frequency up - sweep and a negative W_ℓ (or μ_ℓ) to a frequency down - sweep.

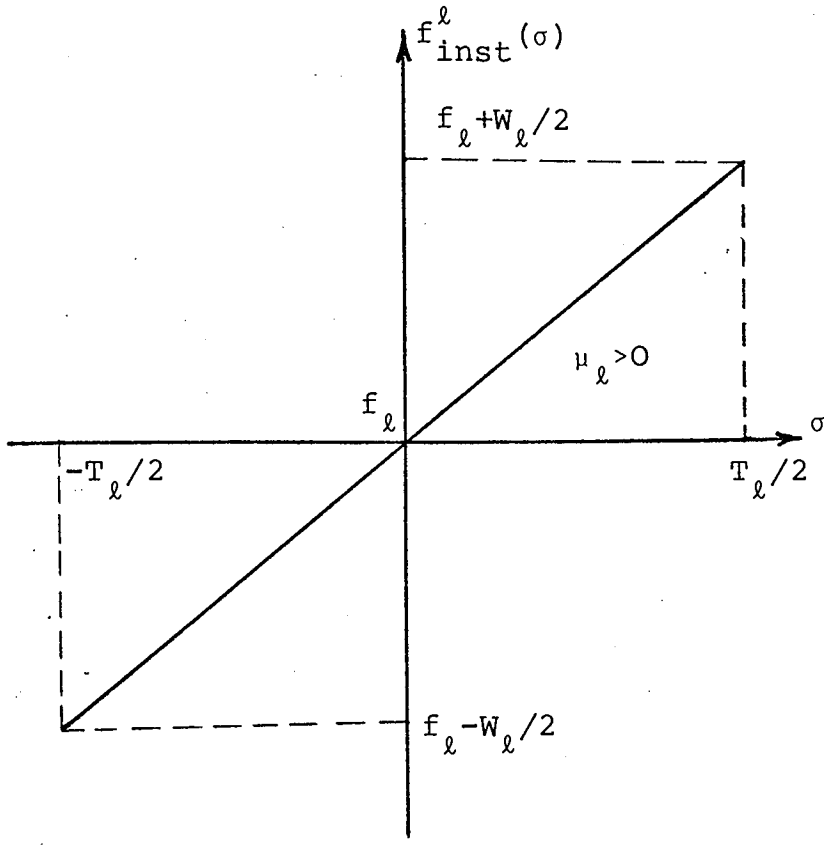

Fig. 3.1 The Linear FM Law

3.1.2. Basic Properties of the LFM Signal

Denoting the number of cycles within $x_\ell(\sigma)$ by n_ℓ and making use of (3.3a) shows that

$$n_\ell = \int_{-T_\ell/2}^{T_\ell/2} f^{\ell}_{inst}(\sigma)\,d\sigma = f_\ell T_\ell \tag{3.4}$$

which indicates that the number of cycles in a LFM pulse is given by the product of its mean frequency and duration.

It is mathematically more convenient to study the real LFM signal set of (3.1) through the following complex LFM

signal set

$$y_\ell(\sigma) = a_\ell(\sigma)e^{j\theta_\ell(\sigma)}, \quad |\sigma| \leq \frac{T_\ell}{2}, \ \ell=1,\ldots,N$$
$$= 0, \quad |\sigma| > \frac{T_\ell}{2}, \ \ell=1,\ldots N \tag{3.5}$$

which implies that

$$x_\ell(\sigma) = \frac{1}{2}\left[y_\ell(\sigma) + y_\ell^*(\sigma)\right] \tag{3.6}$$

and, according to Appendix A, that $y_\ell(\sigma)$ is the exponential complex representation of $x_\ell(\sigma)$.

The spectrum $Y_\ell(f)$ of $y_\ell(\sigma)$ cannot be found unless the exact form of $a_\ell(\sigma)$ is specified. However, it is possible to obtain a fairly accurate expression of $Y_\ell(f)$, for any arbitrary $a_\ell(\sigma)$, in the practically important case where $|W_\ell T_\ell| >> 1$ (e.g $|W_\ell T_\ell| \geq 25$). In this case, making use of (B.9) shows that

$$Y_\ell(f) \approx \frac{a_\ell\left(\frac{f-f_\ell}{\mu_\ell}\right)}{|\mu_\ell|^{\frac{1}{2}}} e^{j\left(\alpha_\ell \pm \frac{\pi}{4} - \frac{\pi(f-f_\ell)^2}{\mu_\ell}\right)}, \quad |f-f_\ell| \leq \frac{|W_\ell|}{2}$$
$$\approx 0, \quad |f-f_\ell| > \frac{|W_\ell|}{2} \tag{3.7}$$

where $\frac{\pi}{4}$ and $-\frac{\pi}{4}$ in the exponent correspond to the two cases where $\mu_\ell > 0$ and $\mu_\ell < 0$ respectively.

Relations (3.5) and (3.7) show that

(i) For $|W_\ell T_\ell| >> 1$, the spectrum $Y_\ell(f)$ of the strictly duration-limited LFM signal $y_\ell(\sigma)$ is effectively limited to the f-range $(f_\ell - \frac{|W_\ell|}{2}, f_\ell + \frac{|W_\ell|}{2})$, which is the same range scanned by $f^\ell_{inst}(\sigma)$ over the duration of $y_\ell(\sigma)$ (see Subsection 2.1.1). Thus, $y_\ell(\sigma)$ has a bandwidth $\tilde{\sim}|W_\ell|$. This indicates that for $|W_\ell T_\ell| >> 1$, the LFM signal can be adapted to make efficient use of any available bandwidth (e.g. an audio channel[145]).

(ii) For $|W_\ell T_\ell| >> 1$, $a_\ell(\sigma)$ and $|Y_\ell(f)|$ have the same functional form. Moreover, the phase function of $y_\ell(\sigma)$ is quadratic in σ and the phase function of $Y_\ell(f)$ is quadratic in f. These facts show that the LFM signal is symmetric in time and frequency. This characteristic LFM property makes it relatively easy to handle the LFM signal in theory and practice and to study its dual properties in both domains. It also makes it relatively easy to tackle, for example, the design, weighting and processing problems associated with the LFM signal.

(iii) For $|W_\ell T_\ell| >> 1$, the LFM signal also has a linear "group delay/frequency characteristic" $\sigma^\ell_g(f)$ which may be obtained from (3.7) as

$$\sigma^\ell_g(f) = \frac{f-f_\ell}{\mu_\ell}, \quad |f-f_\ell| \leq \frac{|W_\ell|}{2} \tag{3.8}$$

This relation and (3.3a) indicate that $\sigma^\ell_g(f)$ and $f^\ell_{inst}(\sigma)$ are inverse functions of each other (See (B.11)). Relation (3.8) also implies that the LFM matched filter

is essentially a linear dispersive delay line (see (1.64)). This indicates that the LFM matched filter is generally easier to realize than those of other pulse compression signals.

(iv) The LFM t-ν coupling law is the law relating t and ν on the geometrical locus of the main peak of the two-dimensional correlation function $\chi_{\ell\ell}(t,\nu)$ of $y_\ell(\sigma)$. As a result of LFM symmetry in time and frequency, this law is linear in both t and ν and may be expressed as $\mu_\ell t + \nu = 0$ (See Section 3.2). This law implies that a ν-shift in the mean frequency f_ℓ of $y_\ell(\sigma)$ translates the $y_\ell(\sigma)$ matched filter response in time from t=0 to t= $-\frac{\nu}{\mu_\ell}$. The t-shifted response is usually distorted. However, the resulting distortions decrease with $|W_\ell/\nu|$ and are negligible for $|\nu| << |W_\ell|$. They also may be compensated for, within certain limits and at some cost of SNR_o-degradation, by making the matched filter bandwidth > input LFM signal bandwidth ($\tilde{\simeq}|W_\ell|$ if $|W_\ell T_\ell| >> 1$) in such a way as to accommodate the largest expected ν-shift of this signal. Thus, it can be stated that a relatively small ν-shift in f_ℓ simply translates the matched filter response of $y_\ell(\sigma)$ in time from t=0 to t= $-\frac{\nu}{\mu_\ell}$. This is a characteristic LFM property which implies that

(a) Without any need for additional complex correcting circuitry, the optimality with which a matched filter processes its LFM signal $y_\ell(\sigma)$ exhibits only minimal

sensitivity to channel (e.g. Doppler) and systematic (e.g. oscillator instability) ν-shifts as long as $|\nu| << |W_{\ell}|$. Firstly, this implies that the LFM technique is advantageous for data transmission over channels where ν-shifts are common (e.g. radio links involving moving terminals). Secondly, this implies that the LFM communication system is unique in that the receiver may be operated asynchronously with minimal degradation in its performance (whereas a system such as the DS system always requires precise code, code-clock and carrier frequency and phase acquisition and tracking). Thirdly, this implies that the LFM communication system is, for example, superior to a narrowband FSK system whose performance deteriorates even for very small ν-shifts[145].

(b) A single matched filter can be used for the processing of different ν-shifted versions of the LFM signal matched to this filter as long as the various ν-shifts can be tracked and can lead only to practically tolerable response distortions. In this case, the LFM matched filter acts as a spectrum analyzer transforming the ν-shifted input LFM signals into corresponding t-shifted responses. This characteristic LFM property has been utilized in such communications applications as the transmission of analogue information signals by the Pulse Amplitude Modulation FM (PAM-FM) method[146], spectrum analysis[146], binary and M'ary FSK signal detection[147,148], frequency acquisition[21] and digital data transmission

using spectrum-overlapping LFM signals in order to achieve higher transmission rates under bandwidth constraints[149,150]. On the one hand, this property makes the LFM system considerably simpler and cheaper than other pulse compression systems where a bank of matched filters (correlators) is usually needed because every ν-shifted (t-shifted) version of the same non-LFM signal requires its own matched filter (correlator) in order to avoid intolerable response distortions [66,70]. On the other hand, this property complicates the problem of simultaneous range/range-rate resolution in a LFM radar system[66,115]. This LFM deficiency can be removed by transmitting two similar consecutive LFM pulses with reversed slopes instead of a single LFM pulse[151]. However, this method can be used only in the case where a single target is involved and the pulse repetition rate is so high that the target range-rate does not change noticeably between two consecutive pulses.

The importance of the LFM signal stems from the above-mentioned as well as the following facts:

(v) LFM communication systems can be implemented with circuitry well within the state-of-the-art, exploiting a wealth of experience gained in sonar and radar. They are typical of all pulse compression communication systems and have the general properties, limitations, capabilities and fields of application outlined in

Chapter 2. In fact, communication systems employing FM signals in general, and LFM signals in particular, are relatively simpler, easier to synchronize and implement, cheaper and (in case of successful hostile detection) less capable of enhancing privacy than those systems which employ discrete coded pulse compression signals (e.g. DS, FH and TH signals). LFM capability of enhancing communication privacy can be improved, however, by making use of secure information codes and variable data rates. It can also be improved by employing such hybrid techniques as the FH/LFM technique, whereby the starting frequency of the LFM signal is hopped according to a secure code.

(vi) It was mentioned in Subsection 2.2.2 that the same matched filter can be used for both the generation and optimum processing of a certain category of signals by making use of sideband inversion prior to optimum processing. A typical example of such signals is the LFM signal[66,151] which is also characterized by the additional advantage that the same matched filter can, within certain limits, handle many of its ν-shifted versions.

(vii) The progressive pulse compression processing techniques described in Subsection 1.7.3 are most relevant in the case of the LFM signal. This is due to the linearity of the FM and group delay laws of this signal as well as to the fact that a single matched filter can, within

certain limits, process many of its ν-shifted versions. The implementation of the progressive pulse compression processing techniques is substantially more difficult in the case of other pulse compression signals, where a bank of processors is needed for the optimum predetection processing of the ν-shifted versions of the same signal.

(viii) Both the FSK and PSK signals can be obtained from the LFM signal by putting $\mu_\ell=0$. This implies that the FSK and PSK signal theories can be seen as two special cases of the LFM signal theory.

(ix) A phase-shift (frequency-shift) coded pulse compression signal may be viewed as a phase-quantized (frequency-quantized) version of a corresponding FM signal. Moreover, any nonlinear FM law may be approximated by a sequence of disjoint linear FM segments[66]. These facts imply that the LFM theory may in principle be extended to the case of phase-shift coded signals, frequency-shift coded signals and nonlinear FM signals, which are generally more difficult to handle, both in theory and in practice. Thus, the LFM signal is not only the basic FM pulse compression signal, but is also basic to the concept of pulse compression in general. A thorough understanding of the LFM pulse compression theory provides a better insight into the problems associated with the other more involved forms of pulse compression.

3.1.3 The Chirp Signal

The present work is mainly concerned with the LFM signal with rectangular envelope. This signal will be conveniently called the "chirp" signal in this work. The name "chirp" was first introduced by B. M. Oliver (now vice-president, Hewlett-Packard Co.) in 1951 in an internal Bell Telephone Laboratories memorandum, probably because the sound effect of an audio LFM signal bears a resemblance to a sound heard in nature. Oliver's words, "Not with a Bang, but a Chirp", referred to a new radar LFM pulse compression technique which has both high range and high range-resolution capabilities. Bell Laboratories were then involved in some of the earliest efforts concerning the development of pulse compression radars[152].

The real chirp signal set corresponding to the real shaped LFM signal set of (3.1) may be expressed as

$$r_\ell(\sigma) = A_\ell R_{T_\ell}(\sigma)\cos\theta_\ell(\sigma), \quad \ell=1,\ldots,N \tag{3.9}$$

where $r_\ell(\sigma)$ is the ℓth real chirp signal (see Fig. 3.2), A_ℓ is an arbitrary real constant, $R_{T_\ell}(.)$ is the real Rect function defined by (2.14) and $\theta_\ell(\sigma)$ is given by (3.2).

Again, it is mathematically more convenient to study the real chirp signal set of (3.9) through the following complex chirp signal set

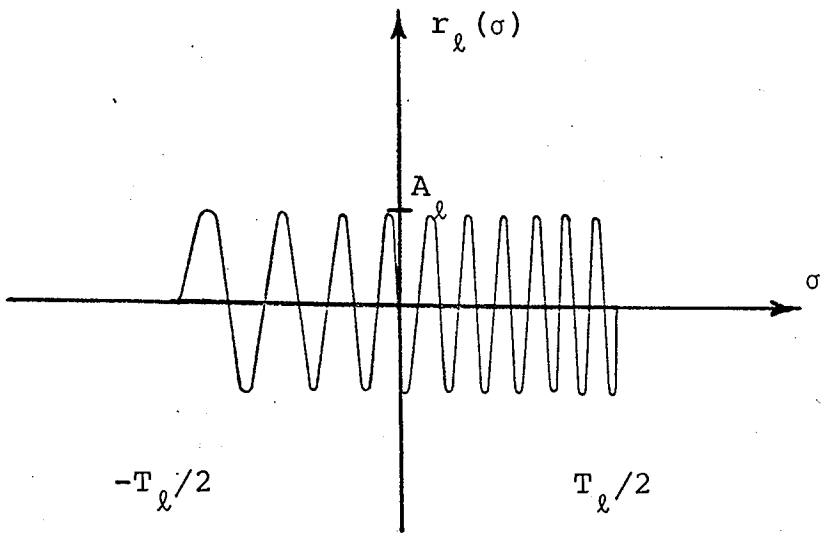

Fig. 3.2 The Chirp Signal ($\mu_\ell > 0$)

$$s_\ell(\sigma) = A_\ell R_{T_\ell}(\sigma) e^{j\theta_\ell(\sigma)}, \qquad \ell = 1, \ldots, N \tag{3.10}$$

which corresponds to the complex shaped LFM signal set of (3.5).

Making use of (3.7) shows that for $|W_\ell T_\ell| >> 1$, the chirp $s_\ell(\sigma)$ has a nearly rectangular spectrum $S_\ell(f)$ given by

$$S_\ell(f) \simeq \frac{A_\ell}{|\mu_\ell|^{\frac{1}{2}}} R_{|W_\ell|}(f-f_\ell) e^{j(\alpha_\ell \pm \frac{\pi}{4} - \frac{\pi(f-f_\ell)^2}{\mu_\ell})} \tag{3.11}$$

where $\frac{\pi}{4}$ and $-\frac{\pi}{4}$ in the exponent correspond to the two cases where $\mu_\ell > 0$ and $\mu_\ell < 0$ respectively.

Denoting the energy of $s_\ell(\sigma)$ by $2E_\ell$, one has

$$2E_\ell \triangleq \int_{T_\ell} |s(\sigma)|^2 d\sigma = A_\ell^2 T_\ell \tag{3.12}$$

which implies that E_ℓ is the energy of the real chirp $r_\ell(\sigma)$ of (3.9).

Numerically integrating the relation $2E_\ell \triangleq \int_{-\infty}^{+\infty} |S_\ell(f)|^2 df$ shows that, for $|W_\ell T_\ell| \geq 10$, the chirp signal energy is effectively confined to the f-range $(f_\ell - |W_\ell|/2,\ f_\ell + |W_\ell|/2)$ and that the small energy portion lying outside this range decreases with $|W_\ell T_\ell|$[152].

As a LFM signal, the chirp signal shares the properties and capabilities outlined in the preceding subsection. The chirp signal also has the additional advantage that it can be used to operate the transmitter at constant power level and that it is relatively easier to handle in both theory and practice. However, the chirp signal may have to be replaced, usually at the cost of more sophistication, by a shaped LFM signal or any other suitable non-LFM pulse compression signal in the case where it is desirable to have a signal autocorrelation function with lower side-lobe level and/or weaker t-ν coupling properties.

A chirp signal with an ideally rectangular envelope cannot be achieved in practice. This is mainly due to the fact that a physical signal has finite rise and fall times and that distortion and shaping of the signal envelope usually takes place because of system nonlinearities and the unavoidable truncation of the signal bandwidth. Nevertheless, the present discussion assumes that a chirp signal has a strictly rectangular envelope.

3.1.4 Applications of the LFM Pulse Compression Technique

Like other pulse compression techniques, the LFM technique was originally intended (and is now often used) to make it possible for a radar system to have a long range capability (by transmitting a high energy pulse with low peak-power and long duration) along with a high range-resolution capability (by compressing the duration and increasing the effective power of the received echo) under the restrictive system peak-power constraints[46,66,113,152].

The fact that the LFM technique combines the typical capabilities of pulse compression with a relative ease of implementation, made it inevitable that great interest should be generated in extending this technique to a constantly increasing number of fields in addition to radar. Such fields include, for example, communications[108,131-137,145-150,153-161], space exploration[137,162], navigation[149,163], sonar[78], seismology[164], meteorology[133], signal processing[146-148,165], charged-particle accelerators and measurement technology[166].

The utilization of the LFM technique in the field of analogue communication can be achieved by making use of the Pulse Amplitude Modulation FM (PAM-FM) method described by S. Darlington[146]. The utilization of this technique in the field of digital communications, which will be studied in this chapter, was first proposed by M. R. Winkler[145]. This author noted that in a variety of applications, digital data can be advantageously transmitted by employing two identical chirps

with reversed slopes (i.e. a slope-reversal chirp pair) in such a way that one of these two chirps conveys the bit 1 and the other chirp conveys the bit 0. This method was later considered by a number of workers[131,132,134-137,153,161]. A hybrid combination of this method and frequency hopping has also been described for the protection of the command/control data links of Remotely-Piloted Vehicles (RPV) from hostile interception and measures[155,159]. In addition to the slope-reversal method, two other methods for the transmission of digital data by chirp techniques have also been reported. The first method employs a suitable chirp signal in an on/off mode[133,157]. The second method employs a suitable chirp signal either in a CPSK mode or in a DPSK mode[154,156]. Other methods will be described later in this chapter.

It is anticipated that the utilization of the LFM technique in the field of communications as well as in other fields will continue to increase with passing time. Accordingly, it is hoped that the present study of this technique will prove to be of practical interest.

3.2 Correlation of Two LFM Signals Having Equal Slopes

This section considers the correlation of two chirp signals in particular, and that of two shaped LFM signals in general, on the assumption that the two correlated signals have equal slopes, mostly have large duration-bandwidth products and have equal or different amplitudes, phases, frequencies and durations (or bandwidths).

3.2.1 Autocorrelation Function of the Chirp Signal

Consider the kth member of the complex chirp set (3.10) and let $\mu_k \triangleq \mu$. The normalized autocorrelation function $\chi^n_{kk}(t,0)$ of this chirp can be obtained by substituting it for $s_k(\sigma)$ and putting i=k and ν=0 in (1.4a), making use of (1.1a) and (3.12). Thus,

$$\chi^n_{kk}(t,0) = \frac{e^{j(2\pi f_k t - \pi\mu t^2)}}{T_k} \int_\sigma R_{T_k}(\sigma) R_{T_k}(\sigma - t) e^{j2\pi\mu t\sigma} d\sigma \tag{3.13a}$$

The integration limits in this relation can be obtained from (1.2) as $(-\frac{T_k}{2}, t+\frac{T_k}{2})$ for $t \leq 0$ and $(t-\frac{T_k}{2}, \frac{T_k}{2})$ for $t \geq 0$. Making use of these limits in (3.13a) shows that

$$\chi^n_{kk}(t,0) = (1-\frac{|t|}{T_k})\ \mathrm{sinc}[\mu t(T_k - |t|)] e^{j2\pi f_k t} \tag{3.13b}$$

A detailed study of $\chi^n_{kk}(t,0)$ is possible by making use of Subsections 1.3.2 and 1.7.1. $\chi^n_{kk}(t,0)$ describes the normalized response of the kth chirp matched filter to this chirp. This response is a constant frequency oscillation with mean frequency f_k. It has its peak amplitude at t=0 with a normalized value 1, an actual duration extending over $|t| \leq T_k$ and an effective duration $\simeq \frac{1}{\text{bandwidth of kth chirp}}$ ($\simeq \frac{1}{|W_k|}$ if $|W_k T_k| >> 1$). Thus, the input chirp undergoes a duration compression ratio and a processing power gain which are of the order of its duration-bandwidth product (i.e. $\simeq |W_k T_k|$ if $|W_k T_k| >> 1$).

The normalized envelope $|\chi^n_{kk}(t,0)|$ is given by

$$|\chi^n_{kk}(t,0)| = |(1-\frac{|t|}{T_k})\text{sinc}[\mu t(T_k-|t|)]| \qquad (3.13c)$$

This relation shows that $|\chi^n_{kk}(t,0)|$ is even in t and has its peak amplitude = 1 at t=0. It also shows that only the central part of $|\chi^n_{kk}(t,0)|$ which lies in the vicinity of t=0 has an essentially |sinc(.)| form in t. Moreover, it shows that $|\chi^n_{kk}(t,0)|$ has its first side-peak 13.2dB below the main peak and the next few side-peaks falling off gradually with |t|.

The actual shape of $|\chi_{kk}(t,0)|$ depends on A_k, T_k and W_k and generally looks as illustrated in Fig. 1.4. According to Subsection 2.4.6., $|\chi_{kk}(t,0)|$ can be considered as quasi-optimal under the constraint of high side-lobe level.

3.2.2 Correlation of Two Chirps with Only Phase and Frequency Mismatch

Consider a chirp which differs from the kth chirp of (3.10) only in that its phase = $\alpha_k+\alpha$ and its mean frequency = $f_k+\nu$. The normalized correlation function of these two chirps may be denoted as $\chi^n_{kk}(t,\nu)$ and obtained by the same method used to obtain $\chi^n_{kk}(t,0)$ in the previous subsection. Thus,

$$\chi^n_{kk}(t,\nu) = \frac{e^{j(\alpha+2\pi f_k t-\pi\mu t^2)}}{T_k}\int_\sigma R_{T_k}(\sigma)R_{T_k}(\sigma-t)e^{j2\pi(\mu t+\nu)\sigma}d\sigma \qquad (3.14a)$$

The integration limits in this relation are identical to those obtained for (3.13a). Accordingly,

$$\chi^{n}_{kk}(t,\nu) = (1-\frac{|t|}{T_k})\,\mathrm{sinc}\left[(\mu t+\nu)(T_k-|t|)\right]e^{j\left[2\pi(f_k+\frac{\nu}{2})t+\alpha\right]} \qquad (3.14b)$$

A detailed study of $\chi^{n}_{kk}(t,\nu)$ is not intended in the present discussion. Theoretically, $\chi^{n}_{kk}(t,\nu)$ exists for all ν-values. However, it will be effectively negligible for all $|\nu|>|W_k|$ if $|W_kT_k|>>1$. This can be seen from Subsection 3.1.2(i) along with comment on (1.3), noting that the sweeps of the two chirps have the same sign. $\chi^{n}_{kk}(t,\nu)$ satisfies the general properties outlined in Subsection 1.3.2.

For a given ν, $\chi^{n}_{kk}(t,\nu)$ describes the normalized response of the kth chirp matched filter to an input which is a phase and frequency shifted version of this chirp. This response is a constant frequency oscillation with mean frequency = $f_k+\frac{\nu}{2}$. Also, this response has an actual duration = $2T_k$ extending over the range $|t|\leq T_k$ and an effective duration $\approx \frac{1}{\text{bandwidth of reference chirp } -|\nu|}$ ($\approx \frac{1}{|W_k|-|\nu|}$ if $|W_kT_k|>>1$). Thus, it can be seen that the response effective duration increases with $|\nu|$ and that the input chirp undergoes a duration compression ratio and a processing power gain which are of the order of the difference between its duration-bandwidth product and the quantity $|T_k\nu|$ (i.e. both decrease linearly with $|\nu|$).

The envelope $|\chi^{n}_{kk}(t,\nu)|$ corresponds to the normalized

ambiguity function of the kth chirp. This envelope can be plotted and studied as a surface extending over the t-ν plane[46,66]. It is given by

$$|\chi^n_{kk}(t,\nu)| = |(1-\frac{|t|}{T_k})\mathrm{sinc}[(\mu t+\nu)(T_k-|t|)]| \qquad (3.14c)$$

This relation shows that for a given ν, only the part of $|\chi^n_{kk}(t,\nu)|$ which lies in the vicinity of t=0 has an essentially |sinc(.)| form in t. It also shows that $|\chi^n_{kk}(t,\nu)|$ has its peak amplitude at $t=-\frac{\nu}{\mu}$ (i.e. where μt+ν=0) with a value $1-|\frac{\nu}{W_k}|$ which can be obtained by substituting $-\frac{\nu}{\mu}$ for t in the expression $1-\frac{|t|}{T_k}$. Noting that this expression describes the normalized triangular autocorrelation function of the envelope $A_k R_{T_k}(\sigma)$ of the kth chirp, it can be seen that this function bounds $|\chi^n_{kk}(t,\nu)|$ and, hence, $\chi^n_{kk}(t,\nu)$. These are characteristic LFM properties that can be extended to the case of any shaped LFM signal (see Subsection 3.2.4).

$\chi^n_{kk}(t,0)$ corresponds to the special case of $\chi^n_{kk}(t,\nu)$ where α=ν=0. Thus, the effects of phase and frequency mismatch between the input and reference chirps on the matched filter response can be studied by comparing $\chi^n_{kk}(t,0)$ and $\chi^n_{kk}(t,\nu)$. Thus, comparing (3.13b) and (3.14b) shows that an isolated phase mismatch α leaves $\chi^n_{kk}(t,0)$ unchanged except for an equal phase shift α. Again, making use of the previous discussion in relation to (3.13b) through (3.14c) indicates that an isolated frequency mismatch ν: (a) translates the main peak of $\chi^n_{kk}(t,0)$ in time from t=0 to $t=-\frac{\nu}{\mu}$ and reduces this peak from 1 to $1-|\frac{\nu}{W_k}|$, (b) increases the effective

duration of $\chi^n_{kk}(t,0)$ and deforms its envelope $|\chi^n_{kk}(t,0)|$, and (c) shifts the mean frequency of $\chi^n_{kk}(t,0)$ from f_k to $f_k + \frac{\nu}{2}$. These frequency mismatch effects form the basis of the LFM t-ν coupling property as described in Subsection 3.1.2 .

3.2.3 General Correlation Function of Two Chirps Having Equal Slopes

Consider the ith and kth members of the complex chirp set (3.10). Let $\mu_i=\mu_k \triangleq \mu$, $|\alpha_i-\alpha_k| \triangleq \alpha$ and $f_i-f_k \triangleq \nu$. The normalized correlation function $\chi^n_{ik}(t,\nu)$ of these two chirps can be obtained by substituting the ith chirp for $s_i(\sigma)e^{j2\pi\nu\sigma}$ and the kth chirp for $s_k(\sigma)$ in (1.4a) making use of (1.1a) and (3.12). Thus,

$$\chi^n_{ik}(t,\nu) = \frac{e^{j(\alpha+2\pi f_k t-\pi\mu t^2)}}{\sqrt{T_i T_k}} \int_\sigma R_{T_i}(\sigma) R_{T_k}(\sigma-t) e^{j2\pi(\mu t+\nu)\sigma} d\sigma \qquad (3.15a)$$

The integration limits in this relation can be obtained from (1.2). They depend on whether $T_i>T_k$, $T_i<T_k$ or $T_i=T_k$. If $T_i>T_k$, (1.2) shows that these limits are given by $(-\frac{T_i}{2}, t+\frac{T_k}{2})$ for $t\leq -\frac{T_i-T_k}{2}$, by $(t-\frac{T_k}{2}, t+\frac{T_k}{2})$ for $|t|\leq \frac{T_i-T_k}{2}$ and by $(t-\frac{T_k}{2}, \frac{T_i}{2})$ for $t\geq \frac{T_i-T_k}{2}$. If $T_i<T_k$, these limits are $(-\frac{T_i}{2}, t+\frac{T_k}{2})$ for $t\leq -\frac{T_k-T_i}{2}$, by $(-\frac{T_i}{2}, \frac{T_i}{2})$ for $|t|\leq \frac{T_k-T_i}{2}$ and by $(t-\frac{T_k}{2}, \frac{T_i}{2})$ for $t\geq \frac{T_k-T_i}{2}$. If $T_i = T_k$, $T_k-T_i \to 0$ and these limits reduce to those obtained for (3.13a). Making use of

these limits along with comment on (1.2) indicates that $\chi^n_{ik}(t,\nu)$ is always limited to the range $|t| \leqslant \frac{T_i+T_k}{2}$ in all cases $T_i \gtrless T_k$ and for all ν.

Consider, for example, the case where $T_i < T_k$. Substituting the integration limits for this case in (3.15a) shows that:

(a) In the range $|t| \leqslant \frac{T_k-T_i}{2}$,

$$|\chi^n_{ik}(t,\nu)| = \left|\left(\frac{T_i}{T_k}\right)^{\frac{1}{2}} \operatorname{sinc}[T_i(\mu t+\nu)]\right| \tag{3.15b1}$$

$$\arg \chi^n_{ik}(t,\nu) = \alpha + 2\pi f_k t - \pi\mu t^2 \tag{3.15b2}$$

(b) In the range $\frac{T_k-T_i}{2} \leqslant |t| \leqslant \frac{T_i+T_k}{2}$,

$$|\chi^n_{ik}(t,\nu)| = \left|\frac{1}{\sqrt{T_i T_k}}\left(\frac{T_i+T_k}{2} - |t|\right) \operatorname{sinc}\left[(\mu t+\nu)\left(\frac{T_i+T_k}{2} - |t|\right)\right]\right| \tag{3.15c1}$$

$$\arg \chi^n_{ik}(t,\nu) = \alpha \pm \frac{\pi\nu}{2}(T_k-T_i) + 2\pi\left(f_k + \frac{\nu}{2} \pm \mu \cdot \frac{T_k-T_i}{4}\right)t \tag{3.15c2}$$

where the lower and upper signs in (3.15c2) correspond to the two cases were $t \gtrsim \frac{T_k-T_i}{2}$ and $t \lesssim -\frac{T_k-T_i}{2}$ respectively.

Again, a detailed study of $\chi^n_{ik}(t,\nu)$ is beyond the scope of the present discussion. Theoretically, $\chi^n_{ik}(t,\nu)$ exists for all ν-values. However, it will be effectively negligible for all $|\nu| > \frac{|W_i| + |W_k|}{2}$ if $|W_i T_i| \gg 1$ and $|W_k T_k| \gg 1$. $\chi^n_{ik}(t,\nu)$

has the general properties outlined in Subsection 1.3.2. Thus, $\chi^n_{ki}(t,\nu)$ can be derived and studied through $\chi^n_{ik}(t,\nu)$ itself by making use of (1.5).

For a given ν, $\chi^n_{ik}(t,\nu)$ describes the normalized response of the kth chirp matched filter to the ith chirp. This response vanishes outside the range $|t| \leq \frac{T_i+T_k}{2}$ and consists of two parts lying inside and outside the range $|t| \leq \frac{T_k-T_i}{2}$. Relation (3.15b) shows that the first part has the form of a LFM oscillation with phase α, mean frequency f_k and slope $-\mu$. Relation (3.15c) shows that the second part has the form of a constant frequency oscillation with phase $\alpha \pm \frac{\pi\nu}{2}(T_k-T_i)$ and mean frequency $f_k + \frac{\nu}{2} \pm \frac{W_k-W_i}{4}$.

For a given ν, the effective duration of $\chi^n_{ik}(t,\nu)$ depends on whether the main lobe of $|\chi^n_{ik}(t,\nu)|$ lies inside and/or outside the range $|t| \leq \frac{T_k-T_i}{2}$ (see below). If the main lobe lies inside this range, (3.15b1) shows that effective duration of $\chi^n_{ik}(t,\nu) \tilde{\simeq} \frac{1}{|W_i|}$. If the main lobe lies outside this range, (3.15c1) shows that effective duration of $\chi^n_{ik}(t,\nu) \tilde{\simeq} \frac{1}{(|W_i|+|W_k|)/2 - |\nu|}$.

The envelope $|\chi^n_{ik}(t,\nu)|$ corresponds to the normalized cross-ambiguity function of the ith and kth chirps. It may be plotted and studied as a surface extending over the t-ν plane. For a given ν, it consists of two parts lying inside and outside the range $|t| \leq \frac{T_k-T_i}{2}$. Relation (3.15b1) shows that the first part has a perfect $|\mathrm{sinc}(.)|$ form in t while

(3.15c1) shows that the second part has a distorted $|\text{sinc}(.)|$ form in t. Both (3.15b1) and (3.15c1) indicate that the peak amplitude of this envelope is at $t = -\frac{\nu}{\mu}$ (i.e. the envelope's main lobe is centred at this instant). This peak amplitude can be obtained from (3.15b1) or (3.15c1) depending on whether $t = -\frac{\nu}{\mu}$ lies inside or outside the range $|t| \leq \frac{T_k - T_i}{2}$. Thus,

(a) If $|t| = |-\frac{\nu}{\mu}| \leq \frac{T_k - T_i}{2}$,

$$\text{Peak amplitude} = \left(\frac{T_i}{T_k}\right)^{\frac{1}{2}} \tag{3.16a}$$

which is ≤ 1 and independent of t.

(b) If $|t| = |-\frac{\nu}{\mu}| \geq \frac{T_k - T_i}{2}$,

$$\text{Peak amplitude} = \frac{1}{\sqrt{T_i T_k}} \left[\frac{T_i + T_k}{2} - |t|\right] \tag{3.16b}$$

which is $< \left(\frac{T_i}{T_k}\right)^{\frac{1}{2}}$ and decreases linearly with $|t|$ until it vanishes at $|t| = \frac{T_i + T_k}{2}$.

Noting that (3.16) describes the normalized trapezoidal correlation function of the two envelopes $A_i R_{T_i}(\sigma)$ of the ith chirp and $A_k R_{T_k}(\sigma)$ of the kth chirp, it can be seen that this function bounds $|\chi^n_{ik}(t,\nu)|$ and, hence, $\chi^n_{ik}(t,\nu)$. Again, this is a characteristic LFM property that can be extended to the case of any two shaped LFM signals (see Subsection 3.2.4).

Making use of the fact that $\frac{W_i}{T_i} \triangleq \frac{W_k}{T_k}$ shows that (3.16) can also be expressed as

(a) If $|\nu| \leq \frac{|W_k|-|W_i|}{2}$,

$$\text{Peak amplitude} = \left(\frac{W_i}{W_k}\right)^{\frac{1}{2}} \tag{3.17a}$$

which is ≤ 1 and independent of ν.

(b) If $|\nu| \geq \frac{|W_k|-|W_i|}{2}$,

$$\text{Peak amplitude} = \frac{1}{\sqrt{W_i W_k}}\left[\frac{|W_i|+|W_k|}{2} - |\nu|\right] \tag{3.17b}$$

which is $< \left(\frac{W_i}{W_k}\right)^{\frac{1}{2}}$ and decreases linearly with $|\nu|$ until it vanishes at $|\nu| = \frac{|W_i|+|W_k|}{2}$.

Relation (3.17) implies that a slight mismatch $|W_k| - |W_i| > 0$ reduces the peak amplitude slightly from 1 to $\left(\frac{W_i}{W_k}\right)^{\frac{1}{2}} < 1$ and keeps it constant for all $|\nu| \leq \frac{|W_k|-|W_i|}{2}$. Combining this with the fact that a frequency shift translates the peak amplitude in time from t=0 to $t=-\frac{\nu}{\mu}$ indicates that a frequency shift ν in the range $|\nu| \leq \frac{|W_k|-|W_i|}{2}$ can, at minimum cost of SNR_o - degradation, be accommodated by making the matched filter bandwidth ($\simeq |W_k|$ if $|W_k T_k| >> 1$) slightly larger than that of the input chirp ($\simeq |W_i|$ if $|W_i T_i| >> 1$). This characteristic LFM property has already been mentioned in Subsection 3.1.2.

$\chi^n_{ik}(t,\nu)$ is a generalization of $\chi^n_{kk}(t,\nu)$ and, hence, $\chi^n_{kk}(t,0)$. Thus, $\chi^n_{kk}(t,0)$ corresponds to the special case of (3.15) where $i=k$, $\alpha=\nu=0$ and $T_i=T_k$ ((3.15b) vanishes identically in this case). Similarly, $\chi^n_{kk}(t,\nu)$ corresponds to the special case of (3.15) where $i=k$ and $T_i=T_k$ ((3.15b) vanishes identically in this case).

$\chi^n_{kk}(t,0)$, $\chi^n_{kk}(t,\nu)$ and $\chi^n_{ik}(t,\nu)$ may be used to carry out a variety of studies related to chirps having equal slopes. These studies are concerned with such areas as weighting, signal design and mismatching effects.

Chirp weighting[46,66] is beyond the scope of this work. However, results obtained in the next subsection may be utilized in this respect in the case of chirps having equal slopes. Signal design for chirps having equal slopes will be considered in the next section. General distortion mismatching effects were considered in Subsection 1.6.2.

Effects of phase and frequency mismatch between the ith and kth chirps on the response of the latter's matched filter to the former were considered in the previous subsection. The combined effects of phase, frequency and duration (or bandwidth) mismatch may be obtained by comparing (3.13), (3.14) and (3.15). It suffices here to consider the effects of an isolated duration (or bandwidth) mismatch.

Duration mismatch effects can be obtained by putting

$\alpha=\nu=0$ in (3.15) and comparing the result with (3.13). Bandwidth mismatch effects can be obtained by applying this same procedure and substituting $\frac{W_i}{\mu}$ for T_i and $\frac{W_k}{\mu}$ for T_k in (3.13) and (3.15). Thus, it can be seen that duration (or bandwidth) mismatch: (a) introduces a residual LFM component with mean frequency f_k and slope $-\mu$ as the central part of the response extending over the range $|t|\leq\frac{T_k-T_i}{2}$, (b) leaves the response peak at t=0 and reduces this peak from 1 to $(\frac{T_i}{T_k})^{\frac{1}{2}}<1$, (c) increases the response effective duration and decreases its actual duration from $(-T_k,T_k)$ to $(-\frac{T_i+T_k}{2}, \frac{T_i+T_k}{2})$, and (d) shifts the mean frequency of the part of the response lying outside the range $|t|\leq\frac{T_k-T_i}{2}$ by $\pm\frac{\mu}{4}(T_k-T_i)$ and distorts the envelope of this part changing it from the form described by (3.13c) to a form which can be obtained by putting $\nu=0$ in (3.15c1).

3.2.4 Correlation of Two Shaped LFM Signals With Equal Slopes

Consider the two shaped LFM signals $y_i(\sigma)$ and $y_k(\sigma)$ of the complex LFM signal set(3.5). Let $\mu_i = \mu_k \triangleq \mu$, $|\alpha_i-\alpha_k| \triangleq \alpha$ and $f_i-f_k \triangleq \nu$. The correlation function $\chi_{ik}(t,\nu)$ of these two signals can be obtained by substituting $y_i(\sigma)$ for $s_i(\sigma)e^{j2\pi\nu\sigma}$ and $y_k(\sigma)$ for $s_k(\sigma)$ in (1.4a) making use of (1.1a). Thus,

$$\chi_{ik}(t,\nu) = e^{j(\alpha+2\pi f_k t-\pi\mu t^2)}\int_\sigma a_i(\sigma)a_k(\sigma-t)e^{j2\pi(\mu t+\nu)\sigma}d\sigma \qquad (3.18a)$$

which is a generalization of (3.15a) and, hence, (3.14a) and (3.13a).

Relation (3.18a) cannot be used to obtain a closed-form expression for $\chi_{ik}(t,\nu)$ unless the explicit forms of $a_i(\sigma)$ and $a_k(\sigma)$ are specified. However, a few comments are in order. Theoretically, $\chi^n_{ik}(t,\nu)$ exists for all ν-values. However, it will be effectively negligible for all $|\nu| > \frac{|W_i|+|W_k|}{2}$ if $|W_iT_i| >> 1$ and $|W_kT_k| >> 1$. $\chi_{ik}(t,\nu)$ has the general properties outlined in Subsection 1.3.2. Thus, $\chi_{ki}(t,\nu)$ can be derived and studied through $\chi_{ik}(t,\nu)$ itself by making use of (1.5). For a given ν, $\chi_{ik}(t,\nu)$ describes the response of the matched filter of $y_k(\sigma)$ to $y_i(\sigma)$. This response is always limited to the range $|t| \leq \frac{T_i+T_k}{2}$ in all cases $T_i \gtrless T_k$ and for all ν. It can be used to obtain the normalized response by making use of (1.4).

The envelope $|\chi_{ik}(t,\nu)|$ corresponds to the cross-ambiguity function of $y_i(\sigma)$ and $y_k(\sigma)$ and may be plotted and studied as a surface extending over the t-ν plane. It can be obtained from (3.18a) as

$$|\chi_{ik}(t,\nu)| = \left|\int_\sigma a_i(\sigma)\, a_k(\sigma-t)\, e^{j2\pi(\mu t+\nu)\sigma} d\sigma\right| \qquad (3.18b1)$$

which, for small t, can be expressed as

$$|\chi_{ik}(t,\nu)| \tilde{=} \left|\int_\sigma a_i(\sigma)\, a_k(\sigma)\, e^{j2\pi(\mu t+\nu)\sigma} d\sigma\right|, \quad t \to 0 \qquad (3.18b2)$$

In this relation, the integral may be viewed as the Fourier transform of the product $a_i(\sigma)a_k(\sigma)$ with ν taken as a parameter and μ as a scaling factor in the t- domain. Also, the product $a_i(\sigma)a_k(\sigma)$ is real and even in σ. Making use of these facts and the fact that the Fourier transform of a real even function is purely real, relation (3.18b2) can be written as

$$|\chi_{ik}(t,\nu)| \tilde{\simeq} \int_\sigma a_i(\sigma)a_k(\sigma)e^{j2\pi(\mu t+\nu)\sigma}d\sigma, \quad t\to 0 \qquad (3.18b3)$$

This relation implies that for a given ν, there is a Fourier pair relationship in the vicinity of t=0 between the envelope $|\chi_{ik}(t,\nu)|$ of the matched filter response and the product of the two envelopes $a_i(\sigma)$ and $a_k(\sigma)$ of the input and reference LFM signals. This is a characteristic LFM property that may be exploited in such areas as LFM weighting, mismatching effects and signal design. It holds for any two identical or different LFM signals having equal slopes and rectangular or shaped envelopes. In fact, relations similar to (3.18b3) can be derived from (3.13a), (3.14a) and (3.15a). Such relations are special cases of (3.18b3) and lead to expressions which coincide with those obtained by putting $t\tilde{\simeq}0<<T_k$ in (3.13c) and (3.14c) and taking $|t| \leq \frac{T_k-T_i}{2}$ in (3.15b1). These relations and expressions reveal that there is always a Fourier pair relationship between the envelope of the matched filter response and the product of the two envelopes

of the input and reference chirps. Such a relationship is almost exact in the vicinity of t=0 but becomes distorted as t increases.

It can be seen from (3.18b1) that for a given ν, $|\chi_{ik}(t,\nu)|$ has its peak amplitude at $t=-\frac{\nu}{\mu}$ (i.e. where $\mu t+\nu=0$) and that this peak amplitude can be obtained by substituting $-\frac{\nu}{\mu}$ for t in the expression $|\int a_i(\sigma)a_k(\sigma-t)d\sigma|$. Assuming that both $a_i(\sigma)$ and $a_k(\sigma)$ are positive-valued, this expression reduces to their correlation function $\int a_i(\sigma)a_k(\sigma-t)d\sigma$. Thus, it can be seen in this case that the correlation function $\int a_i(\sigma)a_k(\sigma-t)d\sigma$ bounds $|\chi_{ik}(t,\nu)|$ and, hence, $\chi_{ik}(t,\nu)$. These are characteristic LFM properties which hold for any two identical or different LFM signals having equal slopes and rectangular or shaped envelopes. They have already been highlighted in the previous two subsections in relation to chirp signals.

It can also be seen that $|\chi_{ik}(t,\nu)|$ always has its peak amplitude at $t=-\frac{\nu}{\mu}$ irrespective of the shapes of the envelopes of the two involved LFM signals. This is another characteristic LFM property which indicates that LFM envelope shaping does not affect the peak amplitude location on the t-axis, although it may affect the magnitude of this amplitude and the side-lobe behaviour of $|\chi_{ik}(t,\nu)|$.

$\chi_{ik}(t,\nu)$ can be used in the case where $y_i(\sigma)$, $y_k(\sigma)$ or

$y_i(\sigma)$ and $y_k(\sigma)$ reduce to corresponding FSK or PSK signals. Thus, (3.18) describes the correlation between two FSK signals in the case where $\mu=0$ and describes the correlation between two PSK signals in the case where $\mu=\nu=0$. Similar comments also apply in the case of (3.13), (3.14) and (3.15). These facts confirm a previous conclusion that FSK and PSK signal theories may be viewed as two special cases of LFM signal theory (see Subsection 3.1.2). They also indicate that (3.13), (3.14), (3.15) and (3.18) can also be used, for example, as a basis for: (a) PSK signal design, (b) FSK signal design, (c) mixed LFM, PSK and FSK signal design, and (d) LFM-FSK (or PSK) interference studies.

3.3 Signal Design for Chirps Having Equal Slopes

This section considers the problem of designing signal sets consisting of chirps having equal slopes for digital data transmission. It assumes optimum processing in an AWGN background and practically tolerable slope distortions and deviations and mutual interferences. The results obtained can be used as a basis for the corresponding case of shaped-LFM signal design.

3.3.1 The Conventional Detection Theoretical Method

This method was introduced in Subsection 1.4.1. It may

be used in both the coherent and noncoherent cases. In this method, the optimum demodulator comprises a bank of optimum predetection processors and a decision device for deciding on the outputs of these processors. Each member of the modulator signal set requires its own processor. Assuming AWGN, this processor may be a correlator or a matched filter-sampler in the coherent case. In the noncoherent case, this processor is predominantly a square-envelope correlator or a matched filter-envelope detector-sampler (see Subsection 1.2).

3.3.1.1 The Coherent Case

This case is described in Subsection 1.4.2. This subsection indicated that in the coherent case, the design and performance of a particular signal set such as that of (1.10) are based on its correlation matrix $[\lambda^{n}_{ik}(0,\nu)]^{N}_{i,k=1}$. Also, this subsection was mainly concerned with the performance of signal sets which consist of real, equiprobable and equal energy signals. These sets may be N'ary equicorrelated signal sets or arbitrarily correlated signal pairs.

Consider the ith and kth chirps of the real chirp set (3.9) assuming that they are equiprobable and have the same slope μ. Also, let $T_i < T_k$, $|\alpha_i - \alpha_k| \triangleq \alpha$ and $f_i - f_k \triangleq \nu$. If the bandwidth of the kth chirp does not exceed 2× mean frequency f_k and that of the ith chirp does not exceed 2× mean frequency f_i, the normalized correlation coefficient of these two chirps may be obtained by making use of (3.15a) in

(1.14a). Thus,

$$\lambda_{ik}^{n}(0,\nu) = \left(\frac{T_s}{T_\ell}\right)^{\frac{1}{2}} \operatorname{sinc}(T_s\nu)\cos\alpha \qquad (3.19a)$$

where T_s is the smaller and T_ℓ is the larger of T_i and T_k.

This relation indicates that $\lambda_{ik}^{n}(0,\nu)$ is determined by T_i, T_k, ν and α and is independent of μ. Also, the fact that $-0.218 \leq \operatorname{sinc}(T_s\nu) \leq 1$ and $-1 \leq \cos\alpha \leq 1$ indicates that

$$-\left(\frac{T_s}{T_\ell}\right)^{\frac{1}{2}} \leq \lambda_{ik}^{n}(0,\nu) \leq \left(\frac{T_s}{T_\ell}\right)^{\frac{1}{2}} \qquad (3.19b)$$

where the lower limit corresponds to the case where $\nu=0$ and $\alpha=\pi$ and the upper limit corresponds to the case where $\nu=\alpha=0$.

Relation (3.19) can be used as a basis for the design of a a variety of coherent chirp signal pairs and sets of various correlation properties such as those described in Subsection 1.3.4. If these pairs and sets are assumed to consist of chirps having the same energy E, their performance can be obtained by making use of the appropriate expressions in Subsection 1.4.2. These pairs and sets include, for example,

3.3.1.1.1 The Antipodal Chirp Pair

The ith and kth chirps form an antipodal pair if $E_i=E_k \triangleq E$

and $\lambda_{ik}^{n}(0,\nu)=-1$. Relation (3.19a) indicates that this corresponds to the case where $T_i=T_k$, $\nu=0$ and $\alpha=\pi$. The antipodal chirp pair can be used for both CPSK signalling[154] and DPSK signalling[156].

The fact that α should be kept equal to π for the antipodal chirp pair and that $\lambda_{ik}^{n}(0,\nu)$ is sensitive to variations in α questions the utility of this pair in practice where such variations are usually unavoidable due to both systematic and channel instabilities. In fact, this problem has usually been considered as a limitation on the practical utility of any chirp system based on the assumption of coherent reception[132,134,153]. However, it should be noted here that this problem is not peculiar of chirps, that great strides are being currently made in the field of phase acquisition and tracking[98] and that: (i) chirp signalling can achieve good phase-recovery because it is capable of providing higher bit synchronization channel signal-to-noise ratio due to its pulse compression properties (see Subsection 2.4.2), (ii) small phase errors can only produce some amplitude jitter of the compressed pulses in a coherent chirp system which employs chirp pulses with large numbers of cycles[132,134], (iii) the effects of phase errors in a coherent chirp system may be reduced by slightly increasing the width of the main peak of the compressed pulse by making use of progressive pulse compression (see Subection 1.7.3) or by introducing a

slight duration (or bandwidth) mismatch between the matched filter input and reference chirps (see Subsection 3.2.3) , and (iv) in such an important application as data transmission over dispersive multipath channels, a coherent chirp system excels over ordinary coherent systems in that its echo rejection capability (see Section 2.5) enables it to consider the phase of only one multipath component instead of the phase of the resultant of many such components at a time.

3.3.1.1.2 Orthogonal Chirp Pairs

Relation (3.19a) indicates that the ith and kth chirps form an orthogonal chirp pair if: (i) T_i, T_k and ν are arbitrary and $\alpha = \frac{\pi}{2}$, or (ii) T_i, T_k and α are arbitrary and $T_s|\nu|$ = positive integer.

Relation (3.19a) also indicates that the ith and kth chirps form a quasi-orthogonal pair if: (i) α and T_k are arbitrary and $T_s|\nu|$ is large (e.g. >5), or (ii) α and ν are arbitrary and $(\frac{T_s}{T_\ell})^{\frac{1}{2}} = (\frac{W_s}{W_\ell})^{\frac{1}{2}} < \varepsilon$, where ε is an arbitrarily small positive quantity.

3.3.1.1.3 An Orthogonal Chirp Set

The method of constructing such a set will be illustrated here for the case of three chirps. The case of more than three chirps can be treated similarly.

Let the first three chirps of the real chirp set of (3.9) have identical slopes as well as equal energies. Let these three chirps be chosen in such a way that $T_1 \leq T_2 \leq T_3$ and that $T_1|f_1-f_2|=m_1$, $T_1|f_1-f_3|=m_2$ and $T_2|f_2-f_3|=m_3$, where the m's are different and may be positive integers or any large positive numbers (e.g. >5). It can readily be seen from (3.19a) that these three chirps are mutually orthogonal or quasi-orthogonal. It can also be seen that the available bandwidth determines the permissible values of $|f_1-f_2|$, $|f_1-f_3|$ and $|f_2-f_3|$ and, hence, the possible m-values. Moreover, it can be seen that these possible m-values are also governed by the permissible maximum mutual interference level.

3.3.1.2 The Noncoherent Case

This case is described in Subsections 1.4.3, 1.4.4 and 1.4.5. In this case, the design and performance of a particular signal set such as that of (1.10) are both based on the in-phase component $[\rho_{ik}(0,\nu)]_{i,k=1}^{N}$ and the quadrature component $[\hat{\rho}_{ik}(0,\nu)]_{i,k=1}^{N}$ of its correlation matrix $[\lambda_{ik}^{n}(0,\nu)]_{i,k=1}^{N}$.

Consider the ith and kth chirps described in Subsection 3.3.1.1 disregarding their phases. The in-phase correlation coefficient $\rho_{ik}(0,\nu)$ and the quadrature correlation coefficient $\hat{\rho}_{ik}(0,\nu)$ of these two chirps may be obtained by making use of (3.15 a) in (1.27). Thus,

$$\rho_{ik}(0,\nu) = \left(\frac{T_s}{T_\ell}\right)^{\frac{1}{2}} \operatorname{sinc}(T_s \nu) \tag{3.20a}$$

$$\hat{\rho}_{ik}(0,\nu) = 0 \tag{3.20b}$$

Making use of the fact that $-0.218 \leq \operatorname{sinc}(T_s \nu) \leq 1$, (3.20a) indicates that

$$-0.218 \left(\frac{T_s}{T_\ell}\right)^{\frac{1}{2}} \leq \rho_{ik}(0,\nu) \leq \left(\frac{T_s}{T_\ell}\right)^{\frac{1}{2}} \tag{3.20a1}$$

Relation (3.20) can be used as a basis for the design of a variety of noncoherent chirp signal pairs or sets of various correlation properties such as those described in Subsection 1.4.3. For example, it can be used along with (1.29) to design noncoherent orthogonal chirp signal pairs and sets. However, it cannot be used along with (1. 30) to construct a noncoherent antipodal pair. This is due to the fact that $\rho_{ik}(0,\nu)$ cannot be made equal to -1 in this case as can be seen from (3.20a1). The performance of noncoherent chirp signal pairs or sets can be found by making use of the appropriate relations in Section 1.4.

It has been stated above that ν is the shift between the mean frequencies f_i and f_k of the ith and kth chirps of equal slopes. It can be seen from (3.19a) and (3.20a) that this shift plays an important role in determining the correlation properties of these two chirps in both the

coherent and noncoherent cases. This obviously implies that strict ν- control is generally required in implementing both coherent and noncoherent systems employing signal sets consisting of chirps of equal slopes. Such a strict ν-control seems to be possible in view of the current advances in the field of frequency acquisition and tracking[108].

3.3.2 The t-ν Coupling Method

The conventional detection theoretical method described in Subsection 3.3.1 above requires a complex receiver which comprises an optimum predetection processor corresponding to each member of the modulator chirp signal set. However, this receiver complexity may be substantially reduced by making use of an alternative chirp signal design technique based on the characteristic LFM t-ν coupling property introduced in Subsection 3.1.2 and Section 3.2. This technique may be described as below.

First, consider a subset comprising the first $2M-1 \leq N$ members of the real chirp set (3.9). Assume that these members have sufficiently large duration-bandwidth products, are not necessarily phase-coherent and have different mean frequencies. Let these members have the same slope μ, the same energy E, the same duration T and the same sweep W. Second, consider the matched filter of the first chirp in

the assumed subset. According to Subsection 3.2.1, the normalized response of this filter to the first chirp itself has an envelope with a main peak = 1 at t=0, a main lobe centred at t=0 and an effective duration $\simeq \frac{1}{|W|}$. Third, consider the second chirp in the assumed subset and let $f_2-f_1 \triangleq \nu$. According to Subsection 3.2.2, the normalized response of the matched filter of the first chirp to this second chirp has an envelope with a main peak $=1-|\frac{\nu}{W}|$ at $t=-\frac{\nu}{\mu}$, a main lobe centred at $t=-\frac{\nu}{\mu}$ and an effective duration $\simeq \frac{1}{|W|-|\nu|}$ ($\simeq \frac{1}{|W|}$ for $|\nu| << |W|$).

Assuming that $|\nu|<<|W|$, the two responses in the first and second steps above will be separable if the t-shift between the two main peaks $\geq$ response effective duration, i.e. if $|\frac{\nu}{\mu}| \geq \frac{1}{|W|}$, i.e. if $|\nu| \geq \frac{1}{T}$. Separability of the two t-shifted responses implies the quasi-orthogonality of the corresponding two ν-shifted first and second chirps. Thus, these two chirps may be considered to form a quasi-orthogonal pair if $|f_2-f_1| \geq \frac{1}{T}$.

The preceding discussion indicates that it is possible by proper frequency selection to make the assumed chirp subset quasi-orthogonal in such a way that it may be incoherently processed by a single matched filter, namely, the matched filter of the first chirp. This may be achieved, for example, by: (a) assuming that ν_{max} is the maximum permissible ν-shift

from f_1 which corresponds to the minimum acceptable degraded and shifted peak amplitude $1 - |\frac{\nu_{max}}{W}|$, (b) making $f_2-f_1=f_3-f_2=f_4-f_3=\ldots=f_M-f_{M-1}\triangleq\frac{1}{T}$, (c) assuming that $\frac{1}{T}(M-1)\leq\nu_{max}$, and (d) making $f_{M+1}-f_1=f_{M+2}-f_{M+1}=f_{M+3}-f_{M+2}=\ldots$ $=f_{2M-1}-f_{2M-2}\triangleq-\frac{1}{T}$. In this manner, the ν-shifted chirps will be mutually quasi-orthogonal because their corresponding responses through the matched filter of the first chirp will be centred at, and on both sides of, t=0 in such a way that each response occupies a t-slot of width $\simeq\frac{1}{|W|}$ along the t-axis. The first, second, third, ... and Mth chirps will have their responses centred at t=0, $-\frac{1}{W}$, $-\frac{2}{W}$,... and $-\frac{M-1}{W}$ respectively. The (M+1)th, (M+2)th,... and (2M-1)th chirps will have their responses centred at $t=\frac{1}{W}$, $\frac{2}{W}$, ... and $\frac{M+1}{W}$ respectively.

In practice, one has to take into account the fact that the effective duration of the response of the matched filter of the first chirp to any other member of the assumed subset with mean frequency $f_1\pm\nu$ increases with $|\nu|$ and is of the order of $\frac{1}{|W|-|\nu|}$. Also, one has to take into account the fact that distortions in such a response increase with, and may give rise to, intolerable side-lobe interferences.

The chirp signal set construction procedure outlined above may be improved, for example, by introducing a suitable slight duration (or sweep) mismatch between the first chirp and all other chirps. This can be achieved by: (a)

excluding the first chirp from the desired chirp signal set while retaining its matched filter for the processing of this set, and (b) increasing the duration of the first chirp to T_1 and its sweep to W_1 in such a way that $\frac{W_1}{T_1} = \mu$, $T_1 > T$ and $|W_1| > |W|$. This new procedure is advantageous because, according to Subsection 3.2.3, it: (a) makes the main lobes of the responses corresponding to chirps with mean frequency $f_1 \pm \nu$ assume the same perfect $|\text{sinc}(.)|$ form in t if $|\nu| < \frac{|W_1| - |W|}{2}$ and different distorted $|\text{sinc}(.)|$ forms in t if $|\nu| > \frac{|W_1| - |W|}{2}$, (b) makes all such responses have the same effective duration $\tilde{\sim} \frac{1}{|W|}$ if $|\nu| < \frac{|W_1| - |W|}{2}$ and nearly the same effective duration $\tilde{\sim} \frac{2}{|W_1| + |W|}$ if $\frac{|W_1| - |W|}{2} < |\nu| << \frac{|W_1| + |W|}{2}$, (c) reduces the output normalized peak amplitude only slightly from 1 to the stationary level $(\frac{W}{W_1})^{\frac{1}{2}} < 1$ if $|\nu| < \frac{|W_1| - |W|}{2}$ and to the lower decreasing level $\frac{1}{\sqrt{WW_1}}[\frac{|W_1| + |W|}{2} - |\nu|]$ if $|\nu| > \frac{|W_1| - |W|}{2}$, and (d) leaves this peak amplitude at $t = -\frac{\nu}{\mu}$ for all ν. This procedure can pack a set of $|W|(T_1 - T)$ quasi-orthogonal chirps in the range $|\nu| \leq \frac{|W_1| - |W|}{2}$. Other chirps can be added to this set in the range $\frac{|W_1| - |W|}{2} < |\nu| << \frac{|W_1| + |W|}{2}$.

The preceding discussion implies that ν-shifts play the main role in determining the correlation properties and, hence, the performance of chirp signal sets designed according to the t-ν coupling technique. This obviously implies that strict ν-control is always required in this technique.

Again, such a strict ν-control seems to be possible in view of the current advances in the field of frequency acquisition and tracking. In fact, frequency recovery and synchronization in the present case may be easily achieved by using a suitable member of the constructed chirp set as a synchronizing signal.

Assuming a purely AWGN background, an upper bound on the performance of the system employing a quasi-orthogonal chirp set constructed by the t-ν coupling technique can be found by making use of Subsection 1.4.3. However, the exact evaluation of the performance of this system is expected to be difficult. This is due to the fact that such an exact evaluation would also have to take into account such unavoidable performance degrading factors as μ-distortions, μ-mismatches, sidelobe - overlapping and synchronization errors.

3.4 Correlation of Two LFM Signals Having Different Slopes

This section considers the correlation of two chirp signals in particular, and that of two shaped LFM signals in general, on the assumption that the two correlated signals have different slopes, mostly have large duration - bandwidth products and have equal or different amplitudes, phases, mean frequencies and durations (or bandwidths). The application of the results obtained to the special case

where the two slopes become equal may involve laborious limiting processes. This explains why the same - μ and the different - μ cases are treated separately in the present work.

3.4.1 General Correlation Function of Two Chirps Having Different Slopes

Consider the ith and kth members of the complex chirp set (3.10). Let $|\alpha_i-\alpha_k| \triangleq \alpha$ and $f_i-f_k \triangleq \nu$. The normalized correlation function $\chi^n_{ik}(t,\nu)$ of these two chirps can be obtained by substituting the ith chirp for $s_i(\sigma)e^{j2\pi\nu\sigma}$ and the kth chirp for $s_k(\sigma)$ in (1.4a) making use of (1.1a) and (3.12). Thus,

$$\chi^n_{ik}(t,\nu) = \frac{e^{ju}}{\sqrt{T_i T_k}} \int_\sigma R_{T_i}(\sigma) R_{T_k}(\sigma-t) e^{j2\pi\left[(\mu_k t+\nu)\sigma + \frac{\mu_i-\mu_k}{2}\sigma^2\right]} d\sigma \tag{3.21a}$$

where

$$u \triangleq \alpha+2\pi f_k t - \pi\mu_k t^2 \tag{3.21b}$$

Theoretically, $\chi^n_{ik}(t,\nu)$ exists for all ν. However, it will be effectively negligible for all $|\nu| > \frac{|W_i|+|W_k|}{2}$ if $|W_i T_i| >> 1$ and $|W_k T_k| >> 1$. This can be seen from Subsection 3.1.2(i) along with comment on (1.3), noting that W_i and W_k

may have different signs.

Also, $\chi^n_{ik}(t,\nu)$ has the general properties outlined in Subsection 1.3.2. Thus, $\chi^n_{ki}(t,\nu)$ can be derived and studied through $\chi^n_{ik}(t,\nu)$ itself by making use of (1.5).

For a given ν, $\chi^n_{ik}(t,\nu)$ describes the normalized response of the kth chirp matched filter to the ith chirp. The normalized response envelope $|\chi^n_{ik}(t,\nu)|$ corresponds to the normalized ith-kth cross-ambiguity function and may be plotted and studied as a surface extending over the t-ν plane.

Relation (3.21) reduces to (3.15a) in the special case where $\mu_i=\mu_k=\mu$. However, the following analysis generally breaks down in this latter case. This is because this analysis is based on the assumption that $\mu_i\neq\mu_k$ in such a way that the term including σ^2 in the integrand's exponent does not vanish identically. Thus, assuming that $\mu_i\neq\mu_k$ and completing the square in the integrand's phase reduce (3.21) to

$$\chi^n_{ik}(t,\nu)=\frac{e^{jz}}{g\sqrt{T_iT_k}}\int_x R_{T_i}\left(\frac{x}{g}-h\right)R_{T_k}\left(\frac{x}{g}-h-t\right)e^{\pm j\frac{\pi}{2}x^2}dx \qquad (3.22a)$$

where $j\frac{\pi}{2}x^2$ and $-j\frac{\pi}{2}x^2$ correspond to $\mu_i>\mu_k$ and $\mu_i<\mu_k$ respectively and

$$x \triangleq g.(\sigma+h) \tag{3.22b1}$$

$$g \triangleq \sqrt{2|\mu_i-\mu_k|}, \qquad \mu_i \neq \mu_k \tag{3.22b2}$$

$$h \triangleq \frac{\nu+\mu_k t}{\mu_i-\mu_k}, \qquad \mu_i \neq \mu_k \tag{3.22b3}$$

$$z \triangleq (\alpha - \frac{\pi\nu^2}{\mu_i-\mu_k}) + 2\pi(f_k - \frac{\nu\mu_k}{\mu_i-\mu_k})t - \frac{\pi\mu_i\mu_k}{\mu_i-\mu_k}t^2 \tag{3.22b4}$$

3.4.1.1 Integration Limits

The integration limits in (3.21a) depend on whether $T_i<T_k$, $T_i>T_k$ or $T_i=T_k$ and are identical to those obtained for (3.15a). These limits together with comment on (1.2) indicate that $\chi^n_{ik}(t,\nu)$ is always limited to the range $|t| \leqslant \frac{T_i+T_k}{2}$ for all ν in all cases $T_i \gtrless T_k$.

The integration limits in (3.22a) may be obtained from those in (3.21a) through (3.22b). If $T_i<T_k$, these limits may be denoted as (x_1,x_2) for $t \leqslant -\frac{T_k-T_i}{2}$, (x_1,x_3) for $|t| \leqslant \frac{T_k-T_i}{2}$ and (x_4,x_3) for $t \geqslant \frac{T_k-T_i}{2}$. If $T_i>T_k$, these limits are (x_1,x_2) for $t \leqslant -\frac{T_i-T_k}{2}$, (x_4,x_2) for $|t| \leqslant \frac{T_i-T_k}{2}$ and (x_4,x_3) for $t \geqslant \frac{T_i-T_k}{2}$. If $T_i=T_k$, these limits reduce to (x_1,x_2) for $t \leqslant 0$ and (x_4,x_3) for $t \geqslant 0$. The x's are given by

$$x_1 \triangleq \frac{gT_i}{2}(-1+\frac{2h}{T_i}) \tag{3.23a}$$

$$x_2 \triangleq \frac{gT_k}{2}(1+\frac{2(h+t)}{T_k}) \tag{3.23b}$$

$$x_3 \triangleq \frac{gT_i}{2}\left(1+\frac{2h}{T_i}\right) \tag{3.23c}$$

$$x_4 \triangleq \frac{gT_k}{2}\left(-1+\frac{2(h+t)}{T_k}\right) \tag{3.23d}$$

This relation shows that within the duration of $\chi^n_{ik}(t,\nu)$: (a) x_1 and x_2 vanish together only at $t=-\frac{T_i+T_k}{2}$ and may have different signs only in the range ($x_1=0$, $x_2=0$) where $x_1<0$ and $x_2>0$, (b) x_1 and x_3 cannot vanish together and may have different signs only in the range ($x_1=0$, $x_3=0$) where $x_1<0$ and $x_3>0$, (c) x_2 and x_4 cannot vanish together and may have different signs only in the range ($x_2=0$, $x_4=0$) where $x_2>0$ and $x_4<0$, and (d) x_3 and x_4 vanish together only at $t=\frac{T_i^2+T_k}{2}$ and may have different signs only in the range ($x_3=0$, $x_4=0$) where $x_4<0$ and $x_3>0$.

3.4.1.2 A Fresnel Function

Consider the integration limit pairs given above and denote an arbitrary pair by (x_p,x_q) where $p=1,4$ and $q=2,3$. For this pair, the integral in (3.22a) reduces to the Fresnel function $F(x_p,x_q) \triangleq \int_{x_p}^{x_q} e^{j\frac{\pi}{2}x^2}dx$ if $\mu_i>\mu_k$ and to $F^*(x_p,x_q)$ if $\mu_i<\mu_k$. $F(x_p,x_q)$ can also be expressed as $[F(x_q) - F(x_p)]$, where $F(X)\triangleq\int_o^X e^{j\frac{\pi}{2}x^2}dx$ is the complex Fresnel integral which is usually expressed as $F(X) = C(X)+jS(X)$. All $C(X)$, $S(X)$ and $F(X)$ are odd functions of X. Both $C(X)$ and $S(X)$ are available in tabulated form as functions of X[79].

For small X, F(X) is quasi-oscillatory in X. However, $\lim_{X\to\infty} C(X) = \lim_{X\to\infty} S(X) = \frac{1}{2}$ and, thus, $F(X) \simeq \frac{e^{j\frac{\pi}{4}}}{\sqrt{2}}$ for large X (e.g. $X \geq 3.5$).

$|F(x_p,x_q)|^2 = [C(x_q)-C(x_p)]^2 + [S(x_q)-S(x_p)]^2$ and $\arg F(x_p,x_q) = \tan^{-1}\frac{S(x_q)-S(x_p)}{C(x_q)-C(x_p)}$. These two functions are usually difficult to handle because they cannot generally be expressed in closed-form. They may have to be evaluated numerically and plotted as fluctuating functions of x_p and x_q. However, prediction criteria concerning their behaviour can be formulated (See Subsections 4.8.2 through 4.8.6 as well as Sections 4.10 and 4.11).

If x_p and x_q vanish simultaneously, $|F(x_p,x_q)|$ vanishes identically. If this is not the case, $|F(x_p,x_q)|$ generally has a central region flanked by two tails (see Fig. 3.3). The central region covers the range (x_p=0, x_q=0) in which x_p and x_q have different signs or either x_p=0 or x_q=0. In this region, $|F(x_p,x_q)|$ assumes its largest possible values fluctuating about the mean level $\sqrt{2}$ with an oscillation amplitude $\frac{2}{\pi|x_p|}$ in the x_p=0 side and $\frac{2}{\pi|x_q|}$ in the x_q=0 side. In the tails, x_p and x_q have the same sign and $|F(x_p,x_q)|$ undergoes gradual decay fluctuating about the mean level $\frac{1}{\pi|x_p|}$ in the x_p=0 tail and the mean level $\frac{1}{\pi|x_q|}$ in the x_q=0 tail. If the nonvanishing values of $|x_p|$ and $|x_q|$ are large (e.g. ≥ 3.5), the tails tend to disappear,

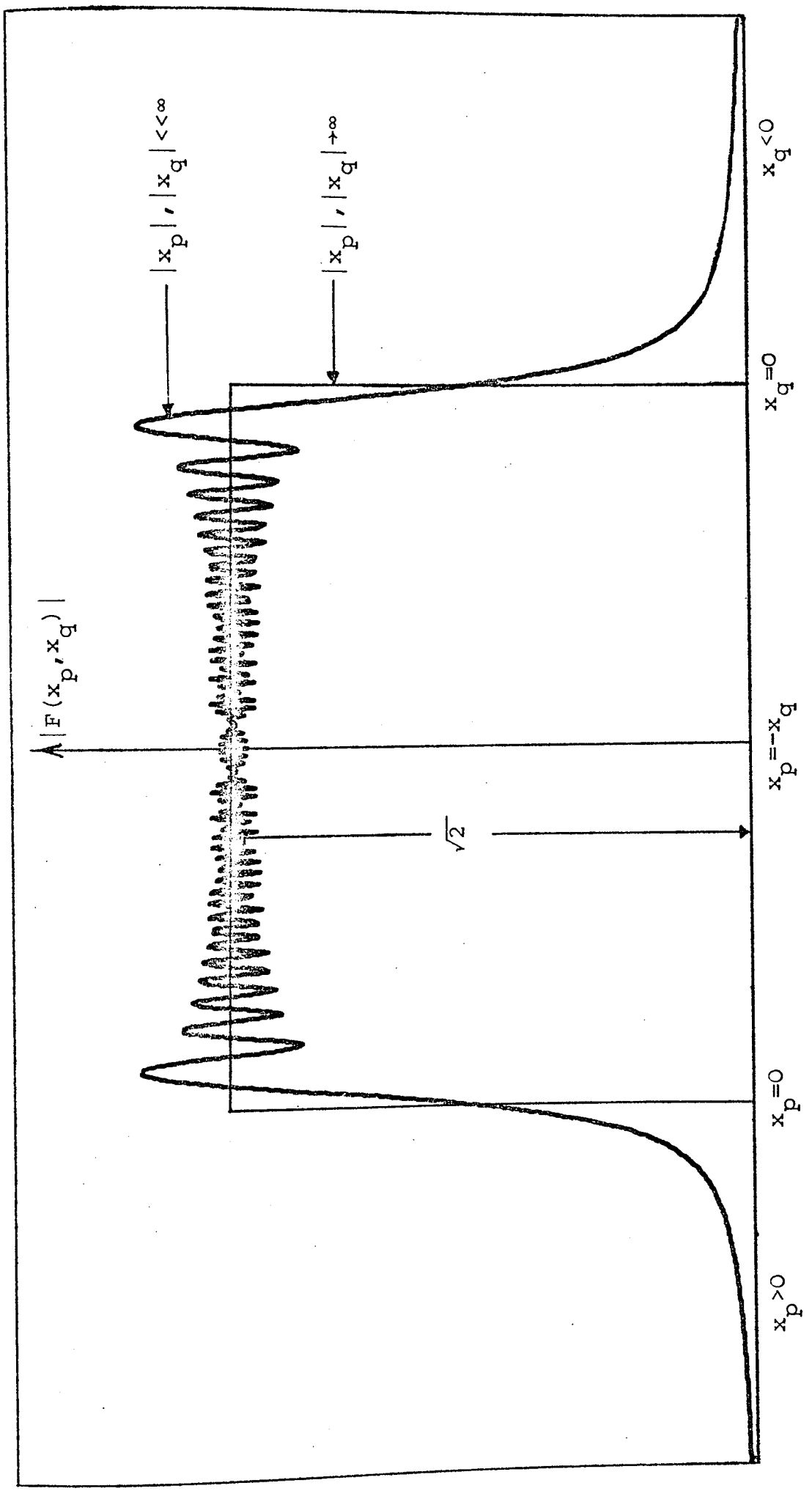

Fig. 3.3 $|F(x_p,x_q)|$ for Large and Small $|x_p|$ and $|x_q|$

the oscillations collapse and $|F(x_p,x_q)|$ becomes mainly confined to the central region assuming a value $\tilde{\sim}$ the mean value $\sqrt{2}$ in this region proper and a value $\tilde{\sim}\frac{1}{\sqrt{2}}$ at its two edges. Conclusions concerning the $F(x_p,x_q)$ phase may be obtained in a similar manner. It suffices here to note that this phase $\tilde{\sim}\frac{\pi}{4}$ in the closed range (x_p=0, x_q=0) if the nonvanishing values of $|x_p|$ and $|x_q|$ are large and fluctuates about this level if these values are small.

3.4.1.3 $\chi^n_{ik}(t,\nu)$ for Large $|x|$'s

The previous discussion indicates that in all cases $\mu_i<\mu_k$, $\mu_i>\mu_k$ and $T_i\lesseqgtr T_k$, $\chi^n_{ik}(t,\nu)$ can be found only if the Fresnel functions $F(x_p,x_q)$, p=1,4, q=2,3 are known. The approach whereby $\chi^n_{ik}(t,\nu)$ is determined through the numerical evaluation of these Fresnel functions cannot be followed here. This is not because this approach is normally tedious, but because it is only possible in the special case where all T_i, T_k, W_i, W_k, t and ν are specified and because it does not generally lead to a closed-form expression of $\chi^n_{ik}(t,\nu)$ which can be used for analytical purposes. However, general conclusions concerning $\chi^n_{ik}(t,\nu)$ and bounds on it may be obtained by making use of those obtained for $F(x_p,x_q)$ in the previous subsection and in Sections 4.8 and 4.11.

The fact that the central region of $F(x_p,x_q)$ is confined

to the range (x_p=0, x_q=0) implies that $\chi^n_{ik}(t,\nu)$ is mainly concentrated in the t-ν plane within the parallelogram whose centre is the origin and whose sides are the following four straight lines corresponding to x_p=0, p=1,4 and x_q=0, q=2,3

$$\mu_k t + \nu = (\mu_i - \mu_k)\frac{T_i}{2} \quad : \quad x_1=0 \tag{3.24a}$$

$$\mu_i t + \nu = (\mu_k - \mu_i)\frac{T_k}{2} \quad : \quad x_2=0 \tag{3.24b}$$

$$\mu_k t + \nu = (\mu_k - \mu_i)\frac{T_i}{2} \quad : \quad x_3=0 \tag{3.24c}$$

$$\mu_i t + \nu = (\mu_i - \mu_k)\frac{T_k}{2} \quad : \quad x_4=0 \tag{3.24d}$$

The vertices of this parallelogram are the points $(\pm\frac{T_i+T_k}{2}, \mp\frac{W_i+W_k}{2})$ and $(\pm\frac{T_k-T_i}{2}, \mp\frac{W_k-W_i}{2})$ and its orientation in the t-ν plane is determined by the signs of W_i and W_k. It provides a simple method for studying $\chi^n_{ik}(t,\nu)$.

Consider, for example, the special case where $\mu_i = 4\mu_k = 2$, $T_k = 2T_i$. The parallelogram corresponding to this case is shown in Fig. 3.4(a). In this case, $\chi^n_{ik}(t,\nu_o)$ for a given $\nu=\nu_o$ is mainly concentrated in the range (t_1,t_2). It is given by (3.22a) with the integral given by $F(x_1,x_2)$ in the range $(-\frac{T_i+T_k}{2}, -\frac{T_k-T_i}{2})$, by $F(x_1,x_3)$ in the range $(-\frac{T_k-T_i}{2}, \frac{T_k-T_i}{2})$ and by $F(x_4,x_3)$

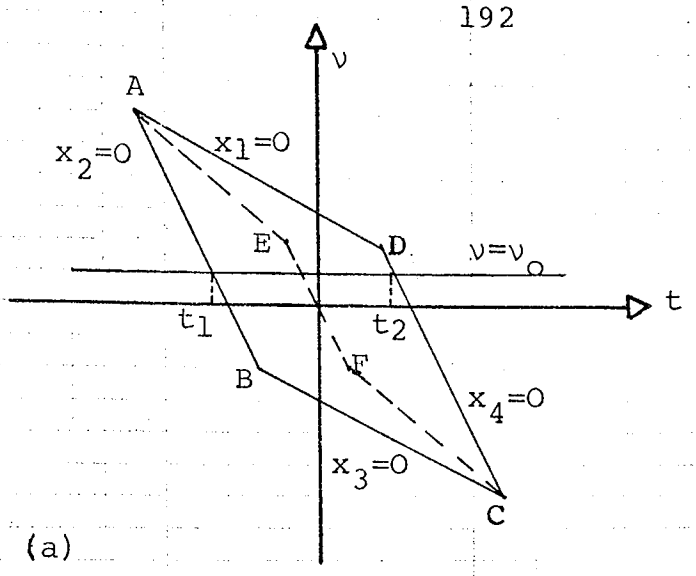

(a)

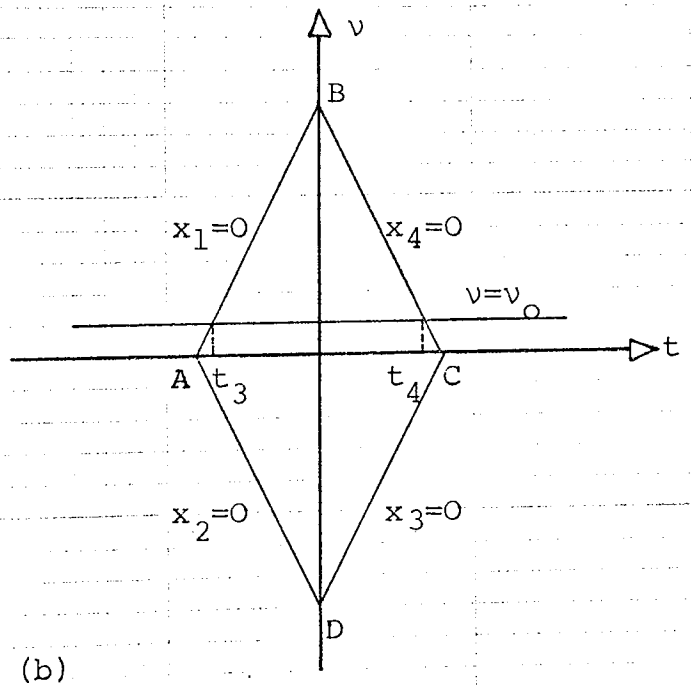

(b)

Fig. 3.4 $\chi^n_{ik}(t,\nu)$ Spread in the t-ν Plane

(a) $\mu_i=4\mu_k=2$, $T_k=2T_i$

(b) $\mu_i=-\mu_k=2$, $T_k=T_i\triangleq T$

$$A \equiv \left(-\frac{T_i+T_k}{2}, \frac{W_i+W_k}{2}\right)$$

$$B \equiv \left(-\frac{T_k-T_i}{2}, \frac{W_k-W_i}{2}\right)$$

$$C \equiv \left(\frac{T_i+T_k}{2}, -\frac{W_i+W_k}{2}\right)$$

$$D \equiv \left(\frac{T_k-T_i}{2}, -\frac{W_k-W_i}{2}\right)$$

in the range $(\frac{T_k-T_i}{2}, \frac{T_i+T_k}{2})$. Also, consider the special case of a slope-reversal chirp pair with $\mu_i=-\mu_k=2$, $T_i=T_k\triangleq T$. The parallelogram corresponding to this case is shown in Fig. 3.4(b). In this case, $\chi_{ik}^n(t,\nu_o)$ is mainly concentrated in the range (t_3,t_4) and is given by (3.22a) with the integral given by $F(x_1,x_2)$ in the range $(-T,0)$ and by $F(x_4,x_3)$ in the range $(0,T)$.

The procedure used in the above-mentioned two special cases can similarly be applied to any other special case in which $\chi_{ik}^n(t,\nu)$ may be treated either as a function of t for a given ν or as a function of ν for a given t. In all cases, the contribution to $\chi_{ik}^n(t,\nu)$ from a particular Fresnel function $F(x_p,x_q)$ or its complex conjugate does not necessarily come from the central region of this function. This implies that each of the amplitude and phase functions of $\chi_{ik}^n(t,\nu)$ may consist of two portions (if $T_i=T_k$) or three (if $T_i\neq T_k$) which may correspond to the central regions and/or tails of the Fresnel functions involved. The actual situation in this respect depends on the particular case under consideration.

It suffices here to consider only the case where the nonvanishing values of all $|x|$'s are large. This case is mathematically tractable and is the main concern of the present discussion. In this case, $F(x_p,x_q)\rightarrow\sqrt{2}e^{j\frac{\pi}{4}}$ in the

central region ($x_p=0$, $x_q=0$) and may be treated as having neither tails nor oscillations. Consequently, contributions to both the amplitude and phase functions of $\chi^n_{ik}(t,\nu)$ in this case come only from the central regions of Fresnel functions. This implies that in this case, $\chi^n_{ik}(t,\nu)$ becomes effectively limited in the t-ν plane to the region lying within the corresponding parallelogram and is given for all $T_i \lesseqgtr T_k$ by

$$|\chi^n_{ik}(t,\nu)| \tilde{\sim} (|\mu_i-\mu_k| T_i T_k)^{-\frac{1}{2}} \tag{3.25a}$$

$$\arg\chi^n_{ik}(t,\nu) \tilde{\sim} z \pm \frac{\pi}{4} \tag{3.25b}$$

where z is given by (3.22b4) and $\frac{\pi}{4}$ and $-\frac{\pi}{4}$ correspond to $\mu_i>\mu_k$ and $\mu_i<\mu_k$ respectively.

Relation (3.25) indicates that for large $|x|$'s, the response $\chi_{ik}(t,\nu)$ of the kth chirp matched filter to the ith chirp always has the form of a LFM oscillation with a mean frequency $f_k + \frac{\nu\mu_k}{\mu_k-\mu_i}$ and a slope $\frac{\mu_i\mu_k}{\mu_k-\mu_i}$. That this response has some residual LFM is due to the mismatch condition between the two chirps.

Unlike $|F(x_p,x_q)|$, $|\chi^n_{ik}(t,\nu)|$ cannot have long tails in t for small $|x|$'s because it vanishes outside the range

$|t| \leq \frac{T_i+T_k}{2}$. Like $|F(x_p,x_q)|$, however, $|\chi^n_{ik}(t,\nu)|$ oscillates for small $|x|$'s. This oscillation takes place about the large $|x|$'s level of (3.25a) as a mean level. The largest oscillation amplitude is generally small compared to this mean level. These conclusions may be obtained by making use of those obtained in Section 4.8 for $|F(x_p,x_q)|$. They imply that (3.25a) can also be taken as a basis for studying $|\chi^n_{ik}(t,\nu)|$ in the small $|x|$'s case.

3.4.1.4 The Large $|x|$'s Assumption

The large $|x|$'s assumption made in the previous subsection will now be considered. Relation (3.23) indicates that the necessary and sufficient condition for the nonvanishing values of all $|x|$'s to be large may be taken as

$$gT_s \geq (2\Delta)^{\frac{1}{2}} \tag{3.26a}$$

i.e.

$$|\mu_i-\mu_k|T_s^2 \geq \Delta \tag{3.26b}$$

where $\Delta >> 1$ and T_s is the smaller of T_i and T_k.

The required Δ-value depends on the desired preciseness. An acceptable such value from the viewpoint of the present

discussion may be based on the assumption that the kth chirp matched filter output is normally sampled at t=0 in search for any possible response characteristic of this chirp. In this case, $t=\nu=0$ and (3.23) gives $|x_1|=|x_3|=\frac{gT_i}{2}$ and $|x_2|=|x_4|=\frac{gT_k}{2}$. These values may be considered to be sufficiently large from a Fresnel viewpoint if $gT_s \geq 3.5$. Making use of this fact, (3.26) gives $\Delta \geq 25$.

Condition (3.26) implies that $|\chi_{ik}^n(t,\nu)|$ in (3.25a) is low compared to unity. That is, (3.25) is more suited for interference studies where the ith and kth chirps are intended to be distinct rather than distortion studies where these two chirps are understood to be slightly mismatched versions of one another. This is convenient from the viewpoint of the present discussion which is mainly concerned with interference studies and signal design. Distortion studies imply that (3.26) and, hence, (3.25) do not hold. In this case, $|\chi_{ik}^n(t,\nu)|$ and $\arg\chi_{ik}^n(t,\nu)$ generally fluctuate about those of (3.25) as their means and one would have to evaluate them through (3.22) by numerical techniques or to predict their behaviour by making use of the methods of Sections 4.8 and 4.11.

3.4.1.5 $\chi_{ik}^n(t,\nu)$ Spread in the t-ν Plane

Subsection 3.4.1.3 indicates that the spread of

$\chi^n_{ik}(t,\nu)$ in the t-ν plane may be effectively limited to any desired parallelogram centred at the origin by a proper choice of T_i, T_k, W_i and W_k that satisfies (3.26). It should be noted, however, that such a choice does also affect the $|\chi^n_{ik}(t,\nu)|$ level through (3.25a).

Condition (3.26) is both necessary and sufficient for $\chi^n_{ik}(t,\nu)$ to be negligible for all $|\nu|>\frac{|W_i|+|W_k|}{2}$. Thus, (3.26) relaxes the two previously stated conditions in this respect that $|W_iT_i|>>1$ and $|W_kT_k|>>1$ (see Subsection 3.4.1).

$\chi^n_{ik}(t,\nu)$ has an effective duration $\leq$ its actual duration. This effective duration may remain constant or change with $|\nu|$. The relationship between the centre of this duration and ν depends on the values of T_i, T_k, W_i, and W_k under consideration and may take the form of a broken line such as AEFC in Fig. 3.4(a) or a straight line such as BD in Fig. 3.4(b). This relationship corresponds to the linear t-ν coupling law $t=-\frac{\nu}{\mu}$ relating this centre and ν for two chirps having the same slope μ.

If $|\chi^n_{ik}(t,\nu)|$ of (3.25a) is plotted as a surface extending over the t-ν plane, it will look as a flat plateau whose altitude is constant and whose projection on the t-ν plane is the parallelogram corresponding to the values of T_i, T_k, W_i and W_k involved.

If (3.26) does not hold, (3.25a) also does not hold and

this plateau fluctuates about the level of (3.25 a) as a mean altitude and its projection on the t-ν plane becomes less defined.

3.4.2 Mismatch Effects

$\chi^n_{ik}(t,\nu)$ may be used to carry out a hierarchy of studies concerning chirps having different slopes. These studies may be related to weighting, signal design or mismatch effects. Some basic results obtained in the next subsection may be used for weighting. Signal design will be considered in the next section. The present subsection considers the effects of mismatch between the ith and kth chirps on the latter's matched filter response to the former.

Isolated and combined phase, frequency and duration (or bandwidth) mismatch effects in the $\mu_i=\mu_k$ case have already been outlined in the previous section. Thus, it remains to consider the effects of μ-mismatch in isolation from, or in combination with, phase, frequency, duration and bandwidth mismatch. It also remains to compare the mismatch effects in the $\mu_i=\mu_k$ case with their counterparts in the $\mu_i\neq\mu_k$ case. A detailed analysis in this respect is not intended here and may be carried out be comparing (3.13), (3.14), (3.15) and an explicit numerical or mathematical expression of (3.22) having a validity and preciseness that match those of the desired results. In any case, a few comments are in order.

Subsection 3.4.1.3 indicates that for a given ν, $|\chi_{ik}^{n}(t,\nu)|$ is rectangular in t as long as (3.26) holds, i.e. it has the same functional form as that of the envelope of the input chirp. This may be compared with a previous result that in the $\mu_i=\mu_k$ case, $|\chi_{ik}^{n}(t,\nu)|$ roughly has the form of the Fourier transform of the rectangular envelope of the input chirp.

The response level in the $\mu_i\neq\mu_k$ case is less than that in the $\mu_i=\mu_k$ case. While the latter has a normalized value = 1, the former has a normalized mean value $\simeq \frac{1}{(|\mu_i-\mu_k|T_iT_k)^{\frac{1}{2}}} < 1$. Response level degradation in moving from the $\mu_i=\mu_k$ condition to the $\mu_i\neq\mu_k$ condition is mainly determined by the dominating μ-mismatch $|\mu_i-\mu_k|$ and is insensitive to α, t and ν.

Relation (3.24) can also be used in the case where $\mu_i=\mu_k\triangleq\mu$. In this case, (3.24) reduces to the single linear relation $\mu t+\nu=0$ corresponding to the main ridge of $|\chi_{ik}^{n}(t,\nu)|$ when viewed as a surface extending over the t-ν plane. This indicates that in moving from the $\mu_i=\mu_k$ condition to the $\mu_i\neq\mu_k$ condition, the main ridge straight line $\mu t+\nu=0$ degenerates into a parallelogram whose sides are given by (3.24) and whose size is proportional to the μ-mismatch $|\mu_i-\mu_k|$.

3.4.3 Correlation of Two Shaped LFM Signals Having Different Slopes

Consider the two shaped LFM signals $y_i(\sigma)$ and $y_k(\sigma)$ of the complex LFM signal set (3.5). Let $\alpha_i-\alpha_k \triangleq \alpha$ and $f_i-f_k \triangleq \nu$. The correlation function $\chi_{ik}(t,\nu)$ of these two signals can be obtained by substituting $y_i(\sigma)$ for $s_i(\sigma)e^{j2\pi\nu\sigma}$ and $y_k(\sigma)$ for $s_k(\sigma)$ in (1.4a) making use of (1.1a). Thus,

$$\chi_{ik}(t,\nu)=e^{ju}\int_\sigma a_i(\sigma)\,a_k(\sigma-t)\,e^{j2\pi\left[(\mu_k t+\nu)\sigma+\frac{\mu_i-\mu_k}{2}\sigma^2\right]}d\sigma \tag{3.27a}$$

where u is given by (3.21b).

Relation (3.27a) is a generalization of, and has the same integration limits as, (3.21). However, it is more difficult to handle even if $a_i(\sigma)$ and $a_k(\sigma)$ are specified. Such a specification does not necessarily simplify the integral or reduce it to a Fresnel form which can be treated in a manner similar to that used for (3.21a). Thus, an exact closed-form expression of (3.27a) is not generally possible. However, it is sometimes possible to obtain an approximate explicit expression for (3.27a) even without specifying $a_i(\sigma)$ and $a_k(\sigma)$. This may be achieved by applying the stationary phase method to the integral and is possible only if the conditions underlying this method are satisfied. Such a satisfaction is conceivable as long as $a_i(\sigma)$ and

$a_k(\sigma)$ are two well behaved physical time functions which are slowly varying in contrast with the integrand's exponential function (i.e. $|\mu_i-\mu_k|$ is sufficiently large).

The stationary phase method implies that in the first approximation, the main contribution to the value of the integral in (3.27a) comes from the vicinity of the integrand's stationary phase where $\frac{d}{d\sigma}\left[(\mu_k t+\nu)\sigma+\frac{\mu_i-\mu_k}{2}\sigma^2\right]=0$, i.e. from the vicinity of $\sigma_o \triangleq \frac{\mu_k t+\nu}{\mu_k-\mu_i}$. Thus, this integral $\approx \int_{\sigma\approx\sigma_o}(.)d\sigma$. Since $a_i(\sigma)$ and $a_k(\sigma)$ are assumed to be slowly varying functions of σ, the product $a_i(\sigma)\ a_k(\sigma-t)\approx a_i(\sigma_o)\ a_k(\sigma_o-t)$ for $\sigma\approx\sigma_o$ and, hence, can be taken outside the integration sign. Thus, the integral $\approx a_i(\sigma_o)a_k(\sigma_o-t)\int_{\sigma\approx\sigma_o} e^{j2\pi\left[(\mu_k t+\nu)\sigma+\frac{\mu_i-\mu_k}{2}\sigma^2\right]}d\sigma$. Also, since σ_o is the only integrand's stationary phase point, the integration may be carried out over all σ and not only over $\sigma\approx\sigma_o$. In this manner, the integral $\approx a_i(\sigma_o)a_k(\sigma_o-t).I$, where I is the integral in (3.21a). Making use of these facts, (3.27a) reduces to

$$\chi_{ik}(t,\nu)\tilde{\approx} a_i\left(\frac{\mu_k t+\nu}{\mu_k-\mu_i}\right)a_k\left(\frac{\mu_i t+\nu}{\mu_k-\mu_i}\right)e^{ju}.I \qquad (3.27b)$$

where u is given by (3.21b) and I is the integral in (3.21a).

It suffices here to consider only the case where condition (3.26) holds. In this case, $I=\frac{e^{j(z-u\pm\frac{\pi}{4})}}{|\mu_i-\mu_k|^{\frac{1}{2}}}$ and (3.27b) reduces

for all $T_i \gtrless T_k$ to

$$|\chi_{ik}(t,\nu)| = \frac{a_i\left(\frac{\mu_k t+\nu}{\mu_k-\mu_i}\right) a_k\left(\frac{\mu_i t+\nu}{\mu_k-\mu_i}\right)}{|\mu_i-\mu_k|^{\frac{1}{2}}}, \quad \mu_i \neq \mu_k \tag{3.27c1}$$

$$\arg \chi_{ik}(t,\nu) = z \pm \frac{\pi}{4} \tag{3.27c2}$$

where in (3.27c2), z is given by (3.22b4) and $\frac{\pi}{4}$ and $-\frac{\pi}{4}$ correspond to $\mu_i > \mu_k$ and $\mu_i < \mu_k$ respectively.

Relation (3.27c) can be used as a basis for a variety of studies concerning LFM signals having different slopes such as weighting, mismatching and signal design. It can be studied in a manner similar to that used to study (3.25).

The normalized form of (3.27c) can be obtained through (1.4). This form is a generalization of (3.25). Although (3.27a) reduces to (3.18a) in the special case where $\mu_i = \mu_k \triangleq \mu$, (3.27c) is like (3.25) in that it can only be used in the case where $\mu_i \neq \mu_k$. As given by (3.27), $\chi_{ik}(t,\nu)$ has the general properties outlined in Subsection 1.3.2 and can be used to derive $\chi_{ki}(t,\nu)$ through (1.5).

For a given ν, $\chi_{ik}(t,\nu)$ describes the response of the $y_k(\sigma)$ matched filter to $y_i(\sigma)$. For all ν, $T_i \lesseqgtr T_k$, $\mu_i > \mu_k$ and $\mu_i < \mu_k$, this response is always limited to the range $|t| \lesseqgtr \frac{T_i+T_k}{2}$. The response envelope $|\chi_{ik}(t,\nu)|$ may be plotted

and studied as a surface extending over the t-ν plane.

$\chi_{ik}(t,\nu)$ is effectively limited in the t-ν plane to the region lying inside the parallelogram whose sides are given by (3.24). This conclusion may be reached in a manner similar to that used for $\chi^{n}_{ik}(t,\nu)$ of (3.25). This conclusion may also be directly based on (3.27c). Thus, noting that $a_i(\sigma)$ and $a_k(\sigma)$ are limited to the ranges $|\sigma| \leq \frac{T_i}{2}$ and $|\sigma| \leq \frac{T_k}{2}$ respectively, it can be seen that the product $a_i(\frac{\mu_k t+\nu}{\mu_k-\mu_i})\, a_k(\frac{\mu_i t+\nu}{\mu_k-\mu_i})$ and, hence, $\chi_{ik}(t,\nu)$ in (3.27c) are confined between the straight lines $\frac{\mu_k t+\nu}{\mu_k-\mu_i} = \pm \frac{T_i}{2}$ and $\frac{\mu_i t+\nu}{\mu_k-\mu_i} = \pm\frac{T_k}{2}$, which are identical to those of (3.24).

The fact that $\chi_{ik}(t,\nu)$ of(3.27c)is effectively confined to the same t-ν parallelogram as $\chi_{ik}(t,\nu)$ of(3.25) indicates that the former has all the properties of Subsection 3.4.1.5.However if $|\chi_{ik}(t,\nu)|$ of(3.27c)is plotted as a surface extending over the t-ν plane,it will generally look as an uneven plateau whose projection on this plane is the parallelogram defined by(3.24)and whose shape and altitude are determined by the product $a_i(\frac{\mu_k t+\nu}{\mu_k-\mu_i})\, a_k(\frac{\mu_i t+\nu}{\mu_k-\mu_i})$. A vertical cut through this plateau will essentially have the same shape as the product $a_i(.)\,a_k(.)$ as long as (3.26) holds. If (3.26) does not hold, this cut will assume a distorted shape fluctuating about the product $a_i(.)\,a_k(.)$ as its mean.

For a given ν and as long as (3.26) holds, the response

envelope $|\chi_{ik}(t,\nu)|$ has the functional form of the product $a_i(.)a_k(.)$ of the envelopes of the two correlated LFM signals $y_i(\sigma)$ and $y_k(\sigma)$. This conclusion is a generalization of that obtained for chirp signals in Subsection 3.4.2.

Relation (3.27a) indicates that $|\chi_{ik}(t,\nu)|<|\int_\sigma a_i(\sigma)a_k(\sigma-t)e^{jc}d\sigma|\leq|\int_\sigma a_i(\sigma)a_k(\sigma-t)d\sigma|$, where c is the integrand's stationary phase. This implies that $|\int_\sigma a_i(\sigma)a_k(\sigma-t)d\sigma|$ is a loose bound on $|\chi_{ik}(t,\nu)|$ and, hence, on $\chi_{ik}(t,\nu)$ itself. This can be compared with a corresponding result obtained in Subsection 3.2.4 for the $\mu_i=\mu_k$ case and indicated that $|\int_\sigma a_i(\sigma)a_k(\sigma-t)d\sigma|$ is a tight bound on $|\chi_{ik}(t,\nu)|$ and, hence, on $\chi_{ik}(t,\nu)$. This difference between the $\mu_i=\mu_k$ and $\mu_i\neq\mu_k$ cases is expected, however, because the μ-mismatch is bound to reduce the response level.

As compared to $\chi_{ik}(t,\nu)$ in the $\mu_i=\mu_k$ case, $\chi_{ik}(t,\nu)$ in the $\mu_i\neq\mu_k$ case can only be used for LFM studies involving a single FSK or PSK element. This is because a different $-\mu$ LFM set can accommodate only one FSK or PSK element with a slope=0.

3.5 Signal Design For Chirps Having Different Slopes

This section considers the problem of designing signal sets consisting of chirps having different slopes for digital

data transmission. It assumes optimum processing in an AWGN background and practically tolerable mutual interferences and slope distortions and deviations. The results obtained may be taken as a basis for the corresponding case of shaped-LFM signal design.

Signal design for chirps with different slopes may be achieved by the conventional detection theoretical method in both the coherent and noncoherent cases (see Subsection 3.3.1).

3.5.1 The Coherent Case

Signal design for chirps having different slopes in the coherent case may be considered through the ith and kth members of the real chirp set (3.9). To this end, let $\mu_i \neq \mu_k$, $|\alpha_i - \alpha_k| \triangleq \alpha$ and $f_i - f_k \triangleq \nu$ and assume that T_i, T_k, W_i and W_k satisfy condition (3.26). If the kth chirp bandwidth $< 2f_k$ and the ith chirp bandwidth $< 2f_i$, the normalized correlation coefficient $\lambda_{ik}^{n}(0,\nu)$ of these two chirps may be obtained by making use of (3.25) in (1.14a). Thus,

$$\lambda_{ik}^{n}(0,\nu) = \frac{\cos\left(\alpha \pm \frac{\pi}{4} - \frac{\pi\nu^2}{\mu_i - \mu_k}\right)}{\left(|\mu_i - \mu_k| T_i T_k\right)^{\frac{1}{2}}} \tag{3.28}$$

where $\frac{\pi}{4}$ and $-\frac{\pi}{4}$ correspond to $\mu_i > \mu_k$ and $\mu_i < \mu_k$ respectively.

Relation (3.28) indicates that $\lambda_{ik}^{n}(0,\nu)$ oscillates about zero-level between the lower and upper bounds $\pm \frac{1}{(|\mu_i-\mu_k|T_iT_k)^{\frac{1}{2}}}$ with an oscillation amplitude $= \frac{2}{(|\mu_i-\mu_k|T_iT_k)^{\frac{1}{2}}}$ Relation (3.28) also indicates that $\lambda_{ik}^{n}(0,\nu)$ depends on α, ν and $(|\mu_i-\mu_k|T_iT_k)$. However, since $|\mu_i-\mu_k|T_iT_k>>1$ according to (3.26), $\lambda_{ik}^{n}(0,\nu)$ is mainly determined by the factor $\frac{1}{(|\mu_i-\mu_k|T_iT_k)^{\frac{1}{2}}}$ in such a way that it is essentially $\simeq 0$ and relatively insensitive to variations in α and ν. Thus, the two chirps under consideration can practically be seen to form a quasi-orthogonal pair in the coherent case. Assuming AWGN and equiprobable chirps with the same energy E, the performance of this pair can be obtained from (1.26).

If α- and ν- control is both possible and desirable, proper selection of α and ν can make $\lambda_{ik}^{n}(0,\nu)$ assume any required value between its lower and upper bounds (e.g. $\lambda_{ik}^{n}(0,\nu)=0$). If either $\mu_i=0$ or $\mu_k=0$, the ith and kth chirp pair reduces to an FSK-chirp pair. Moreover, if condition (3.26) is not strictly satisfied, $\lambda_{ik}^{n}(0,\nu)$ will have two new bounds which fluctuate about their flat counterparts mentioned above as mean levels and, hence, the preceding results will still hold in the mean (see Subsection 3.6.1).

The preceding discussion indicates that in the coherent case, quasi-orthogonality is the only practically conceivable correlation relationship between two or more chirps having

different slopes. Signal sets comprising such chirps will be considered in Subsection 3.5.3 below.

3.5.2 The Noncoherent Case

Signal design for chirps having different slopes in the noncoherent case may be elucidated by considering the ith and kth chirps described in the previous subsection disregarding their phases. The in-phase and quadrature correlation coefficients $\rho_{ik}(0,\nu)$ and $\hat{\rho}_{ik}(0,\nu)$ of these two chirps may be obtained by making use of (3.25) in (1.27). Thus,

$$\rho_{ik}(0,\nu) = \frac{\cos\left(-\frac{\pi\nu^2}{\mu_i-\mu_k} \pm \frac{\pi}{4}\right)}{\left(|\mu_i-\mu_k|T_iT_k\right)^{\frac{1}{2}}} \tag{3.29a}$$

$$\hat{\rho}_{ik}(0,\nu) = \frac{\sin\left(-\frac{\pi\nu^2}{\mu_i-\mu_k} \pm \frac{\pi}{4}\right)}{\left(|\mu_i-\mu_k|T_iT_k\right)^{\frac{1}{2}}} \tag{3.29b}$$

where $\frac{\pi}{4}$ and $-\frac{\pi}{4}$ correspond to $\mu_i>\mu_k$ and $\mu_i<\mu_k$ respectively.

Except for their independence of α and that they are in phase-quadrature, $\rho_{ik}(0,\nu)$ and $\hat{\rho}_{ik}(0,\nu)$ have the same properties as $\lambda^n_{ik}(0,\nu)$ of (3.28). This implies that also in the noncoherent case, the ith and kth chirps under consideration can be seen to form a quasi-orthogonal pair. Assuming AWGN and equiprobable chirps with the same energy E,

the performance of this pair in the noncoherent case may be obtained by making use of the appropriate P_e-expressions characteristic of this case (see Section 1.4).

Again, quasi-orthogonality is the only practically conceivable correlation relationship between two or more chirps having different slopes in the noncoherent case. Signal sets comprising such chirps will be considered in the next subsection.

3.5.3 Chirp Packing

This subsection considers the problem of constructing quasi-orthogonal sets of chirps with different slopes by packing the members of each set in a given μ-space in such a way that the mutual interference between any two members does not exceed a maximum admissible level.

3.5.3.1 Introduction

Let the chirp set to be designed comprise the first M members of the real chirp set (3.9), $M \leq N$. Let each member of this set have its distinct slope and assume that the durations and sweeps of any two of its members may be arbitrarily chosen in such a way that condition (3.26) is satisfied.

The optimum demodulator of the real chirp set to be designed is assumed to comprise an optimum predetection processor for each of its members. Assuming AWGN, this processor may be a correlator or a matched filter-sampler in the coherent case and a square-envelope correlator or a matched filter-envelope detector-sampler in the noncoherent case.

Assume coherent reception and consider the optimum predetection processor of chirp $r_k(\sigma)$, say, of the set to be designed. This processor gives a response $\lambda_{kk}(0,0)$ to $r_k(\sigma)$ itself and a response $\lambda_{ik}(0,\nu)$ to the ith member of the set, i.e. to $r_i(\sigma)$. Making use of (1.12a) and (1.4), (3.13b) gives $\lambda_{kk}(0,0)=E_k$ and (3.25) gives $\lambda_{ik}(0,\nu)=\frac{(E_iE_k)^{\frac{1}{2}}}{(|\mu_i-\mu_k|T_iT_k)^{\frac{1}{2}}}\cos(\alpha\pm\frac{\pi}{4}-\frac{\pi\nu^2}{\mu_i-\mu_k})$. This indicates that in the coherent case, the maximum expected power Interference-to-Signal Ratio (ISR) at the output of $r_k(\sigma)$'s processor due to $r_i(\sigma)$ is $(\frac{\text{maximum } \lambda_{ik}(0,\nu)}{\lambda_{kk}(0,0)})^2=\frac{E_i}{E_k|\mu_i-\mu_k|T_iT_k}\triangleq\beta_{i,k}^{-1}$, where $\beta_{i,k}$ is the corresponding Signal-to-Interference Ratio (SIR). Similarly, it can be seen in the coherent case that the maximum expected ISR at the output of $r_i(\sigma)$'s processor due to $r_k(\sigma)$ is $(\frac{\text{maximum } \lambda_{ki}(0,\nu)}{\lambda_{ii}(0,0)})^2=\frac{E_k}{E_i|\mu_i-\mu_k|T_iT_k}\triangleq\beta_{k,i}^{-1}$. It can also be seen that $\beta_{i,k}\gtrless\beta_{k,i}$ implies $E_k\gtrless E_i$.

Again, assume noncoherent reception and consider the

optimum predetection processor of $r_k(\sigma)$. This processor gives a response = Envelope$[\lambda_{kk}(t,0)]_{t=0}$ to $r_k(\sigma)$ itself and a response = Envelope$[\lambda_{ik}(t,\nu)]_{t=0}$ to $r_i(\sigma)$. Making use of (1.12b) and (1.4), (3.13c) gives Envelope$[\lambda_{kk}(t,0)]_{t=0}$ $= E_k$ and (3.25a) gives Envelope$[\lambda_{ik}(t,\nu)]_{t=0} = \left(\frac{E_i E_k}{|\mu_i - \mu_k| T_i T_k}\right)^{\frac{1}{2}}$. This indicates that in the noncoherent case the maximum expected ISR at the output of $r_k(\sigma)$'s processor due to $r_i(\sigma)$ is $\beta_{i,k}^{-1}$. Similarly, it can be seen in the noncoherent case that the maximum expected ISR at the output of $r_i(\sigma)$'s processor due to $r_k(\sigma)$ is $\beta_{k,i}^{-1}$.

The preceding facts indicate that in both the coherent and noncoherent cases, the interference caused by $r_i(\sigma)$ at the output of $r_k(\sigma)$'s processor does not exceed the ISR level $\beta_{i,k}^{-1}$ and that the interference caused by $r_k(\sigma)$ at the output of $r_i(\sigma)$'s processor does not exceed the level $\beta_{k,i}^{-1}$. These facts also indicate that $\beta_{i,k}$ is generally different from $\beta_{k,i}$ unless $E_i = E_k$.

The previous paragraph implies that in both the coherent and noncoherent cases, the maximum interference levels characterizing the different pairs of the chirp set under consideration may not necessarily be the same. Accordingly, it is desired to construct this set in such a way that the interference between any two of its members does not exceed a maximum admissible ISR level β_O^{-1}, say. Thus, the problem is to construct this set in such a way that: (a) it satisfies

condition (3.26), (b) each of its members has its distinct slope, (c) no member can have a slope outside the specified μ- range (μ_{min}, μ_{max}), and (d) the mutual ISR level of any two members does not exceed β_o^{-1}, i.e. $\beta_{i,k}^{-1} \leq \beta_o^{-1}$; $i \neq k$; $i,k=1,2,3,\ldots,M$. This problem may be tackled by either of the two construction methods suggested below.

3.5.3.2 First Packing Method

This method requires the selection of the energy, slope and duration (or sweep), or any other equivalent set of parameters, of each member of the chirp set to be constructed. It may be outlined in the following four steps:

(i) Assign the energies of the members in such a way that

$$E_m \leq E_{m+1};\ m=1,2,3,\ldots,M-1 \qquad (3.30a)$$

(ii) Assign the slopes of the members in an ascending order in such a way that

$$\mu_1 = \mu_{min} \quad \text{and}$$

$$\mu_m < \mu_{m+1} \leq \mu_{max};\ m=1,2,3,\ldots,M-1 \qquad (3.30b1)$$

Alternatively, assign the slopes of the members in a descending order in such a way that

$$\mu_1 = \mu_{max} \quad \text{and}$$

$$\mu_{min} \leq \mu_{m+1} < \mu_m;\ m=1,2,3,\ldots,M-1 \qquad (3.30b2)$$

(iii) Assign the durations of the consecutive members in any suitable manner is such a way that

$$|\mu_m-\mu_{m+1}|=\beta_O\frac{E_{m+1}}{E_m}\frac{1}{T_mT_{m+1}}\ ;\ m=1,2,3,\ldots,M-1 \qquad (3.30c1)$$

Alternatively, assign the sweeps of the consecutive members in any suitable manner in such a way that

$$\left|\frac{1}{\mu_m}-\frac{1}{\mu_{m+1}}\right|=\beta_O\frac{E_{m+1}}{E_m}\frac{1}{|W_mW_{m+1}|};\quad m=1,2,3,\ldots,M-1 \qquad (3.30c2)$$

Relation (3.30c1) implies that $\beta_{m+1,m}=\beta_O$, i.e. the ISR caused by any member at the output of the processor of the preceding member is equal to the maximum admissible level β_O^{-1}. Also, (3.30a) implies that $\beta_{m,m+1}\geq\beta_{m+1,m}\geq\beta_O$. These facts imply that the mutual relative interference between any consecutive pair of the chirp set under construction does not exceed the ISR level β_O^{-1}. It should be noted here that (3.30c1) and (3.30c2) are equivalent. In fact, dividing (3.30c1) by $|\mu_m\mu_{m+1}|$ reduces it to (3.30c2).

(iv) Assign the durations of the nonconsecutive members in any suitable manner in such a way that

$$|\mu_p-\mu_q|\geq\beta_O\frac{E_p}{E_q}\frac{1}{T_pT_q}; \qquad (3.30d1)$$

$q=1,2,3,\ldots,M-2;$

$p=q+2, q+3,\ldots,M.$

Alternatively, assign the sweeps of the nonconsecutive members in any suitable manner in such a way that

$$\left|\frac{1}{\mu_p} - \frac{1}{\mu_q}\right| \geq \beta_o \frac{E_p}{E_q} \frac{1}{|W_p W_q|}; \qquad (3.30d2)$$

$q=1,2,3,\ldots,M-2;$

$p=q+2,q+3,\ldots,M.$

Relation (3.30d1) indicates that $\beta_{p,q} \geq \beta_o$. Also, (3.30a) implies that $\beta_{q,p} \geq \beta_{p,q} \geq \beta_o$. These facts imply that the mutual relative interference between any two nonconsecutive members of the chirp set under construction does not exceed the required ISR level β_o^{-1}. Thus, (3.30c) and (3.30d) guarantee that the relative interference between any two different members of this subset does not exceed the maximum admissible ISR level β_o^{-1}. Again, it should be noted that (3.30d1) and (3.30d2) are equivalent.

This method is capable of packing chirps in the given μ-space in the most compact manner under the specified ISR ceiling β_o^{-1}, i.e. in such a way that $\beta_{i,k}^{-1} \leq \beta_o^{-1}$; $i \neq k$; $i,k=1,2,3,\ldots,M$. The number M of chirps that can be packed by this method under such constraints may be obtained from (3.30c1) or (3.30c2) by letting m assume all its possible values and summing the results. Thus,

$$|\mu_1-\mu_M| = \beta_O \sum_{m=1}^{M-1} \frac{E_{m+1}}{E_m} \frac{1}{T_m T_{m+1}} \qquad (3.30e1)$$

or

$$|\frac{1}{\mu_1} - \frac{1}{\mu_M}| = \beta_O \sum_{m=1}^{M-1} \frac{E_{m+1}}{E_m} \frac{1}{|W_m W_{m+1}|} \qquad (3.30e2)$$

where (3.30e1) is to be used if the durations are specified and (3.30e2) is to be used if the sweeps are specified.

Relation (3.30e) does not give an explicit expression for M except in the case where $\frac{E_{m+1}}{E_m} \frac{1}{T_m T_{m+1}}$ = constant or $\frac{E_{m+1}}{E_m} \frac{1}{|W_m W_{m+1}|}$ = constant for all m=1,2,3,...,M-1. This case includes, for example, the two special cases where: (a) the ratio $\frac{E_{m+1}}{E_m}$ is fixed (i.e. $E_2=\sqrt{E_1 E_3}$, $E_3=\sqrt{E_2 E_4}$... etc) and either $T_m T_{m+1}$ is fixed (i.e. $T_1=T_3=T_5=...$; $T_2=T_4=T_6=...$) or $|W_m W_{m+1}|$ is fixed (i.e. $|W_1|=|W_2|=|W_5|=....$; $|W_2|=|W_4|=|W_6|...$) and (b) all chirps have the same energy and either have the same duration or have the same sweep (see Subsection 3.5.3.4 below). Other special cases in this category can readily be defined. In any case, it can be seen that relation (3.30e) always implies the logical conclusion that M increases with the available μ-range (μ_{min},μ_{max}) as well as with the admissible ISR level β_O^{-1} and is determined by the actual values of the energies and durations (or sweeps).

In the case where the chirps to be packed have equal energies, $\beta_{i,k}=\beta_{k,i}=|W_iT_k-W_kT_i|$ for any two consecutive or nonconsecutive chirps and the packing steps become much easier and their associated relations become simpler. For example, (3.30c) reduces to $|W_mT_{m+1}-W_{m+1}T_m|=\beta_O$ for a consecutive pair, (3.30d) reduces to $|W_iT_k-W_kT_i|\geq\beta_O$ for a nonconsecutive pair and (3.30e) reduces to

$$|\mu_1-\mu_M|=\beta_O\sum_{m=1}^{M-1}\frac{1}{T_mT_{m+1}} \tag{3.30f1}$$

or

$$\left|\frac{1}{\mu_1}-\frac{1}{\mu_M}\right|=\beta_O\sum_{m=1}^{M-1}\frac{1}{|W_mW_{m+1}|} \tag{3.30f2}$$

3.5.3.3 Second Packing Method

The first packing method outlined above is rather difficult to implement and does not give an explicit M-expression except in some special cases. Accordingly, an alternative method will now be described which may not necessarily have a comparable packing capability but is generally easier to implement and does always give an explicit M-expression. Like the first method, this method also requires the selection of the energy, slope and duration (or sweep) of each member of the chirp set to be constructed. Unlike the first method, however, this method

does not give identical results in terms of both durations and sweeps. This can be seen from the following steps underlying this method:

(i) Assign the energies and slopes of the members as described in steps (i) and (ii) of the first method.

(ii) Assign a minimum admissible duration T_{min}. Alternatively, assign a minimum admissible sweep $|W|_{min}$.

(iii) Assign the slopes of the members in such a way that the slope difference between any two consecutive members is constant and let

$$|\mu_m - \mu_{m+1}| = \beta_o \frac{E_M}{E_1} \frac{1}{T_{min}^2} ; \tag{3.31a1}$$

or

$$\left|\frac{1}{\mu_m} - \frac{1}{\mu_{m+1}}\right| = \beta_o \frac{E_M}{E_1} \frac{1}{|W|_{min}^2} ; \tag{3.31a2}$$

$m=1,2,3,\ldots,M-1.$

This relation can readily be seen to imply that the mutual relative interference between any two consecutive or nonconsecutive members does not exceed the maximum admissible ISR level β_o^{-1} as required.

In this method, an expression for M can be obtained from (3.31a) by letting m assume all its possible values

and summing the results. Thus

$$M = 1 + \frac{1}{\beta_O}|\mu_1-\mu_M|\frac{E_1}{E_M}T_{min}^2 \tag{3.31b1}$$

or

$$M = 1 + \frac{1}{\beta_O}|\frac{1}{\mu_1} - \frac{1}{\mu_M}|\frac{E_1}{E_M}|W|_{min}^2 \tag{3.31b2}$$

This relation explicitly shows that M increases with the available μ-range (μ_{min}, μ_{max}) as well as with the admissible ISR level β_O^{-1}.

In the case where the chirps to be packed have equal energies, $\beta_{i,k}=\beta_{k,i}=|W_iT_k-W_kT_i|$ for any two consecutive or nonconsecutive chirps and the packing steps become slightly easier and their associated relations become simpler. For example, (3.31a1) reduces to $|\mu_m-\mu_{m+1}|=\frac{\beta_O}{T_{min}^2}$, (3.31a2) reduces to $|\frac{1}{\mu_m} - \frac{1}{\mu_{m+1}}|=\frac{\beta_O}{|W|_{min}^2}$ and (3.31b) reduces to

$$M = 1 + \frac{1}{\beta_O}|\mu_1-\mu_M|T_{min}^2 \tag{3.31c1}$$

or

$$M = 1 + \frac{1}{\beta_O}|\frac{1}{\mu_1} - \frac{1}{\mu_M}||W|_{min}^2 \tag{3.31c2}$$

3.5.3.4 Packing of Chirps Having Equal Energies

The preceding two chirp packing methods have been formulated in quite general terms. They may be applied to a variety of special cases concerning the parameters forming the ISR expression, namely, the energy, duration and sweep and their combinations. Such special cases include, for example, those cases where the chirps to be packed have energies, durations, bandwidths ($\simeq$ sweeps), duration-bandwidth products or average powers that are constrained to lie within specific ranges or to satisfy certain algebraic relations (e.g. equal, form an arithmetic progression). A detailed study of such special cases cannot be given here due to space considerations. It suffices here to consider the special case where the chirps to be packed have equal energies. This case is singled out due to its practical importance and because it is the case normally assumed in deriving P_e-expressions in detection theory (see Section 1.4).

Consider for example, the two special cases where the chirps to be packed have equal energies and either have the same duration T or have the same sweep $|W|$. In the former case, the chirps have equal average powers and may be employed to transmit digital data at a fixed rate from

one or more transmitters. In the latter case, the chirps nearly have equal average spectral powers (assuming large duration-bandwidth products so that common bandwidth $\simeq |W|$) and may be used to transmit digital data from different transmitters over a common channel in a spread spectrum multiple-access mode. Mathematically, these two special cases reduce to one another through the transformation $T \overset{\leftarrow}{\rightarrow} |W|$. Thus, it suffices to consider only the former case. In this case, both packing methods become identical. In fact, it can be seen in this special case that step (3.30c) for the consecutive chirps in the first method implies and, hence, cancels the need for step (3.30d) concerning the nonconsecutive chirps. It can also be seen that this step becomes identical to step (3.31a) in the second method requiring only that the duration-bandwidth product difference between any two consecutive chirps be made equal to β_o. Moreover, it can be seen that in this special case, both methods give M as

$$M = 1 + \frac{|W_1 T - W_M T|}{\beta_o} \tag{3.32a}$$

This relation implies that in the special case under consideration, the problem of chirp packing in a given μ-space (μ_{min}, μ_{max}) reduces to a problem of chirp packing in an equivalent duration-bandwidth product space

$(W_{min}T,\ W_{max}T)$ in such a way that the maximum number M of chirps that can be packed in this space is given by

$$M = 1+\text{largest integer in } \frac{|W_{max}T-W_{min}T|}{\beta_O} \tag{3.32b}$$

This relation implies that M increases with the available duration-bandwidth product range as well as with the maximum admissible ISR level β_O^{-1}.

3.5.3.5 Packing Efficiency

Relation (3.30b2) implies that in the first method, the $|\Delta\mu|$-separation between any two nonconsecutive chirps exceeds that between any two consecutive ones. Also, relation (3.30c) implies that in this method, the $|\Delta\mu|$-separation between consecutive chirps is not necessarily fixed. These facts indicate that in the first method, the minimum $|\Delta\mu|$-separation may be obtained from (3.30c) as

$$|\mu_i-\mu_k|_{min} = \beta_O \left(\frac{E_{m+1}}{E_m}\right)_{min} \left(\frac{1}{T_m T_{m+1}}\right)_{min}; \tag{3.33a}$$

$i\neq k,\ i,\ k=1,2,3,\ldots,M;$

$m=1,2,3,\ldots M-1.$

Again, relation (3.30b2) implies that in the second

method, the $|\Delta\mu|$-separation between any two nonconsecutive chirps exceeds that between any two consecutive ones. Also, relation (3.31a) implies that in this method, the $|\Delta\mu|$-separation between consecutive chirps is fixed. These facts indicate that in the second method, the minimum $|\Delta\mu|$-separation may be obtained from (3.31a) as

$$|\mu_i-\mu_k|_{min}=\beta_o \frac{E_M}{E_1}\frac{1}{T_{min}^2} ; \qquad (3.33b)$$

$i\neq k,\ i,\ k=1,2,3,\ldots,M;$

$m=1,2,3,\ldots,M-1$

Assuming the same β_o and the same E- and T- ranges in (3.33a) and (3.33b), the minimum $|\Delta\mu|$-separation in the second method exceeds that in the first method except in the special case of equal energies and durations. These facts imply that given the same β_o, the same μ-space (μ_{min},μ_{max}) and the same E- and T- ranges, the first method is generally more capable of compact chirp packing than the second method. These facts also imply a previous result that both methods become equally capable in this respect in the case where all packed chirps have equal energies and durations.

3.5.3.6 Admissible ISR Levels

In the two chirp packing methods outlined above, it

has been assumed that any two members $r_i(\sigma)$ and $r_k(\sigma)$ of the constructed chirp set satisfy condition (3.26). As applied to this entire set, condition (3.26) requires that

$$|\mu_i-\mu_k|_{\min} T^2_{\min} \geq \Delta \; ; \tag{3.34}$$

$i \neq k$; $i,k=1,2,3,\ldots,M$.

Multiplying both (3.33a) and (3.33b) by $T^2_{\min}$ and comparing the results with (3.34) shows that

$$\beta_o \left(\frac{E_{m+1}}{E_m}\right)_{\min} \left(\frac{T^2_{\min}}{T_m T_{m+1}}\right) \geq \Delta \quad , \tag{3.35a}$$

$m=1,2,3,\ldots,M-1$;

$$\beta_o \frac{E_M}{E_1} \geq \Delta \tag{3.35b}$$

where (3.35a) corresponds to the first method and (3.35b) corresponds to the second method.

It can be seen that (3.35b) and not (3.35a) represents the stronger largeness constraint on β_o except in the case of equal durations and energies where both become identical. Thus, it can be stated that for the entire chirp packing theory developed here to be consistent with condition (3.26),

β_o must be assigned in such a way that it satifies (3.35b).

It was shown in Subsection 3.4.1.4 that for (3.26) to be reasonably satisfied, Δ may be as low as 25. Making use of this fact in (3.35b) indicates that as far as the present chirp packing theory is concerned, the minimum admissible SIR level β_o may be as low as 25($\tilde{=}$14 dB) in the case of equal energies and may even be lower in the case of different energies. This is a logical conclusion since it has been assumed in the present theory (see (3.30a,b)) that the μ-mismatch between any two chirps increases with their E-mismatch, and vice versa.

The fact that the present chirp packing theory will normally be valid for $\beta_o \geq 25$ implies that this theory can accommodate amplitude ISR levels which may be as high as $\frac{1}{5}$. Since such a level would generally be high from a practical point of view, it may well be assumed that this theory holds in all practical situations.

The previous paragraph indicates that requiring the present chirp packing theory to satisfy condition (3.34) does not inconveniently constraint the maximum ISR level β_o^{-1} admissible in this theory. It remains thus to realize the intuitively obvious fact that the validity of this theory is also not undermined by any low choice of β_o^{-1} which may be desirable. In fact, low values of β_o^{-1} would make condition (3.34) more than satisfied.

3.6 The Slope-Reversal Chirp Pair

This section considers the slope-reversal chirp pair and highlights its place within the framework of the general theory concerning LFM signals having different slopes.

3.6.1 Introduction: Correlation of Two Real Chirps Having Different Slopes

Consider the ith and kth members of the real chirp set (3.9) and let $\mu_i \neq \mu_k$, $f_i - f_k \triangleq \nu$ and $|\alpha_i - \alpha_k| \triangleq \alpha$. If the kth chirp bandwidth $< 2f_k$ and the ith chirp bandwidth $< 2f_i$, the normalized correlation function $\lambda^n_{ik}(t,\nu)$ of these two real chirps may be obtained through the normalized correlation function $\chi^n_{ik}(t,\nu)$ of their exponential complex representations by making use of (1.14a). The resulting $\lambda^n_{ik}(t,\nu)$ expression can then be used to obtain the normalized correlation coefficient $\lambda^n_{ik}(0,\nu)$. In this manner, one has

$$\lambda^n_{ik}(0,\nu) = \frac{|F(x_p,x_q)|}{(2|\mu_i-\mu_k|T_iT_k)^{\frac{1}{2}}} \cos\left[\alpha - \frac{\pi\nu^2}{\mu_i-\mu_k} \pm \arg F(x_p,x_q)\right] \tag{3.36}$$

where $+\arg(.)$ and $-\arg(.)$ correspond to $\mu_i > \mu_k$ and $\mu_i < \mu_k$

respectively, p=1 and q=3 if $T_i<T_k$, p=4 and q=2 if $T_i>T_k$, p=1(or 4) and q=2 (or 3) if $T_i=T_k$ and x_1 through x_4 may be obtained by putting t=0 in (3.23).

Relation (3.36) underlies the design and performance of signal sets comprising chirps having different slopes. Coherent transmission is based on $\lambda^n_{ik}(0,\nu)$ itself and noncoherent transmission may be based on $|\lambda^n_{ik}(0,\nu)|$ or on $\rho_{ik}(0,\nu)$ and $\hat{\rho}_{ik}(0,\nu)$.

As described by (3.36), $\lambda^n_{ik}(0,\nu)$ oscillates in the ν- $\lambda^n_{ik}(0,\nu)$ plane about the ν-axis (i.e. about the level $\lambda^n_{ik}(0,\nu)=0$)with a varying instantaneous frequency and with an envelope given by $\frac{|F(x_p,x_q)|}{(2|\mu_i-\mu_k|T_iT_k)^{\frac{1}{2}}}$. Three cases may be identified in this respect, namely,

(i) The case where $|\mu_i-\mu_k|$ is large in such a way that condition (3.26) is satisfied with a sufficiently large Δ. In this case, $|F(x_p,x_q)|\to\sqrt{2}$, $\arg F(x_p,x_q)\to\frac{\pi}{4}$ and (3.36) reduces to (3.28). This implies that the instantaneous frequency of $\lambda^n_{ik}(0,\nu)\to\frac{\nu}{\mu_k-\mu_i}$ (which varies linearly and slowly with ν) and its envelope$\to$ $\frac{1}{(|\mu_i-\mu_k|T_iT_k)^{\frac{1}{2}}}$ (which is low and constant).

(ii) The case where condition (3.26) is not satisfied with

a sufficiently large Δ but $|\mu_i-\mu_k|$ is still large enough to make $|\mu_i-\mu_k|T_s^2 > 7$ (see (iii) below). In this case, the instantaneous frequency and the envelope of $\lambda_{ik}^n(0,\nu)$ fluctuate about the levels $\frac{\nu}{\mu_k-\mu_i}$ and $\frac{1}{(|\mu_i-\mu_k|T_iT_k)^{\frac{1}{2}}}$ as their respective means. The fluctuation amplitude decreases with $|\mu_i-\mu_k|$ (see Fig. 3.3).

(iii) The case where $|\mu_i-\mu_k|\to 0$ in such a way that $|\mu_i-\mu_k|T_s^2<7$. In this case, fluctuation about the mean comes to an end. In fact, it can be shown by methods which will be outlined in Section 4.11 in relation to the chirp spectrum that as $\mu_i-\mu_k\to 0$, the envelope of $\lambda_{ik}^n(0,\nu)\to(\frac{T_s}{T_\ell})^{\frac{1}{2}}|\text{sinc}\nu T_s|$, assuming an essentially $|\text{sinc}(.)|$ form in ν that persists as long as $|\mu_i-\mu_k|T_s^2<7$. This conclusion is in full agreement with the fact that as $\mu_i-\mu_k\to 0$, $|\chi_{ik}^n(0,\nu)|$ of (3.22) approaches $|\chi_{kk}^n(0,\nu)|$ of (3.14c) if $T_i=T_k$ and $|\chi_{ik}^n(0,\nu)|$ of (3.15b1) if $T_i<T_k$.

The behaviour of $\lambda_{ik}^n(0,\nu)$ in case (i) has already been considered in the previous section. In this case, $\lambda_{ik}^n(0,\nu)$ would assume its smallest possible positive and negative values describing an essentially orthogonal chirp pair. In case (ii), $\lambda_{ik}^n(0,\nu)$ may assume relatively larger positive

and negative values. In case (iii), $\lambda_{ik}^{n}(0,\nu)$ would assume its largest possible positive and negative values. These facts imply that if a large negative $\lambda_{ik}^{n}(0,\nu)$ value is desirable (which is usually the case in coherent transmission), one would choose $|\mu_i-\mu_k|$ in such a way that condition (3.26) is not properly satisfied and then choose ν in such a way as to obtain the corresponding largest possible negative $\lambda_{ik}^{n}(0,\nu)$ value. However, such a conclusion is of no practical significance. This is due to the fact that $\lambda_{ik}^{n}(0,\nu)$ in both cases (ii) and (iii) is difficult to compute and is highly sensitive to ν-variations that it may jump from its largest possible negative value to its largest possible positive value for a slight change in ν. This explains why the theory of "signal design for chirps having different slopes" has been based in the previous section on case (i), i.e. on the case where condition (3.26) is properly satisfied.

As mentioned above, $\lambda_{ik}^{n}(0,\nu)$ assumes its largest possible positive value in case (iii). Thus, assuming that $\mu_i-\mu_k\to 0$ and taking $\alpha=0$ in (3.36), the largest possible positive value of $\lambda_{ik}^{n}(0,\nu)$ corresponds to $\nu=0$ and is given by $(\frac{T_s}{T_\ell})^{\frac{1}{2}}$. If, in addition, $T_i\to T_k$, the two chirps become identical and the largest possible positive value $\to 1$ as expected (see (1.15)).

Also, $\lambda_{ik}^{n}(0,\nu)$ assumes its largest possible negative

value in case (iii). However, the precise evaluation of this value is not easy because of the presence of the rapidly fluctuating $|F(x_p,x_q)|$ and $\arg F(x_p,x_q)$ in (3.36). Nevertheless, if $\alpha=0$ and $\mu_i >$ or $< \mu_k$, an estimate of this value has been found numerically to be $\simeq -0.258(\frac{T_s}{T_\ell})^{\frac{1}{2}}$ for $|\mu_i-\mu_k|T_s^2 \simeq 4.7493$ at $|\nu| \simeq 1.09|\mu_i-\mu_k|^{\frac{1}{2}}$ (i.e. for $x_p \simeq 0$ and $x_q \simeq 3.082$ or $x_p \simeq -3.082$ and $x_q \simeq 0$ in (3.36)). It can be seen that as $|\mu_i-\mu_k|$ increases, this value decreases (unless $T_i=T_k$, where it remains fixed at -0.258) and its location along the ν-axis moves away from $\nu=0$.

It can readily be seen that for fixed T's and W's, x_p and x_q in (3.36) are functions of ν only and have different signs only in the range $|\nu| \leq \frac{|\mu_i-\mu_k|T_s}{2}$ (i.e. in the range ($x_p=0$, $x_q=0$)). This implies that the central region of $|F(x_p,x_q)|$ and, hence, the central region of $\lambda_{ik}^n(0,\nu)$ extend over the range $|\nu| \leq \frac{|\mu_i-\mu_k|T_s}{2}$. The preceding paragraphs have been mainly concerned with the behaviour of $\lambda_{ik}^n(0,\nu)$ in this central region. Outside this region, i.e. in the tail region, $\lambda_{ik}^n(0,\nu)$ is generally small. This indicates that the orthogonality of the two chirps would be enhanced in case (i) above and that they may be made essentially orthogonal in cases (ii) and (iii) by making $|\nu|$ sufficiently large. In this manner, the point $(0,\nu)$ lies outside the parallelogram characterizing the effective $\lambda_{ik}^n(t,\nu)$ spread in the t-ν plane (see Fig. 3.4). That is,

the kth matched filter response to ith chirp will be of low level at the sampling instant t=0, may be centred at another instant away from t=0 and generally has an effective duration<effective duration of $\lambda_{ik}^{n}(t,0)$. Thus, ν-shifting may be used to prevent intersystem interference accummulation in the caseof chirp packing presented in the previous section.

3.6.2 The Generalized Slope-Reversal Chirp Pair

The real ith-kth Arbitrary Chirp Pair (ACP) studied in the previous subsection reduces to a Generalized Slope-Reversal Chirp Pair (GSRCP) in the case where $\mu_i=-\mu_k \triangleq \mu$. Accordingly, the results obtained for the ACP can readily be applied to the GSRCP through the transformation $\mu_i \to \mu$, $\mu_k \to -\mu$. This implies, for example, that the only practically conceivable GSRCP is one which satisfies condition (3.26). For such a pair, (3.36) reduces to

$$\lambda_{ik}^{n}(0,\nu) = \frac{\cos\left(\alpha \pm \frac{\pi}{4} - \frac{\pi}{2}\frac{\nu^2}{\mu}\right)}{(2|\mu|T_iT_k)^{\frac{1}{2}}} \qquad (3.37)$$

where $+\frac{\pi}{4}$ and $-\frac{\pi}{4}$ correspond to $\mu>0$ and $\mu<0$ respectively.

Relation (3.37) underlies the design and performance

of the GSRCP in both the coherent and noncoherent modes. It implies that the GSRCP is essentially orthogonal under condition (3.26). Thus, assuming that the energy ratio $\frac{E_i}{E_k}$ is the same for both the ACP and GSRCP, comparing (3.37) and (3.28) indicates that under (3.26), the GSRCP and ACP would roughly have the same performance capability in both coherent and noncoherent transmission. That is, the GSRCP performance would be insensitive to deviation from the slope-reversibility condition (or to any other parameter distortion) as long as the two μ's remain different and constant over signal duration and (3.26) is satisfied. In fact, such a deviation would slightly improve or degrade the performance of the GSRCP depending on whether $\lambda^n_{ik}(0,\nu)$ of (3.28) is larger or less than $\lambda^n_{ik}(0,\nu)$ of (3.37).

Assuming that the two members forming the chirp pair have equal energies and satisfy (3.26), the highest possible ACP interference level may be obtained from (3.28) as $(|\mu_i-\mu_k|T_iT_k)^{-\frac{1}{2}}$. Similarly, the highest possible GSRCP interference level may be obtained from (3.37) as $(2|\mu|T_iT_k)^{-\frac{1}{2}}$. These two levels form the basis for comparing the ACP worst performance with that of the GSRCP.

Consider, for example, the class $C(\gamma,WT)$, say, comprising all ith-kth chirp pairs in such a way that each

pair consists of two real chirps with equal energies that : (i) satisfy (3.26), (ii) have opposite, but not necessarily exactly reversed, slopes (e.g. $\mu_i>0$, $\mu_k<0$, $|\mu_i| \gtrless |\mu_k|$), and (iii) satisfy the condition

$$W_i T_i = -\gamma^2 W_k T_k \triangleq WT \quad \text{for all i and k} \tag{3.38}$$

where γ is a real constant and WT is a fixed reference product.

The highest possible interference level for any pair belonging to this class is given by $z^{-\frac{1}{2}}$, where $z \triangleq |W_i T_k - W_k T_i|$. Writing $\frac{W_i}{W_k} \triangleq y$ and making use of (3.38), $z = |WT(\frac{y}{\gamma^2} + \frac{1}{y})|$. It can readily be seen that z assumes its minimum value $2|\frac{WT}{\gamma}|$ at $y=\pm\gamma$. This corresponds through (3.38) to $\mu_i = -\mu_k$, i.e. to a GSRCP. This implies that compared to all other pairs belonging to class $C(\gamma,WT)$, the GSRCP assumes the maximum "highest possible interference level". That is, all GSRCP's in class $C(\gamma,WT)$ perform equally and are inferior to all other pairs in this class. Thus, any deviation from the slope-reversibility condition within class $C(\gamma,WT)$ would improve the pair performance. This improvement increases as $|\frac{W_i}{W_k}| \to 0,\infty$ away from $\frac{W_i}{W_k} = \pm\gamma$.

3.6.3 A Special Slope-Reversal Chirp Pair

According to the present discussion, both the ACP

and GSRCP introduced above may be employed to convey the bits 1 and 0 in a coherent or noncoherent mode. In contrast reported work in this area has been concerned with conveying these two bits, mainly in an incoherent mode, through a Special Slope-Reversal Chirp Pair (SSRCP) comprising two chirps which, in addition to being slope-reversed, may differ only in their mean frequencies (see Subsection 3.1.4). Obviously, this pair is a special case of the GSRCP and may be treated accordingly.

Consider the ith-kth SSRCP for which $A_i=A_k$, $\alpha=0$, $\mu_i=-\mu_k \triangleq \mu>0$, $T_i=T_k \triangleq T$ and $W_i=-W_k \triangleq W>0$. For this pair, the effective $\lambda^n_{ik}(t,\nu)$ spread in the t-ν plane is confined to a parallelogram such as that shown in Fig. 3.4(b). Also, $\lambda^n_{ik}(0,\nu)$ for this pair may be obtained through (3.36) as

$$\lambda^n_{ik}(0,\nu) = \frac{|F(x_p,x_q)|}{2(WT)^{\frac{1}{2}}} \cos\left[-\frac{\pi}{2}\frac{\nu^2}{\mu} + \arg F(x_p,x_q)\right] \qquad (3.39a)$$

where

$$x_p \triangleq (WT)^{\frac{1}{2}}\left(-1+\frac{\nu}{W}\right) \qquad (3.39b1)$$

$$x_q \triangleq (WT)^{\frac{1}{2}}\left(1+\frac{\nu}{W}\right) \qquad (3.39b2)$$

This relation underlies the design and performance of the SSRCP in both the coherent and noncoherent modes.

It may be studied in a manner similar to that used for studying (3.36). For example, making use of the general results obtained in Subsection 3.6.1, relation (3.39) gives an estimate of the SSRCP largest possible negative $\lambda_{ik}^{n}(0,\nu)$ value as -0.258 for $2(WT)^{\frac{1}{2}} \simeq 3.082$ at $|\nu| \simeq 1.541\mu^{\frac{1}{2}}$. This corresponds either to the case where the two SSRCP chirps have the same initial frequency and a |final frequency separation| $\simeq \frac{4.75}{T}$ (if $\nu>0$) or to the case where these two chirps have the same final frequency and an |initial frequency separation| $\simeq \frac{4.75}{T}$ (if $\nu<0$). In both cases, the SSRCP has a total bandwidth occupancy $\simeq 2W \simeq \frac{4.75}{T}$.

Relation (3.39) is based on the assumption that T covers the range $(-\frac{T}{2}, \frac{T}{2})$. If T covers the range (0,T), (3.39) is replaced by

$$\lambda_{ik}^{n}(0,\nu') = \frac{|F(x_p', x_q')|}{2(WT)^{\frac{1}{2}}} \cos\left[-\frac{\pi}{2}\frac{\nu'^2}{\mu} + \arg F(x_p', x_q')\right] \tag{3.40a}$$

where $\nu' \triangleq$ ith initial frequency - kth initial frequency = $\nu - W$ and

$$x_p' \triangleq \frac{\nu'}{\mu^{\frac{1}{2}}} \tag{3.40b1}$$

$$x_q' \triangleq 2(WT)^{\frac{1}{2}} + \frac{\nu'}{\mu^{\frac{1}{2}}} \tag{3.40b2}$$

Relation (3.40) may be reduced to the less informative

form

$$\lambda_{ik}^{n}(0,\nu') = \frac{1}{v}\{[C(u)-C(u-v)]\cos\frac{\pi}{2}u^2 + [S(u)-S(u-v)]\sin\frac{\pi}{2}u^2\} \tag{3.41a}$$

where C(.) and S(.) are Fresnel cosine and sine integrals introduced in Subsection 3.4.1.2 and

$$u \triangleq -\frac{\nu'}{\mu^{\frac{1}{2}}} \tag{3.41b1}$$

$$v \triangleq 2(WT)^{\frac{1}{2}} \tag{3.41b2}$$

Relation (3.41) checks with a relation obtained by Berni and Gregg[153] in the context of comparing the SSRCP with the PSK and FSK pairs. A detailed analysis of the results obtained by these authors is not intended, but the following comments are in order:

(i) Berni and Gregg base their comparison on the largest possible negative $\lambda_{ik}^{n}(0,\nu')$ value. They obtain this value for the SSRCP as -0.629 for v=2.5 and u=-1.53, i.e. for $2(WT)^{\frac{1}{2}}=2.5$ at $\nu'=1.53\,\mu^{\frac{1}{2}}$ (i.e. at $\nu=2.78\mu^{\frac{1}{2}}$), corresponding to an overall bandwidth occupancy = $\nu' \simeq \frac{1.9}{T}$. However, these estimates are doubtful.

This may be seen from the fact that putting v=2.5 and u=-1.53 in (3.40) or (3.41) gives $\lambda_{ik}^{n}(0,\nu') \simeq +0.015$ and not -0.629. This may also be seen from the fact that for v=2.5, i.e. for $WT \simeq 1.56$, the SSRCP virtually has no LFM modulation and approaches a narrowband FSK pair. That is, the largest possible negative $\lambda_{ik}^{n}(0,\nu')$ value for the SSRCP is expected to approach that of the FSK pair which can be shown to be = -0.218 (>>-0.629) at $|\nu'| \simeq \frac{0.7}{T}$. These conclusions indicate that our estimates given in the paragraph following (3.39) are more realistic in this respect. Thus, the results obtained by Berni and Gregg would have to be modified accordingly. For example, the largest possible negative $\lambda_{ik}^{n}(0,\nu')$ values for the PSK pair, the FSK pair and the SSRCP would respectively be -1, -0.218 and -0.258 (instead of -0.629) corresponding to the overall bandwidth occupancies $\frac{2}{T}$, $\frac{2.7}{T}$ and $\frac{4.75}{T}$ (instead of $\frac{1.9}{T}$). Assuming these $\lambda_{ik}^{n}(0,\nu')$ values and coherent reception in AWGN, the PSK pair, the FSK pair and the SSRCP would respectively require the relative signal energies E_o, 1.64 E_o and 1.59 E_o (instead of 1.22 E_o) in order to give (through (1.26)) the same P_e. That is, assuming coherent reception in AWGN, the PSK pair excels over the FSK pair and the SSRCP in terms of both bandwidth

and signal energy requirements. However, the SSRCP excels over the FSK pair only in terms of required signal energy (and not in terms of both required bandwidth and signal energy). Similar modifications may be extended to the results obtained by Berni and Gregg for partially coherent reception and nonselective fading channels. This can be achieved through $\rho_{ik}(0,\nu')$ and $\hat{\rho}_{ik}(0,\nu')$ making use of Section 1.4.

(ii) That Berni and Gregg base their comparison on the largest possible negative $\lambda^{n}_{ik}(0,\nu')$ value implies that this comparison is misleading from the practical viewpoint. This due to: (a) the fact that the SSRCP with the largest possible negative $\lambda^{n}_{ik}(0,\nu')$ value virtually has no LFM modulation and can hardly be treated as a chirp pair, and (b) the fact that the precise "largest possible negative $\lambda^{n}_{ik}(0,\nu')$ value" is difficult to compute and is highly sensitive to ν'-variations that it may jump to the "largest possible positive $\lambda^{n}_{ik}(0,\nu')$ value" for a slight change in ν'.

(iii) In carrying out their comparison, Berni and Gregg did not take into account the merits of the chirp as a pulse compression signal.

According to Subsection 3.6.1, it is more realistic to base the SSRCP design and performance as well as its

comparison with any other signal pair (e.g. the PSK, FSK and $\mu_i=\mu_k$ pairs) on the case where it properly satisfies condition (3.26), i.e. on the case where $WT \geq \frac{\Delta}{2}$ (with Δ sufficiently large). This case accommodates all practically usable chirps and corresponds through (3.39) to

$$\lambda_{ik}^{n}(0,\nu) = \frac{\cos(\frac{\pi}{4} - \frac{\pi}{2}\frac{\nu^2}{\mu})}{(2WT)^{\frac{1}{2}}} \tag{3.42}$$

This relation indicates that a coherent SSRCP and, through $\rho_{ik}(0,\nu)$ and $\hat{\rho}_{ik}(0,\nu)$, a noncoherent SSRCP are essentially orthogonal under (3.26), i.e. for sufficiently large WT. This implies that: (i) the coherent and noncoherent SSRCP's would roughly have the same performance as their ACP and GSRCP counterparts as long as (3.26) is satisfied, i.e. the SSRCP performance would be insensitive to parameter distortion as long as the two μ's remain different and constant over signal duration and (3.26) is satisfied, (ii) all SSRCP's in class C(1,WT) perform equally and are inferior to all other pairs in this class, (iii) under (3.26), the coherent SSRCP in particular, and the coherent ACP and GSRCP in general, are inferior to the PSK pair and roughly equivalent to the coherent orthogonal FSK pair from the viewpoint of minimizing P_e in AWGN, and (iv) the noncoherent SSRCP, GSRCP and ACP are roughly

equivalent to the noncoherent FSK pair in this respect.

The incoherent SSRCP may also be dealt with through the envelope of $\lambda_{ik}^{n}(0,\nu)$ in particular, and through the envelope of $\lambda_{ik}^{n}(t,\nu)$ in general. Assuming that the chirp bandwidth $< 2\times$ the smaller of f_i and f_k, an expression for the envelope of $\lambda_{ik}^{n}(t,\nu)$ may be obtained through (3.22) and (1.14b) as

$$\text{Envelope of } \lambda_{ik}^{n}(t,\nu) = |\chi_{ik}^{n}(t,\nu)| = \frac{|F(x_p,x_q)|}{2(WT)^{\frac{1}{2}}} \tag{3.43}$$

where $p=1$, $q=2$ for $t\leq 0$, $p=4$, $q=3$ for $t\geq 0$ and x_1 through x_4 may be obtained from (3.23) by putting $\mu_i=-\mu_k=\mu>0$, $T_i=T_k=T$ and $W_i=-W_k=W>0$.

Relation (3.43) implies that $|\chi_{ik}^{n}(t,\nu)|$ is even in t. For $\nu=0$, (3.43) reduces to

$$\text{Envelope of } \lambda_{ik}^{n}(t,0) = |\chi_{ik}^{n}(t,0)| = \frac{|F(x_q)|}{(WT)^{\frac{1}{2}}} \tag{3.44}$$

where $q=2$ for $t\leq 0$ and $q=3$ for $t\geq 0$.

Relation (3.44) checks with a relation obtained by Zaytsev and Zhuravlev[161] in the context of considering the candidacy of a SSRCP with $\nu=0$ for incoherent binary digital data transmission. These authors plot (3.44) as a a function of $\frac{t}{T}$ for different WT. They also plot (3.44) as a function of WT for t=0 showing that for WT>20 (i.e. under condition (3.26)), $\frac{|F(x_q)|}{(WT)^{\frac{1}{2}}} \to \frac{1}{(2WT)^{\frac{1}{2}}}$ and, hence, the SSRCP with $\nu=0$ is essentially orthogonal in incoherent reception.

4

THE LFM SPECTRUM

This chapter presents a systematic study of the LFM spectrum. It formulates rather simple and accurate prediction criteria concerning the form and behaviour of this spectrum as a function of the LFM pulse parameters. Such criteria can readily be used to establish bounds on this spectrum and to find its oscillations in the different frequency regions. They may also be used to establish bounds on the LFM power spectrum. The results may be extended to the dual case concerning the time amplitude function of a passive LFM pulse having a strictly limited bandwidth. They may also be extended to any other quantity which may be expressed in a mathematical form similar to that of the LFM spectrum (e.g. the correlation function of two LFM signals with different slopes).

4.1 Introduction

No signal can be handled properly without an adequate knowledge of its spectrum and the class of LFM signals is no exception in this regard. The LFM spectrum cannot generally be expressed in closed-form (excluding the case where the LFM pulse has a Gaussian envelope). For every single set of pulse parameters, this spectrum usually has to be obtained through carefully prepared and laborious computations (using a digital computer) or to be approximated by the closed-form stationary phase relation (3.7) which can be strictly valid only in the case of infinite duration-bandwidth products.

The LFM signal in common use is the chirp signal introduced in Section 3.1. Previous workers have commonly assumed a chirp pulse with an ideally rectangular envelope, having neither rise nor fall times. Again, the spectrum of this pulse has usually to be obtained through laborious computations or through the closed-form stationary phase relation (3.11) corresponding to an infinite duration-bandwidth product.

The previous two paragraphs imply that it would be constructive to develop rather accurate and manageable

methods for handling the LFM spectrum which obviate the need for the laborious computations and which take the finiteness of the duration-bandwidth product and the rise and fall times of the physical LFM pulse into consideration. Such methods would facilitate the handling of the LFM pulse compression technique in theory and practice and would enhance its utilization in an ever increasing number of fields of application.

The spectrum of a given signal may be studied through the well known methods for evaluating, and finding bounds on, Fourier transforms[6,13,24,167,168]. However, such methods are generally of little use in the case of the LFM spectrum. This spectrum usually involves the Fresnel integral which is neither reducible to a closed-form nor can be easily precisely computed by numerical methods. Nevertheless, asymptotic, series and rational expansions of this integral are available in the literature[79]. Accordingly, the present work studies the LFM spectrum mainly through these expansions. It employs detailed rational and series expansions for the rather accurate numerical computations and short series and asymptotic expansions for the rather approximate theoretical analysis. The adoption of a particular Fresnel expansion for theoretical analysis has been based on intuition with an aim of being consistent and obtaining

reasonably accurate and simple relations which can be easily handled in practice.

The Fresnel integral contributes to both the amplitude and phase functions of the LFM spectrum. The contribution to the phase function is sometimes called the 'residual phase' because it is generally ignored in practice. Accordingly, the present discussion is mainly concerned with the LFM amplitude spectrum. The residual phase may also be studied. It should be noted, however, that this phase is highly sensitive to approximation errors.

The physcial chirp has short, but finite, rise and fall times and, hence, its envelope may be modelled by a trapezoid. Accordingly, the trapezoidal LFM spectrum is studied first with a view of applying the results to the spectrum of the physical chirp as a special case. If the fall and rise times of the physical chirp are too small to be taken into consideration, it may be treated as having an ideally rectangular envelope. Thus, the rectangular LFM spectrum is considered next. The remaining discussion is mainly concerned with the spectrum of the arbitrarily weighted LFM pulse as well as with the limiting case where the LFM spectrum approaches that of a monotone whose duration-bandwidth

product is unity.

For convenience, the results have been obtained for a complex baseband LFM pulse whose central instant is the origin of the time-axis and whose initial phase is zero. These results can readily be extended to a real LFM pulse whose mean frequency >0, whose central instant is shifted from the origin of the time-axis and/or whose initial phase $\neq 0$ (See Subsection A.5, Appendix A).

4.2 The Spectrum of a Trapezoidal LFM Pulse

Consider the following baseband complex LFM pulse with duration T, rise time $T_r < \frac{T}{2}$, fall time $T_f < \frac{T}{2}$ and trapezoidal envelope (see Fig. 4.1)

$$y(\sigma) = y_1(\sigma) + y_2(\sigma) + y_3(\sigma) \tag{4.1a}$$

where

$$y_1(\sigma) \triangleq \frac{1}{T_r}(\sigma + \frac{T}{2})e^{j\pi\mu\sigma^2}, \qquad \sigma_1 \leq \sigma \leq \sigma_2 \tag{4.1b}$$

$$y_2(\sigma) \triangleq e^{j\pi\mu\sigma^2}, \qquad \sigma_2 \leq \sigma \leq \sigma_3 \tag{4.1c}$$

$$y_3(\sigma) \triangleq \frac{1}{T_f}(-\sigma + \frac{T}{2})e^{j\pi\mu\sigma^2}, \qquad \sigma_3 \leq \sigma \leq \sigma_4 \tag{4.1d}$$

and $\sigma_1 = -\sigma_4 = -\frac{T}{2}$, $\sigma_2 = \sigma_1 + T_r$ and $\sigma_3 = \sigma_4 - T_f$.

Making use of the linearity property of Fourier transform, the spectrum Y(f) of y(σ) is given by

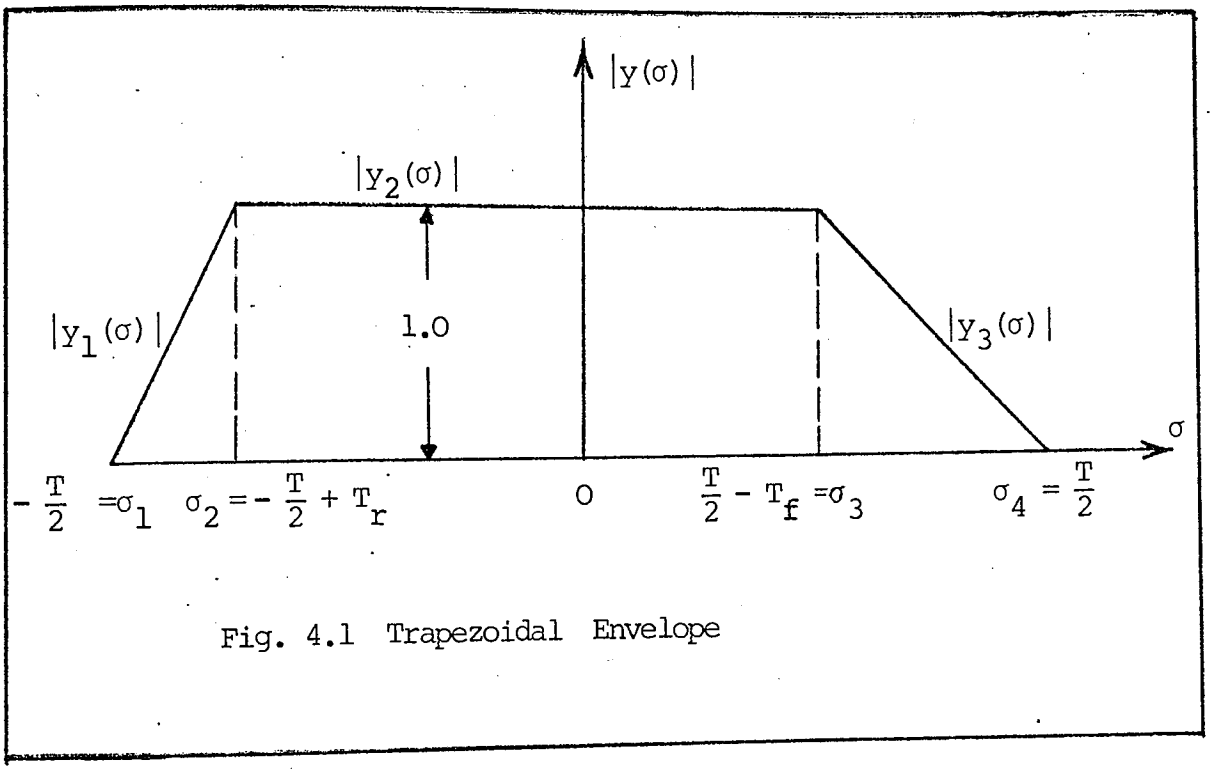

Fig. 4.1 Trapezoidal Envelope

$$Y(f) = Y_1(f) + Y_2(f) + Y_3(f) \tag{4.2}$$

let

$$x \triangleq |2\mu|^{\frac{1}{2}}(\sigma - \frac{f}{\mu}) \tag{4.3}$$

Substituting for σ from this transformation reduces (4.2) to

$$Y_1(f) = \frac{1}{T_r}(\frac{T}{2} + \frac{f}{\mu})I_1 + \frac{1}{T_r} I_2 \tag{4.4a}$$

$$Y_2(f) = I_1 \tag{4.4b}$$

$$Y_3(f) = \frac{1}{T_f}\left(\frac{T}{2} - \frac{f}{\mu}\right) I_1 - \frac{1}{T_f} I_2 \tag{4.4c}$$

where

$$I_1 \triangleq \frac{e^{-j\pi f^2/\mu}}{|2\mu|^{\frac{1}{2}}} \int_x e^{\pm j\frac{\pi}{2}x^2} dx \tag{4.4d}$$

$$I_2 \triangleq \frac{e^{-j\pi f^2/\mu}}{\pm j\pi |2\mu|} \int_x d\left(e^{\pm j\frac{\pi}{2}x^2}\right) \tag{4.4e}$$

in which $j\frac{\pi}{2}x^2$ and $-j\frac{\pi}{2}x^2$ correspond to $\mu>0$ and $\mu<0$ respectively.

Integrals I_1 and I_2 may be compared with that of (3.22a). The integration limits are (x_1, x_2) in the expression for $Y_1(f)$, (x_2, x_3) in the expression for $Y_2(f)$ and (x_3, x_4) in the expression for $Y_3(f)$, where

$$x_1 \triangleq \left|\frac{WT}{2}\right|^{\frac{1}{2}} (-1-\eta) \tag{4.5a}$$

$$x_2 \triangleq \left|\frac{WT}{2}\right|^{\frac{1}{2}} \left(-1-\eta+\frac{2T_r}{2}\right) \tag{4.5b}$$

$$x_3 \triangleq \left|\frac{WT}{2}\right|^{\frac{1}{2}} \left(1-\eta-\frac{2T_f}{2}\right) \tag{4.5c}$$

$$x_4 \triangleq \left|\frac{WT}{2}\right|^{\frac{1}{2}} (1-\eta) \tag{4.5d}$$

in which

$$\eta \triangleq \frac{f}{W/2} \tag{4.5e}$$

is a normalized frequency variable.

Assuming $\mu>0$ and substituting for $(\frac{T}{2} \pm \frac{f}{\mu})$ in (4.4) from (4.3) using the proper σ-value, (4.2) gives

$$Y^n(\eta) = \sum_{\ell=1}^{4} \frac{1}{T_\ell} \left[x_\ell F(x_\ell) + \frac{je^{j\frac{\pi}{2}x_\ell^2}}{\pi}\right] \tag{4.6a}$$

where $F(x)$ is the complex Fresnel integral introduced in Section 3.4 and

$$Y^n(\eta) = Y^n(f) \triangleq |2\mu| e^{j\pi f^2/\mu} \; Y(f) \tag{4.6b}$$

$$T_1 = -T_2 \triangleq T_r \tag{4.6c}$$

$$T_4 = -T_3 = T_f \tag{4.6d}$$

Relation (4.6a) implies that $|Y^n(\eta)|$ will be symmetric in η only if $|y(\sigma)|$ is symmetric in σ. Also, this relation remains valid for $\mu<0$ except that the bracketed quantity $\rightarrow$ its complex conjugate and $\eta \rightarrow -\eta$. These facts imply that $|Y(\eta)|_{\mu<0} = |Y(\eta)|_{\mu>0}$ if $|y(\sigma)|$ is symmetric in σ and that $|Y(\eta)|_{\mu<0} = |Y(-\eta)|_{\mu>0}$ if $|y(\sigma)|$ is asymmetric in σ. These relations can be used to adapt the following discussion concerning the $\mu>0$ case to the $\mu<0$ case.

Relation (4.6) may be used to compute and plot the amplitude and phase sepctra of any symmetric or asymmetric

trapezoidal LFM pulse for different $|WT|$ products (see Figs. 4.2 through 4.4).

4.3 The Trapezoidal LFM Spectrum for $|WT|\to\infty$

The fact that $|WT|\to\infty$ implies that the nonvanishing values of all $|x|$'s are large over the entire η-axis and one may adopt the following asymptotic expansion[79] for all $F(x)$ in (4.6) even in the immediate vicinity of a vanishing x

$$F(x) \simeq \frac{e^{j\frac{\pi}{4}}}{\sqrt{2}} - \frac{je^{j\frac{\pi}{2}x^2}}{\pi x} \tag{4.7}$$

which has been found numerically to give acceptable results for $|x| \geq 0.8$.

Thus, assuming $\mu>0$ and noting the signs of the x's in the different regions of the η-axis, one has

$$|Y^n(\eta)|_\infty = 0, \qquad |\eta|>1 \tag{4.8a}$$

$$= |Y_1^n(\eta)|_\infty = \frac{|WT|^{\frac{1}{2}}}{T_r}(1+\eta), \quad -1<\eta<-1+\frac{2T_r}{T} \tag{4.8b}$$

$$= |Y_2^n(\eta)|_\infty = 2|\mu|^{\frac{1}{2}}, \qquad -1+\frac{2T_r}{T}<\eta<1-\frac{2T_f}{T} \tag{4.8c}$$

$$= |Y_3^n(\eta)|_\infty = \frac{|WT|^{\frac{1}{2}}}{T_f}(1-\eta), \quad 1-\frac{2T_f}{T}<\eta<1 \tag{4.8d}$$

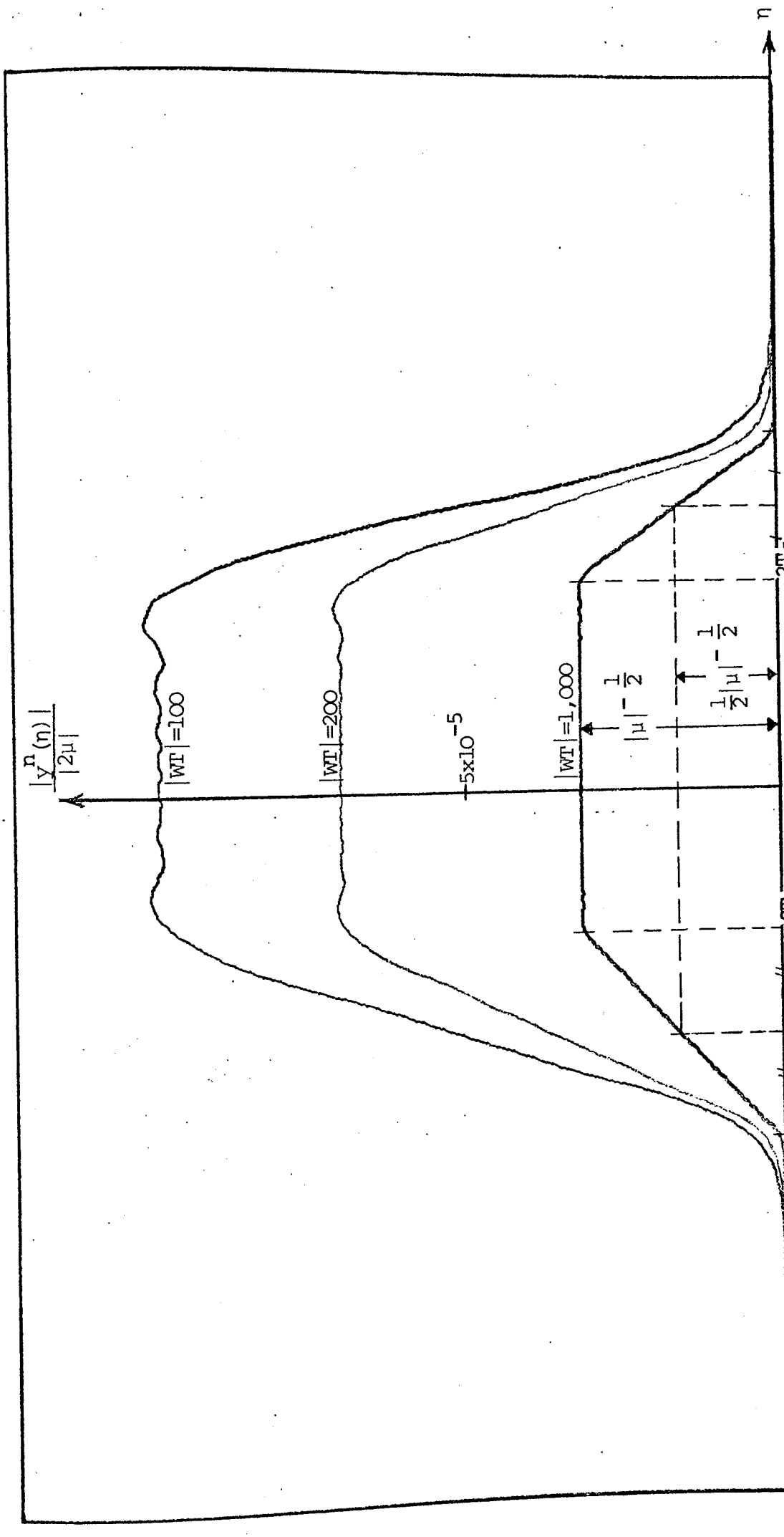

Fig. 4.2 Trapezoidal LFM Amplitude Spectrum; $T = 10^{-3}$sec., $T_r = 1.5\ T_f = 0.3T$ (increasing |WT|).

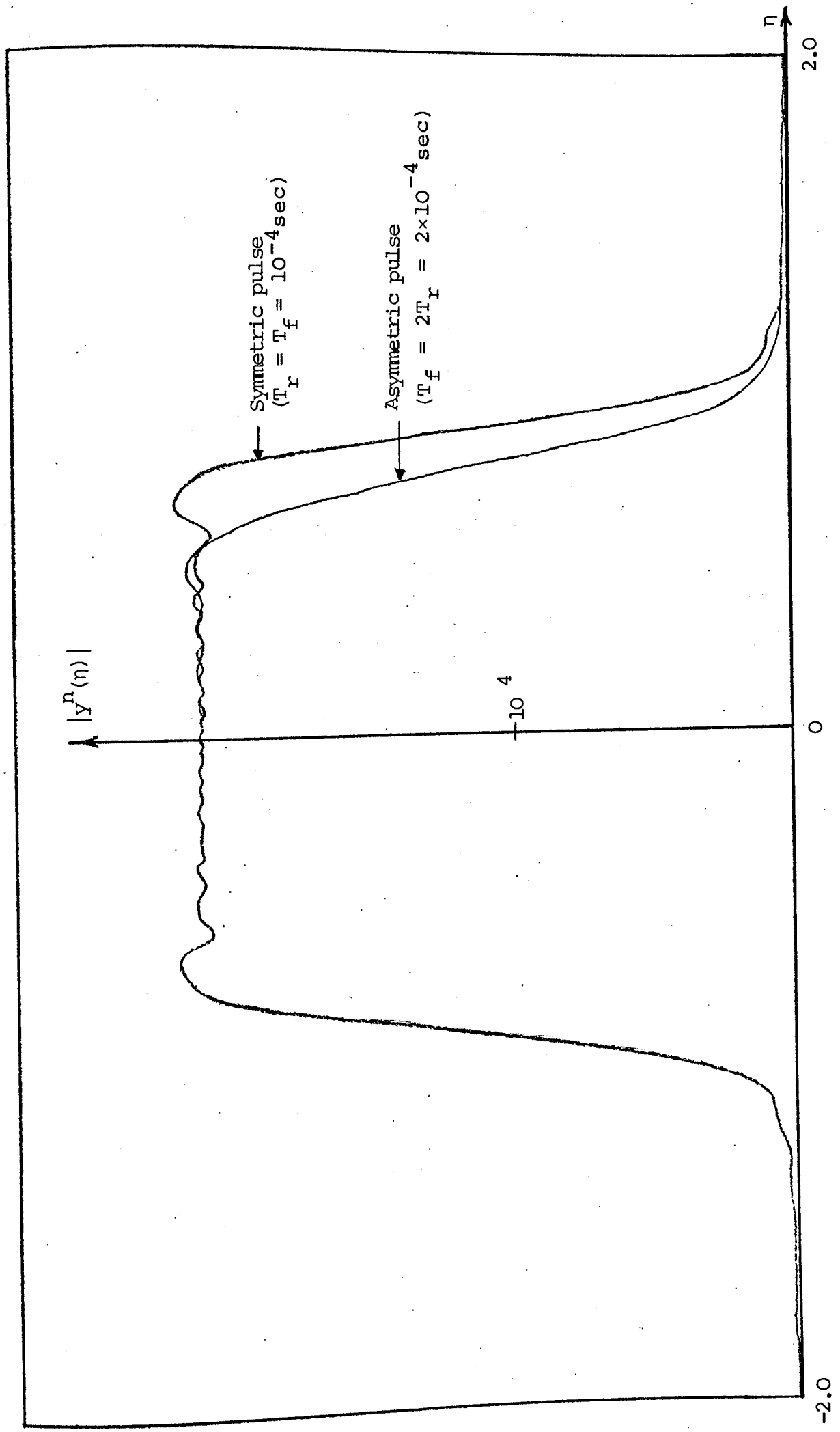

Fig. 4.3 Trapezoidal LFM Amplitude Spectrum; $W=10^5$ Hz, T=1 ms (symmetry effects).

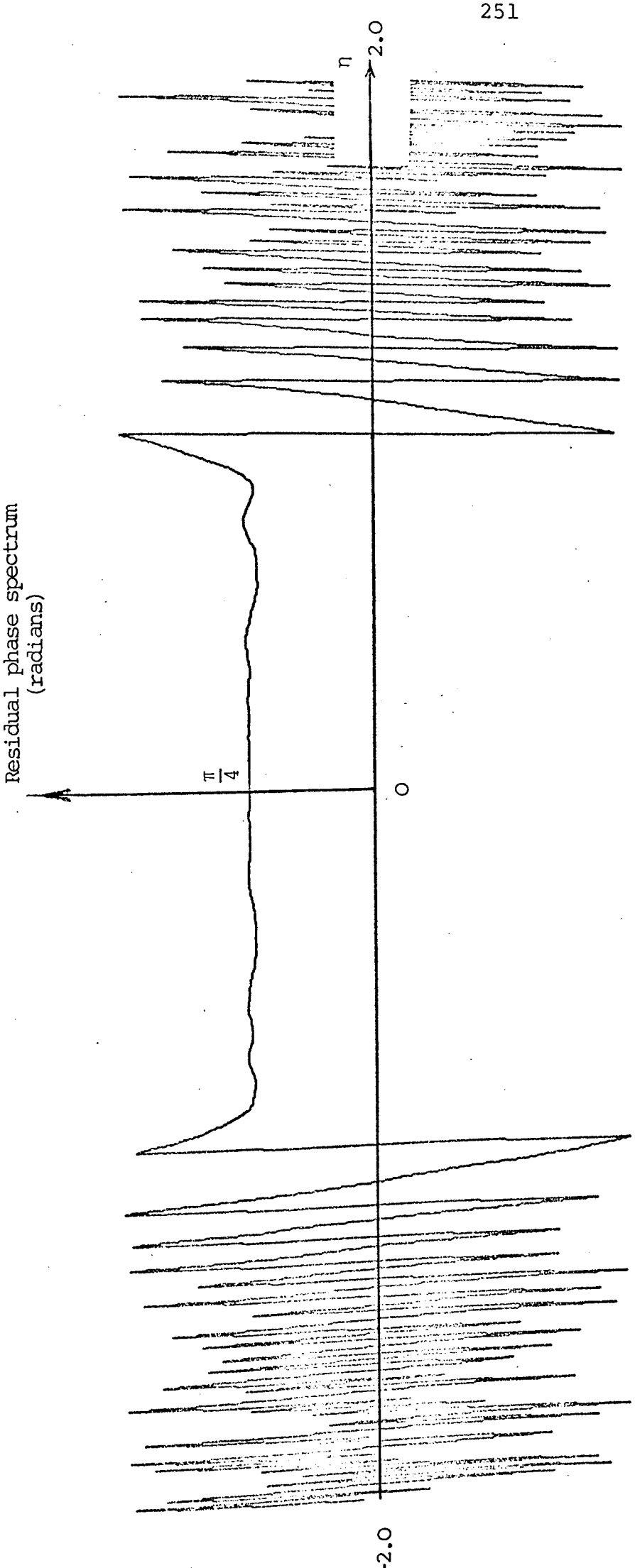

Fig. 4.4 Trapezoidal LFM Residual Phase Spectrum; $W=10^5$ Hz, $T=10^{-3}$ sec., $T_r=1.5\ T_f=0.3\ T$.

This relation is valid even in the immediate vicinities of the edges $\eta=\pm 1$, $-1+\frac{2T_r}{T}$ and $1-\frac{2T_f}{T}$ and is illustrated in Fig. 4.5. It predicts that as $|WT|\to\infty$, $|Y(f)|$ assumes the functional form of $|y(\sigma)|$ in agreement with the stationary phase relation (3.7). This prediction is confirmed by the computer plot corresponding to $|WT|=1{,}000$ in Fig. 4.2

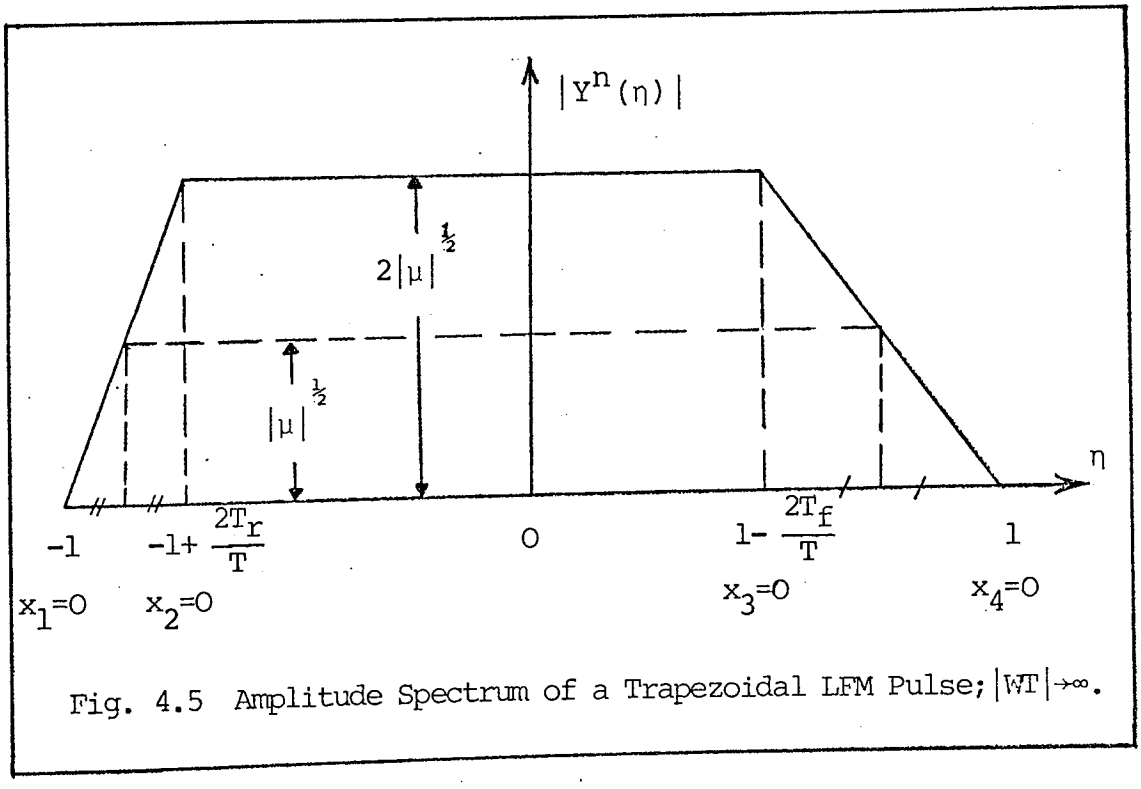

Fig. 4.5 Amplitude Spectrum of a Trapezoidal LFM Pulse; $|WT|\to\infty$.

Relation (4.8) is expected to be most accurate in the vicinities of the frequencies $\eta=-1+\frac{T_r}{T}$, 0 and $1-\frac{T_f}{T}$, where all the $|x|$'s assume their largest values. In fact, (4.8) may remain accurate at these frequencies in general, and at $\eta=0$ in particular, even for relatively moderate $|WT|$- products. However, the

accuracy of (4.8) generally degrades as η moves towards the critical edge frequencies $\eta=-1$, $-1+\frac{2T_r}{T}$, $1-\frac{2T_f}{T}$ and 1. These predictions are confirmed by the computer plots of Fig. 4.2.

4.4 The Trapezoidal LFM Spectrum for Finite |WT| - Introduction

The previous section indicates that for a LFM pulse $y(\sigma)$ with $|WT|\to\infty$, $|Y^n(\eta)|$ is nonoscillatory and is confined to the range $|\eta|\leq 1$. A physical $y(\sigma)$, however, can only have a finite $|WT|$ and, thus, its $|Y^n(\eta)|$ may be expected to fluctuate about that of (4.8) forming both rising and falling tails flanking the central region $|\eta|\leq 1$. Accordingly, the following discussion considers the case where $|WT|$ is finite but large enough to make $|Y^n(\eta)|$ assume a characteristic LFM form. The case where $|WT|$ is small will be considered in Section 4.11.

Expansion (4.7) may not be adopted for all F(x)'s in the finite $|WT|$ case as it was adopted in the $|WT|\to\infty$ case. Such an adoption would give the same $|WT|\to\infty$ results and reflect no effects concerning the finiteness of $|WT|$. Thus, expansion (4.7) may have to be modified or even replaced in the finite $|WT|$ case. However, not any such modification or replacement may lead to acceptable results or manageable mathematics. A compromise between the required accuracy and mathematical complexity is

desirable in this respect. This can be achieved only if a rather localized, but systematic, expansion scheme is followed which takes the comparative largeness of each of the four $|x|$'s in the various η-regions into consideration.

4.5 The Trapezoidal LFM Spectrum For Finite $|WT|$ - The Tail ($|\eta|>1$)

4.5.1 The T_r-Tail Proper ($\eta<-1$)

This tail extends from $\eta=-\infty$ to η_{r2}, say, where it meets the edge $\eta=-1$ outside vicinity. In this tail in general, and in its near side in particular, one may expect that the rising effects exceed those of falling. Such an expectation would imply that for the moderately large $|\eta|$ in the near T_r-tail, it may be reasonable to assume that both $|x_3|$ and $|x_4|$ have roughly the same largeness which comparatively exceeds that associated with $|x_1|$ and $|x_2|$. That is, it may be reasonable in the near T_r-tail to retain expansion (4.7) for $F(x_3)$ and $F(x_4)$ and to adopt the following rather more accurate form of this expansion for $F(x_1)$ and $F(x_2)$.

$$F(x)\simeq \frac{e^{j\frac{\pi}{4}}}{\sqrt{2}} - \frac{je^{j\frac{\pi}{2}x^2}}{\pi x} - \frac{e^{j\frac{\pi}{2}x^2}}{\pi^2 x^3} \qquad (4.9)$$

Adopting the above-mentioned expansion scheme and noting that all x's are positive in the T_r-tail, (4.6) gives

$$Y^n(\eta) \simeq -\frac{1}{T_r}\sum_{\ell=1}^{2}\frac{e^{j\frac{\pi}{2}x_\ell^2}}{(\pi x_\ell)^2} \tag{4.10}$$

which leads through (4.5) to

$$|Y^n(\eta)| \leq \frac{2}{\pi^2|WT|T_r}\left[\frac{1}{(|\eta|-1)^2}+\frac{1}{(|\eta|-1+\frac{2T_r}{T})^2}\right] \tag{4.11a}$$

$$|Y^n(\eta)| \geq \frac{2}{\pi^2|WT|T_r}\left[\frac{1}{(|\eta|-1)^2}-\frac{1}{(|\eta|-1+\frac{2T_r}{T})^2}\right] \tag{4.11b}$$

$$|Y^n(\eta)|_{mean} \simeq \frac{2}{\pi^2|WT|T_r}\cdot\frac{1}{(|\eta|-1)^2} \tag{4.11c}$$

Relation (4.11) predicts that $|Y^n(\eta)|\to 0$ as $|WT|\to\infty$ in full agreement with Section 4.3. It also predicts that $|Y^n(\eta)|\to 0$ as $|\eta|\to\infty$ in full agreement with Fourier transform theory.

Relation (4.10) predicts that $|Y^n(\eta)|$ is oscillatory. Oscillation may be seen to take place between the upper and lower bounds about $|Y^n(\eta)|_{mean}$ with an oscillation amplitude $A(\eta)$ given by

$$A(\eta) \simeq \frac{4}{\pi^2 |WT| T_r (|\eta| - 1 + \frac{2T_r}{T})^2} \tag{4.12}$$

This relation predicts that $A(\eta)$ decreases with $|WT|$ and T_r and is insensitive to T_f. These predictions are in good agreement with reality as can be seen from the computer plots of Fig. 4.6. Relation (4.12) also predicts that $A(\eta)$ decreases with $|\eta|$. This prediction is confirmed by Figs. 4.6 through 4.9. Moreover, (4.12) predicts that $\frac{A(\eta)}{|Y^n(\eta)|_{mean}} \simeq 2$ for $|\eta| >> \frac{T_r}{T}$ and that this ratio decreases slowly as $|\eta|$ decreases. This implies that $A(\eta)$ is comparatively large and, hence, the oscillations can readily be detected. These predictions are confirmed by Figs. 4.8 and 4.9.

The frequencies η_{max} where the oscillations have their maxima would be approximately those frequencies where the modulus of (4.10) equals the upper bound of (4.11a). Similarly the frequencies η_{min} where the oscillations have their minima would be approximately those frequencies where the modulus of (4.10) equals the lower bound of (4.11b). Thus,

$$\eta^k_{max} \simeq -1 + \frac{T_r}{T} - \frac{2k+1}{|WT| . T_r/T} \tag{4.13a}$$

$$\eta^k_{min} \simeq -1 + \frac{T_r}{T} - \frac{2k}{|WT| . T_r/T} \tag{4.13b}$$

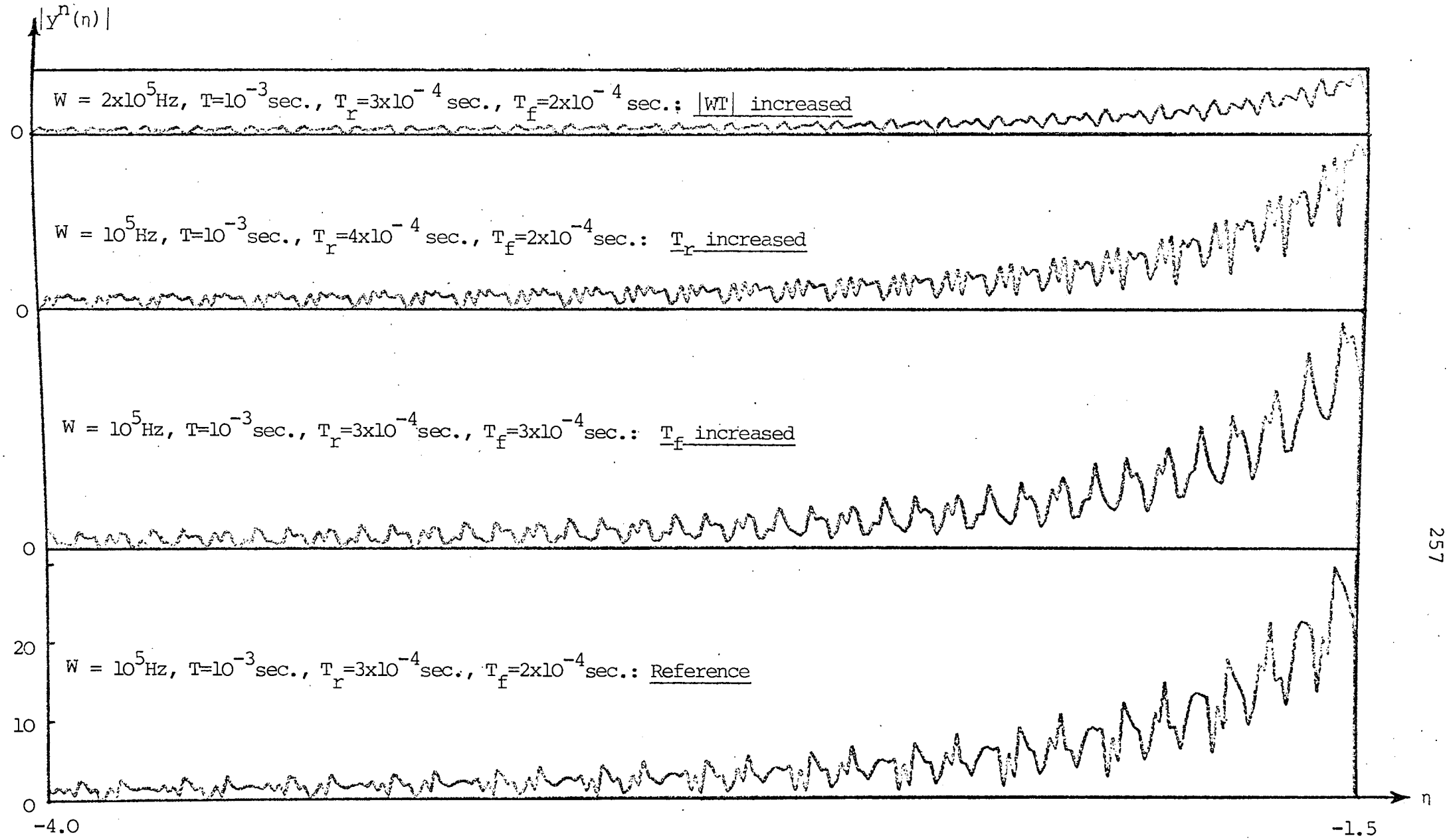

Fig. 4.6 Oscillation Amplitude and Density in the T_r-Tail (drawings are to the same scale).

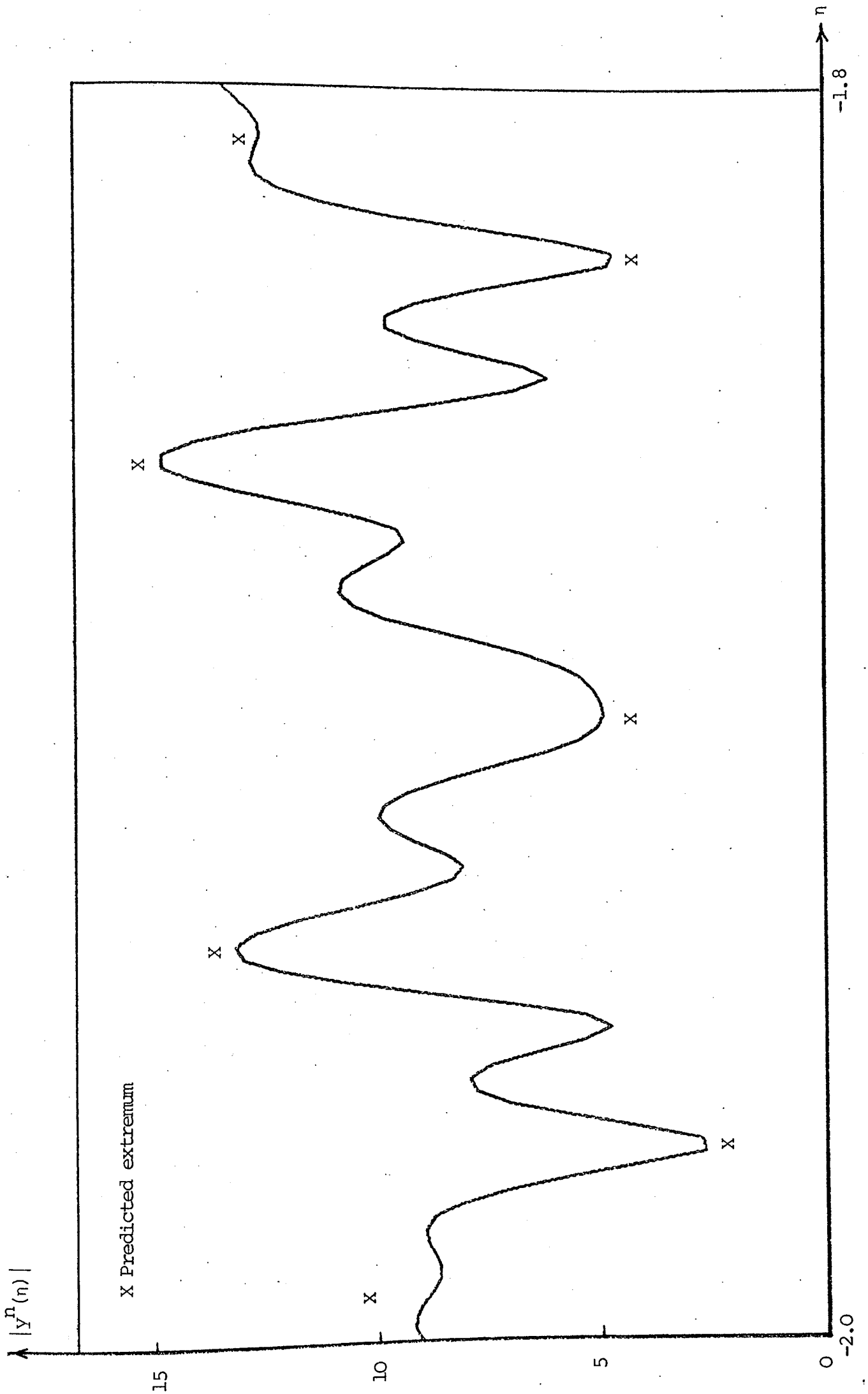

Fig.4.7 Predicted Extrema in the T_r-Tail; W=10^5Hz, T=1 ms, T_r=1.5 T_f=0.3 T.

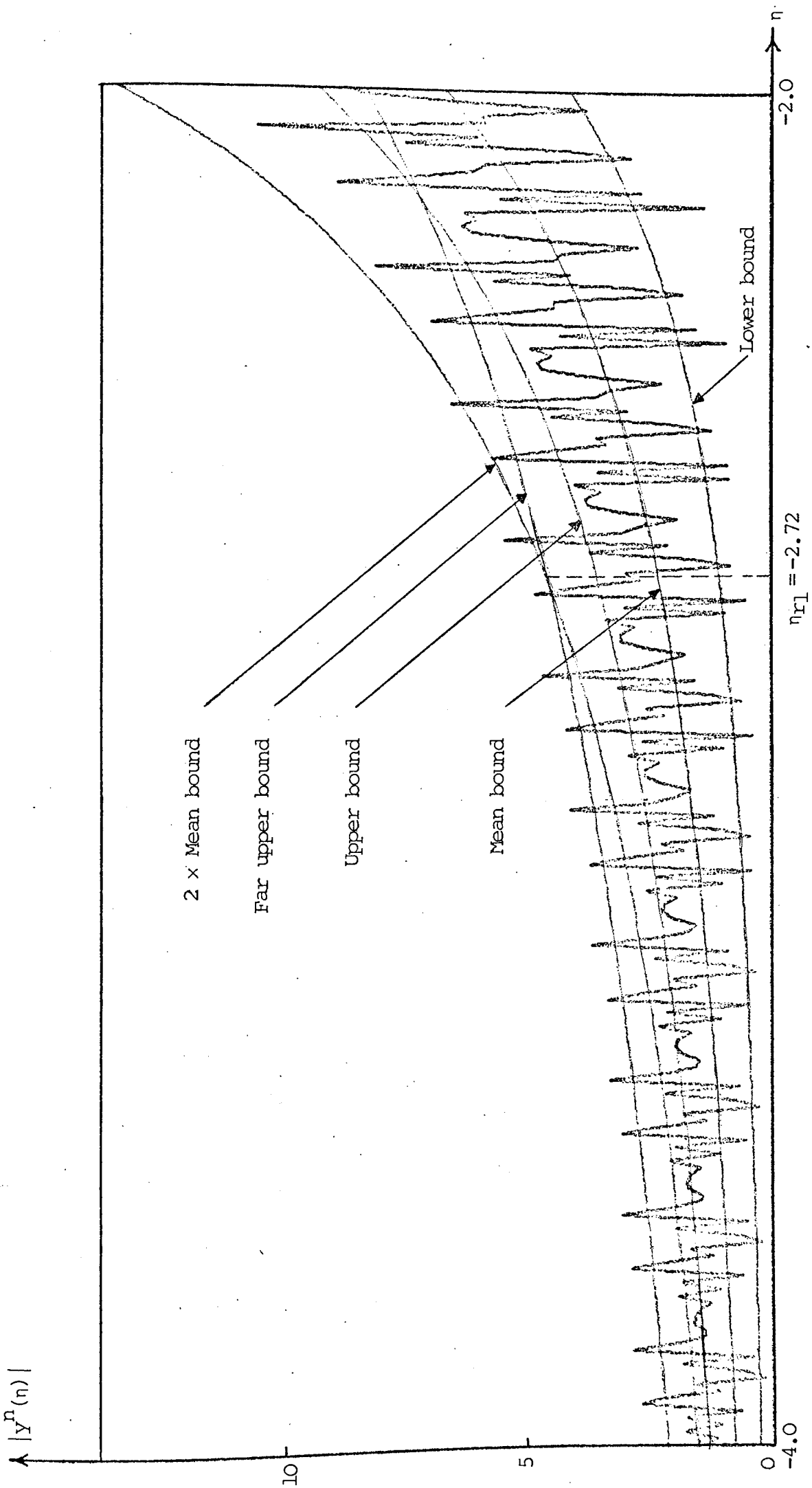

Fig. 4.8 Bounds in the T_r-Tail; $W=10^5$Hz, $T=10^{-3}$sec., $T_r=1.5\ T_f=0.3\ T$.

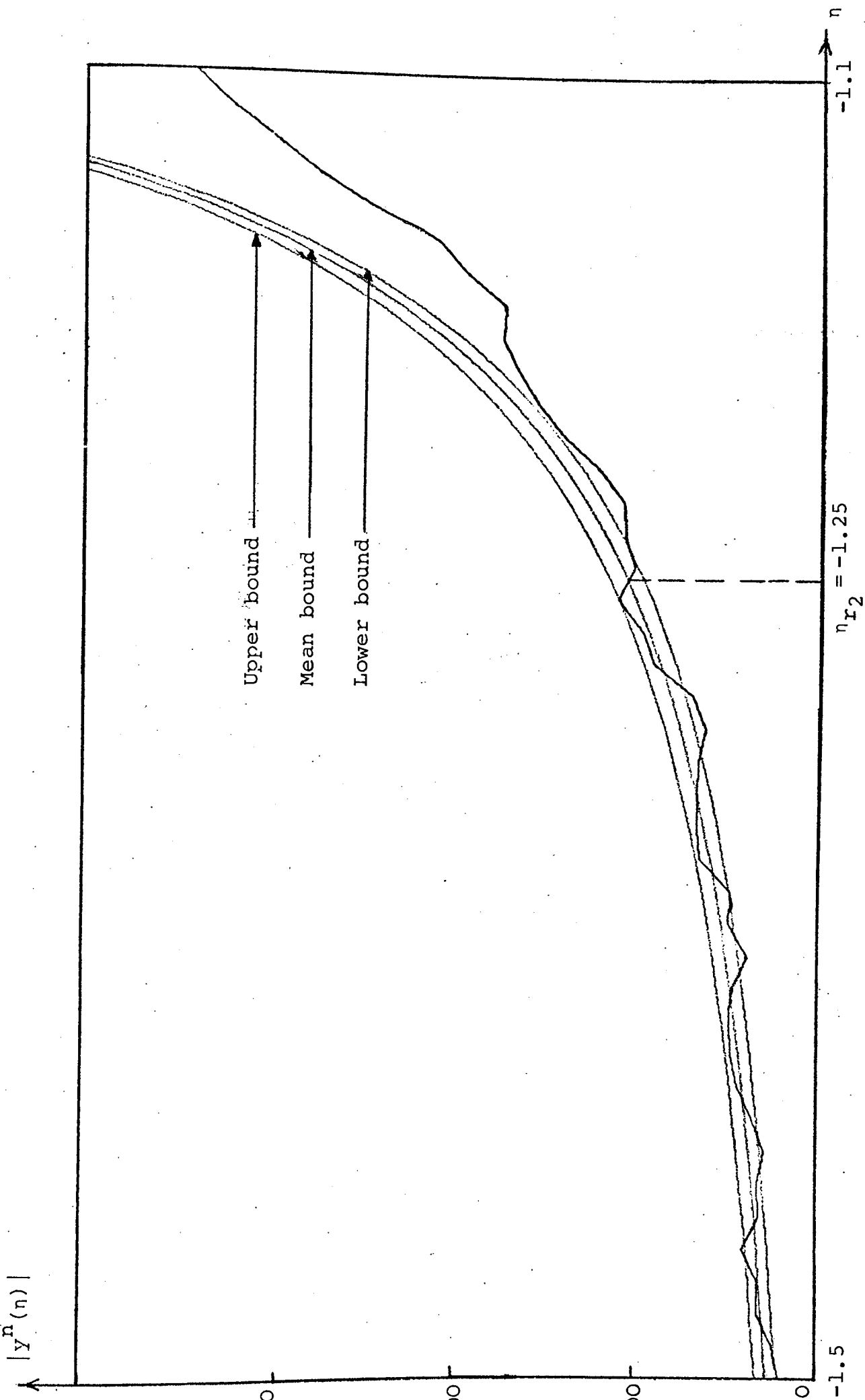

Fig. 4.9 Boundary Between the T_r-Tail and the Edge η=-1 Outside Vicinity; W=10^5Hz, T=10^{-3}sec., T_r=1.5T_f=0.3T.

In this relation, k may be zero or a positive integer indicating extrema order. This order increases along the negative η-axis in the present case.

Relation (4.13) can be used to predict the oscillations in any given range in the near T_r-tail. A computer program was written in this respect and applied to afew arbitrary cases including a study case with W=100 KHz, T = 1ms and $T_r = 1.5\ T_f = 0.3T$ in different η-ranges. The results were then compared with those obtained by detailed and relatively precise computer analyses of these ranges based directly on (4.6). Such a comparison revealed that (4.13) is more capable of predicting those extrema where $|Y^n(\eta)|$ has broad or pronounced fluctuations (see Fig. 4.7). This comparison also showed that the $|Y^n(\eta^k_{max})|$ and $|Y^n(\eta^k_{min})|$ values predicted by making use of (4.13) in (4.11) may deviate slightly from their actual counterparts (see Fig. 4.8).

Relation (4.13) predicts that the oscillation density is uniform in η and is given by $\frac{1}{2}|WT|\frac{T_r}{T}$ per unit of η. That is, this density increases with both $|WT|$ and $\frac{T_r}{T}$ and is insensitive to both η and T_f. These predictions are in good agreement with reality as can be seen from Figs. 4.6 through 4.9.

So far, only the near T_r-tail region has been

considered. Flanking this region from the left is the far T_r-tail region and flanking it from the right is the edge $\eta=-1$ outside vicinity. The boundary between these three regions cannot be exactly defined. The far T_r-tail region is considered below. The edge $\eta=-1$ outside vicinity will be considered in Subsection 4.7.1. The boundary between this vicinity and the T_r-tail proper may be taken as $\eta_{r2} \overset{\Delta}{\simeq} -1-\frac{3}{2}\left|\frac{2}{WT}\right|^{\frac{1}{2}}$. Beyond η_{r2}, $x_1>\frac{3}{2}$ and adopting expansion (4.9) for $F(x_1)$ and $F(x_2)$ in the T_r-tail proper is expected to give reliable results. Obviously, η_{r2} is determined by $|WT|$. As $|WT|\to\infty$, $\eta_{r2}\to$ the edge $\eta=-1$ itself. In the special case where $|WT|=100$, for example, the present theory predicts that $\eta_{r2}\simeq -1.21213$. This is in good agreement with reality as can be seen from Fig. 4.9, which shows that $\eta_{r2}\simeq -1.25$ implying that the T_r-tail bounds of (4.11) become invalid for $\eta> -1.25$ where they $\to\infty$.

For relatively large $|\eta|$, $\frac{2T_r}{T}$ may be neglected in (4.11). The required $|\eta|$ largeness in this respect depends on the actual value of $\frac{T_r}{T}$. In this case, the upper bound of (4.11a) reduces to

$$|Y^n(\eta)|_{\text{large}|\eta|} \lesssim 2 \times |Y^n(\eta)|_{\text{mean}} \tag{4.14}$$

For still larger $|\eta|$-values in the far T_r-tail, all

$|x|$'s become of comparable magnitude and it becomes more appropriate to use expansion (4.9) for all F(x)'s. In this manner, (4.6) yields

$$[Y^n(\eta)]_{far} \simeq -\sum_{\ell=1}^{4} \frac{1}{T_\ell} \frac{e^{j\frac{\pi}{2}x^2_\ell}}{(\pi x_\ell)^2} \tag{4.15}$$

which leads through (4.5) to the following 'far' upper bound

$$|Y^n(\eta)|_{far} \leq \frac{4}{\pi^2 |WT| \eta^2} \left(\frac{1}{T_r} + \frac{1}{T_f}\right) \tag{4.16}$$

This relation displays the well known fact that the amplitude spectrum of a given time pulse exhibits far-tail symmetry in the frequency-domain even if the envelope of this pulse is not symmetric in the time-domain. In the particular LFM case under consideration, this can be seen from Fig. 4.3. Relation (4.16) also indicates that the LFM amplitude spectrum in the far tails decreases with $|WT|$, T_r, T_f and η^2 and that the rise and fall effects on this spectrum diminish as $|\eta|$ increases.

The frequency η_{r1}, say, separating the two T_r-tail regions in which the two approximations (4.14) and (4.16) are used is the frequency where both these approximations can be made. That is, η_{r1} is the solution of the equation

resulting from equating the right hand sides of (4.14) and (4.16). Thus,

$$\eta_{r1} = -1 - \left[\frac{T_f}{T_r} + \sqrt{\frac{T_f}{T_r} + \left(\frac{T_f}{T_r}\right)^2} \right] \tag{4.17}$$

This relation indicates that $|\eta_{r1}|$ is determined only by, and increases with, the ratio $\frac{T_f}{T_r}$. In the special case where $|y(\sigma)|$ is symmetric in σ, $\eta_{r1} \tilde{=} -3.4142$. Also, in the special case where $|y(\sigma)|$ is asymmetric with $\mu>0$ and $\frac{T_f}{T_r} = \frac{2}{3}$, $\eta_{r1} \tilde{=} -2.72077$. This latter case is illustrated in Fig. 4.8, which confirms the tightness of the bounds in the regions where they are intended to be used.

4.5.2 The T_f-Tail Proper ($\eta>1$)

The T_f-tail is a replica of the T_r-tail except that $x_1 \to x_4$, $x_2 \to x_3$ and $T_r \to T_f$. In this manner, $T_r \to T_f$ in (4.11) and (4.12), (4.16) remains unchanged and both (4.13) and (4.17) have to be multiplied by -1 with $T_r \to T_f$.

4.6 The Trapezoidal LFM Spectrum for Finite |WT| - The Central Region ($|\eta|<1$) Excluding Edge Vicinities

4.6.1 Introduction

While all x's are positive in the T_r-tail and negative

in the T_f-tail, they are of mixed signs in the central region. Accordingly, this region may be conveniently divided into the three partial regions $-1<\eta<-1+\frac{2T_r}{T}$ where only x_1 is negative, $-1+\frac{2T_r}{T}<\eta<1-\frac{2T_f}{T}$ where only x_1 and x_2 are negative and $1-\frac{2T_f}{T}<\eta<1$ where only x_4 is positive (see Fig. 4.5).

The F(x) expansions found suitable, and manageable, in the central region are: (a) expansion (4.9) for $F(x_1)$ and expansion (4.7) for the rest in the range $-1<\eta\leq-1+\frac{T_r}{T}$, (b) expansion (4.9) for $F(x_2)$ and expansion (4.7) for the rest in the range $-1+\frac{T_r}{T}\leq\eta\leq 0$, (c) expansion (4.9) for $F(x_3)$ and expansion (4.7) for the rest in the range $0\leq\eta\leq 1-\frac{T_f}{T}$, and (d) expansion (4.9) for $F(x_4)$ and expansion (4.7) for the rest in the range $1-\frac{T_f}{T}\leq\eta<1$. In order that this expansion scheme gives acceptable results, the conditions that $|x_2|\geq 0.8$ at $\eta=-1+\frac{T_r}{T}$, 0 and that $|x_3|\geq 0.8$ at $\eta=1-\frac{T_f}{T}$, 0 must be satisfied. This implies that $|WT|$, $\frac{T_r}{T}$ and $\frac{T_f}{T}$ are constrained by

$$\frac{4}{5}\left|\frac{2}{WT}\right|^{\frac{1}{2}}\leq\frac{T_r}{T},\ \frac{T_f}{T}\leq\frac{1}{2}-\frac{2}{5}\left|\frac{2}{WT}\right|^{\frac{1}{2}} \qquad (4.18)$$

This relation shows that the admissible $\frac{T_r}{T}$, $\frac{T_f}{T}$ range is determined only by, and increases with, $|WT|$. For example, this range extends roughly from $\frac{1}{5}$ to $\frac{2}{5}$ for

$|WT|=32$ and from 0.1131 to 0.4434 for $|WT|=100$.

For all practically important $|WT|$, the upper constraint in (4.18) can always be assumed to be satisfied in the present discussion which is mainly concerned with the case where $\frac{T_r}{T}, \frac{T_f}{T} < \frac{T}{2}$. That is, it is only the lower constraint in (4.18) which determines the validity of the theory developed in this section.

4.6.2 The Region $-1<\eta<<-1+\frac{T_r}{T}$

This region extends from η_{r4}, say, where it meets the edge $\eta=-1$ inside vicinity to $\eta=-1+\frac{T_r}{T}$. In this region, (4.6) yields

$$Y^n(\eta) \simeq -\frac{\sqrt{2}x_1}{T_r} e^{j\frac{\pi}{4}} - \frac{e^{j\frac{\pi}{2}x_1^2}}{T_r(\pi x_1)^2} \tag{4.19}$$

which leads through (4.5) to

$$|Y^n(\eta)| \lesssim |Y_1^n(\eta)|_\infty + \frac{2}{\pi^2 T_r |WT| (1-|\eta|)^2} \tag{4.20a}$$

$$|Y^n(\eta)| \gtrsim |Y_1^n(\eta)|_\infty - \frac{2}{\pi^2 T_r |WT| (1-|\eta|)^2} \tag{4.20b}$$

$$|Y^n(\eta)|_{mean} \simeq |Y_1^n(\eta)|_\infty \tag{4.20c}$$

where $|Y_1^n(\eta)|_\infty$ is given by (4.8b).

These relations predict that $|Y^n(\eta)|$ would oscillate in this region with an oscillation amplitude $A(\eta)$ which is insensitive to T_f, increases with $|\eta|$, decreases with $|WT|$ and T_r and is practically negligible compared to $|Y^n(\eta)|_{mean}$. These predictions are in good agreement with reality as can be seen from Fig. 4.10. These relations also predict that

$$\eta_{max}^k \simeq -1+\left(\frac{8k+5}{|WT|}\right)^{\frac{1}{2}} \tag{4.21a}$$

$$\eta_{min}^k \simeq -1+\left(\frac{8k+1}{|WT|}\right)^{\frac{1}{2}} \tag{4.21b}$$

where the order of extrema k increases along the positive η-axis.

Relation (4.21) predicts that the oscillation density is nonuniform, decreases with $|\eta|$ (see Fig. 4.10), increases with $|WT|$ and is insensitive to T_f.

In the special case where $|WT|=100$ and $\frac{T_r}{T}=\frac{3}{10}$, for example, (4.21a) predicts only one maximum $\eta_{max}^o \simeq -0.77639$ and (4.21b) predicts two minima $\eta_{min}^o \simeq -0.9$ and $\eta_{min}^1 \simeq -0.7$. These results are in good agreement with reality as can be seen from Fig. 4.10.

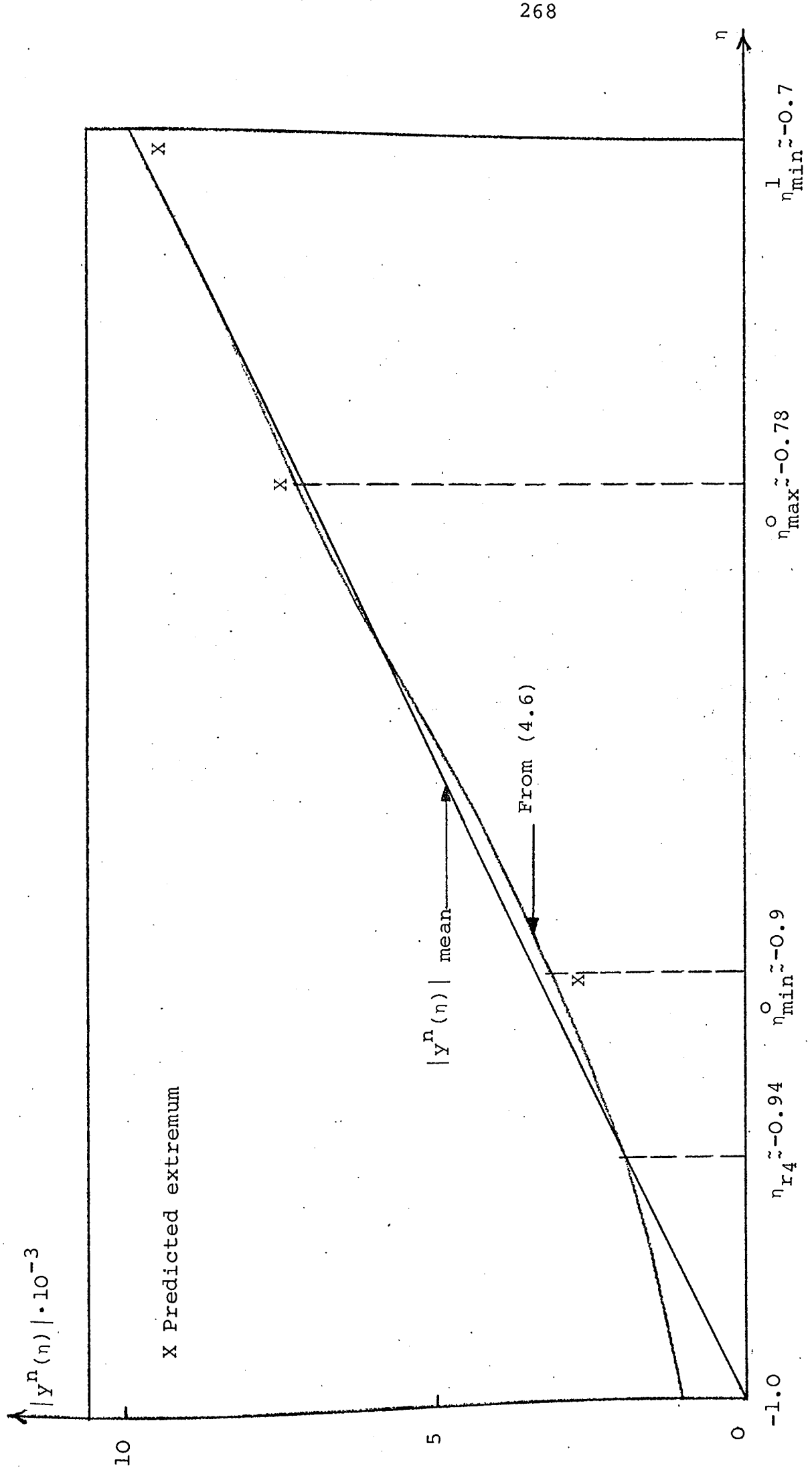

Fig. 4.10 $|y^n(\eta)|$ in the Region $-1 < \eta \lesssim -1 + \frac{T_r}{T}$; $W = 10^5$Hz, $T = 10^{-3}$sec., $T_r = 1.5\ T_f = 0.3T$.

4.6.3 The Region $-1+\frac{T_r}{T} \leq \eta < -1+\frac{2T_r}{T}$

This region extends from $\eta=-1+\frac{T_r}{T}$ to η_{r5}, say, where it meets the edge $\eta=-1+\frac{2T_r}{T}$ external vicinity. In this region, (4.6) yields

$$Y^n(\eta) \simeq -\frac{\sqrt{2}x_1}{T_r} e^{j\frac{\pi}{4}} + \frac{e^{j\frac{\pi}{2}x_2^2}}{T_r(\pi x_2)^2} \tag{4.22}$$

This relation implies that (4.20) still holds in this region and that

$$\eta_{max}^k \simeq -1+\frac{2T_r}{T} - \left(\frac{8k+1}{|WT|}\right)^{\frac{1}{2}} \tag{4.23a}$$

$$\eta_{min}^k \simeq -1+\frac{2T_r}{T} - \left(\frac{8k+5}{|WT|}\right)^{\frac{1}{2}} \tag{4.23b}$$

where the order of extrema k increases along the negative η-axis.

Relation (4.23) predicts that the oscillation density is nonuniform, increases with $|WT|$ and $|\eta|$ (see Fig. 4.11) and is insensitive to T_f.

In the special case where $|WT|=100$ and $\frac{T_r}{T}=\frac{3}{10}$, for example, (4.23a) predicts two maxima $\eta_{max}^o \simeq -0.5$ and $\eta_{max}^1 \simeq -0.7$ and (4.23b) predicts one minimum $\eta_{min}^o \simeq -0.62361$.

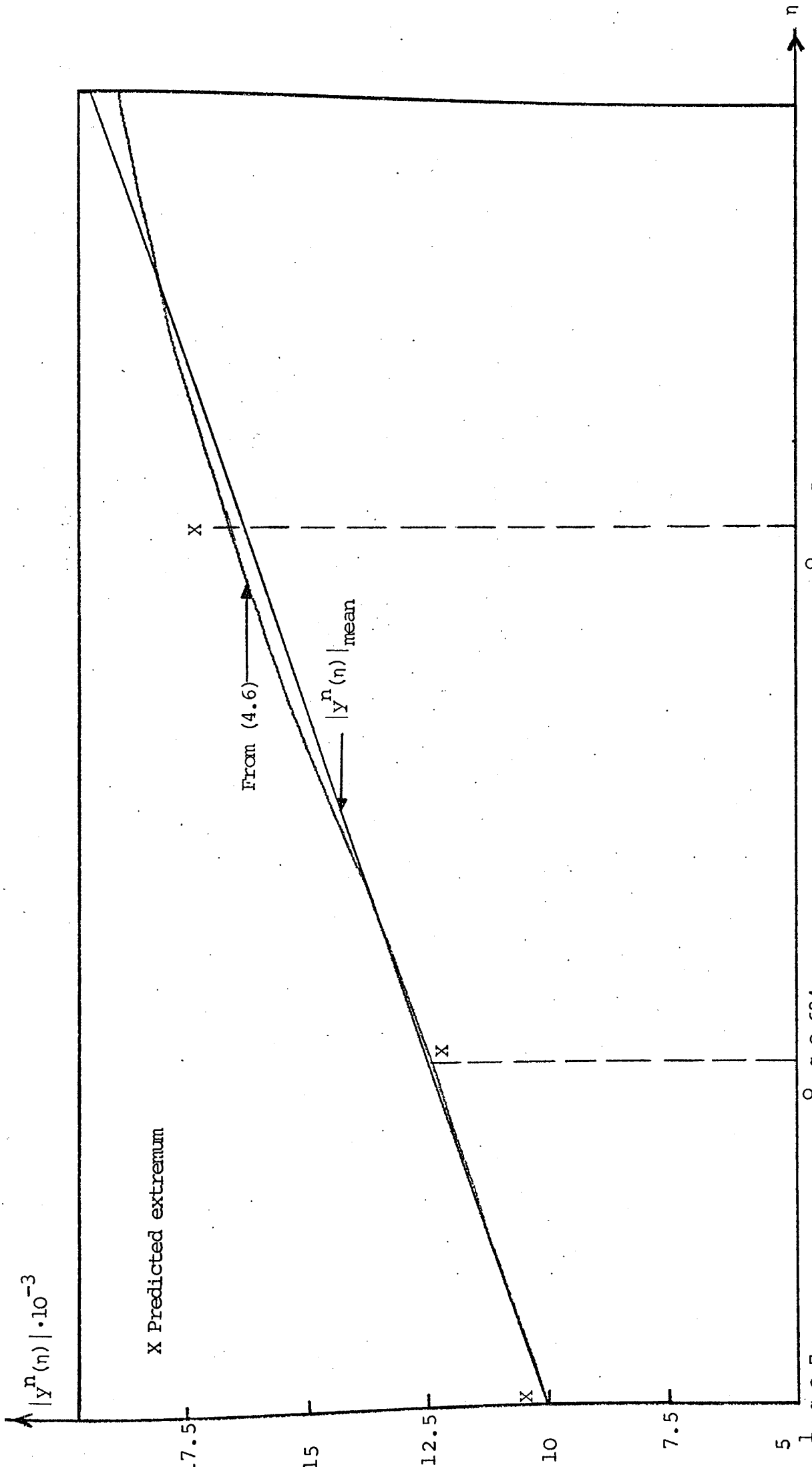

Fig. 4.11 $|y^n(\eta)|$ in the Region $-1+\frac{T_r}{T}\leq\eta<-1+\frac{2T_r}{T}$; $W=10^5$Hz, $T=10^{-3}$sec., $T_r=1.5\,T_f=0.3\,T$.

These results are in good agreement with reality as can be seen from Fig. 4.11.

4.6.4 The Region $-1+\frac{2T_r}{T}<\eta\leq 0$

This region extends from η_{r6}, say, where it meets the edge $\eta=-1+\frac{2T_r}{T}$ internal vicinity to $\eta=0$. In this region, (4.6) yields

$$Y^n(\eta) \simeq 2|\mu|^{\frac{1}{2}} e^{j\frac{\pi}{4}} + \frac{e^{j\frac{\pi}{2}x_2^2}}{T_r(\pi x_2)^2} \tag{4.24}$$

which leads through (4.5) to

$$|Y^n(\eta)| \leq |Y_2^n(\eta)|_\infty + \frac{2}{\pi^2|WT|T_r(1-|\eta|-\frac{2T_r}{T})^2} \tag{4.25a}$$

$$|Y^n(\eta)| \geq |Y_2^n(\eta)|_\infty - \frac{2}{\pi^2|WT|T_r(1-|\eta|-\frac{2T_r}{T})^2} \tag{4.25b}$$

$$|Y^n(\eta)|_{mean} \simeq |Y_2^n(\eta)|_\infty \tag{4.25c}$$

where $|Y_2^n(\eta)|_\infty$ is given by (4.8c).

These relations predict that $|Y^n(\eta)|$ oscillates in this region with an oscillation amplitude $A(\eta)$ which is insensitive to T_f, increases with $|\eta|$ and decreases with $|WT|$ and T_r. These relations also predict that the ratio $\frac{A(\eta)}{|Y^n(\eta)|_{mean}}$ is lower in this region than that

in the T_r-tail and higher than that in the region $-1<\eta<-1+\frac{2T_r}{T}$. These predictions are in good agreement with reality as can be seen from Figs. 4.2, 4.3 and 4.12. Moreover, these relations predict that

$$\eta_{max}^{k} \simeq -1+\frac{2T_r}{T}+\left(\frac{8k+1}{|WT|}\right)^{\frac{1}{2}} \tag{4.26a}$$

$$\eta_{min}^{k} \simeq -1+\frac{2T_r}{T}+\left(\frac{8k+5}{|WT|}\right)^{\frac{1}{2}} \tag{4.26b}$$

where the order of extrema k increases along the positive η-axis.

Relation (4.26) predicts that the oscillation density is nonuniform, decreases with $|\eta|$, increases with $|WT|$ and is insensitive to T_f. These predictions are in good agreement with reality as can be seen from Figs. 4.2, 4.3 and 4.12.

In one example where $|WT|=100$ and $\frac{T_r}{T}=\frac{3}{10}$, (4.26a) predicts two maxima $\eta_{max}^{o} \simeq -0.3$ and $\eta_{max}^{1} \simeq -0.1$ and (4.26b) predicts two minima $\eta_{min}^{o} \simeq -0.17639$ and $\eta_{min}^{1} \simeq -0.03944$. These results are in good agreement with reality as can be seen from Fig. 4.12. In another example where $|WT|=100$ and $\frac{T_r}{T}=\frac{1}{10}$, (4.26) predicts eight maxima and eight minima corresponding to k=0 through k=7. This is in full agreement with reality as shown in

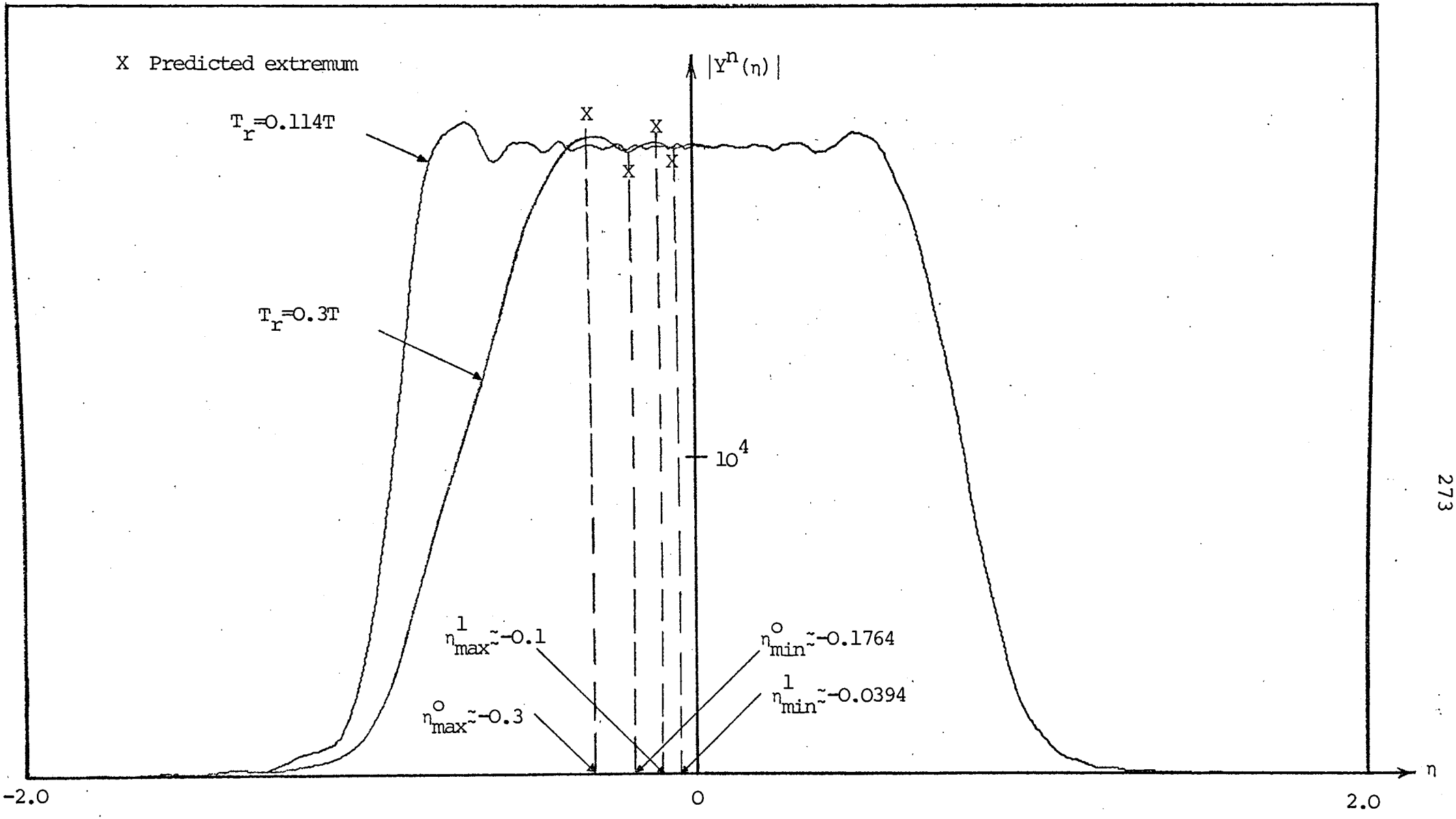

Fig. 4.12 Oscillations in the Region

$-1+\frac{2T_r}{T} < \eta \leq 0$; $W = 10^5$ Hz, $T = 10^{-3}$ sec., $T_f = 0.2T$.

Fig. 4.13, which also confirms the validity of the bounds (4.25) in this region.

4.6.5 The Region $0 \leq \eta < 1$

The previous three subsections have dealt with the left hand side of the central region. The present subsection deals with the right hand side of this region. This side may be divided into the three regions where $0 \leq \eta < 1 - \frac{2T_f}{T}$, $1 - \frac{2T_f}{T} < \eta \leq 1 - \frac{T_f}{T}$ and $1 - \frac{T_f}{T} \leq \eta < 1$.

The region $0 \leq \eta < 1 - \frac{2T_f}{T}$ is a replica of the region $-1 + \frac{2T_r}{T} < \eta \leq 0$ except that $x_2 \rightarrow x_3$ and $T_r \rightarrow T_f$ in (4.24). In this manner, $T_r \rightarrow T_f$ in (4.25) and (4.26) has to be multiplied by -1 with $T_r \rightarrow T_f$.

The region $1 - \frac{2T_f}{T} < \eta \leq 1 - \frac{T_f}{T}$ is a replica of the region $-1 + \frac{T_r}{T} \leq \eta < -1 + \frac{2T_r}{T}$ except that $x_1 \rightarrow -x_4$, $x_2 \rightarrow x_3$ and $T_r \rightarrow T_f$ in (4.22). In this manner, (4.23) has to be multiplied by -1 with $T_r \rightarrow T_f$.

The region $1 - \frac{T_f}{T} \leq \eta < 1$ is a replica of the region $-1 < \eta \leq -1 + \frac{T_r}{T}$ except that $T_r \rightarrow T_f$ and $x_1 \rightarrow -x_4$ in (4.19). In this manner, $T_r \rightarrow T_f$ in (4.20) and (4.21) has to be multiplied by -1.

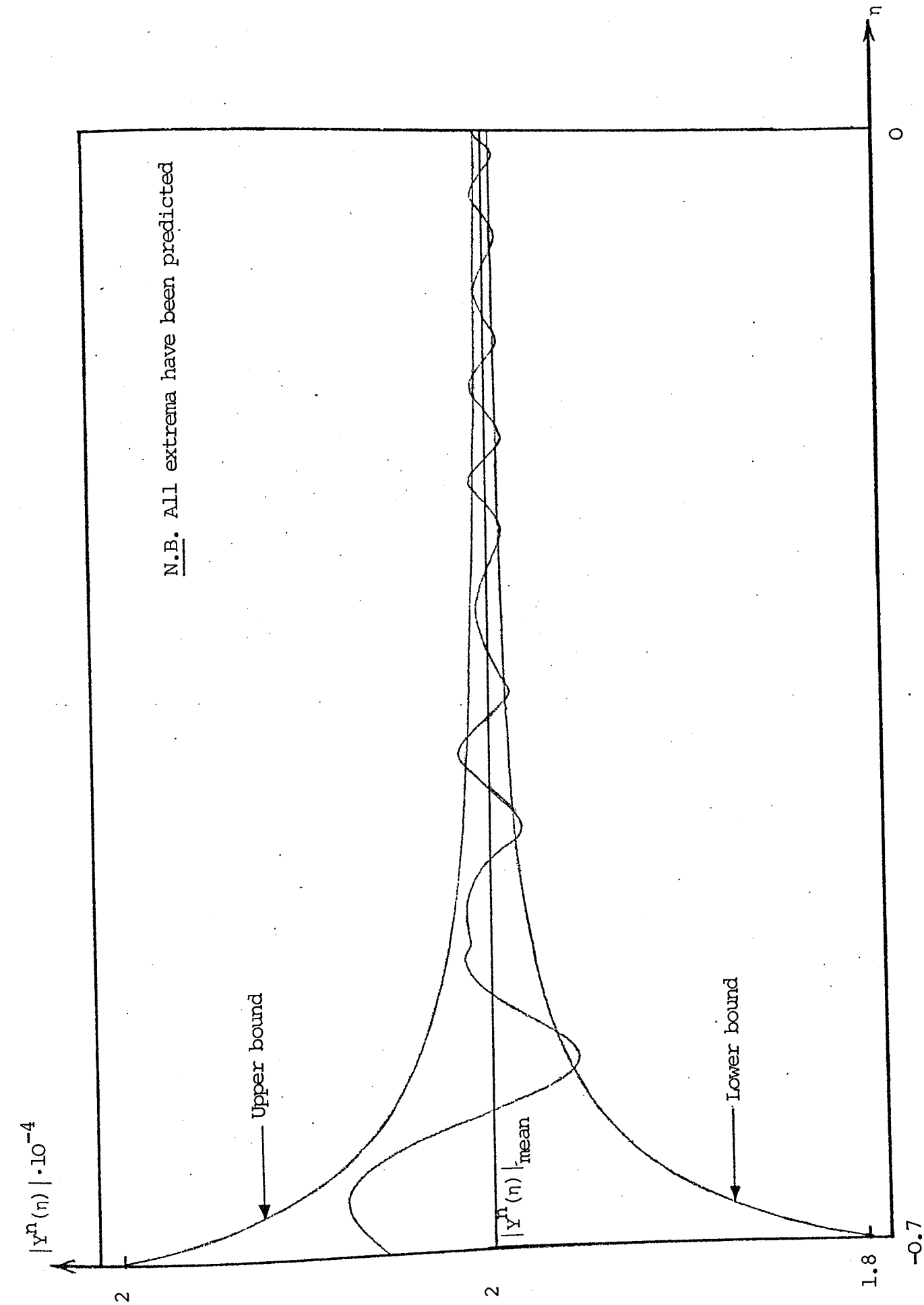

Fig. 4.13 Oscillations and Bounds in the Region

$-1 + \frac{2T_r}{T} < \eta \lesssim 0$; $W = 10^5$Hz, $T = 10^{-3}$sec., $T_f = T_r = 0.1T$

4.7 The Trapezoidal LFM Spectrum - The Edge Vicinities

The previous discussion has avoided any detailed consideration of the vicinities associated with the edges $\eta=\pm 1$, $-1+\frac{2T_r}{T}$ and $1-\frac{2T_f}{T}$. However, this discussion has shown that the preceding results do not hold in these vicinities. Accordingly, these vicinities will be considered below.

4.7.1 The Edge $\eta=-1$ Outside Vicinity ($\eta \lesssim -1$)

This vicinity extends from the edge $\eta=-1$ to $\eta_{r2} \overset{\Delta}{\simeq} -1-\frac{3}{2}\left|\frac{2}{WT}\right|^{\frac{1}{2}}$ where it meets the T_r-tail proper. In this vicinity, one may expect the initial rising effects to exceed those of subsequent rising as well as those of falling. Thus, one may treat x_2, x_3 and x_4 as being comparatively larger than x_1. As one moves towards the near T_r-tail, the subsequent rising effects become comparable with those of initial rising and the largeness of x_1 becomes comparable with that of x_2.

This vicinity may be conveniently divided into two parts. The first part extends from the edge $\eta=-1$ itself to η_{r3}, say. The second part extends from η_{r3} to η_{r2}. In the first part, one may use expansion (4.7) for $F(x_2)$, $F(x_3)$ and $F(x_4)$ and use the following series expansion[79] for $F(x_1)$

$$F(x) \simeq x \tag{4.27}$$

This expansion has been found numerically to give reliable results for $|x| \leq 0.6$. Accordingly, it is reasonable to let $\eta_{r3} \overset{\Delta}{\simeq} -1 - \frac{3}{5}\left|\frac{2}{WT}\right|^{\frac{1}{2}}$.

Adopting the above-mentioned expansion scheme, (4.6) gives

$$Y^n(\eta) \simeq \frac{1}{T_r}\left(x_1^2 - \frac{x_1 e^{j\frac{\pi}{4}}}{\sqrt{2}} + \frac{j e^{j\frac{\pi}{2}x_1^2}}{\pi}\right) \tag{4.28}$$

This relation has been found numerically to predict that in the vicinity part in question, $|Y^n(\eta)|$ decreases slowly and monotonically from a maximum initial value $\simeq \frac{1}{\pi T_r}$ at the edge $\eta=-1$ itself to a minimum value $\simeq \frac{0.115}{T_r}$ at η_{r3} (see Fig. 4.14). Making use of these facts and noting that the vicinity is practically short, $|Y^n(\eta)|$ may be treated in this part as a linear function of η given by the relation

$$|Y^n(\eta)| \simeq \frac{1}{T_r}\left[\frac{1}{\pi} + \frac{1}{3}\left|\frac{WT}{2}\right|^{\frac{1}{2}}(1+\eta)\right] \tag{4.29}$$

whose validity may be judged from Fig. 4.14 concerning the special case where $|WT|=100$ and $T_r=3\times10^{-4}$ sec.

Relations (4.28) and (4.29) may not be used in the second part of this vicinity where $x_1>0.6$ and expansion (4.27) may not give acceptable results. In fact, (4.28)

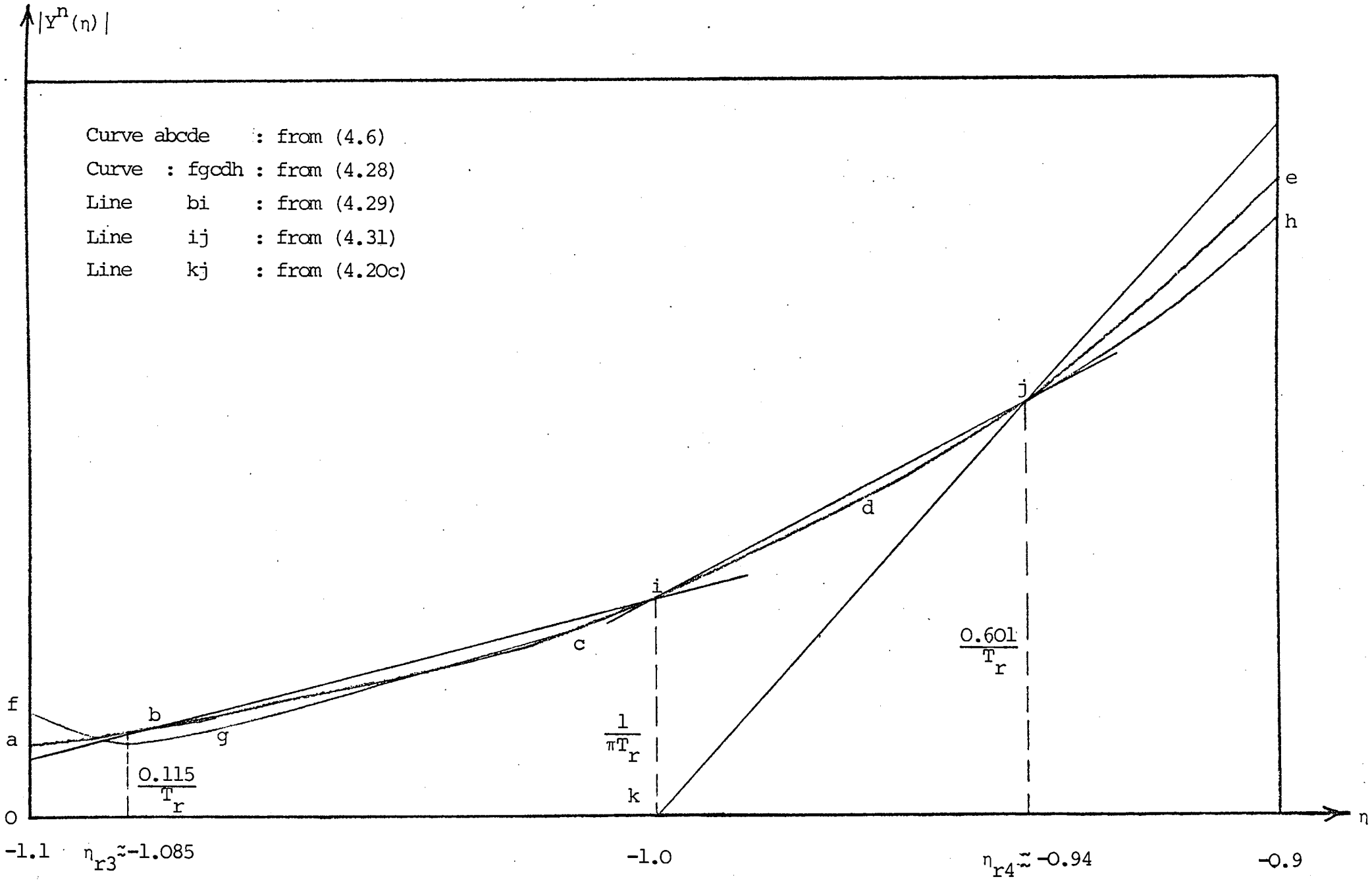

Fig. 4.14 The Edge $\eta=-1$ Vicinity

; $W = 10^5$ Hz, $T = 10^{-3}$ sec., $T_r = 1.5T_f = 3\times10^{-4}$ sec.

predicts that $|Y^n(\eta)|$ increases monotonically with $|\eta|$ in this part and (4.29) predicts that it decreases linearly with $|\eta|$ until it vanishes (see Fig. 4.14). These two predictions cannot be reliable because one expects $|Y^n(\eta)|_{mean}$ in this part to be >0 decreasing monotonically with $|\eta|$ as it does in the neighbouring regions. Thus, a more reliable representation of $|Y^n(\eta)|$ in this part is desirable. Such a representation may be obtained by treating $|Y^n(\eta)|$ as a linear function of η describing the straight line joining the two points in the η-$|Y^n(\eta)|$ plane corresponding to the two ends of this part. The first of these points is $(\eta_{r3}, \frac{0.115}{T_r})$ and the second point is $(\eta_{r2}, \frac{4}{9\pi^2 T_r})$. The ordinate of the second point has been conveniently obtained by substituting η_{r2} in $|Y^n(\eta)|_{mean}$ of (4.11c). Thus, $|Y^n(\eta)|$ may be represented in this part by the linear relation

$$|Y^n(\eta)| \simeq \frac{1}{T_r}\left[\frac{1}{2\pi} + \frac{1}{12}\left|\frac{WT}{2}\right|^{\frac{1}{2}}(1+\eta)\right] \qquad (4.30)$$

whose validity may be judged from Fig. 4.15 concerning the special case where $|WT|=100$ and $T_r=3\times10^{-4}$ sec.

4.7.2 The Edge $\eta=-1$ Inside Vicinity ($\eta\geq-1$)

This vicinity extends from the edge $\eta=-1$ to η_{r4} where it meets the region $-1<\eta\leq-1+\frac{T_r}{T}$. In this vicinity, (4.28)

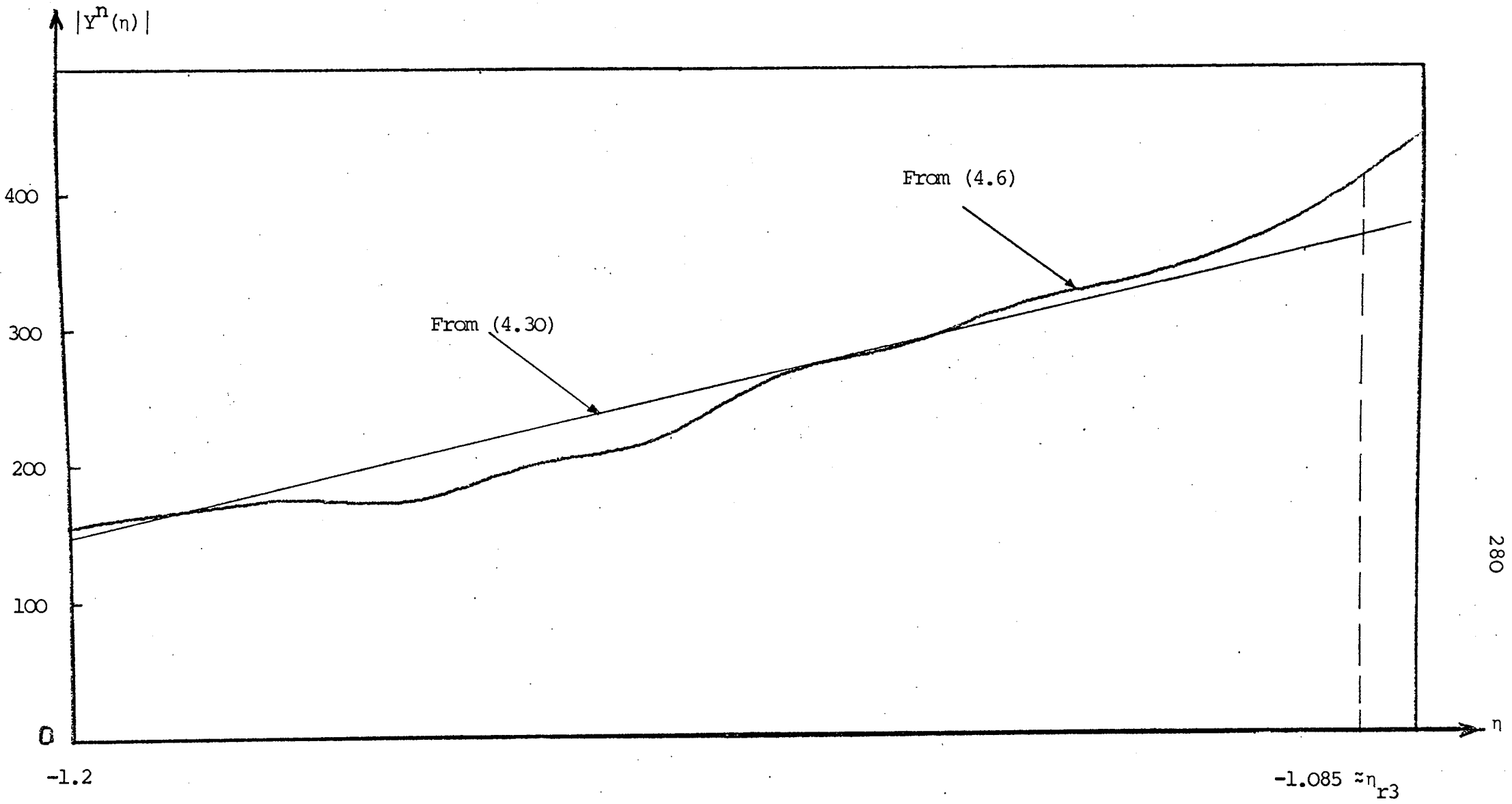

Fig. 4.15 The Edge $\eta=-1$ Outside Vicinity: Second Part;
$W = 10^5$Hz, $T = 10^{-3}$sec., $T_r = 1.5\ T_f = 0.3\ T$.

still holds and predicts that $|Y^n(\eta)|$ increases slowly and monotonically from a minimum initial value $\simeq\frac{1}{\pi T_r}$ at the edge $\eta=-1$ itself until it meets $|Y^n(\eta)|_{mean}$ of (4.20c) at $\eta \simeq -1+0.425|\frac{2}{WT}|^{\frac{1}{2}}$ assuming the value $0.601\ T_r^{-1}$. Accordingly, it is reasonable to let $\eta_{r4} \overset{\Delta}{\simeq} -1+0.425|\frac{2}{WT}|^{\frac{1}{2}}$. It is also reasonable to represent $|Y^n(\eta)|$ in this vicinity by the following linear relation describing the straight line joining the two points corresponding to its two ends in the $\eta-|Y^n(\eta)|$ plane

$$|Y^n(\eta)| \simeq \frac{1}{T_r}\left[\frac{1}{\pi} + \frac{2}{3}\left|\frac{WT}{2}\right|^{\frac{1}{2}}(1+\eta)\right] \tag{4.31}$$

whose validity may be judged from Fig. 4.14 concerning the special case where $|WT|=100$ and $T_r = 3\times10^{-4}$ sec.

4.7.3 The Edge $\eta=-1+\frac{2T_r}{T}$ External Vicinity ($\eta\lessapprox-1+\frac{2T_r}{T}$)

This vicinity extends from the edge $\eta=-1+\frac{2T_r}{T}$ to η_{r5} where it meets the region $-1+\frac{T_r}{T}\lessapprox\eta<-1+\frac{2T_r}{T}$. In this vicinity, one may expect the final rising effects to exceed those of initial rising as well as those of falling. Thus, one may use expansion (4.7) for $F(x_1)$, $F(x_3)$ and $F(x_4)$ and use expansion (4.27) for $F(x_2)$. In this manner, (4.6) gives

$$Y^n(\eta) \simeq 2|\mu|^{\frac{1}{2}}e^{j\frac{\pi}{4}} - \frac{1}{T_r}\left(x_2^2 + \frac{x_2 e^{j\frac{\pi}{4}}}{\sqrt{2}} + \frac{j e^{j\frac{\pi}{2}x_2^2}}{\pi}\right) \tag{4.32}$$

In this relation, the bracketed quantity is identical to the right hand side of (4.28) with $-x_1 \to x_2$. This fact helps in studying (4.32) which is, however, much more difficult to handle because it includes the additional term $2|\mu|^{\frac{1}{2}} e^{j\frac{\pi}{4}}$. In any case, (4.32) can be shown to predict that in this vicinity, $|Y^n(\eta)|$ decreases slowly and monotonically from a maximum initial value $\simeq 2|\mu|^{\frac{1}{2}} - \frac{\sqrt{2}}{2\pi T_r}$ at the edge $\eta = -1 + \frac{2T_r}{T}$ itself until it meets $|Y^n(\eta)|_{mean}$ of (4.20c) at $\eta \simeq -1 + \frac{2T_r}{T} - 0.3841\left|\frac{2}{WT}\right|^{\frac{1}{2}}$ assuming the value $2|\mu|^{\frac{1}{2}} - \frac{0.543}{2T_r T}$. Accordingly, it is reasonable to let $\eta_{r5} \overset{\Delta}{\simeq} -1 + \frac{2T_r}{T} - 0.3841\left|\frac{2}{WT}\right|^{\frac{1}{2}}$. It is also reasonable to represent $|Y^n(\eta)|$ in this vicinity by the following linear relation describing the straight line joining the two points corresponding to its two ends in the $\eta - |Y^n(\eta)|$ plane

$$|Y^n(\eta)| \simeq 2|\mu|^{\frac{1}{2}} - \frac{1}{T_r}\left[\frac{\sqrt{2}}{2\pi} - \frac{4}{5}\left|\frac{WT}{2}\right|^{\frac{1}{2}}(1+\eta-\frac{2T_r}{T})\right] \qquad (4.33)$$

whose validity may be judged from Fig. 4.16 concerning the special case where $W = 10^5$ Hz, $T = 10^{-3}$ sec and $T_r = 0.3\ T$.

4.7.4 The Edge $\eta = -1 + \frac{2T_r}{T}$ Internal Vicinity $(\eta \gtrsim -1 + \frac{2T_r}{T})$

This vicinity extends from the edge $\eta = -1 + \frac{2T_r}{T}$ to η_{r6} where it meets the region $-1 + \frac{2T_r}{T} < \eta \lesssim 0$. In this

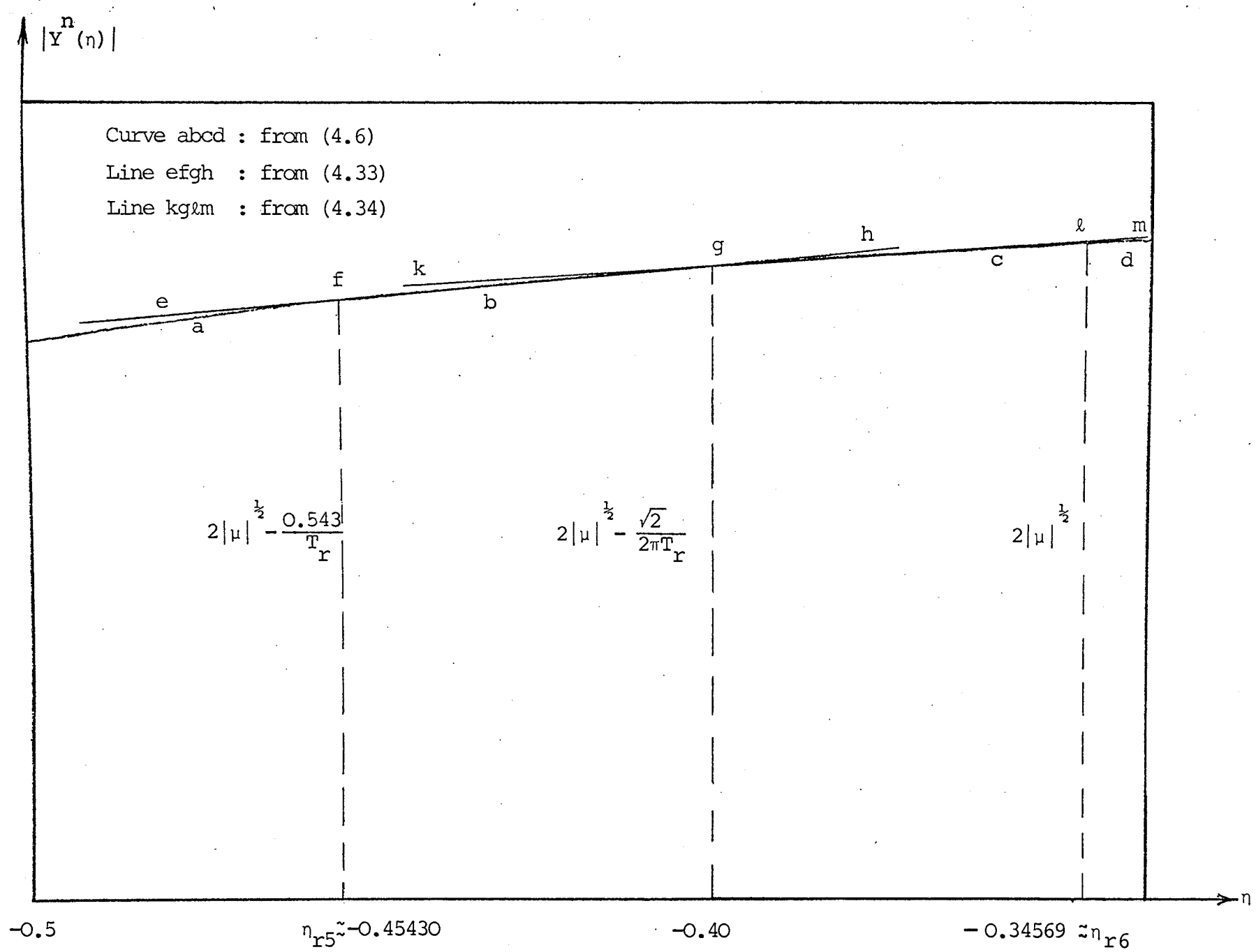

Fig. 4.16 The Edge $\eta=-1+\frac{2T_r}{T}$ Vicinity: $W = 10^5$Hz, $T = 10^{-3}$sec., $T_r = 1.5\ T_f = 0.3T$.

vicinity, (4.32) still holds and predicts that $|Y^n(\eta)|$ increases slowly and monotonically from a minimum initial value $\simeq 2|\mu|^{\frac{1}{2}} - \frac{\sqrt{2}}{2\pi T_r}$ at the edge until it meets $|Y^n(\eta)|_{mean}$ of (4.25c) at $\eta \simeq -1+\frac{2T_r}{T}+0.3841\left|\frac{2}{WT}\right|^{\frac{1}{2}}$ assuming the value $2|\mu|^{\frac{1}{2}}$. Accordingly, it is reasonable to let $\eta_{r6} \triangleq -1+\frac{2T_r}{T}+0.3841\left|\frac{2}{WT}\right|^{\frac{1}{2}}$. It is also reasonable to represent $|Y^n(\eta)|$ in this vicinity by the following linear relation describing the straight line joining the two points corresponding to its two ends in the η-$|Y^n(\eta)|$ plane

$$|Y^n(\eta)| \simeq 2|\mu|^{\frac{1}{2}} - \frac{1}{T_r}\left[\frac{\sqrt{2}}{2\pi} - \frac{3}{5}\left|\frac{WT}{2}\right|^{\frac{1}{2}}(1+\eta-\frac{2T_r}{T})\right] \qquad (4.34)$$

whose validity is evident from Fig. 4.16 concerning the special case where $W = 10^5$ Hz, $T = 10^{-3}$ sec and $T_r = 0.3\ T_r$.

4.7.5 Vicinities of the Edges $\eta=1-\frac{2T_f}{T}$ and $\eta=1$

The edge $\eta=1-\frac{2T_f}{T}$ vicinity is a replica of that of the edge $\eta=-1+\frac{2T_r}{T}$ except that $T_r \to T_f$ and $x_2 \to -x_3$ in (4.32). In this manner, $T_r \to T_f$ and $\eta \to -\eta$ in (4.33) and (4.34).

The edge $\eta=1$ vicinity is a replica of that of the edge $\eta=-1$ except that $T_r \to T_f$ and $x_1 \to -x_4$ in (4.28). In this

manner, $T_r \to T_f$ and $\eta \to -\eta$ in (4.29), (4.30) and (4.31).

4.8 The Spectrum of the Ideal Chirp Pulse

4.8.1 Introduction

The preceding theory can only handle the spectrum of a LFM pulse or a physical chirp pulse having a trapezoidal envelope for which

$$\frac{T_r}{T}, \frac{T_f}{T} \gtrsim \frac{2}{5}\left|\frac{2}{WT}\right|^{\frac{1}{2}} \tag{4.35}$$

It suffices to explain the reasons underlying this constraint in the case of $\frac{T_r}{T}$. To this end, consider the T_r-region where $-1 \lesssim \eta \lesssim -1+\frac{2T_r}{T}$. The methods of Subsections 4.6.2 and 4.6.3 can handle this region's proper for $\frac{T_r}{T} \gtrsim \frac{4}{5}\left|\frac{2}{WT}\right|^{\frac{1}{2}}$ and, less accurately, for $\frac{4}{5}\left|\frac{2}{WT}\right|^{\frac{1}{2}} > \frac{T_r}{T} \gtrsim \frac{2}{5}\left|\frac{2}{WT}\right|^{\frac{1}{2}}$. This region's two edge vicinities can be handled by the methods of Subsections 4.7.2 and 4.7.3.

Thus, the previous theory would not be reliable concerning the T_r-side, the T_f-side or both sides depending on whether (4.35) is not satisfied by $\frac{T_r}{T}$, $\frac{T_f}{T}$ or by both $\frac{T_r}{T}$ and $\frac{T_f}{T}$ respectively. Again, it suffices to consider the case where $\frac{T_r}{T}$ does not satisfy (4.35). In this case, the edge $\eta=-1+\frac{2T_r}{T}$ of the region $-1 \lesssim \eta \lesssim -1+\frac{2T_r}{T}$ moves towards the edge $\eta=-1$ and the two

edge vicinities overlap over a range given by

$$\text{Overlapping range} \simeq 2\left(\frac{2}{5}\left|\frac{2}{WT}\right|^{\frac{1}{2}} - \frac{T_r}{T}\right) \tag{4.36}$$

This relation indicates that the overlapping range increases as $|WT|$ and/or $\frac{T_r}{T}$ decrease(s). It also indicates that no overlapping corresponds to $\frac{T_r}{T} \gtrsim \frac{2}{5}\left|\frac{2}{WT}\right|^{\frac{1}{2}}$, partial overlapping corresponds to $\frac{2}{5}\left|\frac{2}{WT}\right|^{\frac{1}{2}} > \frac{T_r}{T} > \frac{1}{5}\left|\frac{2}{WT}\right|^{\frac{1}{2}}$ and complete overlapping corresponds to $\frac{T_r}{T} \simeq \frac{1}{5}\left|\frac{2}{WT}\right|^{\frac{1}{2}}$.

In the region where the two vicinities overlap, one may use expansion (4.27) for both $F(x_1)$ and $F(x_2)$ and expansion (4.7) for both $F(x_3)$ and $F(x_4)$. In this manner, (4.6) gives

$$Y^n(\eta) \simeq |\mu|^{\frac{1}{2}} e^{j\frac{\pi}{4}} + \frac{x_1^2 - x_2^2}{T_r} + \frac{e^{j\frac{\pi}{2}x_2^2} - e^{j\frac{\pi}{2}x_1^2}}{j\pi T_r} \tag{4.37}$$

which gives

$$|Y^n(\eta)|_{mean} \simeq |\mu|^{\frac{1}{2}} \left[1 + 2|WT|^{\frac{1}{2}}\left(1 + \eta - \frac{T_r}{T}\right)\right] \tag{4.38}$$

A detailed study of the overlapping of edge vicinities and the associated limiting processes is not intended here. It should be noted, however, that (4.38) describes a

straight line in the η-$|Y^n(\eta)|$ plane whose slope is determined by $|W|$ and whose length is determined by $\frac{T_r}{T}$. As $\frac{T_r}{T}$ decreases, i.e. as overlapping increases, the values of $|Y^n(\eta)|$ at the two edges $\eta=-1$ and $\eta=-1+\frac{2T_r}{T}$ approach its value at the midpoint $\eta=-1+\frac{T_r}{T}$ from below and above respectively. As $\frac{T_r}{T}\to 0$, i.e. as the trapezoidal pulse T_r-side becomes rectangular, the edge $\eta=-1+\frac{2T_r}{T}$ of its spectrum moves into the edge $\eta=-1$ with line (4.38) reducing to a single point at this edge and $|Y^n(-1)| \simeq |Y^n(-1)|_{mean} \simeq |\mu|^{\frac{1}{2}}$.

The preceding paragraph implies that if $\frac{T_r}{T}<\frac{1}{5}\left|\frac{2}{WT}\right|^{\frac{1}{2}}$, it is possible to assume that $\frac{T_r}{T} \simeq 0$ and to treat the T_r-side of the trapezoidal pulse as being ideally rectangular. Thus, any physical chirp pulse may be treated as being an ideally symmetric rectangular pulse if

$$\frac{T_r}{T}\ ,\ \frac{T_f}{T} <\frac{1}{5}\left|\frac{2}{WT}\right|^{\frac{1}{2}} \qquad (4.39)$$

This relation implies that a trapezoidal LFM pulse with $W=10^5$ Hz and $T=10^{-3}$sec, for example, may be treated as being ideally rectangular if $T_r, T_f < 2.8\times10^{-5}$sec. The validity of such a conclusion may be judged by comparing Figs. 4.17a and 4.17b which are drawn to the same scale.

The approach whereby an ideally rectangular chirp

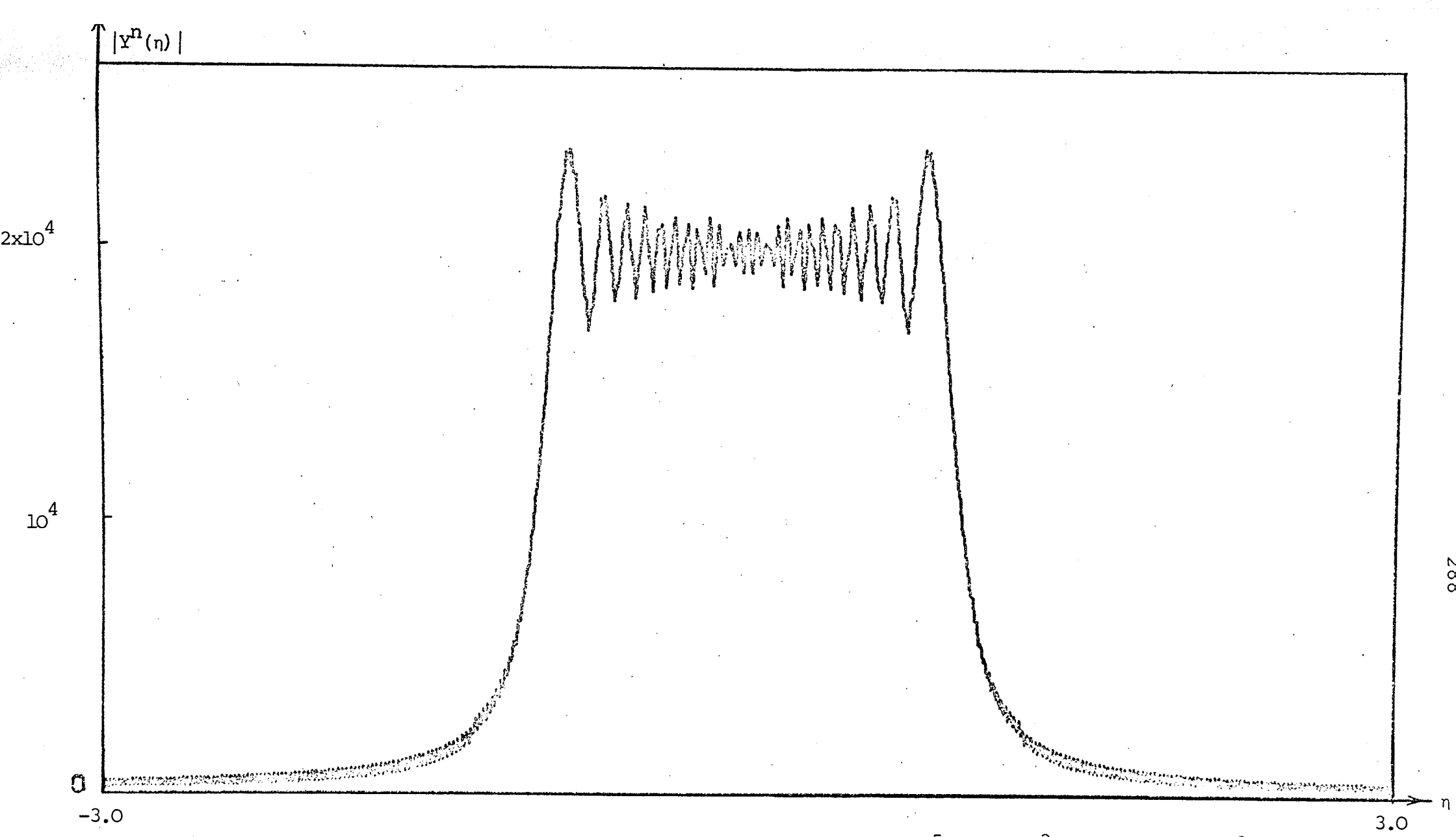

Fig. 4.17a Amplitude Spectrum of a Trapezoidal LFM Pulse; $W=10^5$Hz, $T=10^{-3}$sec., $T_r=T_f=5x10^{-6}$sec.

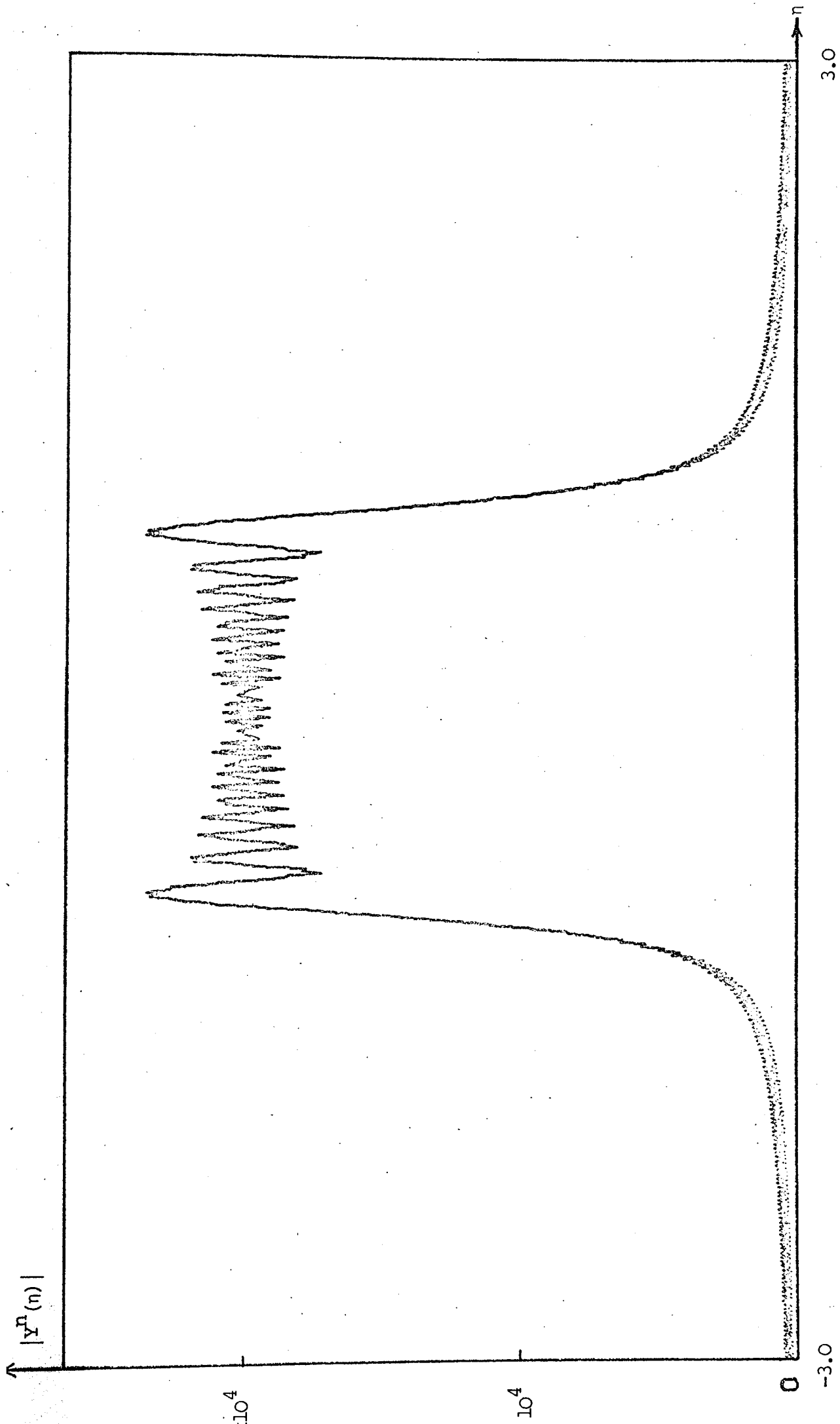

Fig. 4.17b Amplitude Spectrum of a Rectangular Chirp Pulse; $W=10^5$Hz, $T=10^{-3}$sec.

pulse may be treated as a limiting case of the corresponding trapezoidal LFM pulse is rather cumbersome and lengthy. A direct approach in this respect is simpler and straightforward. Accordingly, the following discussion treats the rectangular chirp pulse as an independent case. However, the limiting approach will also be briefly considered in Section 4.9.

4.8.2 The Spectrum of a Rectangular Chirp Pulse

Consider the following baseband complex rectangular chirp pulse

$$y(\sigma) = R_T(\sigma)\ e^{j\pi\mu\sigma^2} \tag{4.40}$$

The spectrum Y(f) of this pulse is given by

$$Y(f) = \int R_T(\sigma)\ e^{j\pi(-2f\sigma+\mu\sigma^2)}d\sigma \tag{4.41a}$$

which reduces through transformation (4.3) to

$$Y(f) = \frac{e^{-j\pi f^2/\mu}}{|2\mu|^{\frac{1}{2}}} \int_{x_p}^{x_q} e^{\pm j\frac{\pi}{2}x^2}\,dx \tag{4.41b}$$

where $+j\frac{\pi}{2}x^2$ and $-j\frac{\pi}{2}x^2$ correspond to $\mu>0$ and $\mu<0$ respectively and

$$x_p \triangleq -\left|\frac{WT}{2}\right|^{\frac{1}{2}}(1+\eta) \tag{4.42a}$$

$$x_q \triangleq \left|\frac{WT}{2}\right|^{\frac{1}{2}}(1-\eta) \tag{4.42b}$$

where η is given by (4.5e).

Thus, making use of (4.41b) in (4.6b) shows that for $\mu>0$,

$$Y^n(\eta) = |2\mu|^{\frac{1}{2}} F(x_p,x_q) \tag{4.43a}$$

where $F(x_p,x_q)$ is a Fresnel function first introduced in Section 3.4 as

$$F(x_p,x_q) \overset{\Delta}{=} F(x_q) - F(x_p) \tag{4.43b}$$

The following discussion is mostly formulated in terms of $F(x_p,x_q)$. The results can readily be applied to $Y^n(\eta)$ through (4.43a).

4.8.3 $|F(x_p,x_q)|$ for $|WT|\to\infty$

For $|WT|\to\infty$, the nonvanishing values of $|x_p|$ and $|x_q|$ are large over the entire η-axis. In this case, it is convenient to use the first term of expansion (4.7) for both $F(x_p)$ and $F(x_q)$. In this manner, (4.43b) gives

$$|F(x_p,x_q)|_\infty = 0 \ , \ |\eta| > 1 \tag{4.44a}$$

$$= \sqrt{2}, \ |\eta| < 1 \tag{4.44b}$$

$$= \frac{1}{\sqrt{2}}, \ |\eta| = 1 \tag{4.44c}$$

This relation is illustrated in Fig. 4.18. It predicts that as $|WT| \to \infty$, $|Y(f)|$ assumes the functional form of $|y(\sigma)|$ in agreement with the stationary phase relation (3.7). This prediction is confirmed by the computer plots of Fig. 4.19.

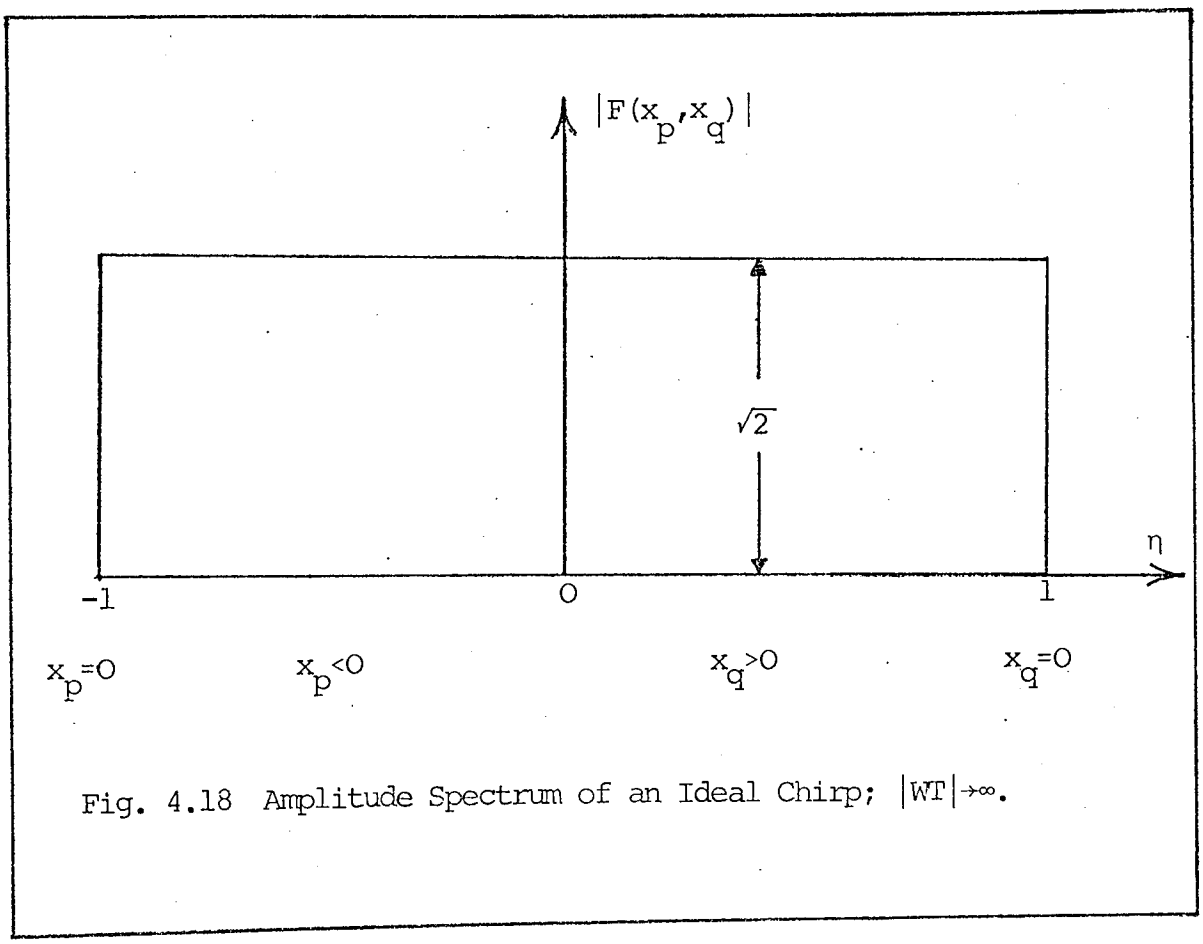

Fig. 4.18 Amplitude Spectrum of an Ideal Chirp; $|WT| \to \infty$.

4.8.4 $|F(x_p,x_q)|$ For Finite $|WT|$ - The Tail Proper ($|\eta|>1$)

For finite $|WT|$, $|F(x_p,x_q)|$ is expected to fluctuate about the limiting level of (4.44) forming both forward

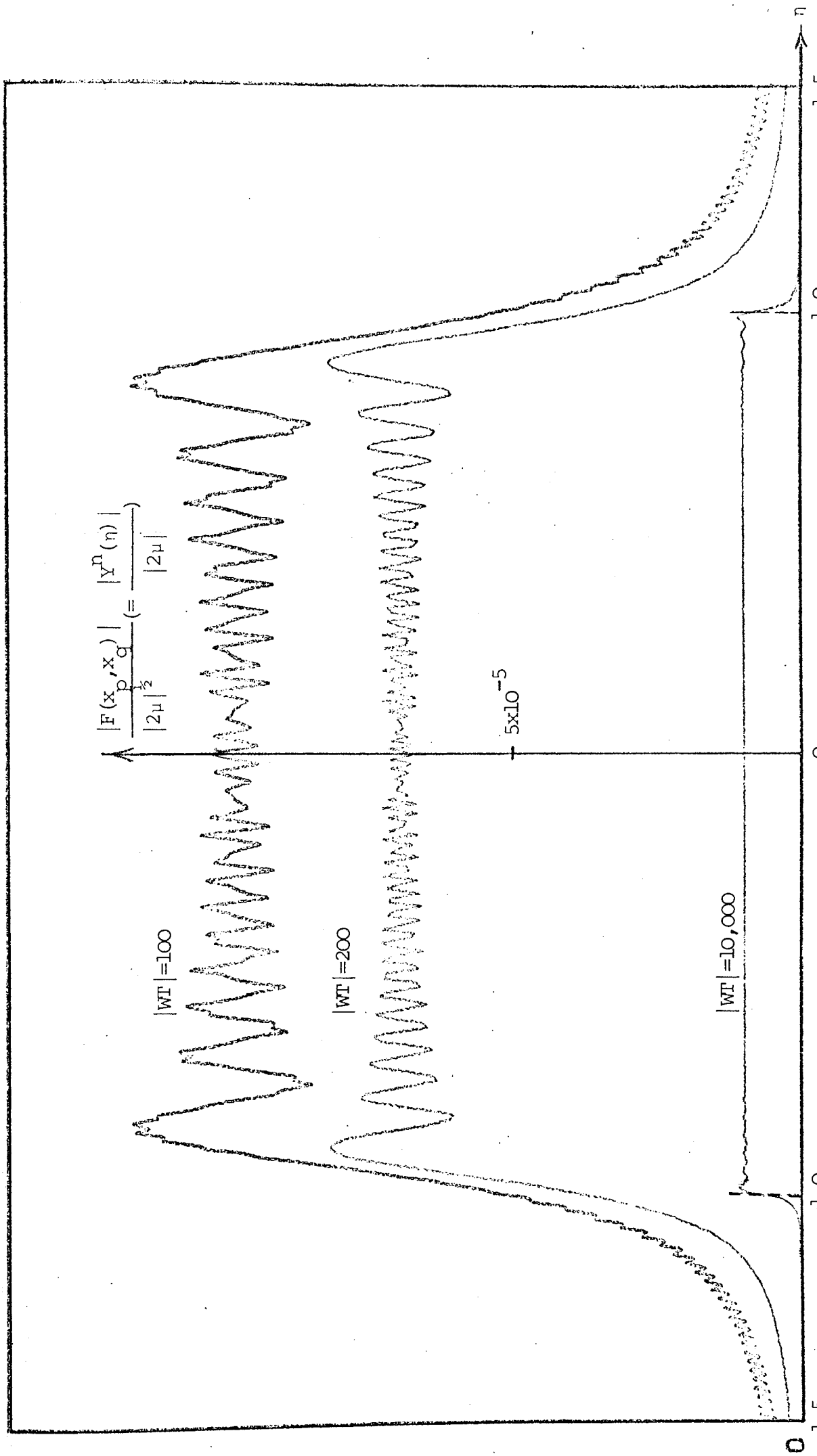

Fig. 4.19 Amplitude Spectrum of an Ideal Chirp; $\mu>0$, $\mu<0$, $T = 10^{-3}$sec. (increasing $|WT|$).

and trailing tails flanking the central region as shown in Fig. 4.17b (see also Fig. 3.3).

Consider the left hand side tail. This tail extends from $\eta=-\infty$ to η_{cl}, say, where it meets the edge $\eta=-1$ outside vicinity. In this tail, it is convenient to expand both $F(x_p)$ and $F(x_q)$ according to (4.7). This gives

$$F(x_p,x_q) \simeq \frac{j}{\pi}\left(\frac{e^{j\frac{\pi}{2}x_p^2}}{x_p} - \frac{e^{j\frac{\pi}{2}x_q^2}}{x_q}\right) \tag{4.45}$$

which implies that

$$|F(x_p,x_q)| \leq \frac{2\sqrt{2}}{\pi|WT|^{\frac{1}{2}}}\cdot\frac{|\eta|}{(|\eta|^2-1)} \tag{4.46a}$$

$$|F(x_p,x_q)| \geq \frac{2\sqrt{2}}{\pi|WT|^{\frac{1}{2}}}\cdot\frac{1}{(|\eta|^2-1)} \tag{4.46b}$$

$$|F(x_p,x_q)|_{mean} \simeq \frac{\sqrt{2}}{\pi|WT|^{\frac{1}{2}}}\cdot\frac{1}{(|\eta|-1)} \tag{4.46c}$$

where it can be seen that the upper bound $=|\eta|\times$ the lower bound.

These relations predict that $|F(x_p,x_q)|$ oscillates with an oscillation amplitude $A(\eta)$ which decreases with both $|WT|$ and $|\eta|$ and that $\frac{A(\eta)}{|F(x_p,x_q)|_{mean}} = \frac{2(|\eta|-1)}{|\eta|+1} \to 2$ for large $|\eta|$. These relations also predict that

$|F(x_p,x_q)|\to 0$ as $|WT|$ and/or $|\eta|\to\infty$ and that

$$|\eta^k_{max}| \simeq \frac{2k+1}{|WT|} \tag{4.47a}$$

$$|\eta^k_{min}| \simeq \frac{2k}{|WT|} \tag{4.47b}$$

where the order of extrema k increases along the negative η-axis.

Relation (4.47) predicts that the oscillation density is uniform in η and is given by $\frac{1}{2}|WT|$ per unit of η.

The above-mentioned predictions are in full agreement with reality as can be seen from Figs. 4.20 through 4.22. Also, these predictions remain valid for the right hand side tail due to perfect symmetry.

4.8.5 $|F(x_p,x_q)|$ for Finite $|WT|$- The Central Region ($|\eta|<1$) Excluding Edge Vicinities

Consider the left hand side of the central region. This side extends from η_{c3}, say, where it meets the edge $\eta=-1$ inside the vicinity to $\eta=0$. In this side, it is convenient to use expansion (4.7) for $F(x_p)$ and the first term of this expansion for $F(x_q)$. This gives

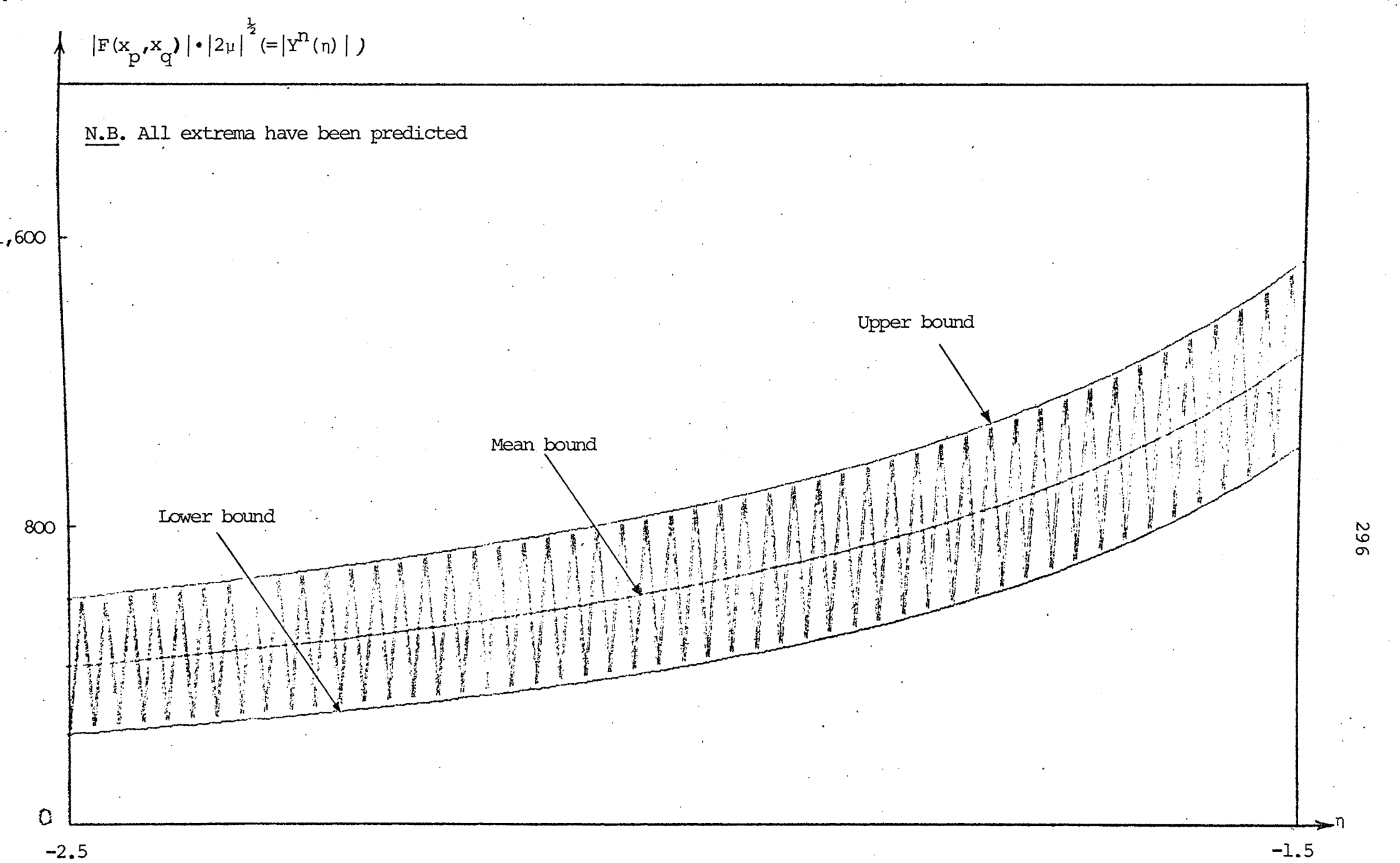

Fig. 4.20 The Tail of the Amplitude Spectrum of an Ideal Chirp; $W=10^5$Hz, $T=10^{-3}$sec.

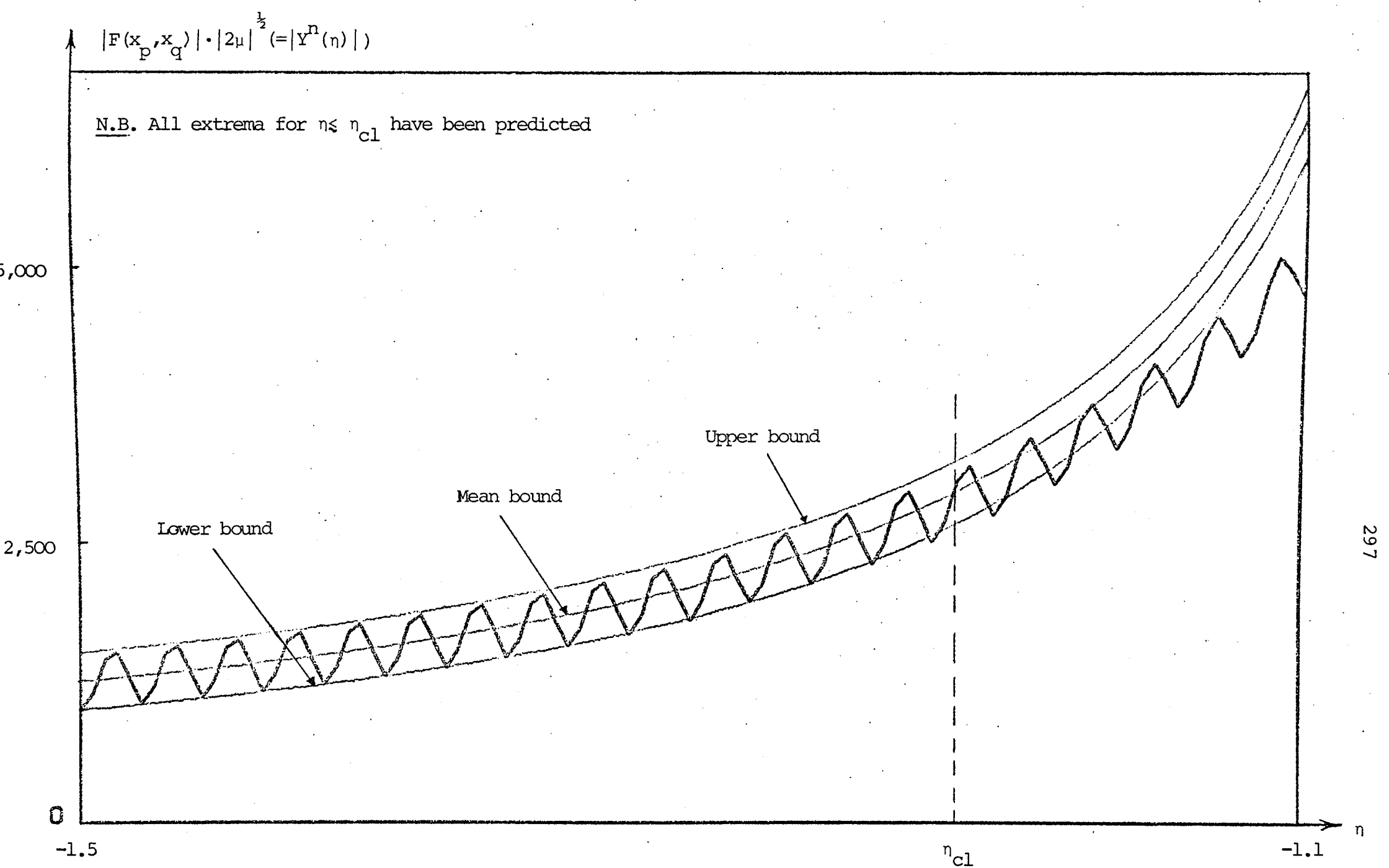

Fig. 4.21 The Tail of the Amplitude Spectrum of an Ideal Chirp; $W=10^5$Hz, $T=10^{-3}$sec.

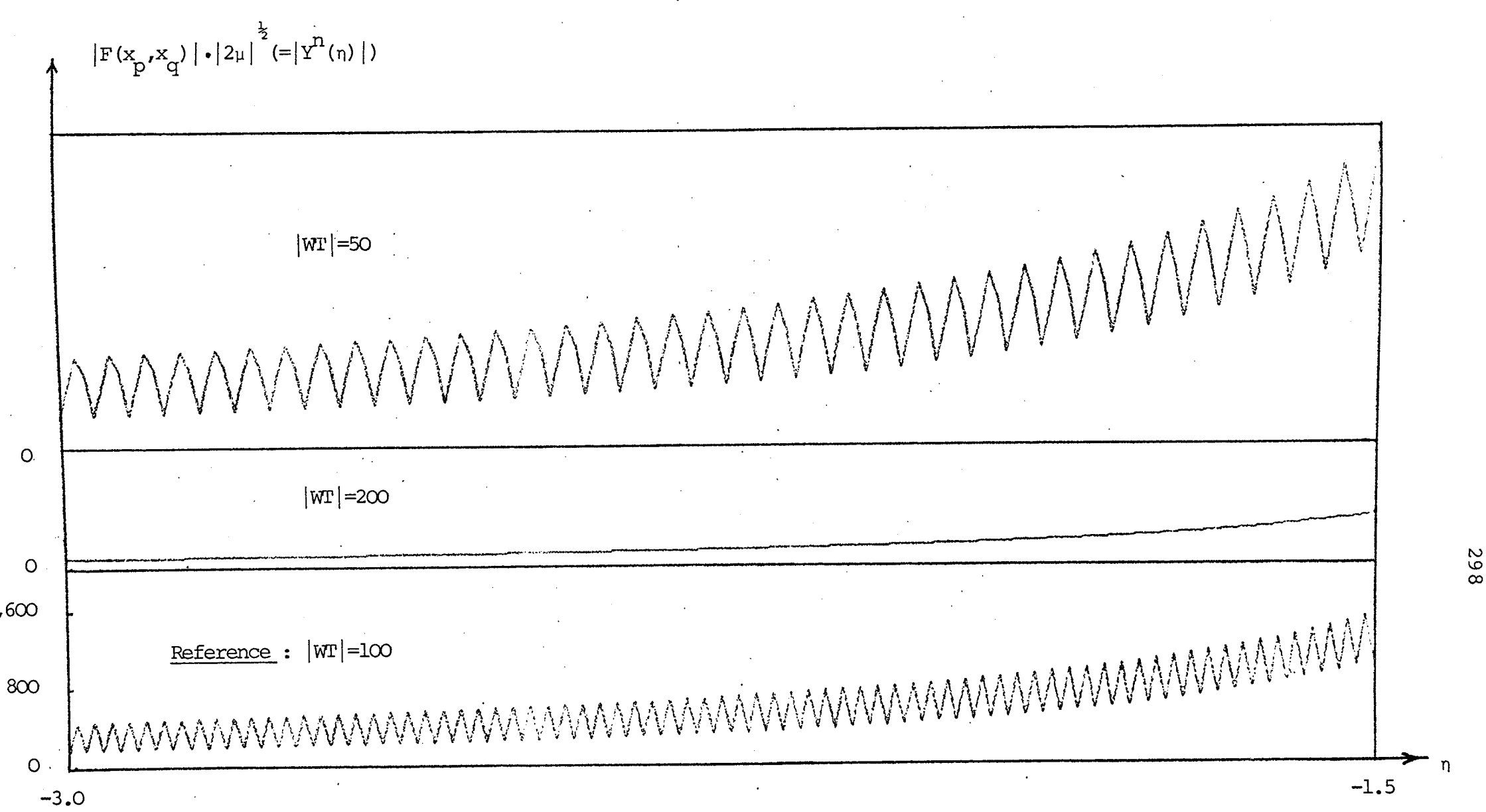

Fig. 4.22 Variation of A(η) with |WT| and |η| in the Tail of the Amplitude Spectrum of an Ideal Chirp; $T = 10^{-3}$ sec. (drawings are to the same scale).

$$F(x_p,x_q) \simeq \sqrt{2}\, e^{j\frac{\pi}{4}} + \frac{j e^{j\frac{\pi}{2}x_p^2}}{\pi x_p} \tag{4.48}$$

which implies that

$$|F(x_p,x_q)| \lesssim \sqrt{2} + \frac{\sqrt{2}}{\pi |WT|^{\frac{1}{2}}(1-|\eta|)} \tag{4.49a}$$

$$|F(x_p,x_q)| \gtrsim \sqrt{2} - \frac{\sqrt{2}}{\pi |WT|^{\frac{1}{2}}(1-|\eta|)} \tag{4.49b}$$

$$|F(x_p,x_q)|_{mean} \simeq \sqrt{2} \tag{4.49c}$$

These relations predict that $|F(x_p,x_q)|$ oscillates with an oscillation amplitude $A(\eta)$ which decreases with $|WT|$ and increases with $|\eta|$. They also predict that

$$|\eta_{max}^k| \simeq 1 - \left(\frac{8k+3}{|WT|}\right)^{\frac{1}{2}} \tag{4.50a}$$

$$|\eta_{min}^k| \simeq 1 - \left(\frac{8k+7}{|WT|}\right)^{\frac{1}{2}} \tag{4.50b}$$

where the order of extrema k increases along the positive η-axis.

Relation (4.50) predicts that the oscillation density is nonuniform, decreases with $|\eta|$ and increases with $|WT|$.

The above-mentioned predictions are in full agreement with reality as can be seen from Figs. 4.19 and 4.23. Also,

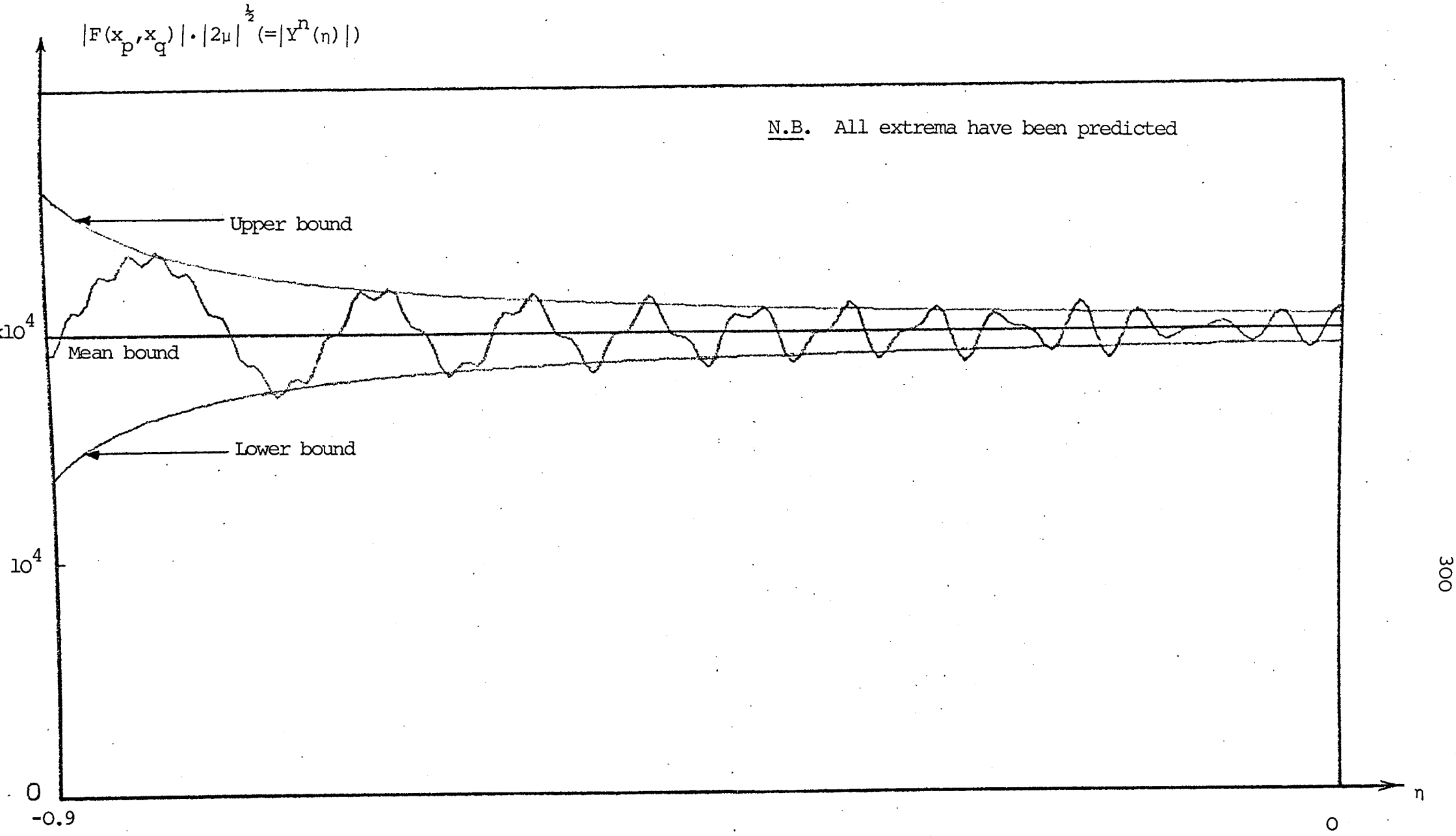

Fig. 4.23 Oscillations and Bounds in the Central Region of the Spectrum of an Ideal Chirp Pulse;
$W = 10^5$Hz, $T = 10^{-3}$sec.

these predictions remain valid for the right hand side of the central region due to perfect symmetry.

4.8.6 $|F(x_p,x_q)|$ - The Edge Vicinities

4.8.6.1 The Edge $\eta=-1$ Outside Vicinity ($\eta \lesssim -1$)

This vicinity extends from the edge $\eta=-1$ to $\eta_{c1} \overset{\Delta}{\simeq} -1- \frac{3}{2}\left|\frac{2}{WT}\right|^{\frac{1}{2}}$ where it meets the left hand tail. It may be divided into two parts. The first part extends from the edge $\eta=-1$ itself to $\eta_{c2} \overset{\Delta}{\simeq} -1- \frac{1}{2}\left|\frac{2}{WT}\right|^{\frac{1}{2}}$ and the second part extends from η_{c2} to η_{c1}. In the first part $0 \lesssim x_p \lesssim \frac{1}{2}$ and one may conveniently use expansion (4.27) for $F(x_p)$ and the first term of expansion (4.7) for $F(x_q)$ to get

$$F(x_p,x_q) \simeq \frac{e^{j\frac{\pi}{4}}}{\sqrt{2}} - x_p \tag{4.51a}$$

implying that

$$|F(x_p,x_q)|^2 \simeq (x_p - \tfrac{1}{2})^2 + (\tfrac{1}{2})^2 \tag{4.51b}$$

which can readily be identified as the upper branch of a vertical hyperbola in the x_p - $|F(x_p,x_q)|$ plane.

Relation (4.51) predicts that $|F(x_p,x_q)|$ decreases slowly and monotonically from a maximum initial value

$\simeq \frac{1}{\sqrt{2}}$ at the η=-1 edge itself where x_p=0 to a minimum value $\simeq \frac{1}{2}$ at η_{c2} where $x_p = \frac{1}{2}$. Noting that the vicinity part under consideration is practically short, one may represent $|F(x_p,x_q)|$ in it by the following linear relation representing the straight line joining the two points corresponding to its two ends in the η- $|F(x_p,x_q)|$ plane

$$|F(x_p,x_q)| \simeq \frac{1}{\sqrt{2}} + (\sqrt{2}-1)\left|\frac{WT}{2}\right|^{\frac{1}{2}}(1+\eta) \qquad (4.52)$$

whose validity may be judged from Fig. 4.2 4 concerning the special case where $|WT|$=100.

In the second part of the edge η=-1 outside vicinity, $|F(x_p,x_q)|$ may be approximated as a linear function of η representing the straight line joining the two points $(\eta_{c2}, \frac{1}{2})$ and $(\eta_{c1}, \frac{2}{3\pi})$ in the η- $|F(x_p,x_q)|$ plane. The ordinate of the second point has been conveniently obtained by substituting η_{c1} for η in (4.46c). Thus, $|F(x_p,x_q)|$ may be represented in this part by the linear relation

$$|F(x_p,x_q)| \simeq (\frac{3}{4} - \frac{1}{3\pi}) + (\frac{1}{2} - \frac{2}{3\pi})\left|\frac{WT}{2}\right|^{\frac{1}{2}}(1+\eta) \qquad (4.53)$$

whose validity may be judged from Fig. 4.24 concerning the special case where $|WT|$=100.

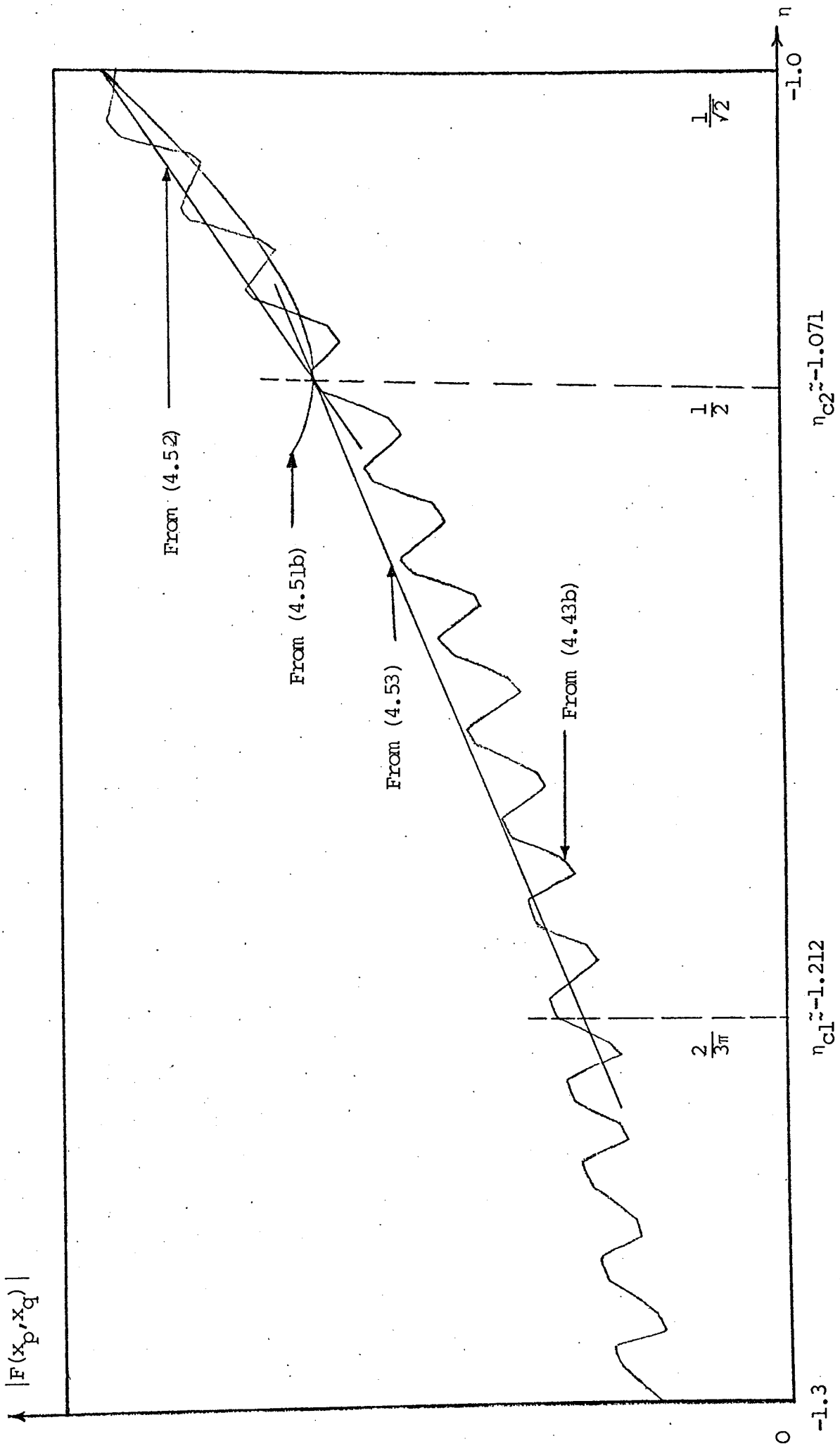

Fig. 4.24 The Edge η=-1 Outside Vicinity; $W = 10^5$ Hz, $T = 10^{-3}$ sec.

4.8.6.2 The Edge $\eta=-1$ Inside Vicinity ($\eta \gtrsim -1$)

This vicinity extends from the edge $\eta=-1$ to η_{c3} where it meets the central region. In this vicinity, (4.51) still holds and predicts that $|F(x_p,x_q)|$ increases slowly and monotonically from a minimum initial value $\simeq \frac{1}{\sqrt{2}}$ at the edge $\eta=-1$ itself until it meets $|F(x_p,x_q)|_{mean}$ of (4.49c) at $\eta \simeq -1+\frac{\sqrt{7}-1}{2}\left|\frac{2}{WT}\right|^{\frac{1}{2}}$ assuming the value $\sqrt{2}$. Accordingly, it is reasonable to let $\eta_{c3} \overset{\Delta}{\simeq} -1+\frac{\sqrt{7}-1}{2}\left|\frac{2}{WT}\right|^{\frac{1}{2}}$. It is also reasonable to represent $|F(x_p,x_q)|$ in this vicinity by the following linear relation describing the straight line joining the two points $(-1, \frac{1}{\sqrt{2}})$ and $(\eta_{c3},\sqrt{2})$ in the η-$|F(x_p,x_q)|$ plane

$$|F(x_p,x_q)| \simeq \frac{1}{\sqrt{2}} + \frac{\sqrt{2}}{\sqrt{7}-1}\left|\frac{WT}{2}\right|^{\frac{1}{2}}(1+\eta) \qquad (4.54)$$

whose validity may be judged from Fig. 4.25 concerning the special case where $|WT| = 100$.

4.8.6.3 The Edge $\eta=1$ Vicinities

These vicinities can be treated in the same manner as their counterparts associated with the edge $\eta=-1$. In fact, results for the former can be obtained by interchanging x_p and x_q in the results for the latter.

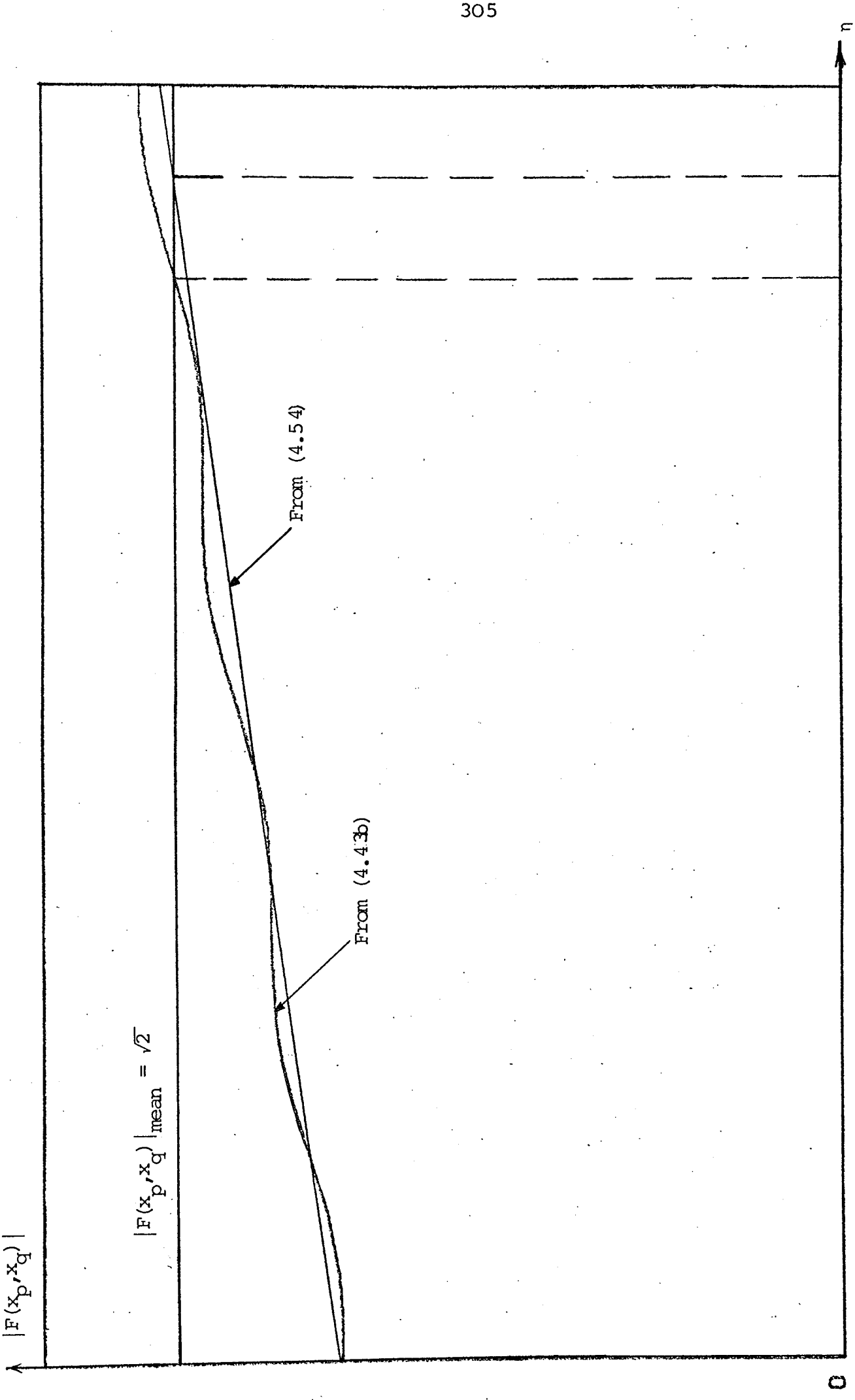

Fig. 4.25 The Edge η=-1 Inside Vicinity; $W = 10^5$ Hz, $T = 10^{-3}$ sec.

4.9 The Limiting Approach

Consider the trapezoidal LFM pulse of (4.1). Let, for example, $|WT|\to\infty$. In this case, all nonvanishing $|x|$-values are large over the entire η-axis and one may assume that $|x_1| \simeq |x_2|$ and $|x_3| \simeq |x_4|$. Thus, noting that $e^{j\frac{\pi}{2}x_1^2} \overset{\rightarrow}{\leftarrow} e^{j\frac{\pi}{2}x_2^2}$ and $F(|x_1|)\overset{\rightarrow}{\leftarrow}F(|x_2|)$ faster than $|x_1|\overset{\rightarrow}{\leftarrow}|x_2|$, that $e^{j\frac{\pi}{2}x_3^2} \overset{\rightarrow}{\leftarrow} e^{j\frac{\pi}{2}x_4^2}$ and $F(|x_3|)\overset{\rightarrow}{\leftarrow}F(|x_4|)$ faster than $|x_3|\overset{\rightarrow}{\leftarrow}|x_4|$ and that $\lim_{x\to\infty}F(x)=\frac{e^{j\frac{\pi}{4}}}{\sqrt{2}}$, (4.6) gives

$$|Y^n(\eta)|_{\infty} = \frac{1}{\sqrt{2}} \sum_{\ell=1}^{4} \frac{|x_\ell|}{T_\ell} \tag{4.55}$$

which can readily be seen through (4.5) to be identical to (4.8).

The limiting approach described above underlies the use of expansion (4.7) in Section 4.3 to obtain (4.8) from (4.6). This is obviously due to the fact that this expansion leads to the same results as, but obviates the need for the details of, this limiting approach. Such a limiting approach can also be used to establish the consistency of the F(x) expansions used for the trapezoidal LFM spectrum in the different η-regions.

The limiting approach can also be applied to the cases where the rising side, the falling side or both sides

of the trapezoidal LFM pulse $y(\sigma)$ of (4.1) become rectangular.

Consider first the case where only the rising side of $y(\sigma)$ becomes rectangular, i.e. where $T_r \to 0$. In this case, the spectrum $Y^n(\eta)$ of $y(\sigma)$ can be obtained by making $x_2 \to x_1$ through $x_2=0 \to x_1=0$ in (4.6). Thus, noting that $e^{j\frac{\pi}{2}x_2^2} \to e^{j\frac{\pi}{2}x_1^2}$ and $F(x_2) \to F(x_1)$ faster than $x_2 \to x_1$, (4.6) reduces in this case to

$$Y^n(\eta) = -|2\mu|^{\frac{1}{2}} F(x_1) + \sum_{\ell=3}^{4} \frac{1}{T_\ell} \left[x_\ell F(x_\ell) + \frac{je^{j\frac{\pi}{2}x_\ell^2}}{\pi}\right] \qquad (4.56)$$

Similarly, if $T_f \to 0$ and only the falling side of $y(\sigma)$ becomes rectangular, $x_3 \to x_4$ through $x_3=0 \to x_4=0$ and (4.6) reduces to

$$Y^n(\eta) = \sum_{\ell=1}^{2} \frac{1}{T_\ell} \left[x_\ell F(x_\ell) + \frac{je^{j\frac{\pi}{2}x_\ell^2}}{\pi}\right] + |2\mu|^{\frac{1}{2}} F(x_4) \qquad (4.57)$$

Finally, if T_r, $T_f \to 0$ and the trapezoidal LFM pulse of (4.1) reduces to the rectangular LFM pulse of (4.40), $x_2 \to x_1$ and $x_3 \to x_4$ and (4.6) reduces to (4.43).

The limiting approach whereby (4.6) $\to$ (4.43) may be used to justify the $F(x)$ expansions used for the spectrum of the rectangular LFM pulse and to establish that they are consistent with those used for the spectrum of the trapezoidal LFM pulse. This can be achieved by making

use of the fact that the exponential terms in (4.6) disappear through the limiting process.

The limiting approach whereby (4.6)→(4.43) may also be used to derive the relations obtained for the amplitude spectrum of the rectangular LFM pulse from those obtained for the amplitude spectrum of the trapezoidal LFM pulse.

A comparison of the appropriate relations and plots in the previous sections shows that the mean value (in the tail) as well as the oscillation amplitude and density of the amplitude spectrum of the rectangular LFM pulse exceed their trapezoidal counterparts for any given $|WT|$ and η. These discrepancies are related to edge effects and increase with $\frac{T_r}{T}$ and $\frac{T_f}{T}$. They may be explained by noting that as (4.6)→(4.43), the x_1 and x_2 phasors as well as the x_3 and x_4 phasors add arithmetically rather than vectorially. Also, these discrepancies indicate that the physical chirp pulse has actually less tail power and less pronounced ripples than what is usually assumed by treating it as an ideally rectangular LFM pulse.

4.10 The Spectrum of an Arbitrarily Shaped LFM Pulse

Consider the following arbitrarily weighted complex LFM pulse

$$y(\sigma) = a(\sigma)\ e^{j\pi\mu\sigma^2}, |\sigma| \leq \frac{T}{2} \tag{4.58}$$

The spectrum Y(f) of this pulse is given by

$$Y(f) = \int_{\sigma} a(\sigma) e^{j\pi(-2f\sigma+\mu\sigma^2)} d\sigma \tag{4.59a}$$

This relation may be compared with (3.27a). Its exact evaluation would require an explicit specification of $a(\sigma)$. However, this relation may be studied through the stationary phase method in the case where $a(\sigma)$ is a well behaved physical function whose rate of variation is small compared with that of the integrand's exponential function (i.e. $|\mu|$ is sufficiently large). In this case, (4.59a) reduces to

$$Y(f) \simeq a(\sigma_o) \int_{\sigma} e^{j\pi(-2f\sigma+\mu\sigma^2)} d\sigma \tag{4.59b}$$

where $\sigma_o \triangleq \frac{f}{\mu}$ is the integrand's stationary phase point.

Relation (4.59b) reduces through transformations (4.3) and (4.6b) for $\mu>0$ to

$$Y^n(\eta) \simeq |2\mu|^{\frac{1}{2}} a(\tfrac{\eta T}{2}) F(x_p, x_q) \tag{4.59c}$$

where η is given by (4.5e), x_p and x_q are given by (4.42) and $F(x_p, x_q)$ is given by (4.43b).

Since $a(\sigma)$ is assumed to vanish identically for

$|\sigma| > \frac{T}{2}$, (4.59c) predicts that $Y^n(\eta)$ also vanishes identically for $|\eta| > 1$. Thus, (4.59c) is only capable of handling $Y^n(\eta)$ in the central region $|\eta| \lesssim 1$. In fact, this result is characteristic of the stationary phase method on which (4.59c) is based.

In the case where $|WT| \to \infty$, $|F(x_p, x_q)|$ is given by (4.44) and (4.59c) predicts that $|Y(f)|$ assumes the functional form of $a(\sigma)$ in agreement with (3.7).

In the case where $|WT|$ is finite, (4.59c) may be studied through the relations obtained for $F(x_p, x_q)$ in Subsections 4.8.5 and 4.8.6.2. In this manner, (4.50) remains unchanged and (4.49) and (4.54) have to be multiplied by $|2\mu|^{\frac{1}{2}} a(\frac{\eta T}{2})$.

Relation (4.59) can readily be used for the approximate handling of the spectrum of any arbitrarily weighted LFM pulse in the central region where $|\eta| \lesssim 1$. Such arbitrarily weighted LFM pulses include, for example, the trapezoidal and the Hamming-weighted[46] pulses. The approximate handling of the tails of the spectra of such pulses will be considered in the next section.

4.11 The LFM and the Monotone Spectra

4.11.1 The LFM Spectrum in the Tail Region

The central part of the spectrum of an arbitrarily

shaped LFM signal was considered in the previous section. It remains to consider the tail of this spectrum. To this end, let $s(\sigma)$ be an arbitrary physical signal whose duration covers the range $\sigma_1 \leq \sigma \leq \sigma_2$. The spectrum $S(f)$ of this signal is given by

$$S(f) = \int_{\sigma_1}^{\sigma_2} s(\sigma) e^{-j2\pi f\sigma} d\sigma \tag{4.60a}$$

If $s(\sigma)$ is K times continuously differentiable, (4.60a) reduces through repeated integration by parts to[167]

$$\lim_{|f|\to\infty} S(f) \simeq \sum_{k=0}^{K} \frac{(-j)^{k-1}}{(2\pi f)^{k+1}} \left[e^{-j2\pi f\sigma} \frac{d^k s(\sigma)}{d\sigma^k} \right]_{\sigma_1}^{\sigma_2} \tag{4.60b}$$

which is an asymptotic approximation of $S(f)$ in the tail region.

Substituting the envelope $a(\sigma)$ of the arbitrarily shaped LFM pulse $y(\sigma)$ of (4.58) as well as $y(\sigma)$ itself for $s(\sigma)$ in (4.60b) putting $k = 0, 1$ gives

$$[A(f)]_{|f|>0} \simeq \frac{j}{2\pi f} \left[e^{-j2\pi f\sigma} a(\sigma) \right]_{-\frac{T}{2}}^{\frac{T}{2}} + \frac{1}{(2\pi f)^2} \left[e^{-j2\pi f\sigma} \frac{da(\sigma)}{d\sigma} \right]_{-\frac{T}{2}}^{\frac{T}{2}} \tag{4.61}$$

$$[Y(f)]_{|f|>\frac{|W|}{2}} \simeq \frac{je^{j\frac{\pi WT}{4}}}{2\pi f}\left[e^{-j2\pi f\sigma}a(\sigma)\left(1+\frac{\mu\sigma}{f}\right)\right]_{-\frac{T}{2}}^{\frac{T}{2}} + \frac{e^{j\frac{\pi WT}{4}}}{(2\pi f)^2}\left[e^{-j2\pi f\sigma}\ \frac{da(\sigma)}{d\sigma}\right]_{-\frac{T}{2}}^{\frac{T}{2}} \qquad (4.62)$$

where $A(f)$ is the spectrum of $a(\sigma)$.

Given $a(\sigma)$, (4.62) may be used to obtain an approximate expression for $Y(f)$ in the tail region where $|f|>\frac{|W|}{2}$. Such an approximate expression may also be obtained through (4.61). This alternative approach is based on the fact that except for the phase factor $e^{j\frac{\pi WT}{4}}$, (4.62) reduces to (4.61) for $|f|>>\frac{|W|}{2}$. Also, this alternative approach may be preferable in practice, especially for finding bounds on $|Y(f)|$ through $|A(f)|$ for $|f|>>\frac{|W|}{2}$. This is because expressions for, and bounds on, $A(f)$ are usually available for the envelopes $a(\sigma)$ in common use[6,24,168].

Relations (4.61) and (4.62) can be expressed in closed-form only if $a(\sigma)$ is specified or is even in σ. Consider, for example, the case where $a(\sigma)\rightarrow R_T(\sigma)$. An approximate expression for $Y(f)$ in this case in the tail region may be obtained through (4.62) as

$$[Y^{(1)}(f)]_{|f|>\frac{W}{2}} \simeq e^{j\frac{\pi WT}{4}}\left[T\,\mathrm{sinc}Tf + \frac{jW}{2\pi f^2}\cos\pi Tf\right] \qquad (4.63a)$$

which is essentially equivalent to the following form obtainable from (4.45)

$$[Y^{(2)}(f)]_{|f|>\frac{|W|}{2}} \simeq \frac{[Y^{(1)}(f)]_{|f|>\frac{|W|}{2}}}{1-(\frac{W}{2f})^2} \tag{4.63b}$$

Relations (4.63a) and (4.63b) give the following two corresponding approximations

$$|Y^{(1)}(f)|^2_{|f|>\frac{|W|}{2}} \simeq \frac{W^2}{(2\pi f^2)^2} + [1-(\frac{W}{2f})^2](\text{TsincTf})^2 \tag{4.64a}$$

$$|Y^{(2)}(f)|_{|f|>\frac{|W|}{2}} \simeq \frac{|Y^{(1)}(f)|_{|f|>\frac{|W|}{2}}}{1-(\frac{W}{2f})^2} \tag{4.64b}$$

Approximations (4.63b) and (4.64b) are preferable to (4.63a) and (4.64a) in the very near tail region where $\frac{|f|}{|W|/2}$ is not too large. Relation (4.63) predicts that except for the phase factor $e^{j\frac{\pi WT}{4}}$, Y(f) reduces to the spectrum TsincTf of $R_T(\sigma)$ for all $|f|>>\frac{|W|}{2}$. Relation (4.64a) predicts that $|Y(f)|$ exceeds $|\text{TsincTf}|$ except where this latter has its side-peaks (i.e. where $|\sin\pi Tf|=1$) in which case they are equal. Relation (4.64b) predicts that $|Y(f)|>|\text{TsincTf}|$. Both (4.64a) and

(4.64b) can be used to estimate the ratio between $|Y(f)|$ and $|TsincTf|$ for a given f. The difference between these two relations diminishes as $\frac{|f|}{|W|/2}$ increases and both indicate that $|Y(f)| \to |TsincTf|$ for $|f| >> \frac{|W|}{2}$. These predictions are in good agreement with reality as can be seen from Fig. 4.26. Both (4.63) and (4.64) may be used to obtain bounds on $|Y(f)|$ in the tail region which correspond to those of (4.46). For $|f| >> \frac{|W|}{2}$, such bounds reduce to those obtainable from (4.61), i.e. to

$$0 \leq |Y(f)| \leq \frac{1}{|\pi f|} \tag{4.65}$$

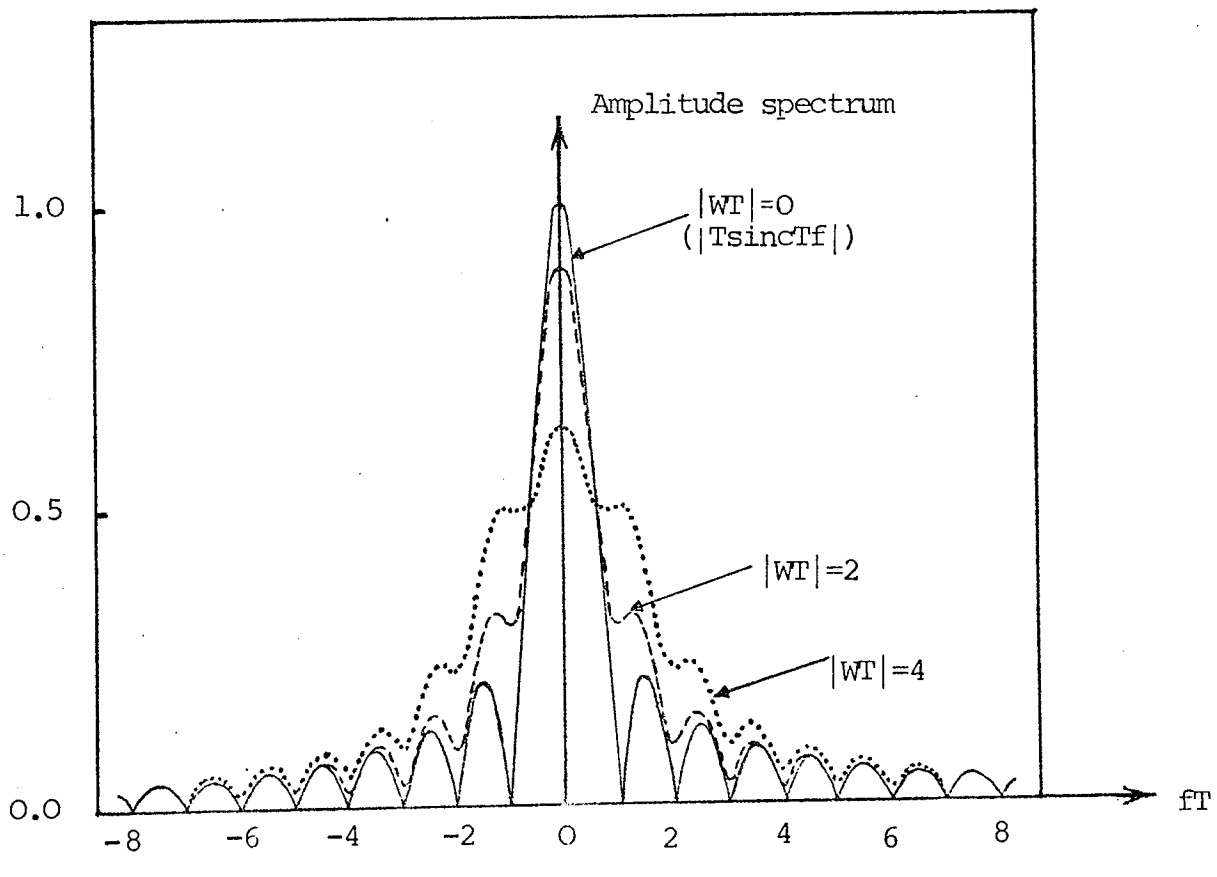

Fig. 4.26 Monotone and LFM Amplitude Spectra; T=1, $|WT| \to 0$.

4.11.2 The LFM Spectrum for $|WT|\to 0$

Consider the arbitrarily shaped LFM pulse $y(\sigma)$ of (4.58) whose envelope is $a(\sigma)$. It can be seen from (4.59a) that as $W\to 0$ (and, hence, $WT\to 0$), the spectrum $Y(f)$ of this pulse reduces to the spectrum $A(f)$ of $a(\sigma)$. Accordingly, one may expect that $Y(f)\simeq A(f)$ for small $|W|$. Two cases may be considered in this regard, namely, the cases where $|f|>\frac{|W|}{2}$ and $|f|<\frac{|W|}{2}$.

In the case where $|W|$ is small and $|f|>\frac{|W|}{2}$, $Y(f)$ may be approximated by (4.62) and the fact that $Y(f)\simeq A(f)$ may be seen by comparing (4.61) and (4.62). If $a(\sigma)\to R_T(\sigma)$, (4.62)$\to$(4.63) and $Y(f)\simeq A(f)=T\,\mathrm{sinc}\,Tf$.

The case where $|W|$ is small and $|f|<\frac{|W|}{2}$ may be considered through $F(x_p,x_q)$ of (4.43b). As $|W|$ decreases, the central region of $F(x_p,x_q)$ described in Subsection 4.8.5 diminishes gradually and the inside vicinities of the two edges $\eta=\pm 1$ eventually dominate the range $|\eta|\leq 1$ and may overlap. Approximate $F(x_p,x_q)$ expressions for small $|W|\neq 0$ and $|f|<\frac{|W|}{2}$ may be obtained by making use of the methods of Subsections 4.8.5 and 4.8.6. Alternatively, one may obtain an $F(x_p,x_q)$ approximation in this respect by using expansion (4.7) for both $F(x_p)$ and $F(x_q)$ in (4.43b). This approximation can then be used in (4.43a) and (4.59c) to obtain corresponding

approximations for the spectra of the rectangular and shaped LFM pulses of (4.40) and (4.58) respectively. The approximation of the rectangular pulse spectrum is given by

$$[Y(f)]_{|f|<\frac{|W|}{2}\neq 0} \simeq \frac{e^{j(\frac{\pi}{4}-\frac{\pi f^2}{\mu})}}{|\mu|^{\frac{1}{2}}} - \frac{e^{j\frac{\pi WT}{4}}}{1-(\frac{2f}{W})^2}\cdot$$

$$[(\frac{2f}{W})^2\cdot T\,\mathrm{sinc}Tf + \frac{j2}{\pi W}\cos\pi Tf] \qquad (4.66a)$$

where the second, subtracted quantity is identical to the right hand side of (4.63b).

It has been found numerically that approximation (4.66a) gives fairly accurate results for $1.5\lesssim|WT|\lesssim 25$ and that its accuracy increases with $|WT|$. For $|WT|\gtrsim 25$, it is preferable to apply the approximations of Subsections 4.8.5. and 4.8.6.2. For $0<|WT|\lesssim 1.5$, one may apply the following approximation obtained by using expansion (4.27) for both $F(x_p)$ and $F(x_q)$ in (4.43b)

$$[Y(f)]_{|f|<\frac{|W|}{2}\neq 0} \simeq T\,e^{-j\pi f^2/\mu} \qquad (4.66b)$$

Approximation (4.66) indicates that for a given T, increasing $|W|$ makes the central f-region of $|Y(f)|$ wider

and the peak amplitude of $|Y(f)|$ lower than those of $|TsincTf|$. However, the central part of $|Y(f)|$ assumes essentially the same form as $|TsincTf|$ only for $|WT| < 7$ (see Fig. 4.26). At $|WT| \simeq 7$, the single main peak at f=0 degenerates into a minimum at f=0 flanked by two maxima at $f \simeq \pm 0.345 \frac{W}{2}$. Any further increase in $|W|$ makes the central part of $|Y(f)|$ still wider until this part starts to fluctuate about a nearly constant mean level $\simeq |\mu|^{-\frac{1}{2}}$ assuming a characteristic LFM form. The ripples may be obtained through (4.50) which remains consistent with (4.66).

The approximation of the shaped LFM pulse spectrum for small $|W| \neq 0$ and $|f| < \frac{|W|}{2}$ may be obtained by multiplying approximation (4.66) by $a(\frac{f}{\mu})$. If $W \to 0$, both approximations become irrelevant because the f-range over which they hold vanishes identically. In this case, (4.63) and (4.62) become, respectively, the sole approximations of the spectra of the rectangular and shaped LFM pulses over the entire f-axis. Moreover, (4.63)$\to$TsincTf and (4.62)$\to$(4.61). This implies that as $W \to 0$, the spectrum $Y(f)$ of the LFM pulse $\to$ the spectrum $A(f)$ of the corresponding monotone $a(\sigma)$ and, hence, $y(\sigma) \to a(\sigma)$ as expected.

The preceding discussion indicates that LFM modulating

a given monotone $a(\sigma)$ distorts its spectrum $A(f)$ over the entire f-axis. The distortion increases with the LFM sweep $|W|$, decreases with $|f|$ and becomes essentially phase distortion for $|f| >> \frac{|W|}{2}$. In fact, increasing $|W|$ widens the central part of the amplitude spectrum (i.e. increases the effective bandwidth) and reduces its main peak in such a way that this part eventually starts to fluctuate about a mean level $\simeq \frac{a(\frac{f}{\mu})}{|\mu|^{\frac{1}{2}}}$ assuming a distinctive LFM form. Also, increasing $|W|$ increases the mean level of the amplitude spectrum in the near tail and leaves this level essentially unchanged in the far tail for $|f| >> \frac{|W|}{2}$.

4.11.3 Correlation of Two LFM Signals with a Relatively Small μ-Mismatch

The correlation of two complex μ-mismatched LFM signals has already been considered in Section 3.4. There, however, the discussion was mainly concerned with signal design. Accordingly, this discussion was mostly confined to the case where condition (3.26) holds, i.e. where the μ-mismatch is large enough to make it justifiable to treat the two correlated signals as being distinct and practically separable. The case where the μ-mismatch does not satisfy (3.26) may arise if this mismatch

is not sufficiently large to make the two correlated signals practically separable. This case may also arise if the two correlated signals are supposed to be identical but they become slightly μ-mismatched due to system imperfections and channel disturbances. In this case where the μ-mismatch $\mu_i-\mu_k\to 0$, the expression for $\chi_{ik}^{n}(t,\nu)$ of (3.22) would approach that obtained in Subsection 3.2.3 for the $\mu_i=\mu_k$ case. A closed-form approximation of this expression can generally be obtained. This may be achieved by obtaining approximate closed-form expressions for the integral in (3.21a) by applying the same approach used above to obtain similar expressions for Y(f) of (4.41a), noting that the integrals in both (3.21a) and (4.41a) have the same Fourier form.

Consider, for example, the correlation coefficient $\chi_{ik}^{n}(0,\nu)$. Intuitively, the approximate closed-form expression of this coefficient in the case where $\mu_i-\mu_k\to 0$ would approach a sinc(.) form in ν (e.g. the form corresponding to $T_i<T_k$ given by (3.15b) with t=0). This expression may be obtained by the procedure outlined at the end of the previous paragraph. Alternatively, this expression may be obtained through (3.22). To this end, the integral in (3.22) is first expressed in terms of the Fresnel functions $F(x_1,x_3)$ if $T_i<T_k$, $F(x_4,x_2)$ if $T_i>T_k$ and $F(x_1,x_2)$ or $F(x_4,x_3)$ if $T_i=T_k$, where x_1 through x_4 are

the integration limits which may be obtained by putting t=0 in (3.23). Approximate closed-form expressions for these Fresnel functions can then be derived by applying the transformations $\mu \to \mu_i - \mu_k$, $|\frac{WT}{2}|^{\frac{1}{2}} \to \frac{gT_i}{2}$, $\frac{gT_k}{2}$ and $\eta \to -\frac{2\nu}{T_i(\mu_i-\mu_k)}$, $-\frac{2\nu}{T_k(\mu_i-\mu_k)}$ to the following $F(x_p,x_q)$ expression corresponding to (4.63) and (4.66) in the appropriate manner

$$[F(x_p,x_q)]_{|\eta|\gtrless 1} = |2\mu|^{\frac{1}{2}} e^{j\frac{\pi WT}{4}\eta^2} [Y(f)]_{|f|\gtrless\frac{|W|}{2}} \qquad (4.67)$$

where $\eta \overset{<}{>} \frac{2f}{W}$.

5

FINAL DISCUSSION

This work has examined the utility of pulse compression techniques for digital data transmission. The general capabilities as well as the problems characterizing these techniques have been highlighted in Chapter 2. However, the main contributions of this work are related to the LFM pulse compression technique. These contributions are of a rather basic nature and cover the two main areas concerning the utility of the class of LFM signals for digital data transmission and the LFM spectrum.

The utility of the class of LFM signals for digital data transmission has been considered in Chapter 3. The capabilities of this class have been outlined and compared with those of other pulse compression signal classes. The correlation properties of this class have been formulated. The usefulness of these properties for handling LFM weighting and mismatching has only been indicated. Nevertheless, these properties have been exploited for establishing a systematic basis for LFM parameter selection and signal design. For mathematical convenience, the class of LFM signals has been divided into two subclasses depending on whether these signals have equal or different slopes. It has been shown that the LFM technique provides a relatively large number of degrees of parameter selection freedom. Making use of the results obtained, a variety of signal sets comprising LFM signals with equal and/or unequal

slopes and having different correlation properties have been, and may be, constructed for both coherent and noncoherent unilink and multiplex digital signalling. Experimental work concerning the performance of this variety of sets in the different transmission environments and in the presence of the unavoidable distortions and system instabilities and imperfections would be of practical interest. A project concerning the utilization of the LFM t-ν coupling property for FSK detection (see Subsection 3.1.2(iv)b) has been proposed to, and is being carried out,by a Ph.D. research student.

The LFM spectrum has been studied in Chapter 4. The bulk of this chapter is new material which has been developed through predominantly tedious and complicated mathematical and numerical analyses whose details have not been given so that the discussion remains reasonably brief and clear. The criteria obtained for predicting the spectrum behaviour would facilitate the handling of the LFM technique in theory and practice. The validity of these criteria has been confirmed through digital computer simulations.

The results have been obtained assuming analogue signal generation and processing. However, these results may be extended to the digital case, where they are expected

to remain valid for sufficiently high sampling rates. The dependence of this validity on the sampling rate would have to be investigated.

Finally, it is hoped that the present work would enhance the utilization of the LFM technique in the field of digital data transmission as well as in an ever increasing number of other fields.

APPENDICES

APPENDIX A

COMPLEX REPRESENTATION OF DETERMINISTIC REAL SIGNALS[46,52,72,73]

This appendix outlines the basic theory of complex representation of deterministic real signals and considers the application of this theory to the class of Linear FM (LFM) signals.

A.1 Introduction

Consider the following deterministic real signal

$$r_\ell(\sigma) = a_\ell(\sigma)\ \cos\theta_\ell(\sigma) \tag{A.1a}$$

where σ indicates time, ℓ may be any positive integer and the phase function $\theta_\ell(\sigma)$ is given by

$$\theta_\ell(\sigma) \triangleq \alpha_\ell + 2\pi f_\ell \sigma + \xi_\ell(\sigma) \tag{A.1b}$$

in which α_ℓ is the initial phase and f_ℓ is the mean frequency of $r_\ell(\sigma)$.

It is mathematically more convenient to handle $r_\ell(\sigma)$ through its complex representation. This representation may be 'analytic' or 'exponential'.

A.2 Analytic Complex Representation

Consider a signal $s_\ell^a(\sigma)$ with a single-sided spectrum $S_\ell^a(f)$ given by

$$S_\ell^a(f) \triangleq \begin{cases} 2R_\ell(f), & f \geq 0 \\ 0, & f < 0 \end{cases} \tag{A.2}$$

where $R_\ell(f)$ is the spectrum of $r_\ell(\sigma)$.

Relation (A.2) may also be expressed as

$$S_\ell^a(f) = R_\ell(f) + j\hat{R}_\ell(f) \tag{A.3a}$$

where

$$\hat{R}_\ell(f) \triangleq e^{-j\frac{\pi}{2}}.\text{sgnf}.R_\ell(f) \tag{A.3b}$$

in which sgnf indicates the 'sign' or 'signum' function which may be defined as

$$\text{sgnf} \triangleq \begin{cases} 1, & f \geq 0 \\ -1, & f < 0 \end{cases} \tag{A.3c}$$

If $\hat{R}_\ell(f)$ is the spectrum of $\hat{r}_\ell(\sigma)$, say, it can be seen from (A.3b) that $r_\ell(\sigma)$ and $\hat{r}_\ell(\sigma)$ are orthogonal and form a Hilbert transform pair[72], i.e.

$$\hat{r}_\ell(\sigma) = \frac{1}{\pi} P \int_{-\infty}^{+\infty} \frac{r_\ell(\tau)}{\sigma-\tau} d\tau \qquad (A.4a)$$

$$r_\ell(\tau) = \frac{1}{\pi} P \int_{-\infty}^{+\infty} \frac{\hat{r}_\ell(\sigma)}{\sigma-\tau} d\sigma \qquad (A.4b)$$

where P indicates the Cauchy principal value implying that in (A.4a), for example,

$$P\int_{-\infty}^{+\infty} = \lim_{\varepsilon \to 0} \left(\int_{-\infty}^{\sigma-\varepsilon} + \int_{\sigma+\varepsilon}^{\infty} \right), \qquad \varepsilon > 0 \qquad (A.4c)$$

Relation (A.4a) indicates that $\hat{r}_\ell(\sigma)$ is real. Relation (A.3a) implies that

$$s_\ell^a(\sigma) = r_\ell(\sigma) + j\, \hat{r}_\ell(\sigma) \qquad (A.5)$$

which indicates that $s_\ell^a(\sigma)$ is a complex signal whose real part is $r_\ell(\sigma)$ and whose imaginary part is the Hilbert transform $\hat{r}_\ell(\sigma)$ of $r_\ell(\sigma)$.

Relation (A.2) and the fact that $R_\ell(-f) = R_\ell^*(f)$ imply that $S_\ell^a(f)$ defines $R_\ell(f)$ over the entire f-axis. That is, $s_\ell^a(\sigma)$ may be taken as a complex representation of $r_\ell(\sigma)$. In fact, $s_\ell^a(\sigma)$ is usually known as the analytic complex representation of $r_\ell(\sigma)$. The word 'analytic' has its origin in the theory of functions of complex variables[2,73].

Assuming that $r_\ell(\sigma)$ is a bandpass signal, $s^a_\ell(\sigma)$ will also be a bandpass signal. In this case, the lowpass version of $s^a_\ell(\sigma)$ is $s^a_\ell(\sigma)e^{-j2\pi f_\ell \sigma}$ which has a spectrum $S^a_\ell(f+f_\ell)$ and is usually described as the "complex envelope" for $r_\ell(\sigma)$. In this context, $s^a_\ell(\sigma)$ is sometimes called the "pre-envelope" for $r_\ell(\sigma)$[73]. If $u_\ell(\sigma)$ and $v_\ell(\sigma)$ are two real lowpass signals which represent the real and imaginary parts of the complex envelope for $r_\ell(\sigma)$ respectively, one has

$$r_\ell(\sigma) = u_\ell(\sigma)\cos 2\pi f_\ell \sigma - v_\ell(\sigma)\sin 2\pi f_\ell \sigma \tag{A.6}$$

which implies that $u_\ell(\sigma)$ and $v_\ell(\sigma)$ are also the "in-phase" and "quadrature" components of $r_\ell(\sigma)$ respectively.

A.3 Exponential Complex Representation

Making use of the identity $\cos\theta_\ell(\sigma) = \frac{e^{j\theta_\ell(\sigma)} + e^{-j\theta_\ell(\sigma)}}{2}$ in (A.1), $r_\ell(\sigma)$ may also be expressed as

$$r_\ell(\sigma) = r_{\ell+}(\sigma) + r_{\ell-}(\sigma) \tag{A.7a}$$

where

$$r_{\ell+}(\sigma) = \frac{1}{2}a_\ell(\sigma)e^{j\theta_\ell(\sigma)} \tag{A.7b}$$

$$r_{\ell-}(\sigma) = r^*_{\ell+}(\sigma) \tag{A.7c}$$

Relation (A.7) implies that

$$R_\ell(f) = R_{\ell+}(f) + R_{\ell-}(f) \tag{A.8}$$

where $R_{\ell+}(f)$ is the spectrum of $r_{\ell+}(\sigma)$ concentrated at f_ℓ, $R_{\ell-}(\sigma)$ is the spectrum of $r_{\ell-}(\sigma)$ concentrated at $-f_\ell$ and $R_{\ell-}(f) = R^*_{\ell+}(-f)$.

Relation (A.7) also implies that $r_\ell(\sigma)$ can be represented by the complex signal $s^e_\ell(\sigma) \triangleq 2r_{\ell+}(\sigma)$. In fact, $s^e_\ell(\sigma)$ is usually known as the exponential complex representation of $r_\ell(\sigma)$ and may also be expressed as

$$s^e_\ell(\sigma) = r_\ell(\sigma) + jr'_\ell(\sigma) \tag{A.9a}$$

where

$$r'_\ell(\sigma) \triangleq a_\ell(\sigma)\sin\theta_\ell(\sigma) \tag{A.9b}$$

The spectrum $S^e_\ell(f)$ generally extends over the entire f-axis and may be expressed as

$$S^e_\ell(f) = 2R_{\ell+}(f) \tag{A.10}$$

A.4 Comparison of the Analytic and Exponential Complex Representations

The fact that $S^a_\ell(f) = 0$ for $f<0$ simplifies the handling

of the analytic representation. However, this representation is generally difficult to obtain because it entails the derivation of the Hilbert transform $\hat{r}_\ell(\sigma)$ of $r_\ell(\sigma)$ which cannot usually be expressed in a closed-form.

The exponential representation can readily be derived. However, the handling of this representation is usually difficult because $S^e_\ell(f)$ generally extends over the entire f-axis.

Comparing (A.5) and (A.9a) shows that the analytic and exponential representations can be identical only if $r'_\ell(\sigma) = \hat{f}_\ell(\sigma)$, i.e. if

$$a_\ell(\sigma)\sin\theta_\ell(\sigma) = H[a_\ell(\sigma)\cos\theta_\ell(\sigma)] \qquad (A.11)$$

where $H[.]$ indicates the Hilbert transform of $[.]$.

Expanding $\sin\theta_\ell(\sigma)$ and $\cos\theta_\ell(\sigma)$ through (A.1b), noting that $H[\cos 2\pi f_\ell\sigma] = \sin 2\pi f_\ell\sigma$ and $H[\sin 2\pi f_\ell\sigma] = -\cos 2\pi f_\ell\sigma$ and making use of the linearity property of the Hilbert transform along with a special case of a theorem* due to Bedrosian[169], it can be shown that (A.11) may be valid only if both $a_\ell(\sigma)\sin[\alpha_\ell+\xi_\ell(\sigma)]$ and $a_\ell(\sigma)\cos[\alpha_\ell+\xi_\ell(\sigma)]$ are strictly limited to the frequency band below f_ℓ. This implies that the analytic and exponential representations may be identical

*This special case may be stated as follows: Given two real time functions $f_1(\sigma)$ and $f_2(\sigma)$ with nonoverlapping spectra and with the frequency band of $f_1(\sigma)$ below that of $f_2(\sigma)$, then $H[f_1(\sigma).f_2(\sigma)] = f_1(\sigma).H[f_2(\sigma)]$.

only if $R_{\ell+}(f) = 0$ for $f<0$ and $R_{\ell-}(f) = 0$ for $f>0$. In this case, $r_\ell(\sigma)$ is a bandpass signal whose frequency spread is confined to the range $(-2f_\ell, 2f_\ell)$, i.e. whose bandwidth $\lesssim 2f_\ell$. Such a signal will be referred to as a "narrowband" signal.

The preceding discussion implies that $s_\ell^a(\sigma)$ and $s_\ell^e(\sigma)$ will be different if, for example, $r_\ell(\sigma)$ is a duration-limited RF pulse with an effectively narrow, but theoretically infinite, bandwidth or if $r_\ell(\sigma)$ is a bandpass signal whose bandwidth is effectively wide and whose $R_{\ell\pm}(f)$ has a spillover in the $(\mp)$ frequency region. In this case, one has

$$s_\ell^e(\sigma) - s_\ell^a(\sigma) = j4\,\mathrm{Im} \int_{-\infty}^{0} R_{\ell+}(f) e^{j2\pi f\sigma} df \qquad (A.12)$$

where "Im" indicates the "Imaginary part of".

Relation (A.12) has been obtained by noting that $S_\ell^a(f) = 2\left[R_{\ell+}(f) + R_{\ell+}^*(-f)\right]$ with $f\gtrless 0$, subtracting $S_\ell^a(f)$ from $S_\ell^e(f)$ of (A.10) to get $S_\ell^e(f) - S_\ell^a(f) = j4\ \mathrm{Im}\ R_{\ell+}(f)$ with $f<0$ and Fourier transforming $S_\ell^e(f) - S_\ell^a(f)$. Relation (A.12) indicates that the difference $s_\ell^e(\sigma) - s_\ell^a(\sigma)$ is a function of the spillover of $R_{\ell+}(f)$ in the negative frequency region. The case where $r_\ell(\sigma)$ is a "narrowband" signal has been considered above. In this case, the spillover$\to 0$ and $s_\ell^e(\sigma) \to s_\ell^a(\sigma)$. The case where $r_\ell(\sigma)$ is a

duration-limited RF pulse with an effectively narrow, but theoretically infinite, bandwidth was considered by Rubin and DiFranco[170]. These authors show that $s_\ell^e(\sigma) \simeq s_\ell^a(\sigma)$ in this case. No general results are available for other cases. However, it is obvious in such cases that the difference $s_\ell^e(\sigma) - s_\ell^a(\sigma)$ depends on the explicit form of $r_\ell(\sigma)$ and may be found by numerical methods.

Consider the special case where $r_\ell(\sigma)$ is a Linear FM (LFM) signal. In this case, bounds on $s_\ell^e(\sigma) - s_\ell^a(\sigma)$ may be established through the results obtained for Y(f) in Chapter 4 (noting that Y(f) corresponds to $2R_{\ell+}(f+f_\ell)$ in this appendix). Now let $\xi_\ell(\sigma) = \pi\mu_\ell\sigma^2$ in (A.1b) in such a way that $r_\ell(\sigma)$ is a bandpass real LFM signal of duration T_ℓ and sweep W_ℓ. According to (3.7), $R_{\ell+}(f)$ for this signal will be effectively confined to the range $(f_\ell - \frac{|W_\ell|}{2}, f_\ell + \frac{|W_\ell|}{2})$ for sufficiently large $|W_\ell T_\ell|$ (e.g. ≥ 25). That is, this signal will be narrowband with $s_\ell^e(\sigma) \to s_\ell^a(\sigma)$ as long as $|W_\ell T_\ell|$ is sufficiently large and $f_\ell \geq \frac{|W_\ell|}{2}$. The LFM signal is unique in this respect.

A.5 Applications

Complex representation of real signals may be used to facilitate their mathematical handling in a variety of applications, e.g. concerning their generation and

processing as well as the formulation of their properties[2,46,72,171]. It suffices for the purposes of the present work, however, to consider only the formulation of the spectra, correlation and energy for these signals.

Consider the real signal $r_\ell(\sigma)$ of (A.1). The spectrum $R_\ell(f)$ of this signal may be obtained through $R_{\ell\pm}(f)$ by making use of (A.8). In the special case where $r_\ell(\sigma)$ is a narrowband signal (e.g. a LFM signal with sufficiently large $|W_\ell T_\ell|$ and $f_\ell \geq \frac{|W_\ell|}{2}$), $R_{\ell\mp}(f)$ has no spillover in the $(\pm)$ frequency region and coincides with $R_\ell(f)$ in the $(\mp)$ frequency region.

The correlation of two real signals such as $r_i(\sigma)$ and $r_k(\sigma)$ will be obtained through their analytic complex representations $s_i^a(\sigma)$ and $s_k^a(\sigma)$. The replacement of these analytic representations by the corresponding exponential representations in the result can be accurate only if both $r_i(\sigma)$ and $r_k(\sigma)$ are narrowband signals.

Making use of Parseval's relation* along with the fact that both $S_i^a(f)$ and $S_k^a(f)$ are single-sided, it can be shown that

---

*Parseval's relation may be expressed as $\int x(\sigma)y^*(\sigma)d\sigma = \int X(f)Y^*(f)df$, where $X(f)$ and $Y(f)$ are the spectra of $x(\sigma)$ and $y(\sigma)$ respectively. This relation is often used for establishing time-frequency duality properties.

$$\int_\sigma s_i^a(\sigma) s_k^a(\sigma-t)\,d\sigma = 0 \qquad \text{(A.13)}$$

Noting that $r_\ell(\sigma) = \frac{s_\ell^a(\sigma)+s_\ell^{a*}(\sigma)}{2}$, $\ell=i,k$, and making use of (A.13), one obtains the following relation which underlies relation (1.12)

$$\int_\sigma r_i(\sigma) r_k(\sigma-t)\,d\sigma = \frac{1}{2}\mathrm{Re}\int_\sigma s_i^a(\sigma) s_k^{a*}(\sigma-t)\,d\sigma \qquad \text{(A.14)}$$

where "Re" indicates the "real part of".

Taking $i=k=\ell$ and $t=0$, (A.14) reduces to

$$\int_\sigma r_\ell^2(\sigma)\,d\sigma = \frac{1}{2}\int_\sigma |s_\ell^a(\sigma)|^2 d\sigma \qquad \text{(A.15a)}$$

This relation indicates that the energy E_ℓ of $r_\ell(\sigma)$ is given by $\frac{\text{energy of } s_\ell^a(\sigma)}{2}$. Noting that $|s_\ell^a(\sigma)| = a_\ell(\sigma)$, (A.15a) reduces to

$$E_\ell = \frac{1}{2}\int_\sigma a_\ell^2(\sigma)\,d\sigma \qquad \text{(A.15b)}$$

This is the familiar expression for the energy of a narrowband real signal (which may also be obtained by substituting for $r_\ell(\sigma)$ from (A.1) in the relation $E_\ell \triangleq \int_\sigma r_\ell^2(\sigma)\,d\sigma$). It indicates that the energy of such a signal is determined only be its time-envelope and is independent of its phase function.

APPENDIX B

THE STATIONARY PHASE METHOD

This appendix introduces the stationary phase method in a way that comports with the utilization of this method in the present work.

B.1 Introduction

A complex signal $s(\sigma) \triangleq |s(\sigma)|e^{j\theta(\sigma)}, \sigma\varepsilon(\sigma_1,\sigma_2)$ and its spectrum $S(f) \triangleq |S(f)|e^{j\phi(f)}, f\varepsilon(f_1,f_2)$ are related by the Fourier integral transform pair

$$S(f) = \int_{\sigma_1}^{\sigma_2} |s(\sigma)| e^{j[\theta(\sigma)-2\pi f\sigma]} d\sigma \qquad \text{(B.1a)}$$

$$s(\sigma) = \int_{f_1}^{f_2} |S(f)| e^{j[\phi(f)+2\pi f\sigma]}\, df \qquad \text{(B.1b)}$$

where σ and f indicate time and frequency respectively.

An exact closed-form description of the $s(\sigma) \rightleftarrows S(f)$ relationship through (B.1) is generally difficult. This explains why use is frequently made of approximate methods for the evaluation of the Fourier integrals in (B.1)[6,13,24,167,168]. One such method is the so-called stationary phase method.

The stationary phase method was first suggested by Lord Kelvin[172]. Since then, it has been applied to a variety of mathematical and physical problems[46,70,167,172-174]. The present appendix considers its application to the two Fourier integrals in (B.1) on the assumption that $s(\sigma)$ is an FM signal. The results obtained can readily be extended to any generalizations of these integrals (e.g. the correlation integral in (1.1a) with t as a parameter and both $s_i(\sigma)$ and $s_k(\sigma)$ being FM signals).

B.2 The Direct Fourier Integral

Consider the Fourier integral in (B.1a) and let:

(i) $|s(\sigma)|$ be continuous and slowly varying compared to the integrand's phase function $\theta(\sigma)-2\pi f\sigma \triangleq \psi(\sigma,f)$ except perhaps at σ_1 and σ_2, (ii) $\psi(\sigma,f)$ be at least twice continuously differentiable in σ, and (iii) $\psi(\sigma,f)$ have a single stationary phase point $\sigma_o \varepsilon (\sigma_1,\sigma_2)$ of the first integral order[167] at which $\frac{d\psi(\sigma,f)}{d\sigma}=0$ and $\frac{d^2\psi(\sigma,f)}{d\sigma^2}\neq 0$, i.e.

$$\frac{d\theta(\sigma_o)}{d\sigma_o} = 2\pi f \tag{B.2a}$$

$$\frac{d^2\theta(\sigma_o)}{d\sigma_o^2} \neq 0 \tag{B.2b}$$

Kelvin's conjecture is that the main contribution to the value of the integral in (B.1a) comes from the vicinity of the stationary phase point σ_o and, to a lesser extent, from the vicinities of the two end-points σ_1 and σ_2.

Compared to the contribution from the vicinity of σ_o, the contribution from the vicinities of σ_1 and σ_2 is generally small and may be treated as an error term. Accordingly, the present discussion is only concerned with the main contribution from the vicinity of σ_o (i.e. with the stationary phase method as an optimization method for Fourier integrals).

Let the vicinity of σ_o be $(\sigma_o-\delta,\sigma_o+\delta)$, where δ is small and positive. Expand the integrand's phase function $\theta(\sigma)-2\pi f\sigma$ into a Taylor's series in this vicinity. Noting that the second term in this series $\to 0$ according to (B.2) and that the fourth and higher terms $\to 0$ (if $\theta(\sigma)$ is quadratic) or may be neglected (since a non-quadratic $\theta(\sigma)$ behaves approximately as a quadratic function in the vicinity of σ_o), (B.1a) reduces to

$$S(f) \simeq \int_{\sigma_o-\delta}^{\sigma_o+\delta} |s(\sigma)| e^{j\left[\theta(\sigma_o)-2\pi f\sigma_o+\frac{(\sigma-\sigma_o)^2}{2}\cdot\frac{d^2\theta(\sigma_o)}{d\sigma_o^2}\right]} d\sigma \qquad (B.3)$$

where the right hand side has to be multiplied by $\frac{1}{2}$ if σ_o coincides with σ_1 or σ_2.

Since $|s(\sigma)| \simeq |s(\sigma_o)|$ in the vicinity of σ_o, (B.3) reduces to

$$S(f) \simeq |s(\sigma_o)| \int_{\sigma_o-\delta}^{\sigma_o+\delta} e^{j\left[\theta(\sigma_o)-2\pi f\sigma_o+\frac{(\sigma-\sigma_o)^2}{2}\cdot\frac{d^2\theta(\sigma_o)}{d_o\sigma^2}\right]} d\sigma \qquad (B.4)$$

Since σ_o is the integrand's only stationary phase point in (σ_1,σ_2), the lower and upper integration limits in (B.4) may be replaced by σ_1 and σ_2 respectively and

$$S(f) \simeq \frac{|s(\sigma_o)|}{\left|\frac{1}{\pi}\frac{d^2\theta(\sigma_o)}{d\sigma_o^2}\right|^{\frac{1}{2}}} e^{j\left[\theta(\sigma_o)-2\pi f\sigma_o\right]} \int_{x_1}^{x_2} e^{\pm j\frac{\pi}{2}x^2} dx \qquad (B.5a)$$

where $j\frac{\pi}{2}x^2$ and $-j\frac{\pi}{2}x^2$ correspond to $\frac{d^2\theta(\sigma_o)}{d\sigma_o^2}>0$ and $\frac{d^2\theta(\sigma_o)}{d\sigma_o^2}<0$ respectively and

$$x \triangleq (\sigma-\sigma_o)\left|\frac{1}{\pi}\frac{d^2\theta(\sigma_o)}{d\sigma_o^2}\right|^{\frac{1}{2}} \qquad (B.5b)$$

which implies that $x_1 \leq 0$ and $x_2 \geq 0$.

Relation (B.5a) implies that according to the stationary phase method, S(f) differs from 0 only for those f-values which correspond through (B.2a) to σ_o. The

present discussion is only concerned with the case where there is a single such f-value f_o, say. That is, this discussion is only concerned with the following form of (B.2a)

$$f_o = \frac{1}{2\pi} \frac{d\theta(\sigma_o)}{d\sigma_o} \tag{B.6a}$$

which, on replacing f_o and σ_o by the current variables f and σ, reduces to

$$f = \frac{1}{2\pi} \frac{d\theta(\sigma)}{d\sigma} \tag{B.6b}$$

where it is to be understood that σ is a stationary phase point and that σ and f are related by a 1-1 correspondence (i.e. they are monotonic functions of each other).

The preceding discussion indicates that according to the stationary phase principle, the signal energy is simultaneously concentrated at the instant σ in the time-domain and at the frequency f in the frequency-domain, where σ and f are related by (B.6b). This implies that assuming a limited signal spread in one domain, the stationary phase method can only give the effective signal spread in the dual domain.

The instantaneous frequency $f_{inst}(\sigma)$ of $s(\sigma)$ is given

by

$$f_{inst}(\sigma) = \frac{1}{2\pi} \frac{d\theta(\sigma)}{d\sigma} \tag{B.7}$$

This relation checks with (B.6b) implying that:
(i) $f_{inst}(\sigma)$ is the frequency at which the signal energy is concentrated in the frequency-domain when this energy is concentrated at instant σ in the time-domain, and
(ii) the effective signal bandwidth is confined to the range of frequency values which $f_{inst}(\sigma)$ assumes over the signal duration.

Replacing σ_o by σ in (B.5a) gives

$$|S(f)| \simeq \frac{|s(\sigma)|}{\left|\frac{1}{\pi} \frac{d^2\theta(\sigma)}{d\sigma^2}\right|^{\frac{1}{2}}} \; |F(x_1,x_2)| \tag{B.8a}$$

$$\phi(f) \simeq \theta(\sigma) - 2\pi f\sigma \pm \arg F(x_1,x_2) \tag{B.8b}$$

where $F(x_1,x_2)$ is a Fresnel function introduced in Section 3.4, the signs + and - in (B.8b) correspond to $\frac{d^2\theta(\sigma)}{d\sigma^2} > 0$ and $\frac{d^2\theta(\sigma)}{d\sigma^2} < 0$ respectively and σ has to be expressed in terms of f through (B.6b).

Relation (B.8) is an approximation of (B.1a). It is generally difficult to handle because it involves the

Fresnel integral which cannot usually be expressed in a closed-form. Nevertheless, this relation may reduce to a simple form. Consider, for example, the case where both $|\frac{d^2\theta(\sigma)}{d\sigma^2}|$ and (σ_1,σ_2) are large. In this case, $s(\sigma)$ has a large duration-bandwidth product (see Subsection 2.1.1), $F(x_1,x_2)\rightarrow\sqrt{2}\,e^{j\frac{\pi}{4}}$ and (B.8) reduces to

$$|S(f)| \simeq \frac{|s(\sigma)|}{|\frac{1}{2\pi}\frac{d^2\theta(\sigma)}{d\sigma^2}|^{\frac{1}{2}}} \tag{B.9a}$$

$$\phi(f) \simeq \theta(\sigma)-2\pi f\sigma \pm\frac{\pi}{4} \tag{B.9b}$$

which reduces to (3.7) in the case where $s(\sigma)\rightarrow$ the Linear FM (LFM) signal of (3.5) (by substituting for σ from (3.3a)).

Relation (B.9) may be used for synthesizing a large duration-bandwidth product FM signal from a given autocorrelation function[70,174]. To this end, one finds $|S(f)|$ for the required signal by making use of the synthesis procedure explained in Subsection 2.4.6. The required signal may then be obtained by substituting $|S(f)|$ in (B.9a) either to find $|s(\sigma)|$ if $\theta(\sigma)$ is specified or to find $\theta(\sigma)$ if $|s(\sigma)|$ is specified.

B.3 The Inverse Fourier Integral

So far, the stationary phase method has been applied to the Fourier relation (B.1a). In a similar manner, this method may also be applied to the inverse Fourier relation (B.1b). In fact, the previous discussion concerning (B.1a) remains essentially valid for (B.1b) except that $\sigma, f, \sigma_o, \sigma_1, \sigma_2, -j2\pi\sigma f, \theta(\sigma), s(\sigma)$ and $S(f) \rightarrow f, \sigma, f_o, f_1, f_2, j2\pi\sigma f, \phi(f), S(f)$ and $s(\sigma)$ respectively. In this manner, the application of the stationary phase method to (B.1b) gives the following relation corresponding to (B.6b)

$$\sigma = -\frac{1}{2\pi}\frac{d\phi(f)}{df} \tag{B.10a}$$

This relation checks with the "spectral group delay $\sigma_g(f)$" relation

$$\sigma_g(f) = -\frac{1}{2\pi}\frac{d\phi(f)}{df} \tag{B.10b}$$

Relations (B.10a) and (B.10b) indicate that $\sigma_g(f) = \sigma$. Similarly, relations (B.6b) and (B.7) indicate that $f_{inst}(\sigma) = f$. These facts imply that $f_{inst}(\sigma)$ and $\sigma_g(f)$ are inverse functions of each other, i.e.

$$\sigma_g(f) = f_{inst}^{-1}(f) \tag{B.11a}$$

$$f_{inst}(\sigma) = \sigma_g^{-1}(\sigma) \tag{B.11b}$$

LIST OF PRINCIPAL SYMBOLS AND ABBREVIATIONS

Subscripts and superscripts may be used with symbols (e.g. to refer to a particular signal, order or region).

A	constant
A(f)	spectrum of $a(\sigma)$ (Section 4.11)
$A(\eta)$	oscillation amplitude of LFM amplitude spectrum at η
ACP	arbitrary chirp pair
AM	amplitude modulation
ASK	amplitude-shift keying
AWGN	additive white Gaussian noise
$a(\sigma)$	arbitrary time amplitude function
arg	argument of
C(X)	Fresnel cosine integral $\int_0^X \cos(\frac{\pi}{2}x^2)\,dx$
CCD	charge-coupled devices
CPSK	coherent PSK
DPSK	differentially coherent PSK
DS	direct sequence

E	energy of a real signal
erf(.)	error function (relation (1.21))
erfc(.)	complementary erf(.) (relation (1.20))
F	bandwidth
F(X)	Fresnel complex integral $\int_0^X e^{j\frac{\pi}{2}x^2} dx$
$F(x_p, x_q)$	$F(x_q) - F(x_p)$
FDM	frequency-division multiplexing
FH	frequency hopping
FM	frequency modulation
FSK	frequency-shift keying
f	current frequency variable
$f_{inst}(\sigma)$	instantaneous frequency at instant σ
f_ℓ	mean frequency of ℓth signal
GSRCP	generalized slope reversal chirp pair
H[.]	Hilbert transform of [.]
H(f), h(σ)	transfer function, impulse response (subsection 1.5.2)
$I_o(.)$	modified Bessel function of the first kind and zeroth order (relation (1.37))

Im	imaginary part of
ISR	interference-to-signal ratio
i,K,k	integers
LFM	Linear FM
LPF	low pass filter
L, ℓ, M	integers
m	integer, positive number
max, min	maximum value of, minimum value of
ms	millisecond
N_o	AWGN single-sided spectral power density
N,n	integers
PAM-FM	pulse amplitude modulation FM
P_e	demodulator error probability
P_e'	decoder error probability
PSK	phase-shift keying
p	integer, signal power
Q(.,.)	Marcum's Q-function (relation (1.36))

q	integer, spectral power
R(f)	spectrum of r(σ)
$R_T(.)$	(temporal) rect function (relation (2.14))
Re	real part of
RPV	remotely-piloted vehicles
r(σ)	real signal
RF	radio frequency
S(f)	spectrum of s(σ)
S(X)	Fresnel sine integral $\int_0^X \sin(\frac{\pi}{2} x^2)\,dx$
SAW	surface acoustic wave
SIR	signal-to-interference ratio
SM	structural multiplexing
SNR	signal-to-noise ratio
SNR_i, SNR_o	input SNR, output SNR
SS	spread spectrum
SSRCP	special slope-reversal chirp pair
s(σ)	complex signal

$s^a(\sigma)$	analytic complex representation
$s^e(\sigma)$	exponential complex representation
sinc x	sinc function $\frac{\sin\pi x}{\pi x}$
T	duration
T_s, T_ℓ	the smaller T, the larger T (Sections 3.3 - 3.6)
TDM	time-division multiplexing
TH	time-hopping
T_f	fall time
T_r	effective duration (Section 1.7), rise time (Chapter 4)
t	time-shift
W	LFM frequency sweep
X(f)	spectrum of $x(\sigma)$
x	arbitrary variable
$x(\sigma)$	arbitrarily shaped real LFM signal (relation (3.1))
Y(f), Y(η)	spectrum of $y(\sigma)$
$Y^n(\eta)$	normalized Y(η)
y	arbitrary variable

$y(\sigma)$	arbitrarily shaped complex LFM signal
α	initial phase shift
α_{ℓ}	initial phase of ℓth signal
β	mean SNR in phase-locked loop bandwidth (relation (1.42))
β_o^{-1}	maximum admissible ISR level
$\beta_{i,k}$	kth-ith SIR at kth matched filter output (Section 3.5)
Δ	arbitrarily large positive quantity (relation (3.26)), difference in (Subsection 3.5.3.5)
δ	small positive quantity, arbitrary parameter
$\delta(.)$	Dirac's delta function
ε	belongs to, small positive quantity
η	normalized frequency variable (relation (4.5e)), arbitrary parameter
η_{max}^{k}	LFM amplitude spectrum maximum point of order k
η_{min}^{k}	LFM amplitude spectrum minimum point of order k
$\theta(\sigma)$	temporal phase function

λ	fixed correlation coefficient
$\lambda_{ik}(t,\nu)$	time/frequency correlation function of the ith and kth real signals
$\lambda^{n}_{ik}(t,\nu)$	normalized $\lambda_{ik}(t,\nu)$
μ	LFM frequency slope
ν	frequency-shift
$\xi(\sigma)$	temporal phase function
$\rho_{ik}(t,\nu)$	in-phase component of $\lambda^{n}_{ik}(t,\nu)$
$\hat{\rho}_{ik}(t,\nu)$	quadrature component of $\lambda^{n}_{ik}(t,\nu)$
Σ	summation
σ	current time variable
$\sigma_{g}(f)$	group delay/frequency characteristic
τ	time delay
$\phi(f)$	spectral phase function
$\chi_{ik}(t,\nu)$	time/frequency correlation function of the ith and kth complex signals
$\chi^{n}_{ik}(t,\nu)$	normalized $\chi_{ik}(t,\nu)$
$(.,.)$	open or closed range

$[.,.]$	closed range
$\lvert\ .\ \rvert$	absolute value of
$\triangleq$	equal by definition
$\neq$	not equal to
$\approx$	approximately equal to
$>,>>$	larger than, much larger than
$<,<<$	less than, much less than
$(.)^*$	complex conjugate of (.)
$\rightarrow$	approaches

REFERENCES

1. Bell Telephone Laboratories, Inc., Transmission Systems for Communications; 1970.

2. Bennett, W. R., Introduction to Signal Transmission, McGraw-Hill, New York; 1970.

3. Fano, R. M., Transmission of Information, M.I.T. Press, Cambridge, Mass., and Wiley, New York; 1961.

4. Gallager, R. G., Information Theory and Reliable Communication, Wiley, New York; 1968.

5. Glinski, G. S., "Adaptive Communication Systems", IEEE Trans. Commun. Electronics, Vol. 83, pp.176-181; March 1964.

6. International Telephone and Telegraph Corp., Reference Data for Radio Engineers, New York; 1969.

7. Lucky, R. W., Salz, J. and Weldon Jr., E. J., Principles of Data Communication, McGraw-Hill, New York; 1968.

8. Panter, P. F., Modulation, Noise, and Spectral Analysis, McGraw-Hill, New York; 1968.

9. Shannon, C. E., "Communication in the Presence of Noise", Proc. IRE, Vol. 37, No. 1, pp.10-21; Jan. 1949.

10. Turin, G. L., Notes on Digital Communication, Van Nostrand Reinhold, New York; 1969.

11. Wozencraft, J. M., and Jacobs, I. M., Principles of Communication Engineering, Wiley, New York; 1967.

12. Bruce, J. D., Optimum Quantization, Tech. Rept. 429, Research Lab. Electronics, M.I.T., Cambridge, Mass.;1963.

13. Cattermole, K. W., Principles of Pulse Code Modulation, Iliffe, London; 1969.

14. Goblick, Jr., T. J., and Holsinger, J. L., "Analog Source Digitization: A Comparison of Theory and Practice", IEEE Trans. Inform. Theory, Vol. IT-13, pp.323-326; April 1967.

15. Kurtenbach, A. J., and Wintz, P. A., "Quantizing for Noisy Channels", IEEE Trans. Comm., Vol. COM-17, No. 2, pp.291-302; April 1969.

16. Linden, D. A., "A Discussion of Sampling Theorems," Proc. IRE, Vol. 47, pp.1219-1226; July 1959.

17. Max, J., "Quantizing for Minimum Distortion", IRE Trans. Inform. Theory, Vol. IT-6, pp.7-12; March 1960.

18. Oliver, B. M., Pierce, J. R., and Shannon, C. E., "The Philosophy of PCM", Proc. IRE, Vol. 36, pp. 1324-1331; Nov. 1948.

19. Purton, R. F., "A Survey of Telephone Speech-Signal Statistics and their Significance in the Choice of a PCM Companding Law", Proc. IEE, Vol. B109, pp.60-66; Jan.1962.

20. Spang, H. A., and Schultheiss, P. M., "Reduction of Quantizing Noise by Use of Feedback", IRE Trans. Comm. Systems, Vol. CS-10, pp.373-380; Dec. 1962.

21. Viterbi, A. J., Principles of Coherent Communication, McGraw-Hill, New York; 1966.

22. Wiggins, M. J., and Branham, R. A., "Reduction in Quantizing levels for Digital Voice Transmission", IEEE Int. Conv. Rec.,Pt. 8, pp.282-288; 1963.

23. Hamsher, D. H. (ed.), Communication System Engineering Handbook, McGraw-Hill, New York; 1967

24. Landee, R. W., Davis, D. C., and Albrecht, A. P., Electronic Designers' Handbook, McGraw-Hill, New York; 1957.

25. Martin, J., Telecommunications and the Computer, Prentice-Hall, Englewood Cliffs, N.J.; 1969.

26. Costas, J. P., "Synchronous Communication", Proc. IRE, Vol. 44, pp.1713-1718; Dec. 1956.

27. Gagliardi, R. M., "Rapid Acquisition Signal Design in a Multiple-Access Environment", IEEE Trans. Aerosp. Electronic Systems, Vol. AES-10, No. 3, pp.359-363; May 1974.

28. Lindsey, W. C., Synchronization Systems in Communication and Control, Prentice-Hall, Englewood Cliffs, N.J.; 1972.

29. Pierce, J. R., "Synchronizing Digital Networks", BSTJ, Vol. 48, pp.615-636; March 1969.

30. Stiffler, J. J., Theory of Synchronous Communications , Prentice-Hall, Englewood Cliffs, N.J.; 1971.

31. Cooper, G. R., "Decision Theory", System Engineering Handbook, (R. E. Machol, ed.), Chap. 24, McGraw-Hill, New York; 1965.

32. Hancock, J. C., and Wintz, P. A., Signal Detection Theory, McGraw-Hill, New York; 1966.

33. Harman, W. W., Principles of the Statistical Theory of Communication, McGraw-Hill, New York; 1963.

34. Helstrom, C. W., Statistical Theory of Signal Detection, Pergamon Press, New York; 1968.

35. Kotel'nikov, V. A., The Theory of Optimum Noise Immunity, (R. A. Silverman, Trans.), McGraw-Hill, New York; 1959.

36. Middleton, D., An Introduction to Statistical Communication Theory, McGraw-Hill, New York, 1960.

37. Selin, I., Detection Theory, Princeton University Press, Princeton, N.J.; 1965.

38. Smith, J. W., "The Joint Optimization of Transmitted Signal and Receiving Filter for Data Transmission Systems", BSTJ; Dec. 1965.

39. Turin, G. L., "An Introduction to Matched Filters", IRE Trans. Inform. Theory, Vol. IT-6, No. 3, pp.311-329; June 1960.

40. Van Trees, H. L., Detection, Estimation and Modulation Theory, Parts I, II and III, Wiley, New York; 1968, 1969.

41. Wainstein, L. A., and Zubakov, V. D., Extraction of Signals from Noise (R. A. Silverman, Trans.), Prentice-Hall, Englewood Cliffs, N. J.; 1962.

42. Weber, C. L., Elements of Detection and Signal Design, McGraw-Hill, New York; 1968.

43. Algazi, V. R., and Lerner, R.M., "Optimum Binary Detection in Non-Gaussian Noise", IEEE Trans. Inform. Theory, Vol. IT-12, No. 2, p.269; 1965.

44. Kailath, T., "The Detection of Known Signals in Colored Gaussian Noise", Proc. Nat. Electronics Conf., Vol. 21; 1965.

45. Sherman, H., and Reiffen, B., "An Optimum Demodulator for Poisson Processes: Photon Source Detectors",Proc. IEEE, Vol. 51, pp.1316-1320; Oct. 1963.

46. Cook, C. E., and Bernfeld , M., Radar Signals, Academic Press, New York; 1967.

47. Lehmann, E. L., Testing Statistical Hypotheses, Wiley, New York; 1959.

48. Neyman, J., and Pearson, E. S., "On the Problem of the Most Efficient Tests of Statistical Hypotheses", Phil. Trans. Roy. Soc., Ser. A, Vol. 231, pp.289-333; 1933.

49. North, D. O., "An Analysis of the Factors which Determine Signal/Noise Discrimination in Radar", Proc. IEEE, Vol. 51, pp.1016-1027; July 1963.

50. Wald, A., Statistical Decision Functions, Wiley, New York; 1950.

51. Weiss, L., Statistical Decision Theory, McGraw-Hill, New York; 1961.

52. Woodward, P. M., Probability and Information Theory, with Applications to Radar, McGraw-Hill, New York; 1955.

53. Berlekamp, E. R., Algebraic Coding Theory, McGraw-Hill, New York; 1968.

54. Ferguson, M. J., "Optimal Signal Design for Sequential Signalling over a Channel with Feedback", IEEE Trans. Inform. Theory, Vol. IT-14, pp.331-340; March 1968.

55. Forney, Jr., G. D., Concatenated Codes, M.I.T. Press, Cambridge, Mass.; 1967.

56. Green, P. E., "Feedback Communication Systems", Chap. 14 in E. J. Baghdady (ed.), Lectures on Communication System Theory, McGraw-Hill, New York; 1961.

57. Hayes, J. F., "Studies of Sequential Detection Systems with Uncertainty Feedback", IEEE Trans. Inform. Theory, Vol. IT-14, pp.63-70; Jan.1968.

58. Horstein, J., "On the Design of Signals for Sequential and Nonsequential Detection Systems with Feedback", IEEE Trans. Inform. Theory, Vol. IT-12, pp.448-455; Oct. 1966.

59. Kramer, A. J., "Improving Communication Reliability by Use of an Intermittent Feedback Channel", IEEE Trans. Inform. Theory, Vol. IT-15, pp.52-60; Jan. 1969.

60. Peterson, W. W., and Weldon, E., Error Correcting Codes, M.I.T. Press, Cambridge, Mass., 1972.

61. Shannon, C. E., "A Mathematical Theory of Communication", BSTJ, Vol. 27, pp.379-423 and 623-656; July and Oct. 1948; "The Zero-Error Capacity of a Noisy Channel", IRE Trans. Inform. Theory, Vol. IT-2, pp.S8-S19; Sep. 1956.

62. Sugimoto, S., "Performance of Suboptimum Feedback Functions for Sequential Detection Systems with Feedback", IEEE Trans. Comm. Technology, Vol. COM-15, pp.215-222; April 1967.

63. Viterbi, A. J., "Information Theory in the Sixties", IEEE Trans. Inform. Theory, Vol. IT-19, No. 3, pp.257-262; May 1973.

64. Lee, Y. W., Statistical Theory of Communication, Wiley New York; 1960.

65. Price, R., and Hofstetter, E. M., "Bounds on the Volume and Height Distributions of the Ambiguity Function", IEEE Trans. Inform. Theory, Vol. IT-11, No. 2, pp.207-214; April 1965.

66. Rihaczek, A. W., Principles of High-Resolution Radar, McGraw-Hill, New York; 1969.

67. Siebert, W. M., "Studies of Woodward's Uncertainty Function", M.I.T. Research Lab. Electronics, Quart. Progr. Rept.; April 15, 1958; "A Radar Detection Philosophy", IRE Trans. Inform. Theory, Vol IT-2, pp.204-221; Sep. 1956.

68. Stutt, C. A., "A Note on Invariant Relations for Ambiguity And Distance Functions", IRE Trans. Inform. Theory, Vol. IT-5, pp.164-167; 1959; "The Application of Time/Frequency Correlation Functions to the Continuous Waveform Encoding of Message Symbols", WESCON, Sect. 9/1; 1961; "Some Results on Real-part/Imaginary-part and Magnitude-Phase Relations in Ambiguity Functions", IEEE Trans. Inform. Theory, Vol. IT-10, pp.321-327; 1964.

69. Urkowitz, H., Hauer, C. A., and Koval, J. F., "Generalized Resolution in Radar Systems", Proc. IRE, Vol. 50, No. 10, pp.2093-2105; Oct. 1962.

70. Vakman, D. E., Sophisticated Signals and the Uncertainty Principle in Radar (E. Jacobs, ed.; K. N. Trirogoff, Trans.), Springer-Verlag, New York; 1968.

71. Wilcox, C. H., The Synthesis Problem for Radar Ambiguity Functions, Rept. 157, Mathematical Research Center, U.S. Army, Univ. of Wisconsin, Madison, Wisc.; April 1960.

72. Franks, L. E., Signal Theory, Prentice-Hall, Englewood Cliffs, N.J.; 1969.

73. Gabor, D., "Theory of Communication", Jour. IEE, Pt. III, Vol. 93, pp.429-457; Nov. 1946.

74. Kay. I., and Silverman, R. A., "On the Uncertainty Relation for Real Signals", Inform. and Control, Vol. 1, No. 1, pp. 64-75; Sep. 1957.

75. Landau, H. J., Pollak, H. O., and Slepian, D., "Prolate Spheroidal Wave Functions, Fourier Analysis and Uncertainty", BSTJ, Vol. 40, No. 1, pp.43-63 and 65-84; Jan. 1961; Vol. 41, No. 4, pp.1295-1336; July 1962.

76. Rihaczek, A. W., "Signal Energy Distribution in Time and Frequency", IEEE Trans. Inform. Theory, Vol. IT-14, pp.369-374; May 1968.

77. Zakai, M., "A Class of Definitions of'Duration'(or 'Uncertainty') and the Associated Uncertainty Relations", Inform. and Control, Vol. 3, No. 2, pp.101-115; June 1960.

78. Glisson, T. H., Black, C. I., and Sage, A. P., "On Sonar Signal Analysis", IEEE Trans. Aerosp. Electronic Systems, Vol. AES-6, No. 1, pp.37-49; Jan. 1970.

79. Abramowitz, J., and Stegun, I. A., Handbook of Mathematical Functions, Dover Publications, New York; 1965.

80. Balakrishnan, A. V., "A Contribution to the Sphere-Packing Problem of Communication Theory", J. Math. Analysis and Appls., Vol. 3, No. 3, pp.485-506; Dec. 1961.

81. Ziv, J., "Generation of Optimal Codes by a 'Pyramid-Packing' Argument", IEEE Trans. Inform. Theory, Vol. IT-10, pp.253-255; July 1964.

82. Landau, H. J., and Slepian, D., "On the Optimality of the Regular Simplex Code", BSTJ, Vol. 45, pp.1247-1272; Oct 1966.

83. Viterbi, A. J., "On Coded Phase-Coherent Communication", IRE Trans. Space Electron. Telemetry, Vol. SET-7, pp.3-12; March 1961.

84. Balakrishnan, A. V., and Abrams, I. J., "Detection Levels and Error Rates in PCM Telemetry Systems", IRE Intern. Conv. Record; 1960.

85. Nuttall, A. H., "Error Probabilities for Equicorrelated M-ary Signals Under Phase-Coherent and Phase-Incoherent Reception", IRE Trans. Inform. Theory, Vol. IT-8, No. 4, pp.305-315; July 1962.

86. Reiger, S., "Error Rates in Data Transmission", Proc. IRE, Vol. 46, pp.919-920; May 1958.

87. Turin, G. L., "The Asymptotic Behaviour of Ideal M'ary Systems", Proc. IRE, Vol. 47, No. 1, pp.93-94; Jan. 1959.

88. Helstrom, C. W., "The Resolution of Signals in White Gaussian Noise", Proc. IRE, Vol. 43, pp.1111-1118; Sep. 1955.

89. Johansen, D. E., New Techniques for Machine Computation of the Q-Functions, Truncated Normal Deviates, and Matrix Eigenvalues, Sylvania ARL, Waltham, Mass., Sci. Rept. No. 2; July 1961.

90. Marcum, J. I., Table of Q-Functions, Rand Corp., Calif., Rpt. RM-339; Jan. 1, 1950.

91. Stein, S., "Unified Analysis of Certain Coherent and Non-Coherent Binary Communications Systems", IEEE Trans. Inform. Theory, Vol. IT-10, pp.43-51; Jan. 1964.

92. Viterbi, A. J., "Optimum Detection and Signal Selection for Partially Coherent Communication", IEEE Trans. Inform. Theory, Vol. IT-11, pp.239-246; April 1965.

93. Turin, G. L., "An Introduction to Digital Matched Filters", Proc. IEEE, Vol. 64, No. 7, pp.1092-1112; July 1976.

94. IEE, Component Performance and Systems Applications of Surface Acoustic Wave Devices, IEE Conf., Aviemore, Scotland; 1973.

95. IEE, Delay Devices for Pulse Compression Radar, IEE Conf. Publ. 20; Feb. 21, 1966.

96. IEEE, Special Issue on Digital Signal Processing, Proc. IEEE; April 1975.

97. IEEE, Special Issue on Optical Computing, Proc. IEEE, Vol. 65, No. 1; Jan. 1977.

98. IEEE, Special Issue on Spread Spectrum Communications, IEEE Trans. Communs., Vol. COM-25, No. 8; August 1977.

99. IEEE, Special Issue on Surface Acoustic Wave Devices and Applications, Proc. IEEE, Vol.64, No. 5; May 1976.

100. IRE, Matched Filter Issue, IRE Trans. Inform. Theory, Vol. IT-6, No. 3; June 1960.

101. Lever, K. V., Patterson, E., Stevens, P. C., and Wilson, I. M., "Surface Acoustic Wave Matched Filters for Communications Systems", The Radio and Electronic Engineer, Vol. 46, No. 5, pp.237-246; May 1976.

102. Lockhart, G. B., "Digital Filtering and Encoding Using Delta Modulation", The Radio and Electronic Engineer, Vol. 42, No. 12, pp.547-551; Dec. 1972.

103. Rabiner, L., and Gold, B., Theory and Applications of Digital Signal Processing, Prentice-Hall, Englewood Cliffs, N.J.; 1975.

104. Cooley, J. W., and Tukey, J. W., "An Algorithm for the Machine Calculation of Complex Fourier Series", Math. Comput., Vol. 19, No. 90, pp.297-301; April 1965.

105. Wheeler, H. A., "The Interpretation of Amplitude and Phase Distortion in Terms of Paired Echoes", Proc. IRE, Vol. 27, pp.359-385; June 1939.

106. Meshkovskiy, K. A., "Advantages of Avoiding the Concept of Signal Volume in Communications", Telecommun., Vol. 22, No. 11, pp.57,58; 1968.

107. Cahn, C. R., Spread Spectrum Applications and State-of-the-Art Equipments, Magnavox Communications and Navigation, Torrance, CA; Jan. 1973.

108. Dixon, R. C., Spread Spectrum Systems, Wiley, New York; 1976. See also Spread Spectrum Techniques (R.C. Dixon, ed.), IEEE Press, New York; 1976.

109. NATO, Spread Spectrum Communications, AGARD Lecture Series No. 58,National Technical Information Service AD-766-914; July 1973.

110. Naval Electronics Lab. Center, Proceedings of the 1973 Symposium on Spread Spectrum Communications, San Diego, CA, Tech. Document 271; March 13-16, 1973; Session C.

111. Lerner R. M., "Signals with Uniform Ambiguity Functions", IRE Intern. Conv. Record, pt. IV, pp.27-36; 1958.

112. Row, H. E., "Amplitude Modulation with a Noise Carrier", "Frequency or Phase Modulation with a Noise Carrier", Proc. IEEE, Vol. 52, No. 4, pp.389-408; April 1964.

113. Nathanson, F. E., Radar Design Principles, McGraw-Hill, New York; 1969.

114. Halsted, L. R., "On Binary Data Transmission Error Rates Due to Combinations of Gaussian and Impulse Noise", Wescon Conv. Record, Part 4, pp.1-10; August 1963.

115. Klauder, J. R., "The Design of Radar Signals Having Both High Range Resolution and High Velocity Resolution", BSTJ, Vol. 39, No. 4, pp.809-820; July 1960.

116. Davenport, W. B. Jr., and Root, W. L., An Introduction to the Theory of Random Signals and Noise, McGraw-Hill, New York; 1958.

117. Turin, G. L., "Minimax Strategies for Matched-Filter Detection", IEEE Trans. Commun., Vol. COM-23, pp.1370-1371; Nov. 1975.

118. Barton, D. K., "Comments on 'Signal Resolution via Digital Inverse Filtering'", "Further Comments on Inverse Filtering", IEEE Trans. Aerosp. Elect. Systems, pp.607-608; July 1973 and pp.294-295; March 1974.

119. Senmoto, S., and Childers, D. G., "Signal Resolution via Digital Inverse Filtering", IEEE Trans. Aerosp. Elect. Systems, Vol. AES-8, No. 5, pp.633-640; Sep. 1972.

120. Bodonyi, A. B., "Effects of Impulse Noise on Digital Data Transmission", IRE Trans. Commun. Systems, Vol. 9, pp.355-361; Dec. 1961.

121. Mertz, P. "Model of Impulsive Noise for Data Transmission", IRE Intern. Conv. Record, Part 4; 1960; "Model of Error Burst Structure in Data Transmission", Proc. Nat. Electron. Conf., Vol. 16; 1960.

122. Spaulding, A. D., and Middleton, D., "Optimum Reception in an Impulsive Interference Environment", IEEE Trans. Commun. Vol. COM-25, No. 9, pp. 910-934; Sept. 1977.

123. Anderson, R. R., and Koll, V. G., "The Use of Smear-Desmear Techniques to Improve Error Performance on Data

Transmission Systems Encountering Impulse Noise", Bell Telephone Laboratories Memorandum; Sep. 1963.

124. Wainwright, R. A., "On the Potential Advantages of a Smearing-Desmearing Filter Technique in Overcoming Impulse-Noise Problems in Data Systems", IRE Trans. Commun. Systems, Vol. 9, pp.362-366; Dec. 1961.

125. Kennedy, R. S., Fading Dispersive Communication Channels, Wiley-Interscience, New York; 1974.

126. Krassner, G. N., and Michaels, J. V., Introduction to Space Communication Systems, McGraw-Hill, New York; 1964.

127. McManamon, P., Jones, R. V., and Tsai, S., "Comparison of Diversity, Nondiversity, and Coding on a Parallel FSK HF Channel", IEEE Trans. Commun. Tech., Vol. COM-17, No. 3, pp.355-367; June 1969.

128. Smith, G. H., Cunningham, D. R., and Ziemer, R. E., "Performance Degradation Due to Specular Multipath Intersymbol Interference", IEEE Trans. Aerosp. Elect. Systems, Vol. AES-9, No. 4, pp.548-555; July 1973.

129. Price, R., and Green, Jr., P. E., "A Communication Technique for Multipath Channels", Proc. IRE, Vol. 46, pp.555-570; March 1958.

130. Sussman, S. M., "A Matched Filter Communication System for Multipath Channels", IRE Trans. Inform. Theory, Vol. IT-6, No. 3, pp.367-373; June 1960.

131. Dayton, D. S., "Coming to Grips with Multipath Ghosts", Electronics, Vol. 40, No. 24,pp.104-108; Nov. 27 1967; "FM'Chirp' Communications: Multiple Access to Dispersive Channels", IEEE Trans. Electromag. Compat. Vol. EMC-10, No. 2, pp.296-297; June 1968.

132. Forgan, D. H., A Study of Digital Radio Links Using Chirp Signals, Ph.D. Thesis, University of Nottingham; Jan. 1971.

133. Girard, A. L., "Signal Design and Discrete Addressing in Oceanographic/Meteorological Buoy Telemetry Using HF Radio", Natl. Telemet. Conf. Proc., pp.400-402; 1966.

134. Gott, G. F., An Investigation into the Application of Chirp Signals in H.F. Digital Communication Systems, Ph.D. Thesis, University of Nottingham, Nottingham; Oct. 1966.

135. Gott, G. F., and Newsome, J. P., "H.F. Data Transmission Using Chirp Signals", Proc. IEE, Vol. 118, No. 9, pp.1162-1166; Sep. 1971.

136. Griffiths, A. S., and Smith, W. H., "FM'Chirp' Communications: An easily-Instrumented Multiple-Access Modulation Form for Dispersive Channels", IEEE Intern. Conf. Commun. Digest, Paper 5.1, p.32; 1967.

137. Lee, J. F., "A Mars Lander Telemetry Relay System", Proc. Nat. Telemet. Conf., Paper 10-1, pp.1-7; 1964.

138. Cooper, G. R., "Is There a Communication Compatibility Theory", IEEE Intern. Conf. Commun., pp. 1-2 to 1-5; 1972.

139. Zayezdnyi, A. M., and Fink, L. M., "The Problem of Electromagnetic Compatibility", Telecomm. Radio Engng., Vol. 28, No. 7, Part 2, pp. 59-63; July 1973.

140. Zadeh, L. A., and Miller, K. S., "Fundamental Aspects of Linear Multiplexing", Proc. IRE, Vol. 40, No. 9, pp. 1091-1097; Sep. 1952.

141. Harmuth, H. F., Transmission of Information by Orthogonal Functions, Springer, New York; 1972.

142. Glenn, A. B., "Code Division Multiplex Systems", IEEE Intern. Conv. Record, Vol. 12, Part 6, pp. 53-61; 1964.

143. McCalmont, A. M., "Multiple-Access Discrete-Address Communication Systems", IEEE Spectrum, pp. 87-94; August 1967.

144. Varakin, L. E., and Pyshkin, I. M., "Asynchronous Address Systems - Past, Present Problems and the Future", Telecomm. Radio Engng., Vol. 28, No. 11, Part 2, pp. 55-67; Nov. 1973.

145. Winkler, M. R., "Chirp Signals For Communications", IEEE WESCON, Paper 14.2; August 1962.

146. Darlington, S., "Demodulation of Wideband, Low-Power FM Signals", BSTJ, Vol. 43, No.1, Part 2, pp. 339-374; Jan. 1964.

147. Mancianti, M., Russo, F., and Verrazzani, L., "On the Detection of M-ary FSK Signals by Chirp-Technique", Alta Frequenza (Italy), Vol. 43, No. 3, pp. 167-172; March 1974.

148. Murarka, N. P., "Detection of FSK Signals Using Linear FM Dispersion Method", IITRI Technical Note COMM-108; Oct. 1971.

149. Burnsweig, J., and Wooldridge, J., "Ranging and Data Transmission Using Digital Encoded FM-'Chirp' Surface Acoustic Wave Filters", IEEE Trans. Microwave Theory and Techniques, Vol. MTT-21, No. 4, pp. 272-279; April 1973.

150. Holland-Moritz, E. K., Dute, J. C., and Brundage, D. R., "Swept Frequency Modulation", Proc. Natl. Electronics Conf., Vol. 22, pp. 469-474; 1966.

151. Ramp, H. O., and Wingrove, E. R., "Principles of Pulse Compression", IRE Trans.Military Electronics, Vol. MIL-5, pp. 109-116; April 1961.

152. Klauder, J. R., Price, A. C., Darlington, S., and Albersheim, W. J., "The Theory and Design of Chirp Radars", BSTJ, Vol. 39, No. 4, pp. 745-808; July 1960.

153. Berni, A. J., and Gregg, W. D., "On the Utility of Chirp Modulation for Digital Signaling", IEEE Trans. Commun., Vol. COM-21, pp. 748-751; June 1973.

154. Dorman, M. I., and Sotkinov, V. V., "Phase-Shift Keyed LFM Signals and Their Optimal Processing", Radio Engng. Elect. Phys., Vol. 20, No. 7, pp. 62-64; July 1975.

155. Federhan, H. M., "RPV Command and Control", Signal; August 1975.

156. Gott, G. F.,and Karia, A. J., "Differential Phase-Shift Keying Applied to Chirp Data Signals", Proc. IEE, Vol. 121, No. 9, pp. 923-928; Sept. 1974.

157. Hata, M., "Application of Swept FM Carrier Pulse to A New Digital Data Transmission System", Jour. Institute Elect. Commun. Engineers (Japan), Vol. 49, No. 11, pp. 363-371; Nov. 1966.

158. Lafuse, H. G., "A Wideband Communication System Using Frequency Slope Modulation", Proc. Natl. Electronics Conf., Vol. 19, pp. 346-357; 1963.

159. Otto, J., "Chirping RPV Data Links for ECM Protection", Microwaves, pp. 54-60; Dec. 1974.

160. Pettit, R. H., "Error Probability for NCFSK with Linear FM Jamming", IEEE Trans. Aerosp. Electron. Systems, Vol. AES-8, No. 5, pp. 609-614; Sept. 1972.

161. Zaytsev, D. L., and Zhuravlev, V. I., "Noise Immunity of a Digital Data Transmission System Using Linearly Frequency-Modulated Signals", Telecomm., Vol. 22, No. 4, pp. 13-17; 1968.

162. Andreyev, G. A., Den'gin, G. D., and Savchenko, V. P., "Optoelectronic Methods of LFM Signal Processing", Telecommun. Radio Engng., No. 11, Part 2, Vol. 28, pp. 108-111; Nov. 1973.

163. Grant, P. M., Collins, J. H., Darby, B. J., and Morgan, D. P., "Potential Applications of Acoustic Matched Filters to Air-Traffic Control Systems", IEEE Trans. Microwave Theory and Techniques, Vol. MTT-21, No. 4, pp. 288-300; April 1973.

164. Robinson, J. C., "A Fast-Correlation Algorithm for Swept-Frequency Seismic Data", IEEE Trans. Acoust. Speech Sig. Processing, Vol. ASSP-23, No. 4, pp. 346-352; Aug. 1975.

165. Otto, O. W., "Real-Time Fourier Transform with a Surface-Wave Convolver", Electronics Letters, Vol. 8, No. 25, pp. 623-624; Dec. 14 1972.

166. Belov, L. A., Barabanov, V. B., and Kochemasov, V. N., "A System for the Automatic Control of the Linear Time Dependence of Frequency Modulation", Telecommun. Radio Engng., No. 5 , Part 1, Vol. 27, pp. 42-46; May 1973.

167. Erdélyi, A., Asymptotic Expansions,Dover, New York; 1956.

168. Mason, S. J., and Zimmermann, H. J., Electronic Circuits,Signals and Systems, Wiley, New York; 1965.

169. Bedrosian, E., "A Product Theorem for Hilbert Transforms", Proc. IEEE, Vol. 51, pp. 868-869; 1963.

170. Rubin, W. L., and DiFranco, J. V., "Analytic Representation of Wideband Radio Frequency Signals", Jour. Franklin Institute, Vol. 275, No. 3, pp. 197-204; March 1963.

171. Gray, G. A., and Nathanson, F. E., "Digital Processing of Radar Signals", IEEE EASCON Record, pp. 208-215; Oct. 1971.

172. Kelvin, Lord, Phil. Mag. (5), Vol. 23, pp. 252-255; 1887.

173. Copson, E. T., Asymptotic Expansions, Cambridge Univ. Press; 1965.

174. Key, E. L., Fowle, E. N., and Haggarty, R. D., "A Method of Designing Signals of Large Time-Bandwidth Product", IRE Internl. Conv. Record, Part 4, pp. 146-154; 1961.